Author:
Howarth, L. G

Title:
Rheological studies of bentonite dispersions

II

RHEOLOGICAL STUDIES OF BENTONITE DISPERSIONS

by

LESLIE GEORGE HOWARTH

A dissertation submitted to the University of Bristol

in partial fulfilment of requirements

for the degree of Doctor of Philosophy.

SHEFFIELD

MARCH 1986

TO MY PARENTS

Conclusions made conclusions leapt

Impressions lost and overstepped

Shadows hide the truth with nobody the wiser...

Geoff Mann, 1984

If you want to destroy something,

use bentonite.

C.A. Lewis, 1984

DECLARATION

The work described in this dissertation was carried out in the Department of Physical Chemistry, University of Bristol, under the supervision of Professor R.H. Ottewill, F.R.S. between November 1982 and October 1985. The dissertation is original except where reference is made in the text and has not been previously submitted for a degree at this or any other University.

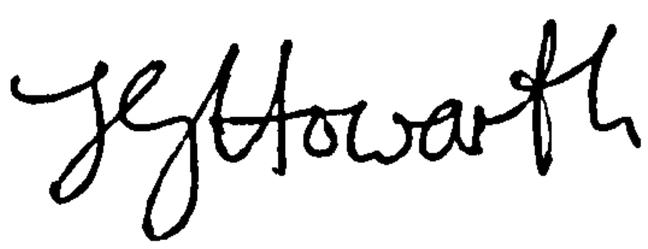

L.G. Howarth, B.Sc.(C.N.A.A.), M.Sc.(Bristol), G.R.S.C.

ACKNOWLEDGEMENTS

I would like to thank Professor Ron Ottewill for his advice and supervision during this work.

Thanks are also due to Roy Goodman, Brian Jepson and Doug Smith, of English Clays Lovering, Pochin and Company, plc, for their assistance during the course of this project.

I also thank all the people, too numerous to mention (appendix 10), who have helped with this work and/or made my time in Bristol so enjoyable.

In particular, I would like to thank (Badman) Bodie Adeniran, for continually insulting me; (Wrecks) Rex Field, for many useless(ish) discussions on aluminium chemistry; and, of course, Isabel MacDonald, for also distracting me from bentonite chemistry.

Finally, I would like to thank Mrs. R. Howarth for typing the script.

ABSTRACT

The properties of Wyoming and Texas bentonite samples were studied and compared. The lower degree of dispersion of crude Texas clay in water compared to that of Wyoming bentonite seemed to be mainly due to the larger amount of Ca montmorillonite present in the former.

Samples of bentonite were dispersed in aqueous solution, coarse accessory minerals were removed (although it was not found to be possible to completely remove opal-CT from the Texas bentonites), converted into a homoionic form and then (with the aid of ion exchange resin treatment) prepared at a range of given electrolyte concentrations. Good reproducibility of rheological properties was found for individual batches of material using this preparation procedure.

The shear moduli of montmorillonite dispersions was measured using a Pulse Shearometer. The Texas bentonite dispersions were found to give lower shear moduli than the Wyoming samples having similar ionic form, volume fraction, pH and electrolyte concentration. The most reasonable explanation for this difference is the presence of montmorillonite-opal-CT aggregates in the Texas bentonites. Reduction of mean particle size by centrifugation or homogenisation seemed to be effective in increasing the shear modulus of the dispersions.

The variations in shear moduli of Wyoming montmorillonite dispersions (at low electrolyte concentration) with volume fraction,

counter ion type and electrolyte concentration could be qualitatively explained using a simple theoretical model considering electric double layer forces and tactoid formation. At higher electrolyte concentrations the dispersions were found to become thixotropic and it seems that flocculation and ordering phenomena may be important.

CONTENTS

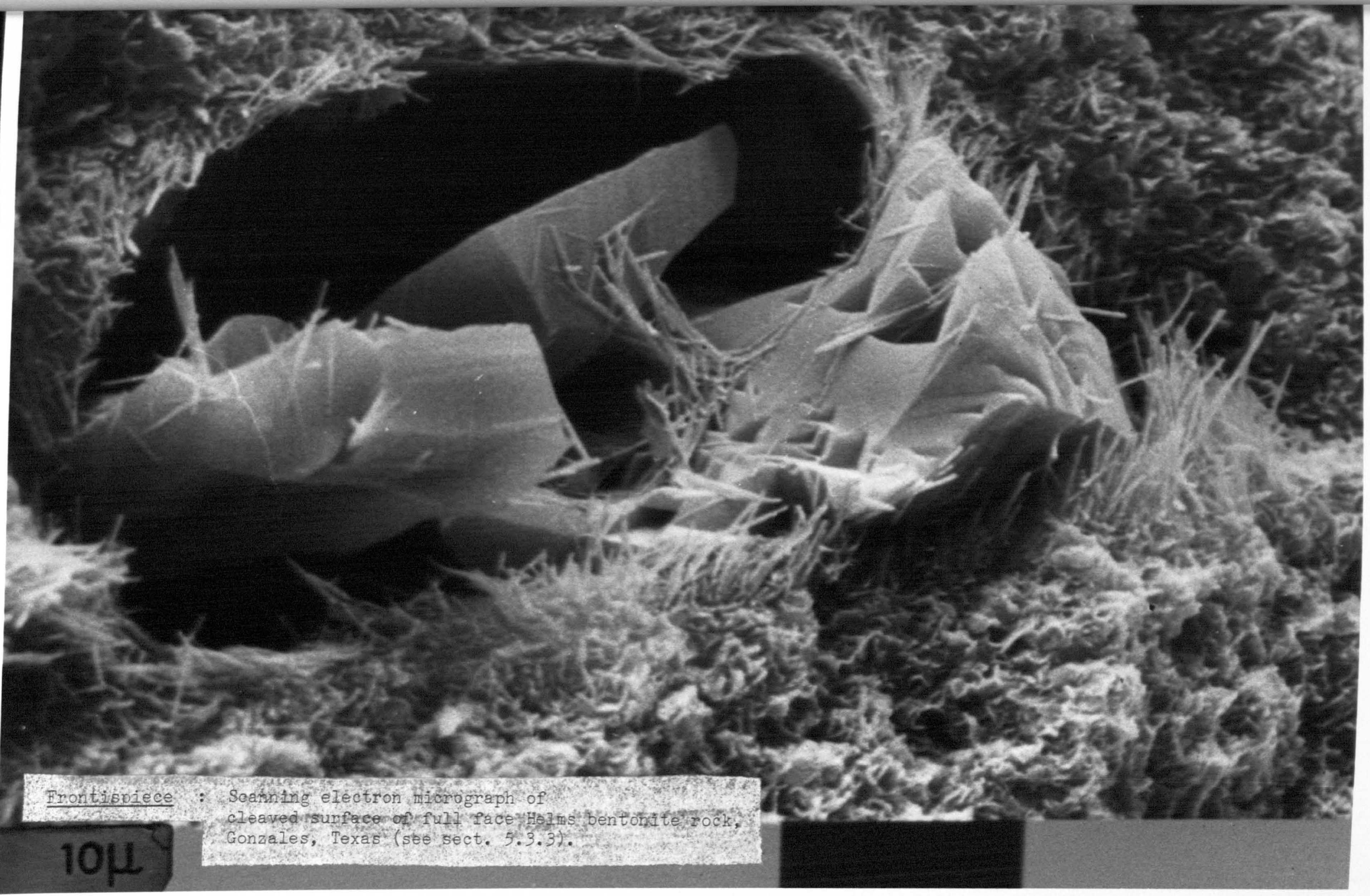

Frontispiece : Scanning electron micrograph of cleaved surface of full face Helms bentonite rock, Gonzales, Texas (see sect. 5.3.3).

CHAPTER ONE

INTRODUCTION

I N T R O D U C T I O N

1.1 BENTONITE

In 1897 Knight (1) reported the occurrence of a clay material having unusual "soapy" properties, near Fort Benton, Wyoming (U.S.A.). He later suggested the name bentonite for this material (2). Ross and Shannon (3) found that bentonite usually contained the mineral montmorillonite or, occasionally, beidellite. The term bentonite is now used for any clay largely composed of a smectite clay mineral and having physical properties due to this clay mineral (4).

The unique physical properties of the Wyoming bentonite led to its use in oil well drilling fluids (5, 6, 7) and for bonding foundry moulding sands (5, 6), and to the development of a bentonite producing industry in the Black Hills region of South Dakota, Wyoming and Montana, (U.S.A.). Bentonites have since been discovered in many areas outside Wyoming (5, 6), such as, for example, in Arizona, California, Mississippi and Texas of the U.S.A. and in England, France, Greece, Spain, Yugoslavia, U.S.S.R., Japan and many other countries. Also, the occurrence of large amounts of montmorillonite containing rock on Mars has been suggested (8). Bentonite now has many other commercial uses (6) including usage in ceramics, catalysts, decolourising agents (Fuller's earth), cements, paints and pesticides.

1.2 OCCURRENCE OF WHITE BENTONITE IN TEXAS

Beds of white bentonite occur in the upper Eocene age (40 million years old) rocks of the Jackson group in south east Texas (U.S.A.) (9, 10 and 42). In Gonzales County, the white bentonite is mined for use in the tile industry, oil bleaching, catalysis and (after processing) as a white gelling agent (11). The Southern Clay Products Company mines two white bentonite pits in Gonzales county, these are the Helms and Clark pits. The Helms pit contains, broadly speaking, two types of white bentonite beds, an upper, soft bentonite with many fractures stained with brown iron oxide and a lower, hard bentonite having fewer, iron stained, fractures. The Clark pit bentonite is similar in physical properties to the soft Helms bentonite. The main constituents of the white bentonites are calcium montmorillonite and cristobalite (10, 12, 13), with the hard Helms bentonite having a higher cristobalite content than the soft (Helms and Clark) bentonites. There is considerable variation in the composition and properties of the bentonites across the deposits (6, 12, 13).

1.3 STATEMENT OF PROBLEM

A typical Wyoming bentonite will readily swell and disperse, in water, forming a colloidal dispersion having a high gel strength (e.g. 5½ to 7% by weight (or ∿2 to 3½ by volume) of Wyoming bentonite, in water, gives an adequate gel strength for a drilling fluid), i.e.

it is a very good gelling agent. However, due to its usual yellow or green colouration, (due to isomorphous substitution of Fe in the clay crystal lattice (section 2.2.4)) Wyoming bentonite is unsuitable for use as a gelling agent in products such as pharmaceuticals and cosmetics; the white Texas bentonites may be.

The iron stains on the fracture surfaces of the hard Helms bentonite are removed manually (cobbing). The soft bentonites are more difficult to cob. The cobbed hard Helms bentonite is then milled, when it is known as "Bentolite L". This material does not disperse as readily, in water, as a Wyoming bentonite, so it is processed further in an attempt to obtain the montmorillonite in the sodium form. This product is not as good a gelling agent as the Wyoming bentonite, i.e. a higher clay concentration is required to achieve a given gel strength.

1.4 AIMS OF PROJECT

The aims of this project were to discover why the white Texas bentonites do not disperse as readily or, after appropriate treatment, do not gel as effectively as an "ideal" Wyoming bentonite.

The properties of Texas and Wyoming bentonites, and other clay samples, were studied and compared using techniques including X-ray diffraction, electron microscopy and pulse shearometry.

CHAPTER TWO

MINERALOGY OF BENTONITE

M I N E R A L O G Y O F B E N T O N I T E

2.1 INTRODUCTION

As stated previously (section 1.1) (4), bentonites are largely composed of smectite clay mineral. Other clay minerals, such as kaolinites and illites, are present in many bentonites (6), as are non-clay minerals (5, 6, 10, 15, 16) such as silica minerals (quartz, tridymite, cristobalite, opal), iron oxides, feldspars and zeolites. The structure of the clay minerals will be described in section 2.2 and the accessory minerals in section 2.3.

2.2 CLAY MINERAL STRUCTURES

2.2.1 Introduction

Clay minerals are hydrous layer-lattice silicates (part of the larger group of phyllosilicates), (5, 17, 18, 19) having a mean particle size in the colloidal range (i.e. less than ~2μm (19)).

Phyllosilicates consist of 2-dimensional sheets of $\{MO_4\}$ tetrahedra (where M = Si^{4+}, Al^{3+} or Fe^{3+}) which are linked to each other at three corners, by sharing (basal) oxygen atoms, forming a hexagonal mesh pattern (fig. 1). The fourth tetrahedral corner (the apical oxygen atom) points in a direction normal to the sheet and forms part of the adjacent octahedral sheet, in which octahedra are linked by sharing octahedron edges (fig. 2). The plane of the junction between the tetrahedral and octahedral sheets consists of

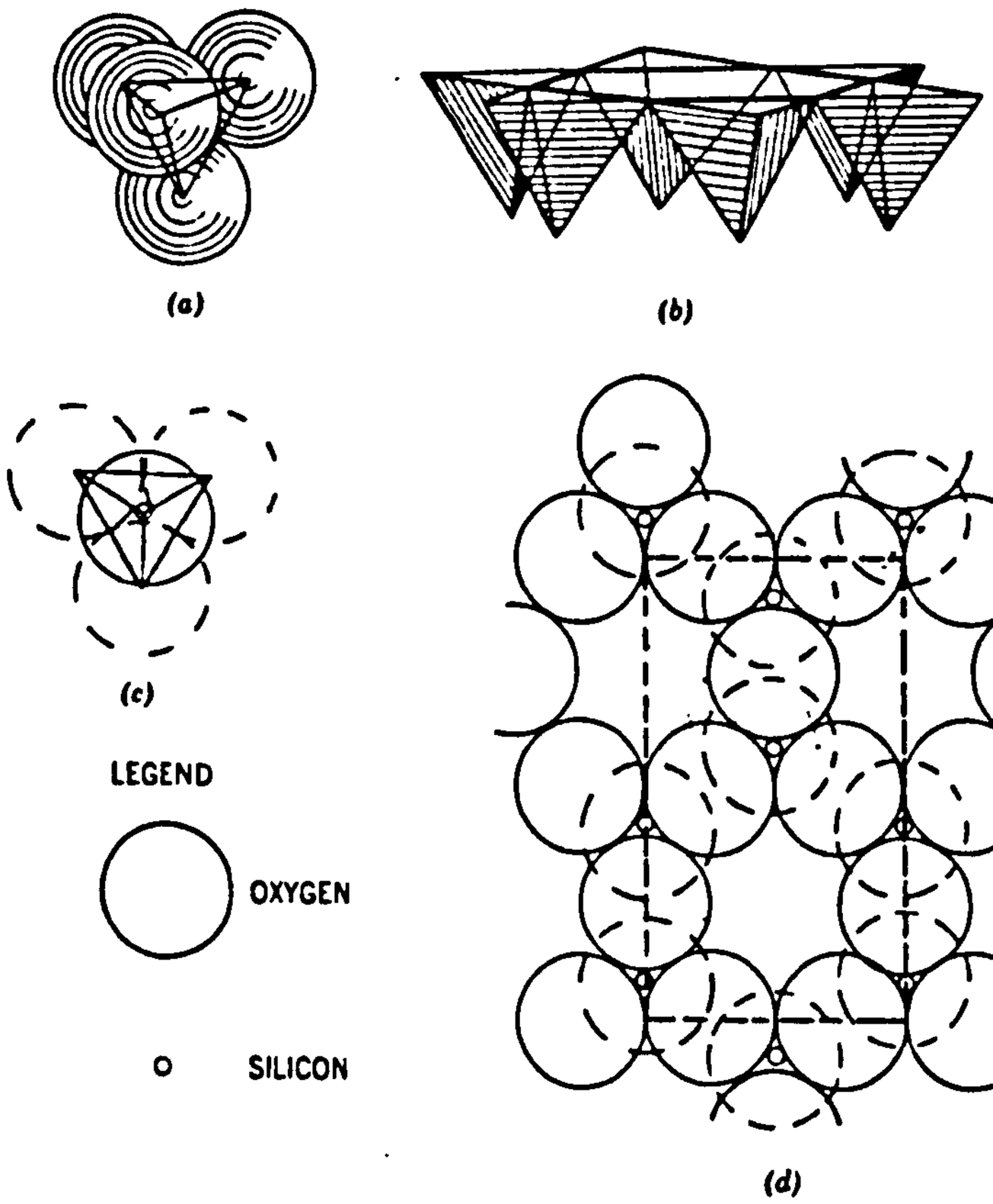

Figure 1 : Structure of the tetrahedral sheet. (*a*) Tetrahedral arrangement of Si and O. (*b*) Perspective sketch of tetrahedral linking. (*c*) Projection of tetrahedron on plane of sheet. (*d*) Top view of tetrahedral sheet (dotted line: unit cell area). Large circles represent oxygen; small circles represent silicon.

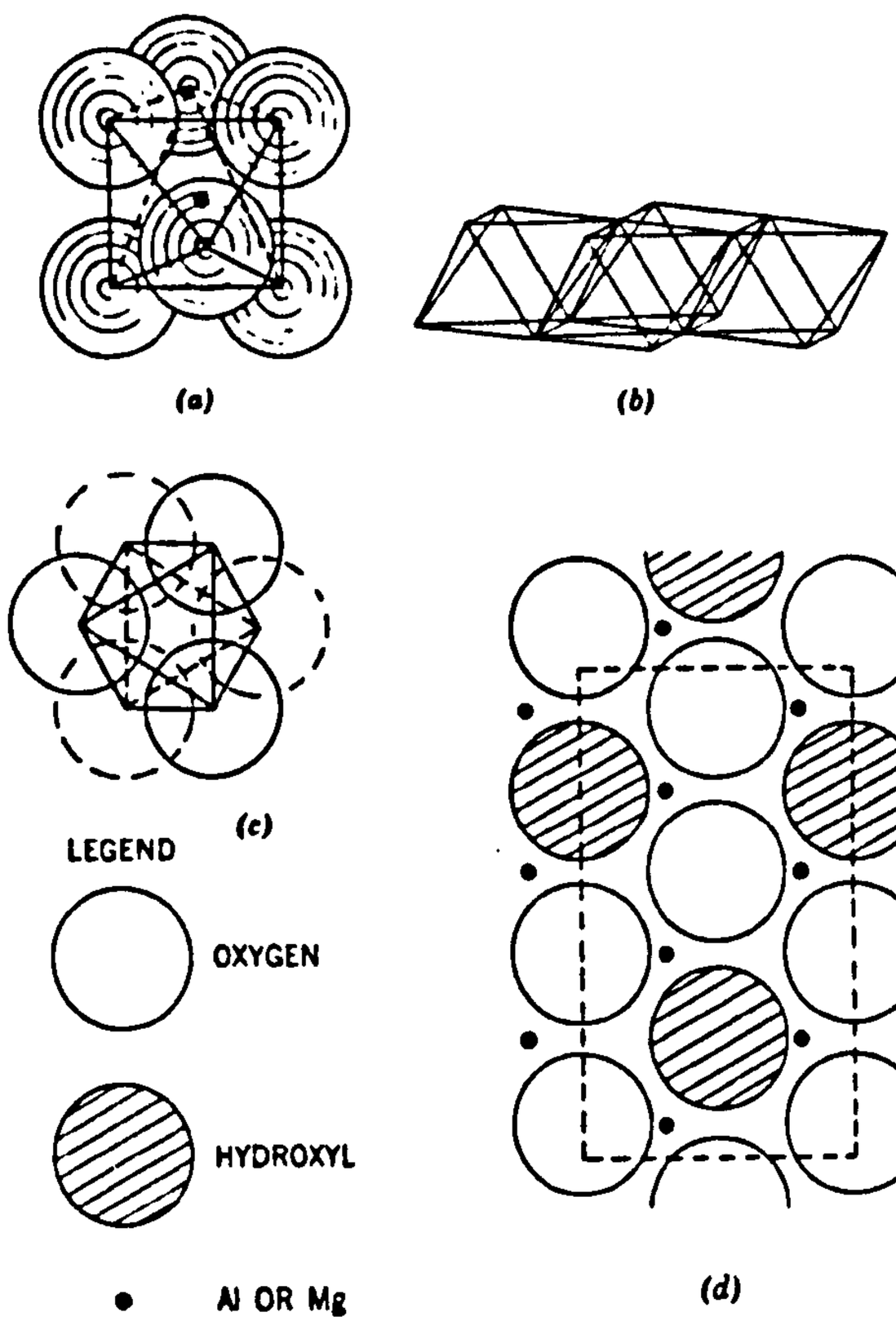

Figure 2: Structure of the octahedral sheet. (*a*) Octahedral arrangement of Al or Mg with O or OH. (*b*) Perspective sketch of octahedral linking. (*c*) Projection of octahedron on plane of sheet. (*d*) Top view of octahedral sheet (dotted line: unit cell area). Large circles represent oxygen; shaded circles represent hydroxyl; small black circles represent aluminum or magnesium.

shared apical oxygen atoms and unshared hydroxyl groups (fluorine atoms may be substituted for some of the hydroxyl groups). Octahedral cations are normally Mg^{2+}, Al^{3+}, Fe^{2+} or Fe^{3+}, but Li, Ti, V, Cr, Mu, Co, Ni, Cu and Zn also occur in some species (18).

The smallest structural unit contains three octahedra. If all three octahedra are occúpied with cations the mineral is termed trioctahedral. If only two of the octahedra are occupied the mineral is dioctahedral.

Linking one tetrahedral sheet to one octahedral sheet gives a 2 (1:1) layer, where the unshared plane of anions in the octahedral sheet consists entirely of hydroxyl groups (fig. 3). A 3 (2:1) layer consists of two tetrahedral sheets linked to one octahedral sheet by their apical oxygen atoms (fig. 4). Both octahedral anion planes have the same O/OH composition.

If 1:1 or 2:1 layers are not electrostatically neutral, the excess layer charge is neutralized by various inter-layer materials such as cations, hydrated cations and octahedral hydroxide groups or sheets (forming a 4 (or 2:1:1) layer (fig. 5).

If the fit between the tetrahedral and octahedral sheets is difficult the places of junction are strained which may have an effect on crystal size, morphology and structure. Some structural adjustment may occur to eliminate the misfit and to give the layer structure. Rotation of adjacent tetrahedra in the 001 plane may occur (20, 21, 22) giving an approximately ditrigonal symmetry to the tetrahedral network. Some adjustment is also possible by thickening the tetrahedral sheet and thinning the octahedral sheet (18). For octahedral sheets occupied with relatively large

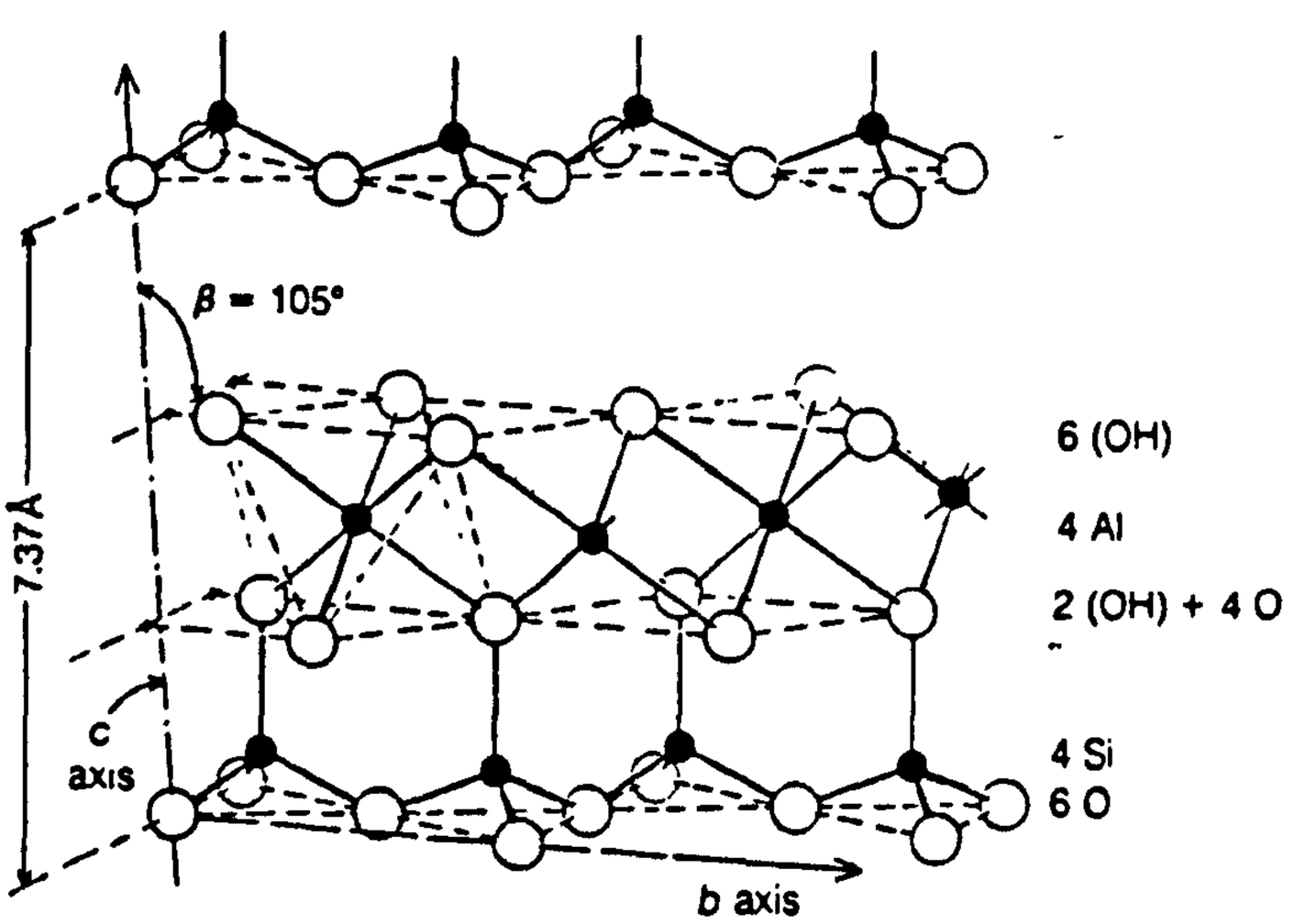

Fig.3: 1:1 layer structure (kaolite)

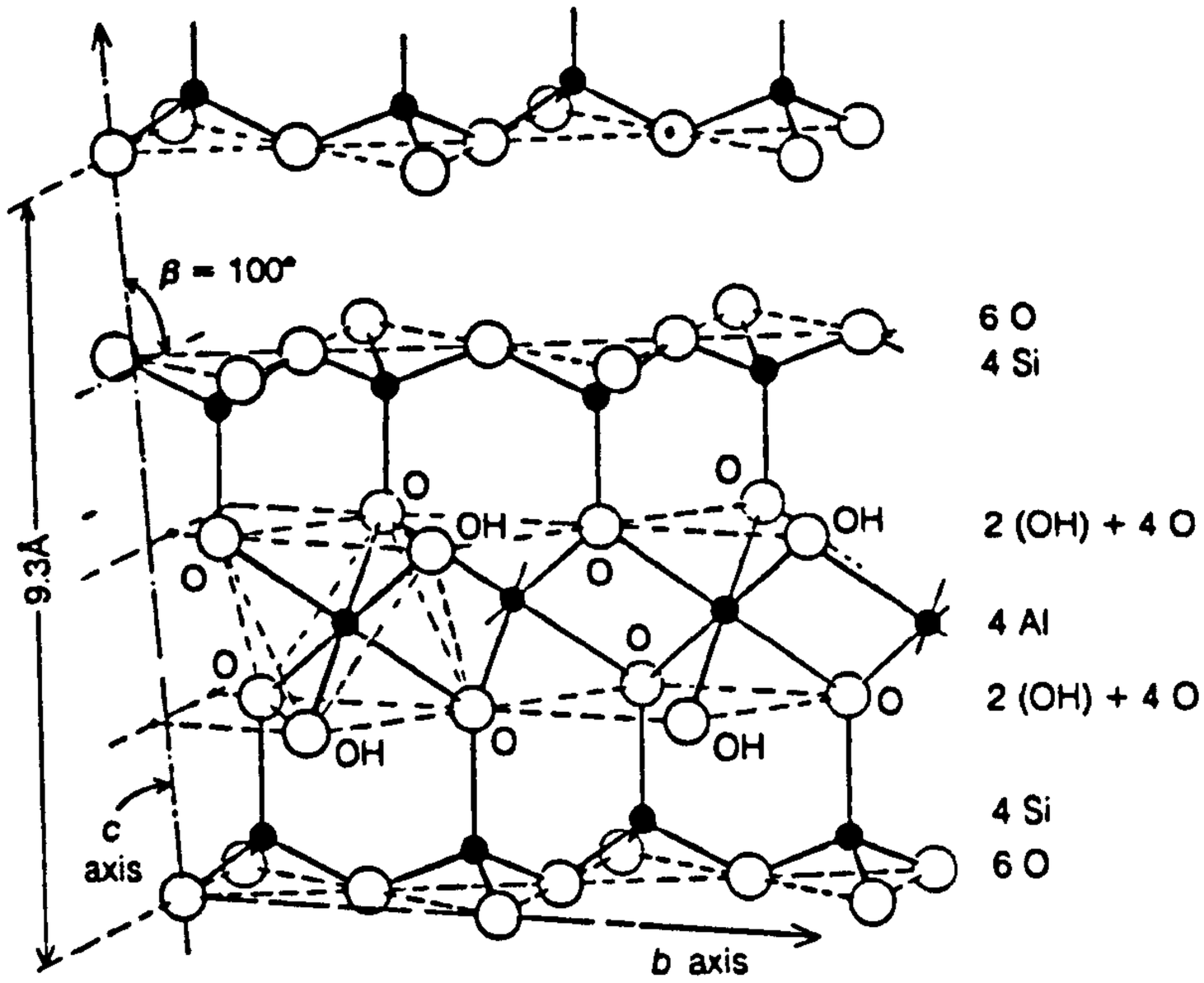

Fig.4: 2:1 layer structure (pyrophyllite)

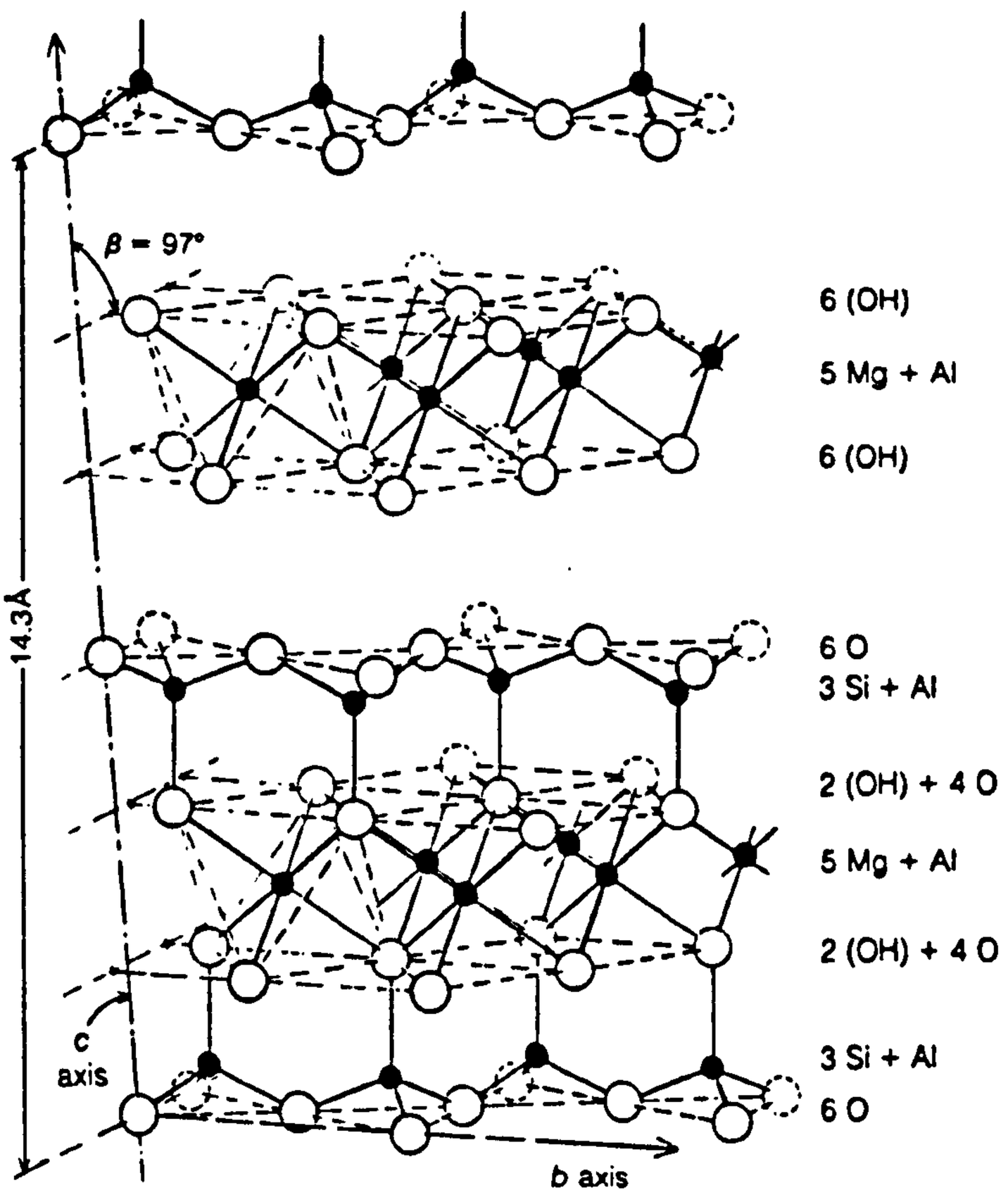

Fig.5: 2:1:1 layer structure (chlorite)

cations (Mg, Ni, Co, Zn, Fe^{2+} and Mn^{2+}) the tetrahedral sheet adjustments may be more drastic e.g. adjustment of sheet thicknesses, tetrahedra tilting (which may lead to curling in 1:1 layers) or inversion of tetrahedra apical directions (18).

2.2.2 Phyllosilicate classification

Layer silicate minerals may be classified on the basis of layer type (1:1 or 2:1), layer charge and type of interlayer into eight major groups. Further subdivision into subgroups and species is made on the basis of octahedral sheet type (di or trioctahedral), chemical composition and geometry of superposition of individual layers and interlayers (18). The classification scheme for phyllosilicates is shown in table 1.

2.2.3 2 layer clays (Serpentine-kaolin group)

2.2.3.1 Kaolinite

Kaolinite is a member of the serpentine-kaolin group of minerals, having a dioctahedral 1:1 layer type. The structure is composed of a single tetrahedral sheet linked to a single octahedral sheet. The unshared plane of anions in the octahedral sheet consists of hydroxyl groups (fig. 3).

The structure is modified considerably by lattice distortion. The octahedral sites form a distorted hexagonal pattern where the larger vacant octahedra are each surrounded

TABLE 1. PHYLLOSILICATE CLASSIFICATION SCHEME

Layer Type	Group	Charge per formula unit	Sub-group	Species (examples)
1:1	Serpentine-kaolin	~0	Serpentines	Chrysolite, Lizardite
			Kaolinites	Kaolinite, Halloysite
2:1	Talc-pyrophyllite	~0	Talcs	Talc, Willemsite
			Pyrophyllites	Pyrophyllite
	Smectites	~0.2-0.6	Saponites	Saponite, hectorite
			Montmorillonites	Montmorillonite, Beidellite, nontronite
	Vermiculites	~0.6-0.9	Trioctahedral vermiculites	Trioctahedral vermiculite
			Dioctahedral vermiculites	Dioctahedral vermiculite
	Mica	~1.0	Trioctahedral micas	Phlogopite, biotite
			Dioctahedral micas	Muscovite, illite
	Brittle Mica	~2.0	Trioctahedral brittle micas	Clintonite, Anandite
			Dioctahedral brittle micas	Margarite
2:1 (inverted ribbons)	Sepiolite-palygorskite	variable	Sepiolites	Sepiolite, Loughlinite
			Palygorskites	Palygorskite
2:1:1	Chlorite	variable	Trioctahedral chlorites	Clinochlore, Chamosite
			Dioctahedral chlorites	Donbassite
			,Ditrioctahedral chlorites	Cookeite, Sudoite

by size smaller occupied sites (23, 24). The tetrahedra linked to the smaller, twisted octahedra edges adjust their orientation by rotation in opposite directions giving a ditrigonal pattern of basal oxygens (22).

The 1:1 layer is planar with each basal tetrahedral oxygen paired with an octahedral OH group, on the adjacent layer, with hydrogen bonds which bond the layers together (25, 26, 27, 28). Cruz et al (29) have, however, calculated that the bonding between the layers is primarily electrostatic in nature.

Kaolinite has the structural formula $Si_4Al_4O_{10}(OH)_8$ (5), having very little substitution, within the lattice, and charge. There may be some isomorphous substitution of iron and/or titanium in some samples (5).

2.2.3.2 Halloysite

Halloysite exists in two forms. 10Å-Halloysite has an X-ray diffraction basal spacing of approximately 10·1Å and the structural formula $Al_4Si_4O_{10}(OH)_8 \cdot 4H_2O$. 10Å-Halloysite may be irreversibly dehydrated by, for example, heating at 70°C or evacuating at room temperature (30, 31, 32, 33, 247, 34), forming 7Å-halloysite. 7Å-Halloysite has a composition similar to kaolinite (structural formula - $Al_4Si_4O_{10}(OH)_8$) and a basal spacing of approximately 7.2Å.

Electron microscopy of halloysites indicates a wide variety of morphologies which are frequently tubular or

rolled (35, 247, 36). The curvature of the (kaolinite-like) layers of halloysite to form tubes is due to either bending of the structural layers (37) or displacements of flat layers (38).

In 10Å-halloysite the water is present in the interlayer, in the form of a planar arrangement (39, 40), the difference in basal spacing between the 10Å- and 7Å-forms, of 2.9Å, being sufficient to accommodate a plane of water molecules. The irreversibility of the 10Å-halloysite hydration is probably due to the absence of interlayer exchangeable cations (37).

2.2.3.3 Other 2-layer minerals

Other examples of dioctahedral 1:1 layer minerals (5, 18) are dickite, nacrite and, possibly, anauxite (5).

Examples of trioctahedral 1:1 layer minerals (serpentines) are lizardite, chrysotite, antigorite, amesite, berthierine, baumite, greenalite, caryopilite, cronstedtite, garnierite, kellyite, brindleyite, chamosite and neponite (5, 18).

2.2.4 3 layer minerals

The 2:1 layer minerals are made up of 2 tetrahedral sheets which "sandwich" an octahedral sheet (sect. 2.2.1). The 2:1 layer

minerals are subdivided into groups depending on the layer charge. Smectites have a layer charge of 0.2 - 0.6 per formula unit while vermiculites have a layer charge of 0.6 - 0.9

The distinction between high charge smectites and low charge vermiculites (layer charge ∿0.6 per formula unit) is not precisely defined. Micas and brittle micas have layer charges of ∿1.0 and 2.0, respectively.

2.2.4.1 Talc-pyrophyllite group

Talc has a trioctahedral 2:1 layer structure in which all the tetrahedral cations are Si and all the octahedral sites are occupied by Mg (i.e. structural formula - $Si_4Mg_3O_{10}(OH)_2$). This mineral has no lattice charge. If the Mg is replaced by Fe^{2+} the mineral is termed minnesotaite (17).

Pyrophyllite is a dioctahedral 2:1 layer mineral having the structural formula $Si_4Al_2O_{10}(OH)_2$ and no lattice charge.

2.2.4.2 Smectites

Smectite structures are derived from the, electrically neutral, talc-pyrophyllite structures by various cation substitutions in both the tetrahedral and octahedral positions (18). Substitution of ions of the same valency, in the octahedral positions, (e.g. Fe^{2+} for Mg and Fe^{3+} for Al substitutions) are common. Anion substitutions (e.g. F for OH) are not common in natural smectites. It is possible for

coupled substitutions to occur (e.g. $Fe^{3+}O$ - $Fe^{2+}OH$). Substitutions by cations of lesser charge (e.g. Al^{3+} for Si in tetrahedral positions and Fe^{2+} or Mg^{2+} for Al^{3+} or Fe^{3+} in octahedral sites) result in negative charges on the layers which are balanced by interlayer cations. Na^{+}, Ca^{2+}, H^{+}, Mg^{2+}, Fe^{2+}, Fe^{3+} and Al species are the most common naturally occurring interlayer cations (41), although a whole range of other cations is possible (18).

2.2.4.3 Dioctahedral smectites - montmorillonites

Montmorillonite group minerals have a dioctahedral 2:1 layer (section 2.2.1) with a layer charge, due to various cation substitutions in the lattice. A general formula for dioctahedral smectites is

$$\{(Si_{4-x}Al_x)(R^{3+}_{2-y}\ R_y^{2+})\ O_{10}(OH)_2\}\ (M^{+}_{x+y}nH_2O) \qquad (1)$$

tetrahedral cations; octahedral cations; anions; interlayer cations

dioctahedral 2:1 layer

where R^{3+} = commonly Al^{3+} and Fe^{3+},

R^{2+} = commonly Mc^{2+} and Fe^{2+}, but other ions may occur,

M^{+} = monovalent exchangeable cations (may be substituted by equivalent numbers of multivalent ions), and

nH_2O = hydration and interlayer water

Substitution of different cations into the above structure yields the various minerals of the montmorillonite group, i.e. montmorillonite, nontronite, beidellite and others. The degree of distortion of the 2:1 layer is usually small (56) in smectites although this depends on the degree and type of substitution.

i) Montmorillonite - The name montmorillonite was first suggested (42) for a mineral from Montmorillon, France in 1847. This mineral was later found to be dioctahedral smectite having Mg for Al substitutions (3, 43). The structural formula for the ideal montmorillonite (43) is:

$$\{Si_4(Al_{2-y}\ Mg_y)O_{10}(OH)_2\}^{y-}\ M_y^+.nH_2O$$

ii) Nontronite - The name nontronite was suggested for a material occurring in the Arrondissement of Nontron, near Saint Pardoux, France (44). This mineral was found to be the iron-rich member of the montmorillonite group (45, 46, 47), having the ideal formula (43):

$$\{(Si_{4-x}Al_x)\ Fe_2^{3+}\ O_{10}(OH)_2\}^{+-}\ M_x^+.nH_2O$$

iii) Beidellite - The name beidellite was first used for a clay mineral occurring at Beidell, Colorado, U.S.A. (48). However, many clays identified as beidellite were found to be mixtures of clay minerals (49, 5), usually inter-stratified illite and smectite (5).

Beidellite is now defined (43) as a member of the montmorillonite group having mainly Al^{3+} for Si substitutions in the tetrahedral sheet and the ideal formula:

$$\{(Si_{4-x}Al_x)Al_2O_{10}(OH)_2\}^{x-}M_x^+.nH_2O$$

Some studies of beidellites have shown good 3-dimensional order (50, 51, 52, 53, 54, 55), due to orderly stacking of layers and uniform layer spacings, caused by bonding of exchangeable cations to the isomorphous substitution sites.

The ideal end-member minerals of the montmorillonite group, described above, occur rarely, if ever, in nature. Most montmorillonite minerals have some intermediate composition. For example, Weaver and Pollard (41) calculated the mean structural formula ($\pm$standard deviation) of 101 samples of montmorillonite-beidellite to be

$$\{(Si_{3.837\pm0.127}\ Al_{0.158\pm0.137})(Al_{1.492\pm0.158}Fe^{3+}_{0.187\pm0.132}\ Fe^{2+}_{0.007\pm0.016}\ Mg_{0.354\pm0.153})O_{10}(OH)_2\}^{0.41-}$$

$$Ca^{2+}_{0.007\pm0.050}\ Na^{+}_{0.010\pm0.051}\ K^{+}_{0.004\pm0.022}$$

Grim and Güven (6) analysed 152 samples of bentonite, and found that members of the montmorillonite-

beidellite series were the most common smectites present. They found no beidellite or nontronite end-member minerals, although they found end-member montmorillonite in Mexico, Algeria, Argentina and England (6). They found that smectite in Wyoming, and many other, bentonites was close to the montmorillonite-beidellite boundary (where tetrahedral Al = octahedral divalentions). They also found that the most common interlayer cations were Na and Ca (Mg being present in few samples in large quantities), and that dioctahedral smectites occurred in all but four (from Nevada) of the samples examined.

2.2.4.4 Trioctahedral smectites - saponites

Trioctahedral smectites are much less abundant than the dioctahedral subgroup (41). Examples of trioctahedral smectites are (5):

Hectorite $\{Si_4(Mg_{3-y}Li_y)O_{10}(OH)_2\}^{y-}\ M^{+}_{g}.nH_2O$,

Saponite $\{(Si_{4-x}Al_x)(Mg_{3-y}Al_y)O_{10}(OH)_2\}^{(x+y)-}M^{+}_{x+y}.nH_2O$

and other minerals such as (37) sauconite, volkhonskoite, medmonite, stevensite and lembergite.

2.2.4.5 Vermiculite group

Vermiculites have a 2:1 layer structure with a charge of approximately 0.6 to 0.9 per formula unit (18). Di- and trioctahedral forms of vermiculite are found in clays (5).

2.2.4.6 Mica group

Muscovite has a dioctahedral 2:1 layer structure with the structural formula:

$$\{(Si_3Al)\ Al_2O_{10}(OH)_2\}\ ^-K^+$$

The tetrahedra are distorted into a ditrigonal arrangement such that the K^+ ions are approximately octahedrally co-ordinated by oxygen atoms of the adjacent tetrahedral sheets. This arrangement leads to the 2:1 layers being bonded together in a very regular manner (24, 56, 57, 58).

The illites are clay minerals (i.e. particle size $<\sim 0.2\mu m$) that differ from the well-crystallised micas in that they tend to have less Al for Si substitution (resulting in a lower charge on the lattice), the interlayer K^+ ions may be replaced by Mg^{2+}, Ca^{2+} or H^+ cations and the stacking of the unit layers is less regular (59). Illites are the commonest clay minerals (41), most of them being dioctahedral (68).

Other examples of dioctahedral micas include paragonite, roscoelite, chernykhite, phengite, glauconite and celadonite. Examples of trioctahedral micas include phlogopite, biotite,

lepidolite, zinnwaldite, siderophyllite, annite, ephesite and hendricksite (14).

2.2.4.7 Other 3-layer minerals

The brittle micas are 3-layer silicates having a formula unit charge of approximately 2·0 (18). Examples are clintonite, anandite, margarite and bityite (14).

Sepiolite-palygorskite minerals have a different arrangement of the tetrahedral and octahedral sheets to the other 2:1 minerals, in which there is a periodic inversion of the direction in which the tetrahedral apical oxygens point (5). Examples of such minerals are sepiolite, loughlinite, palygorskite and attapulgite (5, 18).

2.2.5 "4-layer" clays - chlorites

The chlorites have a 2:1:1 structure, which consists of 2:1 layers having interlayer brucite-like sheets of general composition $(Mg{\cdot}Al)_3(OH)_6$ (5, 62). Three categories of chlorites can be described (63):

i) Chlorites having a trioctahedral 2:1 layer and a dioctahedral interlayer sheet (tri, dioctahedral chlorites), no well crystallised examples of this type are yet known (62), or having a dioctahedral 2:1 layer and a trioctahedral interlayer

sheet (di, trioctahedral chlorites), for example the minerals cookeite and sudoite.

ii) Chlorites with two dioctahedral sheets (di, dioctahedral), e.g. donbassite, and

iii) Less well crystallised layer silicates comparable to i) and ii) above but with imcompletely developed interlayer material (62). Similar material (the so-called pillared interlayer clays - PILCs) may be found or prepared with interlayer polynuclear hydroxy metal cations such as aluminium (64, 65, 66, 248, 129, 260) iron (249) or silicon (67, 68) species.

2.2.6 Interstratified clay minerals

Interstratification, interlayering or mixed-layering of clay minerals occurs when 2 or more kinds of layer are stacked in some regular or random sequence (5, 69, 70) along the c axis, i.e. normal to the layers. The interstratified structures are possible because of the similarity in geometry of the basal tetrahedral oxygen surfaces of the individual layers.

Most reports of interstratified clays comprise 2 components (69) although 3 component materials have been reported (69). Most 2 component interstratified clays seem to have layers with the same octahedral classification (69). Interstratified materials are very common (73) and examples are chlorite-montmorillonite (74),

chlorite-beidellite (75) and mica-smectite (76, 77, 78, 79) interstratifications. Interstratified mica-smectite is the major component of "metabentonite" rocks (6).

Mixtures of clay minerals as discrete particles, rather than interstratification, in clays is also possible (5).

2.3 ASSOCIATED MINERALS

2.3.1 Silica minerals

The silica group of minerals have structures which are made up of SiO_4 tetrahedra, linked to each other by the four oxygen atoms. There are several silica minerals including varieties of quartz, tridymite, cristobalite, coesite, chalcedony and opal (17).

2.3.1.1 Quartz

Low, α- or common quartz has a trigonal trapezohedral structure (17, 80), and is a common mineral in all kinds of rocks, including bentonites (5, 6). Quartz is one of the purest minerals known (81) consisting of >99% SiO_2. Trace impurities of quartz include Al, Ti, Fe, Na, Li, K, Mg and Ca occurring interstially or by substitution (81, 82). Quartz normally exists as sand-size grains of rounded or angular morphology (80, 83), but quartz grains <100µm in size are often flat plates due to a cleavage mechanism (54).

At a temperature of 573° (and atmospheric pressure) low quartz inverts to high or β-quartz (17, 85), which has a hexagonal trapezohedral structure (17).

2.3.1.2 Tridymite and Cristobalite

At 870°C high quartz inverts to high tridymite which inverts to high cristobalite at a temperature of 1470°C (15, 17, 80, 85). The high tridymite and high cristobalite structures consist of stacked sheets of 6 SiO_4 tetrahedra rings (86). Vertices of alternate tetrahedra within the rings are inverted forming links, through the oxygen atoms, with adjacent sheets. In high cristobalite the tetrahedra are arranged in a cubic close packing arrangement giving a repeating ABC-ABC regular interstratification of the sheets (80). High tridymite has AB-AB-AB stacking of the sheets in a hexagonal close packing arrangement.

Tridymite and cristobalite are usually less pure than quartz, the major impurity being Al (80, 81). These impurities may stabilize the tridymite and cristobalite structures, allowing them to exist at temperatures below their phase transition temperatures (87, 88, 89). Tridymite and cristobalite usually exist as small (<1mm), often platy, particles (80, 87).

Middle and low forms of tridymite and a low form of cristobalite also exist (81). At a temperature of 1713°C high cristobalite melts giving liquid silica (80).

2.3.1.3 Opals

Opal is often considered to be amorphous (17, 87) although there is evidence that it exists in a variety of forms (16, 81, 90, 91, 92). Jones and Segnit (92) divided the natural opals into 3 groups i.e. Opal A (near amorphous), Opal CT (disordered stacking of cristobalite- and tridymite-like micro-crystallites) and Opal C (mainly well ordered cristobalite).

Opals have the general structural formula $SiO_2 \cdot nH_2O$, the water-content usually being 4 - 9% (81). Opal is 85 - 95% SiO_2 with significant amounts of impurities (80, 81).

The morphology of opal particles varies depending on the mode of origin. Precious opal consists of close packed aggregates of, approximately monodisperse silica spheres 150 to 300 nm in diameter (91) while other opals, or inorganic origin, often consist of disordered aggregates of silica particles, ranging in diameter from 100 to 830 nm (93), in various macroscopic forms (81, 87, 94).

Biogenic opal has the form of the skeletons of the sponges, radiolaria or diatoms etc. from which it originates, unless subsequently fragmented (16, 80, 99).

2.3.1.4 Other silicas

High temperature, high pressure forms of silica (e.g.

coesite, stishovite and keatite (81)) are rarely found associated with clays (15).

2.3.2 Iron oxides

Iron oxides, hydroxides and oxyhydroxides are generally the commonest accessory minerals in clays (15). Goethite (αFeOOH) and lepidocrocite (γ-FeOOH) are relatively common, akaganéite (β-FeOOH) occurs occasionally and feroxyhyte (δ′-FeOOH) has also been reported (15). Poorly crystalline hydrated iron oxide (ferrihydrate or limonite (17)) also occurs naturally (15).

2.3.3 Manganese minerals

Manganese minerals occurring in clays normally consist of a poorly crystalline mixture (wad) of fine grained minerals such as pyrolusite, romanedite and others (87).

2.3.4 Feldspars

Feldspars (or Felspars (17)) occur frequently in clays, normally in the coarse (<1-2μm) fraction (15). The Feldspar minerals are silicates having a 3-dimensional arrangement of the SiO_4 tetrahedra (tectosilicates). They may be divided into two groups of minerals; the alkali-feldspars, having structural formulae ranging from $KAlSi_3O_8$ (sanidine) to $NaAlSi_3O_8$ (albite),

and the plagioclase group minerals, ranging from albite to $CaAl_2Si_2O_8$ (anorthite) (15, 17, 87).

2.3.5 Zeolites

Zeolites are hydrated tektosilicates that often occur with clay (15). The commonest zeolites that occur in clays are heulandite ($(Na_1Ca)_{2-3}Al_3(Al_1Si)_2 \ Si_{13}O_{36}\cdot 12H_2O$), clinoptilolite, analcime ($NaAlSi_2O_6\cdot H_2O$) and phillipsite (15).

2.3.6 Carbonates and sulphates

Carbonate minerals that occur in clays include calcite ($CaCO_3$), aragonite ($CaCO_3$), magnesite ($MgCO_3$), dolomite ($CaMg(CO_3)_2$), ankerite ($(Ca, Fe, Mg)_2 (CO_3)_2$), siderite ($FeCO_3$) and rhodochrosite ($MnCO_3$) (15).

Calcium sulphate occurs in clays as gypsum ($CaSO_4\cdot 2H_2O$), bassamite ($CaSO_4\cdot \frac{1}{2}H_2O$) or anhydrite ($CaSO_4$) (15). Alunite ($KAl_3(SO_4)_2(OH)_6$ (15) and jarosite ($KFe_3(SO_4)_2(OH)_6$ (10) may also occur.

2.3.7 Titanium oxides

TiO_2 occurs frequently (in small amounts) in clays as anatase (15). Rutile occurs occasionally (15).

2.3.8 Allophane and imogolite

Allophane and imogolite are poorly crystalline aluminosilicate clay minerals, having variable composition (15, 36). Imogolite consists of long flexible thread-like particles (19, 36, 95, 96, 98) and allophane seems to consist of very small (3 - 5nm) approximately spherical particles (19, 36, 96, 98).

2.3.9 Other minerals

Other minerals associated with clays include apatites (e.g. fluoroapatite - $Ca_{10}(PO_4)_6F_2$) (15) and sulphide minerals such as pyrite (FeS_2) and marcasite (FeS_2) (10).

CHAPTER THREE

BENTONITE PROPERTIES

B E N T O N I T E P R O P E R T I E S

3.1 MONTMORILLONITE PROPERTIES

As stated previously (sect. 1.1), montmorillonite is usually the major clay mineral component of bentonites. The properties of montmorillonite, especially with respect to its behaviour in dispersion, will now be discussed in more detail. The difference in behaviour of other clay minerals present in bentonite will be discussed later (sect. 3.3).

3.1.1 Particle morphology

Güven and Pease (6, 100) classified the montmorillonite group mineral morphologies into three groups:-

i) Lath-shaped or L-type particles: consisting of genuine laths or laths formed by folding of thin sheets,

ii) Euhedral lamellae or E-type particles: these are lamellae having well developed 3-dimensional crystal structures and having polygonal shapes, usually hexagonally or diamond (rhomb) shaped.

iii) Subhedral lamellae or S- and H-type particles: these particles are lamellae having irregular outlines. S- and H-type particles are classified as those having thicknesses below and above 6 - 7nm respectively.

Montmorillonite aggregates show a wide range of morphologies (6). Some of the aggregates may contain more than one type of mineral (6). Smectite aggregate morphologies may be classified as follows (6):-

i) Globular aggregates (Otay-type): consisting of randomly arranged tiny globules.

ii) Mossy aggregates (Cheto-type): seem to consist of aggregates formed by the curling of very thin ribbons.

iii) Lamellar aggregates: are aggregates of sheet-like (S-, H- or E-type) particles. Three types may be described:-

a) Foliated aggregates: consist of thin folded and crumpled sheets loosely packed together.

b) Compact lamellar aggregates: similar to foliated aggregates but more compact, they may resemble an H-type particle.

c) Reticulated aggregates (Sants Rita-type): are made up of E-type particles forming a reticular (net-like) arrangement.

For the following discussion of montmorillonite properties it will be assumed that montmorillonite exists as thin sheet-like particles. The presence of montmorillonite aggregates or other minerals in a bentonite would be expected to alter the clay properties to some extent (6).

3.1.2 Structural formulae of montmorillonites

As stated previously (sect. 2.2.4.3) there is some variation in the composition of the montmorillonite group minerals, a general structural formula being

$$\{(Si_{4-x}Al)\{(Al^{3+},Fe^{3+})_{2-y}(Mg^{2+},Fe^{2+})_{y}\}O_{10}(OH)_2\}\ \ M^{+}_{x+y} \qquad (2)$$

For the following calculation (in section 3.1) an 'ideal' sodium montmorillonite (19) having the structural formula

$$\{Si_4(Al_{1.67}Mg_{0.33})O_{10}(OH)_2\}^{0.33-}\ Na^{+}_{0.33}$$

will be assumed.

3.1.3 Calculation of unit cell molecular weight

The unit cell formula of the above ideal montmorillonite is,

$$\{Si_8(Al_{3.34}Mg_{0.66})O_{20}(OH)_4\}^{0.66-}\ Na^{+}_{0.66}$$

and has a relative molecular mass (molecular weight) of 734·04.

3.1.4 Calculation of charge deficit per unit cell

The charge deficit per unit cell, for the ideal montmorillonite, is equal to the number of Mg^{2+} for Al^{3+} substitutions in the octahedral

layer or, since there is electroneutrality, the number of equivalents of counter ions. Therefore, the charge deficit is 0·66 per unit cell, for the ideal montmorillonite. (This is equal to a charge deficit of 0·33 per formula unit - i.e. the mineral has a charge corresponding to a smectite group mineral (sect. 2.2.2)).

3.1.5 Calculation of cation exchange capacity

The cation exchange capacity (cec) of the mineral is given by

$$\text{cec} = \frac{\text{charge deficit per unit cell}}{\text{unit cell molecular weight}} \qquad (3)$$

$$= 0{\cdot}66/734{\cdot}04 \qquad \text{eq g}^{-1}$$

$$\text{cec} = 89{\cdot}91 \qquad \text{meq/100g}$$

This cation exchange capacity is that due to the isomorphous substitution in the mineral lattice. There may be some cation exchange capacity (and anion exchange capacity) due to "broken bonds" at the crystallite edges (5, 19, 101, 120).

3.1.6 Calculation of unit cell dimensions

The unit cell dimensions may be calculated using the following formulae (102, 103):

$$b = 0{\cdot}891 + 0{\cdot}006r + 0{\cdot}0034s + 0{\cdot}0048t \quad \text{nm} \qquad (4)$$

where r = number of Al^{3+} in tetrahedral layer,

s = number of Mg^{2+} in octahedral layer and

t = number of Fe^{2+} and Fe^{3+} in octahedral layer of the unit cell.

$$a = b/\sqrt{3} \quad \text{nm} \qquad (5)$$

Hence, for the ideal montmorillonite

$$b = 0{\cdot}893 \quad \text{nm}$$

and $$a = 0{\cdot}516 \quad \text{nm}$$

The unit cell occupies a rectangular area of b x a in each face of the 2:1 layer, the thickness of the unit cell being c (≃0·913 nm with no counter ions (pyrophyllite) (19), varies if counterions and/or water are present (sect. 3.1.11)).

More details on unit cell dimensions and structures are given by Radoslovich et al (57, 56, 58, 24).

3.1.7 Calculation of specific surface area

The face surface area of the unit cell = 2ba

The mass per unit cell = unit cell molecular weight/N_A

Therefore, the specific surface area of the mineral is given by

$$\text{specific surface area} = \frac{2baN_A}{\text{unit cell molecular weight}} \qquad (6)$$

so for the ideal montmorillonite

$$\text{specific surface area} = \frac{2 \times 0{\cdot}893 \times 0{\cdot}516 \times N_A \quad (\text{nm})^2 g^{-1}}{734{\cdot}04}$$

$$= 756 \quad m^2 g^{-1}$$

This is the face surface area of the montmorillonite. The edge surface area of montmorillonite particles is usually small compared to the face area (table 2). For a square montmorillonite particle of side length d and thickness t

$$\text{Face area} = 2d^2 \qquad (7)$$

$$\text{Edge area} = 4dt \qquad (8)$$

$$\text{Face area : edge area} = d/2t \qquad (9)$$

Therefore:

Table 2: Face:edge area ratios for square plates

d/nm	n*	t/nm	Face area:edge area
1·0	1	1	500:1
0·5	1	1	250:1
0·2	1	1	100:1
0·1	1	1	50:1
0·5	2	2·5	100:1
0·2	2	2·5	40:1
0·5	3	4	62·5:1
0·2	3	4	25:1

* - n = number of plates per tactoid, see sections 3.2.2 and 8.2.1

The edge area becones more significant as the montmorillonite plates (or tactoids - sect. 3.2.2) become smaller (in length) and/or thicker (table 2).

3.1.8 Calculation of surface charge density

The surface charge density (σ_0) can be calculated by dividing the cec by the specific surface area. Hence for ideal montmorillonite plates,

$$\sigma_0 = \frac{\text{cec}}{\text{specific surface area}} \qquad (10)$$

$$= \frac{89{\cdot}91\times10^{-5}}{756}$$

$$= 1{\cdot}19\times10^{-6}\ \text{eqm}^{-2}$$

$$= 1{\cdot}19\times10^{-6}\ N_A \qquad \text{charges m}^{-2}$$

$$= 7{\cdot}16\times10^{17} \qquad \text{charges m}^{-2}$$

$$= 7{\cdot}16\times10^{17}e \qquad \text{Cm}^{-2}$$

$$= 0{\cdot}1148 \qquad \text{Cm}^{-2}$$

$$\sigma_0 = 11{\cdot}48 \qquad \mu\text{Ccm}^{-2}$$

---

where e = electron charge = $1{\cdot}6021\times10^{-19}$C.

The surface area per counter ion can be calculated from

$$\text{surface area per cation} = \frac{ve}{\sigma_0} \qquad (11)$$

where v is the cation valency.

Therefore for the ideal montmorillonite plate,

$$\text{the surface area per cation} = \frac{v}{7{\cdot}16\times10^{17}} \quad m^2 ion^{-1}$$

$$= 1{\cdot}39\times10^{-18}v \quad m^2 ion^{-1}$$

$$= 1{\cdot}39v \quad nm^2 ion^{-1}$$

This corresponds to a distance between monovalent charges, if homogenously distributed, of the order of 1·2nm (see also appendix 1).

3.1.9 Surface heterogeneity of montmorillonite

The distribution of charge sites on a montmorillonite surface, due to isomorphous substitutions in the 2:1 layer, may not be homogenous. There is evidence (104, 105, 106, 222, 107) that there may be an uneven charge distribution on the mineral surface, and this may affect some of the montmorillonite properties (104, 105, 106, 107, 108, 109, 110, 260).

3.1.10 Cation exchange reactions

The negative charge on the montmorillonite faces is balanced by exchangeable cations. The ion exchange process has the general characteristics (111) of being reversible, diffusion controlled, stoichiometric and, usually, there is some selectivity for one ion over the other by the surface.

These characteristics are demonstrated by a pure montmorillonite dispersion where (103)

i) The equivalents of counter ions = charge deficit on the crystal structure.

ii) The exchange of one counter ion for another occurs at an observable rate (if the dispersion is rapidly stirred).

iii) One counter ion species can be stoichiometrically exchanged for another.

iv) The montmorillonite usually exhibits ion exchange selectivity.

Ion exchange selectivity may be predicted by Coulomb's Law (112) i.e. For ions of equal valency the ion having the smaller "effective" radius will be preferentially adsorbed onto the surface. It has been shown (112, 113, 114, 101, 115) that ions having the smaller hydrated size (or larger crystalline size) are preferred by clay surfaces. This is shown by the lyotropic series of monovalent cation preference by clays (5, 101, 103, 116) which takes the form, (hydrated ionic radii/nm in brackets (103)):-

$$Cs^{+}(0{\cdot}329) > K^{+}(0{\cdot}331) > Na^{+}(0{\cdot}358) > Li^{+}(0{\cdot}382)$$

Multivalent ion selectivities may be predicted by electric double layer theory (116, 117, 118). Multivalent ions are normally adsorbed in preference to monovalent cation (5, 101, 103, 116), normally adsorbing more strongly as the valency is increased (5).

Exceptions to this behaviour are K^{+} ions "fixed" on mica surfaces (103), which are only exchanged for other cations very

slowly, and H^+ ions, which tend to attack the crystal lattice ("hydrolysis") releasing polyvalent cations (e.g. Mg^{2+}, Al^{3+}) which are then adsorbed on the mineral surface (119, 271, 272, 273, 19).

Na^+, Ca^{2+}, Mg^{2+}, K^+ and H^+ are the most common exchangeable cations found in natural montmorillonites (41). The exchangeable cation composition of a natural montmorillonite may develop during the formation of the bentonite (121) or during later cation exchange processes (6). The exchange of ions on montmorillonite surfaces may be affected by factors such as the degree of compaction of the clay (122, 123), the ions involved in the exchange process (5, 124), the concentration of ions in solution (16, 125), temperature (126, 127) and the nature of the adsorption site (101, 128).

It is possible to prepare homoionic samples of montmorillonite having various exchangeable cations, such as simple inorganic cations (e.g. Li^+, Na^+, K^+, Cs^+, Mg^{2+}, Ca^{2+}), more complex inorganic species and organic cationic species (5, 6, 130). The type of interlayer cation affects the montmorillonite properties (5, 19)(sections 3.1.11 and 3.2).

3.1.11 Swelling of montmorillonite

The swelling of clays by water and other solvents is a very important property that can be of great commercial (5, 6, 19) or economic (131) importance.

The swelling of montmorillonite proceeds by two difference mechanisms:-

i) hydration, interlamellar or type 1 swelling (sect. 3.1.11.1)

and ii) osmotic or type 2 swelling (sect. 3.1.11.2).

The transition between the two types of swelling is quite sharp.

3.1.11.1 Hydration swelling

The first stage in the swelling process of a (dry) clay by water (hydration swelling) has been shown to proceed by a stepwise process (119, 132, 133, 134, 135) as water molecules are adsorbed between the sheets in 1, 2, 3 and 4 layers. The swelling behaviour is dependent on the exchangeable cation type and the type of clay mineral (132, 135). It is possible to get interstratification between two different hydration states (130).

Different cations give different swelling behaviour. Li saponite gives 5 hydration steps (132) with much interstratification between the hydration states. Na and K smectites swell in 4 hydration steps (130), although the basal spacing (d(001)) may change in a different manner upon swelling for different minerals, e.g. Na montmorillonite has more extensive interstratification between hydration states than Na beidellite (132, 135). In Ca and Mg smectites the 2 layer hydrate predominates over a wide range of relative humidities (130, 135, 136, 250).

The interlayer water has an ice-like structure (137)

where the water molecules are linked in a disordered hexagonal arrangement, to the tetrahedral sheet surfaces by hydrogen bonds (40, 138, 139, 140, 141, 143) the exchangeable cations being arranged in an ordered manner between the 2:1 layers. The exchangeable cations of tetrahedrally substituted minerals (e.g. beidellite) tend to be associated with the sites of substitution (132, 140) forming weak "chains" which hold the adjacent tetrahedral sheets in a fixed relative position (132). This link is not found between octahedral isomorphous substitution sites and interlayer cations (130) since the surface negative charge is more diffuse(130). The stronger bonds between the exchangeable cations and the surface of beidellite as compared to montmorillonite may help to explain the results of compression studies (144, 145, 146).

Interlamellar swelling of clays may also occur by incorporation (intercalation) of organic molecules (e.g. glycerol, ethylene glycol, urea) between the layers (130). Glycerol or ethylene glycol-clay complexes are frequently used for X-ray diffraction identification of smectites since they swell the minerals to uniform layer spacings of 1•77nm (17•7Å) (147) and 1•69 - 1•71nm (16•9 - 17•1Å) (148) respectively, independent of cation saturations.

3.1.11.2 Osmotic swelling

Smectites and vermiculites saturated with certain

cations are capable of swelling to much larger separations than those normally observed with interlamellar complexes (119). This can result in the formation of a stable colloidal dispersion of clay particles having fully developed electric double layers (sect. 3.1.12). This type of swelling, osmotic or type 2 swelling (149), differs from hydration swelling in the larger spacings observed and in the nature of the forces between the layers. These forces are, mainly, electric double layer and van der Waals' forces, as described by colloid stability theory (sect. 3.1.13). The distance between the layers is a distribution over a fairly large range of distances and depends on factors such as clay volume fraction, particle size and shape distributions, electrolyte concentration and type, temperature and sample history.

Na and Li montmorillonite layers dissociate almost completely as the water content is increased (119, 150). Initially the separation increases in steps corresponding to various organised water structures (hydration swelling - sect. 3.1.11.1) until 2nm is reached and then jumps to ∿4nm after which it increases steadily. The system has a broad distribution of separations although the layers tend to remain parallel even in the most highly swollen dispersions (151).

Osmotic swelling is dependent on surface charge localization. Complete dissociation of the layers may or

may not occur with a Na beidellite (132); however, unlimited swelling occurs with a Li beidellite (130).

With divalent cations (e.g. Ca^{2+}, Mg^{2+}) unlimited osmotic swelling is not observed (130). K montmorillonite may disperse but if an expanded Na montmorillonite is treated with dilute K^{+} solution it does not contract, but if treated with Ca^{2+} solution it does (130). If an expanded Na-smectite is treated with H^{+} solution (acid) it initally remains expanded and then, after a few days, contracts. This is due to release of polyvalent octahedral cations (e.g. Mg^{2+}, Al^{3+}), by attack of the clay mineral structure (hydrolysis), which then occupy the exchange sites (119). This process may even occur in dispersions at low ionic strength ($<10^{-3}moldm^{-3}$) and neutral pH (152) and may depend on cation type, Na, K and Cs montmorillonites being hydrolysed more than Li, NH_4, Mg and Ca montmorillonites (152).

The swelling of 2:1 layer clays is also dependent on surface charge density with low (pyrophyllite) and high charge (vermiculite) minerals swelling less than intermediately-charged minerals (smectites).

Montmorillonite particles in samples that do not disperse completely remain as associated units termed tactoids (sect. 3.3.3).

3.1.11.3 Dehydration

All montmorillonites lose interlayer water in the temperature range 100 - 200°C giving a "collapsed" structure (130) which normally has an interlayer spacing of <1nm (10Å), although this is dependent on the interlayer cation (153) or the presence of any other interlayer material (sect. 2.2.5) (130, 64, 155, 10).

The rehydration behaviour is dependent on cation and mineral type (130). Rehydration of Li montmorillonite is insignificant after heatint above 250°C (154) probably because the Li^+ ions diffuse into the vacant sites in the (di) octahedral sheet where they neutralize the layer charge (127). This reaction may be used to distinguish montmorillonite and beidellite (sect. 6.1.3).

3.1.12 Electric double layer theory

In clay-water dispersions the counter-ions (those ions having opposite charge to the mineral surface) tend to diffuse into the bulk aqueous phase because of their thermal motion until balanced by the electrostatic attraction of the mineral surface. This results in a region, adjacent to the surface, where there is a redistribution of the ions in solution, termed the electric double layer.

The electric double layer may be regarded as consiting of two regions: an inner region, which may contain adsorbed ions, and a

diffuse outer layer which is the region of redistribution of ions in the solution phase. The Stern model (156) of the electric double layer regards these two regions as being separated by the Stern plane, which is located at a distance δ (approximately one hydrated counter-ion radius) from the surface and has an electrical potential (the Stern potential) ψ_δ.

3.1.12.1 Gouy-Chapman theory

The diffuse part of the electric double layer may be described by the Gouy (157)-Chapman (158) theory. The potential ψ_x at a distance x from the Stern plane can be given by (159)

$$\psi_x = \frac{2kt}{ve} \ln \left[\frac{1 + \gamma \exp(-\kappa x)}{1 - \gamma \exp(-\kappa x)} \right] \qquad (12)$$

$$\text{where } \gamma = \frac{\exp(z) - 1}{\exp(z) + 1}, \qquad (13)$$

$$\text{with } z = \frac{ve\psi_\delta}{2kT}, \qquad (14)$$

$$\text{and } \kappa = \left[\frac{2e^2 N_A c_e v^2}{\varepsilon kT} \right]^{\frac{1}{2}}, \qquad (15)$$

In equation 15 the various quantities are defined as follows:-

k = Boltzmann's constant = $1{\cdot}38054 \times 10^{-23} JK^{-1}$,

T = temperature /K,

v = valency of counter-ion

c_e = electrolyte concentration/$moldm^{-3}$ and

ε = permittivity of the medium, where

$\varepsilon = \varepsilon_0 \varepsilon_r$, with

ε_0 = permittivity of a vacuum = $8{\cdot}8542 \times 10^{-12} Fm^{-2}$

ε_r = the relative permittivity of the medium

If ψ_δ is low the Debye-Hückel approximation can be made and equation 12 simplifies to

$$\psi_x = \psi_\delta \exp(-\kappa x) \qquad (16)$$

The charge density in the Gouy layer σ_2 may be given by (159),

$$\sigma_2 = (8N_A c_e \varepsilon kT)^{\frac{1}{2}} \sinh z, \qquad (17)$$

which at low ψ_δ reduces to

$$\delta_2 = \varepsilon \kappa \psi_\delta \qquad (18)$$

3.1.12.2 Stern theory

Stern theory (156) may be used to describe the inner

part of the electric double layer. The surface charge density of the Stern layer (σ_1) is given by,

$$\sigma_1 = \frac{N_1 ve}{1 + \frac{\rho_w}{c_e M_w} \exp\left[-2z - \frac{\Phi}{kT}\right]} \tag{19}$$

where N_1 = surface density of adsorption sites, i.e. number per unit area,

ρ_w = density of solvent,

M_w = molecular weight of solvent and

Φ = specific adsorption potential

The surface charge density σ_o is given by

$$\sigma_o = \frac{\varepsilon'}{\delta} (\psi_o - \psi_\delta) \tag{20}$$

where ε' = permittivity of Stern layer and

ψ_o = the surface potential

For overall electrical neutrality it follows that,

$$|\sigma_o| = |\sigma_1| + |\sigma_2| \tag{21}$$

A schematic diagram of the electric double layer is shown in fig. 6. This shows ψ decreasing linearly from the surface potential ψ_o to ψ_δ at the Stern plane and then decreasing exponentially to zero, as suggested by eq. 16. The distance $1/\kappa$ is regarded as the double layer "thickness".

Fig. 6: Schematic diagram of the electric double layer.

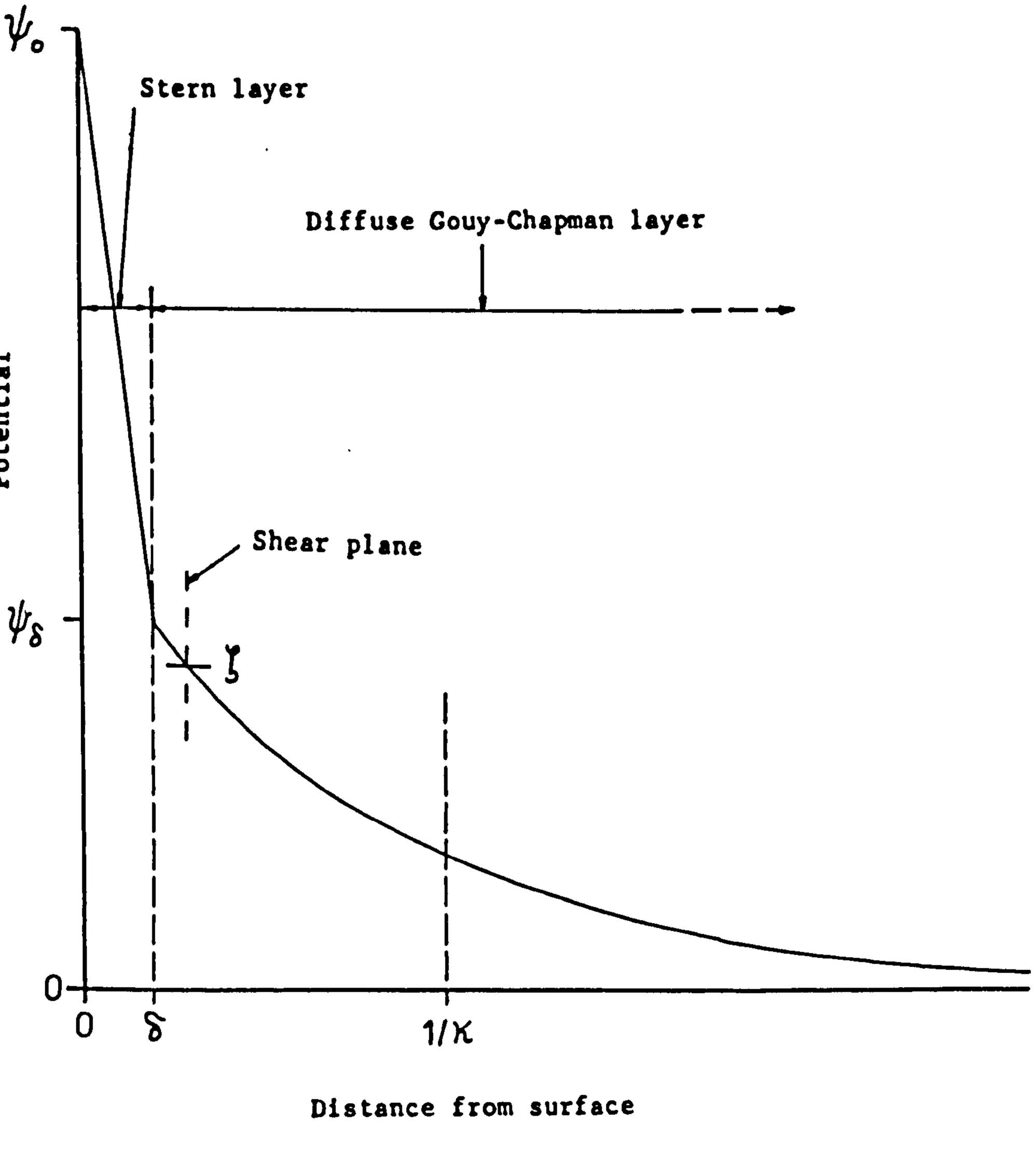

The electrokinetic or ζ potential, which may be measured experimentally occurs at the (ill-defined) plane of shear, a small distance further out from the surface than δ. The difference between ψ_δ and ζ depends on the distance between the shear and Stern planes as well as the magnitude of ψ_δ (i.e. as $\psi_\delta \to 0$ so $\psi_\delta \to \zeta$).

3.1.12.3 Calculation of Stern potentials of montmorillonite

The Stern potential of the "ideal" montmorillonite (sect. 3.1.2) may be calculated from equations 20, 21, 17 and 19.

If the relative permittivity of the Stern layer is assumed to be 6 (103, 160), δ is assumed to be 5×10^{-10}m (103, 160) and the value of δ_o calculated in section 3.1.8 is used then, from equation 20

$$(\psi_o - \psi_\delta) = \frac{0{\cdot}1148\times5\times10^{-10}}{6\times8{\cdot}8542\times10^{-12}} \quad V$$

$$\psi_o - \psi_\delta = 1{\cdot}080 \ V$$

$$\therefore \text{ potential gradient in Stern layer} = \frac{1{\cdot}080}{5\times10^{-10}} = 2{\cdot}16\times10^{6} Vmm^{-1}$$

and, from equation 21

$$\sigma_1 + \sigma_2 = 0{\cdot}1148 \quad Cm^{-2}$$

It is now possible to substitute for σ_1 and σ_2 in equation 17 and 19 and to solve for ψ_δ (103) i.e.

$$\text{Assuming } 1 \ll \frac{\rho_w}{c_e M_w} \cdot \exp\left[-\left(\frac{(2z+\frac{\Phi}{kT})}{}\right)\right]$$

then from equation 19 we obtain (160),

$$\sigma_1 = \frac{N_1 v e c_e M_w}{\rho_w} \exp\left[2z+\frac{\Phi}{kT}\right] \tag{22}$$

and from equation 21

$$\sigma_o = \frac{N_1 v e c_e M_w}{\rho_w} \exp\left[2z+\frac{\Phi}{kT}\right] + (8N_A c_e \varepsilon kT)^{\frac{1}{2}} \sinh z \tag{23}$$

$$\therefore z = \frac{1}{2} \ln\left[\frac{(\rho_w(\sigma_o-(8N_A c_e \varepsilon kT)^{\frac{1}{2}} \sinh z))}{N_1 v e c_e M_w}\right] - \frac{\Phi}{kT} \tag{24}$$

Equation 24 is now solved for z by iteration (program 1, appendix 2) and ψ_δ found from equation 14.

For $\rho_w = 1000 \quad gdm^{-3}$,

$N_1 = 10^{19}$ sites m^{-2} (103),

$Mw = 18{\cdot}0154 \quad g\ mol^{-1}$,

$T = 298$ K,

$v = 1$ and

$\varepsilon_r = 78{\cdot}5$

ψ_δ may be calculated for a range of Φ and c_e values, using the values of Φ obtained by Middleton (145), see table 3.

Table 3: Calculated values of ψ_δ

cation	Φ/kT	c_e/moldm^{-3}	ψ_δ/mV (calculated)	ψ_δ/mV (experimental) (145)	(161)
-	1	10^{-3}	187	-	-
-	2	10^{-3}	161	-	-
(ref.103)	4	10^{-3}	110	-	-
Li^+	4.92	10^{-4}	146	145	90
		10^{-3}	87	117	
		10^{-2}	27	101	
Na^+	5.77	10^{-4}	124	123	69
		10^{-3}	65	91	
		10^{-2}	6	-	
K^+	7.43	10^{-4}	81	81	44
		10^{-3}	22	70	
		10^{-2}	0	52	
Cs^+	9.99	10^{-4}	15	16	12
		10^{-3}	0	19	

It can be seen from the calculated values of ψ_δ that ψ_δ decreases as c_e increases or the counter ions are adsorbed more strongly (Φ increases). These trends seem to be confirmed by experimental result (145, 161).

Novich and Ring (162) have calculated ψ_δ for montmorillonite in 0·29 mol dm^{-3} KCl to be 21·2mV, although their use of the Reerink and Overbeek theory (163) may be invalid (164).

3.1.12.4 Calculation of surface potential of montmorillonite

Knowing ψ_δ and $(\psi_o-\psi_\delta)$, ψ_o may be calculated, i.e.

$$\psi_o = (\psi_o-\psi_\delta)+\psi_\delta$$

$\therefore$ If ψ_δ = 0 110·V then

$$\psi_o = 1{\cdot}080 + 0{\cdot}110 \quad V$$

$$= 1{\cdot}19 \quad V$$

3.1.12.5 Calculation of Stern and Gouy layer charge densities

Knowing ψ_δ it is possible to solve equations 19 and 17 for σ_1 and σ_2 respectively, i.e. if ψ_δ = 0·110V, c_e = 10^{-3}mol dm^{-3} and ϕ = 4kT then

$$\sigma_1 = \frac{10^{19} \times 1 \times 1{\cdot}6021 \times 10^{-19}}{1 + \frac{1000}{10^{-3} \times 18{\cdot}0154}\ \{-(2 \times 2{\cdot}142 + 4)\}}$$

$$= 0{\cdot}1067\ Cm^{-2}$$

and

$$\sigma_2 = (8 \times 6{\cdot}0225 \times 10^{23} \times 10^{-3} \times 10^{3} \times 78{\cdot}5 \times 8{\cdot}8542 \times 10^{-12} \times 1{\cdot}38054 \times 10^{-23} \times 298)^{\frac{1}{2}} \sinh 2{\cdot}142$$

$$= 0{\cdot}0156\ Cm^{-2}$$

and hence,

$$\sigma_1/\sigma_2 = 6{\cdot}843$$

3.1.13 Colloid Stability theory (DLVO theory)

There are three major types of interaction involved in the stability of colloidal dispersions. These are:

i) London-van der Waals forces of attraction (165

ii) Coulombic forces between charged particles, and

iii) solvation effects.

The Derjaguin-Landau (166) and Verwey-Overbeek (160) (D.L.V.O.) theory of the stability of lyophobic dispersions considers that the effects of (i) and (ii) are additive and any solvation effects are ignored.

If the potential energies of repulsion and attraction

between two, similarly charged, colloidal particles are V_R and V_A respectively, then (according to the D.L.V.O. theory) the potential energy of interaction V_T is given by

$$V_T = V_R = V_A \tag{25}$$

3.1.13.1 Potential energy of repulsion

The D.L.V.O. theory considers that V_R is due to the overlap of the electric double layers, surrounding the particles, only. It is possible to calculate the repulsive force between two charged spheres (160, 167, 168), flat plates (160, 169) or other shaped particles (170, 171). The treatment for flat plates is most applicable to ordered montmorillonite dispersions and this will be the only treatment discussed here.

Various methods of calculation of the force between two parallel charged flat plates have been published (160, 167, 169). Langmuir (169) calculated the repulsive pressure, P_R (force per unit area), to be given by

$$P_R = 2c_e N_A kT \, (\cosh u - 1) \tag{26}$$

where u may be calculated for constant charge or constant potential conditions and is given by

$$u = \frac{ve\psi_d}{kT} \tag{27}$$

ψ_d is the mid-plate potential. For weak interaction it may be assumed that the electric double layers are unperturbed and u is given by the approximation,

$$u = 8 \gamma \exp \{- \kappa H_0/2\} \qquad (28)$$

where γ and κ are given by equations 13 and 15 respectively, and H_δ is the distance between the plates. This result was also calculated by Derjaguin et al (167).

Verwey and Overbeek (160) also found that,

$$V_R = \left[\frac{64\ c_e N_A kT}{\kappa} \right] \gamma^2 \exp (-\kappa Ho) \qquad (29)$$

The D.L.V.O. theory ignores the very short range Born repulsions due to orbital overlap and any possible "hydration" forces due to "structuring" of water adjacent to the montmorillonite surfaces (172, 173, 174, 175, 176, 177, 178).

3.1.13.2 Potential energy of attraction

The main source of the attraction between colloidal particles are the London-van der Waals dispersion forces, (179, 180, 181, 182). Assuming only London forces are important, then the energy of attraction, V_A is given by (160, 182)

$$V_A = - \frac{A}{12\pi} \left[\frac{1}{Ho^2} + \frac{1}{(Ho+2t)^2} - \frac{2}{(Ho+t)^2} \right] \qquad (30)$$

where A is the Hamaker constant (183) for the system, and t is the plate thickness.

In the following calculations a value for A of $2{\cdot}2 \times 10^{-20}$J is used (175).

The DLVO theory ignores the contribution of the Debye- and Keesom-van der Waals forces to V_A. Also the retardation effect (184, 185), which is a "weakening" of V_A at separations $\gtrsim$ 10nm, is ignored.

Hunter (339) has given a modification to equation 30 to allow for the retardation effect. This effect becomes more important as Ho or t is increased (339).

3.1.13.3 Potential energy diagrams

The total potential energy of interaction, between two colloidal particles, is given by

$$V_T = V_R + V_A \qquad (25)$$

The shape of the potential energy-distance curve depends on the properties and magnitudes of the two forces.

Potential energy diagrams may be calculated from equations 29, 30 and 25, assuming $A = 2{\cdot}2 \times 10^{-20}$J (175) and other constants have values as given in section 3.1.12. An example of a potential energy diagram is shown in fig. 7. At small particle separations V_A will predominate resulting in the deep primary minimum of the potential energy curve. A repulsive energy barrier (the primary maximum) may occur

Fig. 7: Potential energy diagram

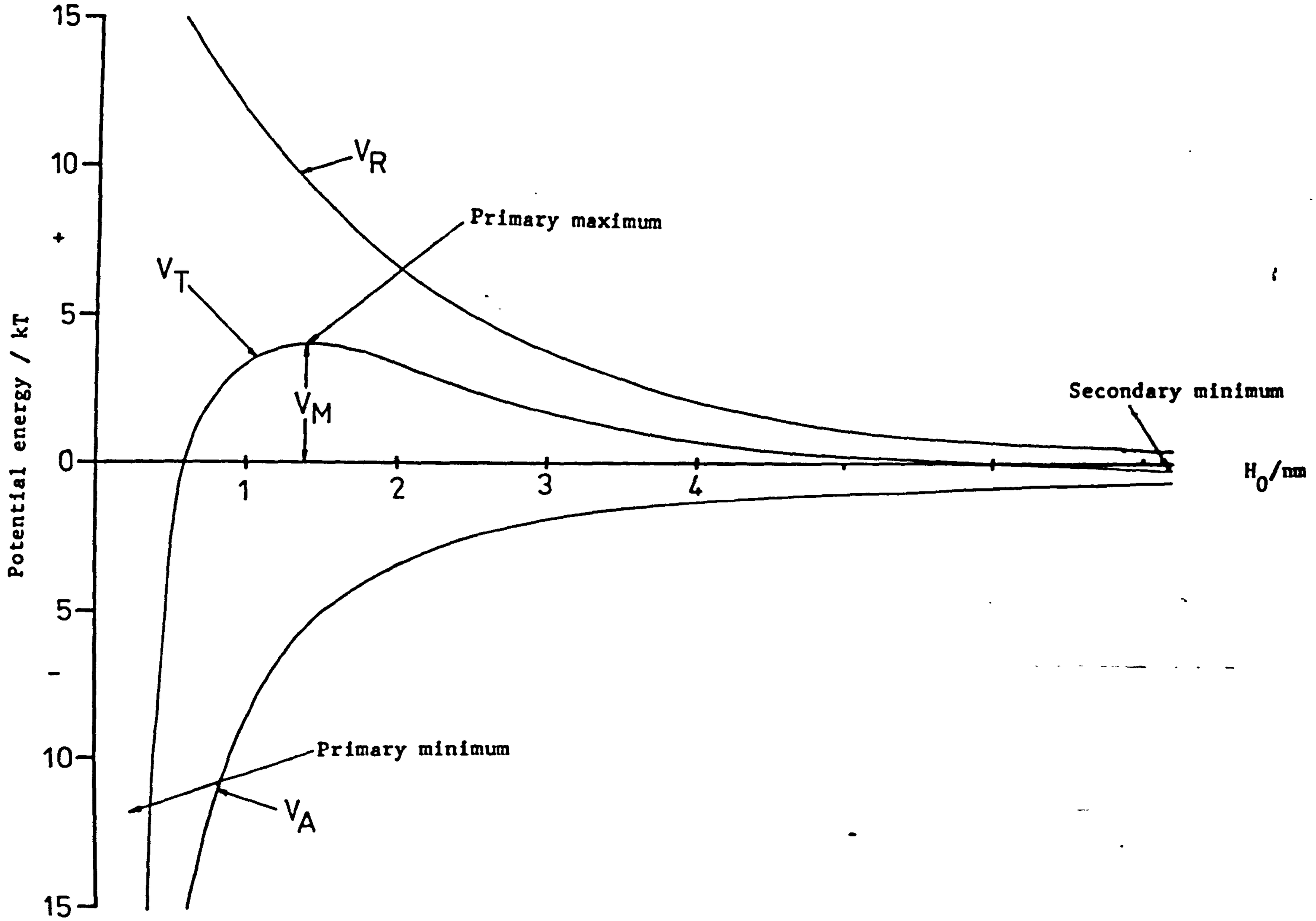

in the potential energy curve which if large compared with the thermal energy of the particles, will render the system "stable" (kinetically inert) with respect to coagulation (aggregation in the primary minimum). At larger values of H_o a secondary minimum may occur which, if it is deep enough, will cause flocculation (aggregation in the secondary minimum) of the particles.

The general shape of these potential energy diagrams, as predicted by the D.L.V.O. theory, have been confirmed by measurement of the forces between macroscopic bodies (186, 187, 176, 177, 178, 146), experimental studies of thin soap films (189, 190) and compression studies of montmorillonite dispersions (146, 172, 145, 144, 191).

3.2 PROPERTIES OF MONTMORILLONITE DISPERSIONS

The properties of montmorillonite dispersions may be dependent upon factors such as montmorillonite volume fraction, particle size and shape, electrolyte concentration, counter ion valency and type, pH and dispersion history (7, 19, 145, 146, 162, 169, 193, 194, 195, 196, 197, 198, 199).

Potential energy diagrams may be used to help explain the properties of dilute colloidal dispersions.

An example of a dilute dispersion (i.e. a dispersion in which there is little interparticle interaction (200)) of montmorillonite would be <1% w/w Li or Na montmorillonite in 10^{-3} mol dm^{-3} electrolyte (151, 169, 194). This is a stable colloidal system consisting of a random arrangement of clay particles in random thermal (Brownian)

motion (151, 169) that shows Newtonian rheological behaviour (194). A potential energy diagram calculated for this system is shown in fig. 8. This shows the large repulsive energy barrier (∿800kT (d = 0•1μm)(sect. 8.7.2)) that renders the system "stable" (kinetically inert) to coagulation into the primary minimum, and that the range of the repulsive potential (∿100nm) is significally smaller than the mean interparticle separation (∿250nm for 1% dispersion (151) (sect. 10.2.1).

3.2.1 Flocculation

If the electrolyte concentration (or counter-ion valency) of the above system is increased, flocculation may occur (19, 195, 201, 163). This is because the range of the double layer repulsive forces will be reduced and the depth of the secondary minimum may become large enough to prevent redispersion of the particles by thermal energy. The effect of increasing the electrolyte concentration upon the potential energy diagram is shown in fig. 9. At electrolyte concentrations of ∿0•1 mol dm^{-3} the depth of the secondary minimum is sufficient to cause weak flocculation. At high electrolyte concentrations ($>^{\sim}$ 1 mol dm^{-3}) strong aggregation may occur in the secondary minimum, although under these conditions the primary minimum occurs at such short range (<1nm) that it is likely to be overcome by the short range Born and, possibly, hydration repulsion i.e. the behaviour of the system is similar to coagulation (into the >∿3nm minimum).

Fig. 8 : Potential energy diagram for parallel flat plates

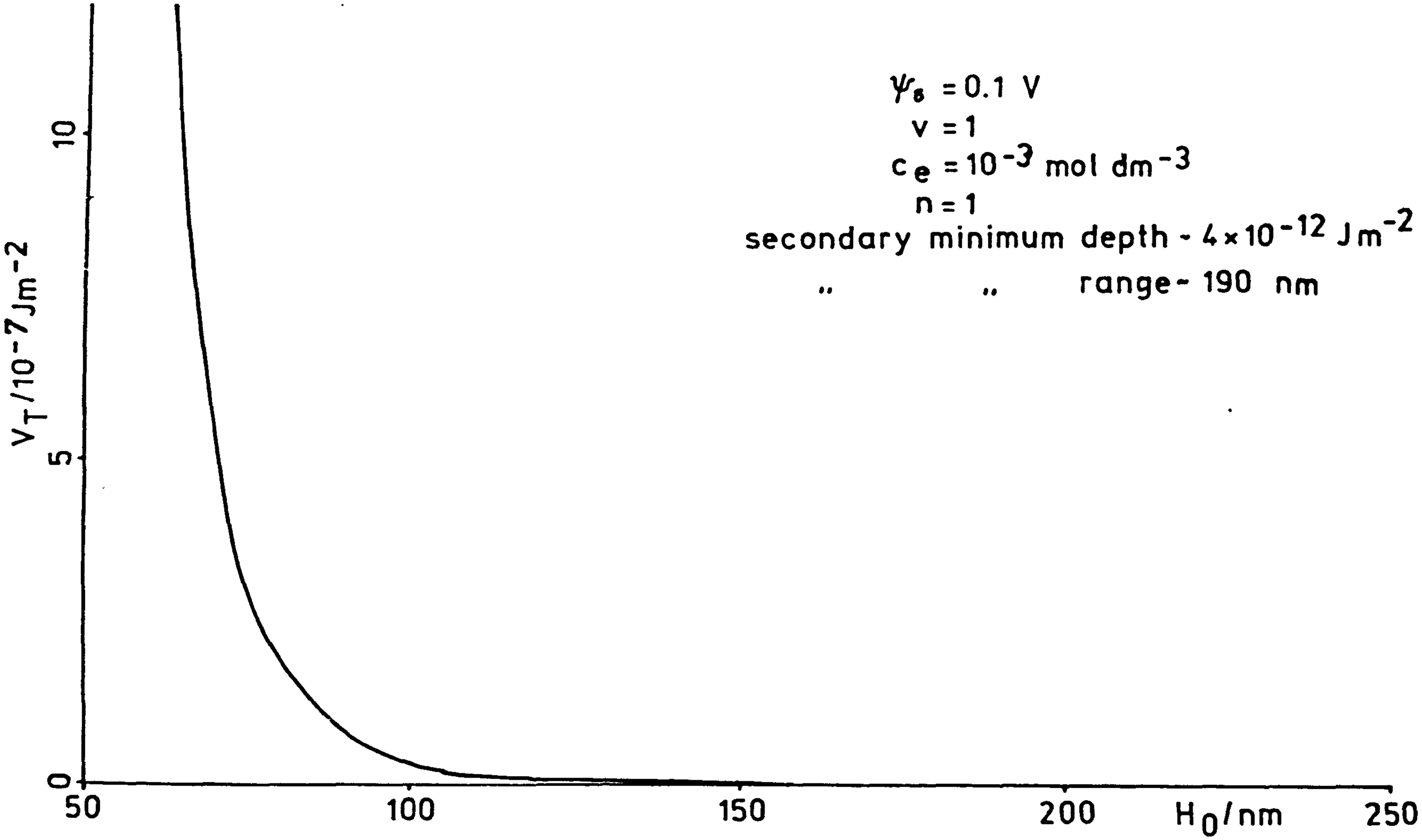

Fig. 9 : Potential energy diagrams for parallel flat plates

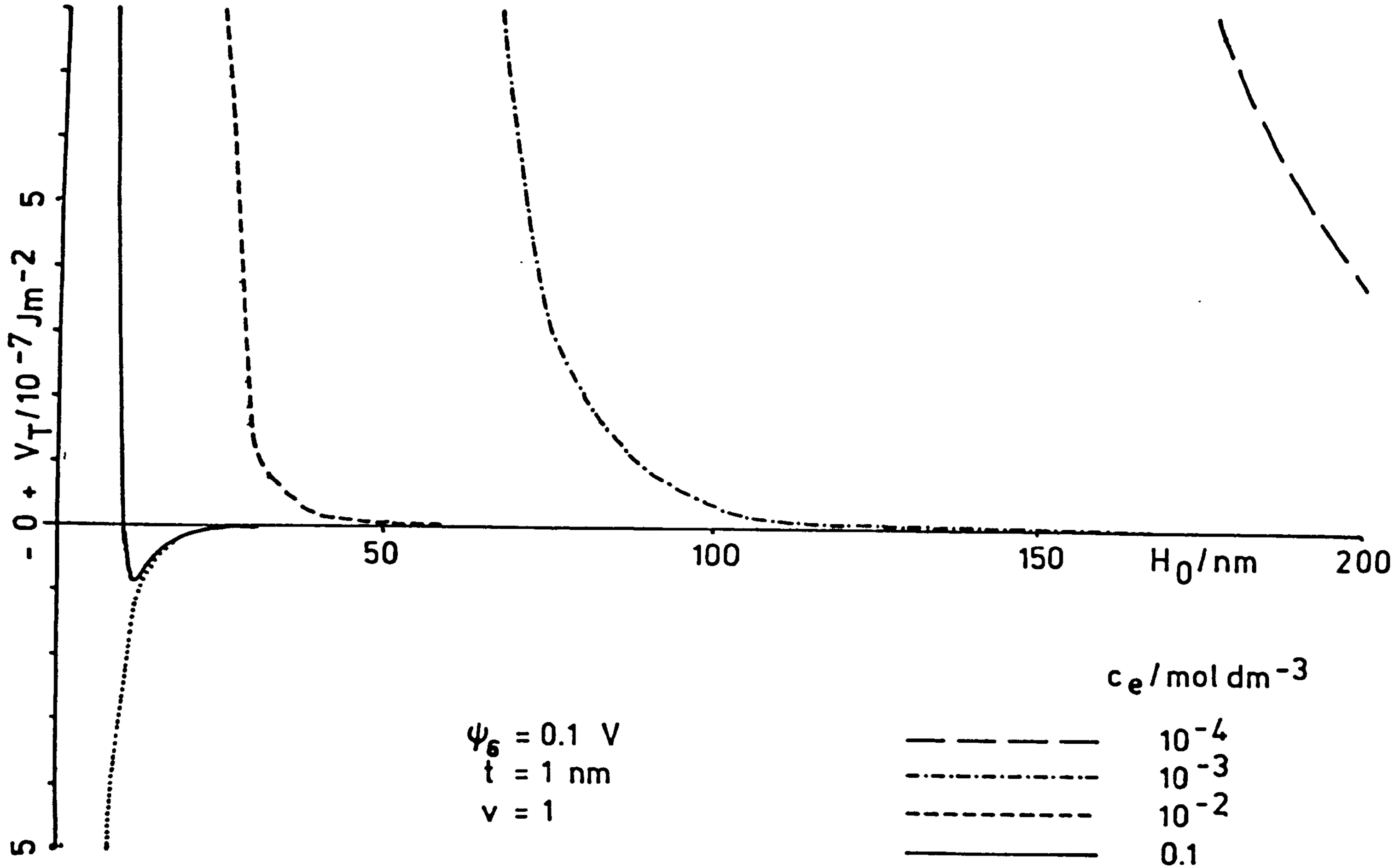

3.2.2 Tactoid formation

Under appropriate conditions montmorillonite particles in dispersion may associate with each other in a face-face arrangement, these stacks of particles have been referred to as tactoids (19, 169, 197, 199, 202, 203, 204). In this work the term tactoid will be used for stacks of parallel montmorillonite particles equally spaced at separations of ~1nm (197, 203, 204). The parallel orientation of clay particles, or tactoids, at separations much larger than 1nm (19, 169, 199, 194, 151, 193) will be discussed later (sections 3.2.3 and 3.2.4.1).

The formation and properties of tactoids of montmorillonite are dependent on counter ion type and valency (202, 197, 203, 205, 206, 207), the surface charge density of the clay mineral (204, 145, 195, 146), shear forces due to thermal motion or hydrodynamic flow (204, 195) or electrolyte concentration (195, 204).

The short range interactions that seem to cause the formation of tactoids are not accounted for by DLVO theory. This is also indicated by the small effect of changing ψ_δ, at $c_e = 10^{-3}$ mol dm^{-3}, on the potential energy diagram, as shown in fig. 10. The formation of tactoids cannot be explained by flocculation (19) or entropy (208) considerations, although these may be important for longer range ordering (sect. 3.2.3).

Tactoids may be considered to form as stacks of montmorillonite particles such that the face size of the tactoids are similar to those of the individual particles, the main difference being the increased thickness of the tactoid (195). It is also possible for tactoids to

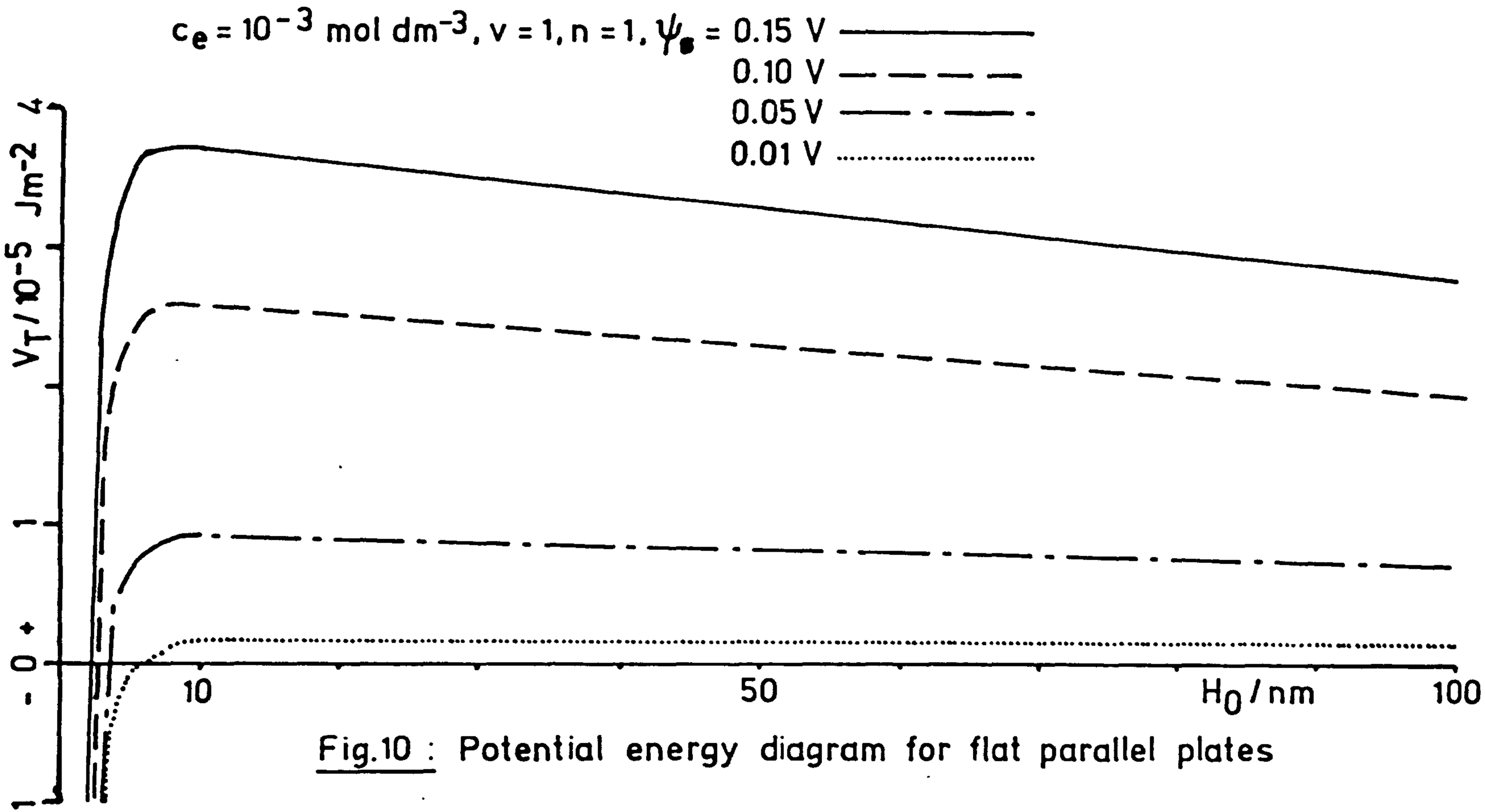

Fig.10 : Potential energy diagram for flat parallel plates

form (probably under conditions of low shear) such that the individual montmorillonite layers overlap each other forming extended ribbons or lamellae whose face areas are considerably larger than those of the individual particles (195, 199, 209, 210, 211).

Neutron diffraction (151, 203, 212), electron microscopy (145) and compression studies (145, 146) suggest that Li montmorillonite disperses as single layers (i.e. number of plates per tactoid, n = 1). As the counter ion hydrated radius decreases, or valency increases, the resultant tactoid size increases (table 4) (197).

The cause of the formation of tactoids is still not clear, but its strong dependence upon cation type (table 4) suggests that it may be due to changes in the affinity of the cations for the clay surface (145, 146) and consequent changes in the short range hydration and electrostatic interactions (204).

Table 4. Number of layers per montmorillonite tactoid (197)

Counter ion	n
Li^+	1·0 (assumed)
Na^+	1·0 - 1·7
NH_4^+	1·7 - 2·0
K^+	1·4 - 2·7
Rb^+	1·5 - 2·6
Cs^+	1·7 - 4·6
Mg^{2+}	2·9 - 9·6
Ca^{2+}	2·7 - 10·9
Ba^{2+}	6·3 - 11·2

3.2.3 Ordering of montmorillonite dispersions

Montmorillonite particles or tactoids may be face-face ordered at larger particle separation than those involved in tactoid formation (19, 169, 151, 194, 199, 193). This ordering may occur naturally (sects. 3.2.3.1 and 3.2.3.2) or by application of external forces (sect. 8.7.1) by shear (sect. 3.2.5), compression (sect. 3.2.4.1), electrical fields (sect. 7.2.6) or other procedures (251). Some of this behaviour may be explained by DLVO theory.

3.2.3.1 Phase separation

Under appropriate conditions, montmorillonite dispersions may separate into 2 phases (169, 151). Such phase separation has also been shown to occur with other colloidal systems (169, 213, 214, 215, 216, 217). As the particle concentration in a montmorillonite dispersion is increased, a point is reached (at ~2% w/w Li or Na montmorillonite (151, 169)) where phase separation occurs. The transition from the disordered (isotropic) state to a more ordered state is known as the Onsager transition (208).

Onsager (208) has used a statistical mechanical approach to explain the phase separation of highly anisotropic particles. A qualitative explanation for the phase transition in a system in which the interactions are all repulsive (as in Li montmorillonite in 10^{-3} mol dm^{-3} LiCl,

say) may be given (193). If the particle concentration of a dilute dispersion (say <1% w/w Li montmorillonite in 10^{-3} mol dm^{-3} LiCl) of montmorillonite is increased, a point will be reached where the montmorillonite layers will experience a loss in entropy since they are no longer free to rotate without interacting with adjacent particles. If some of the layers become arranged in a parallel face-face arrangement, they are more efficiently packed than particles having a random orientation. Therefore the ordered layers will form a denser phase than the disordered layers. The remaining, disordered, layers will now have a greater freedom to rotate, and hence they will gain in entropy. At some point the gain in entropy of the disordered phase will "outweigh" the loss of entropy in the ordered phase, and the system will spontaneously separate into two phases. The Onsager theory for a hard disc fluid (208, 193) is given below.

The number of discs $\rho(\Omega)$ per unit volume having orientation, between the normal to the disc and the preferred axis, between the solid angle Ω to $\Omega+d\Omega$, is given by

$$\rho(\Omega) = \rho_o f(\Omega) d\Omega \qquad (31)$$

where $f(\Omega)$ is the probability distribution function and ρ_o is the total particle number density.

$$\text{(For random orientation } F(\Omega) = 1/4\pi) \qquad (32)$$

The free energy F of a fluid of hard discs is given by (208)

$$\frac{F}{N_A kT} = \mu_o(T) + \log\rho_o + \int f(\Omega)\log\{4\pi f(\Omega)\}d\Omega$$

$$+ \frac{\rho_o}{2}\iint \beta_1(\Omega\,\Omega^1)f(\Omega)f(\Omega^1)d\Omega d\Omega^1$$

$$+ \frac{\rho_o^2}{3}\iiint \beta_2(\Omega,\Omega^1,\Omega'')f(\Omega)f(\Omega^1)f(\Omega'')$$

$$d\Omega d\Omega^1 d\Omega'' + \ldots. \qquad (33)$$

where $\mu_o(T)$ represents the kinetic energy of the discs, $\beta_1(\Omega,\Omega^1)$ is the "excluded volume" of two discs of respective orientation Ω,Ω^1 and $\beta^2(\Omega,\Omega^1,\Omega'')$ represents the probability that three particles of orientations Ω,Ω^1,Ω'' will overlap simultaneously.

For low particle density dispersions higher order terms in this expansion may be ignored, and Equation 33 can be approximated by,

$$\frac{F}{N_A kT} = \mu_o(T) + 10g\rho_o + \int f(\Omega)\log\{4\pi f(\Omega)\}d\Omega$$

$$+ \frac{\rho_o}{2}\iint \beta_1(\Omega,\Omega^1)f(\Omega)f(\Omega^1)d\Omega d\Omega^1 \qquad (34)$$

The first two terms in equation 34 represent the free energy of an ideal gas. The third and fourth terms are entropy corrections due to the finite size of the discs, being minimised by random orientation and perfect ordering respectively (218).

For particles of thickness t and diameter d, $\beta_1(\Omega,\Omega^1)$ is given by

$$\beta_1(\Omega,\Omega^1) = \frac{\pi}{2} d^3 \sin\gamma + \frac{\pi}{2} td^2 + \frac{\pi}{2} td^2 |\cos\gamma| + 2td^2 E(\sin\gamma) + 2t^2 d\sin\gamma \qquad (35)$$

where γ is the angle between the normals to the two discs, E (sin γ) is a complete elliptic integral of the second kind.

The errors involved in the use of equation 34 rather than equation 33 would be expected to be small (193).

Equation 34 may be used to calculate the disc number at which phase separation will occur for given values of t/d (193) Polydispersity of the particles in the system would be expected to affect the results (261, 262).

Colloidal montmorillonite layers are not "hard" but interact through the "soft" electric double layer repulsions (at low electrolyte concentrations) (section 3.2.4 (219)). The effect of the electric double layer, in terms of the hard disc model will be to increase the effective size of the particles (193). Since the range of the electric double layer repulsions is dependent upon factors such as the

electrolyte concentration (sect. 3.1.12), the volume fraction of clay particles at which phase separation occurs would also be expected to depend on electrolyte concentration, counter ion valency, temperature and Stern potential.

If the volume fraction of the clay is increased further, past the stage where phase separation occurs, then the whole system tends to become ordered, this order generally increasing with volume fraction. A "normal" concentrated dispersion (219) of montmorillonite would be expected to consist of randomly oriented regions of ordered layers (145, 203), separated by "crystal grain boundaries". This system may be converted to a well oriented "single crystal" system by compression (sect. 3.2.4.1).

3.2.3.2 Schiller layers

Under appropriate conditions montmorillonite dispersions may sediment with time forming an ordered parallel arrangement of the montmorillonite layers or tactoids such that the electric double layer repulsive forces are balanced by the sedimentation tendency of the clay particles under gravity (220, 221). If the resultant interparticle separations are of the order of the wavelength of light then the ordered phase will show a brilliant irridescence, due to Bragg diffraction effects and light scattering by the clay particles. Such ordered arrays of particles are termed schiller layers (214).

3.2.4 Rheology of montmorillonite dispersions

Rheology is the study of the deformation and flow of matter. The application of a stress, defined as a force per unit area, to a body induces a relative deformation described as a strain. The relationship between the applied stress and the observed strain depends on the inherent properties, the experimental timescale and the magnitude of the stress (223, 224).

For an ideal elastic body, obeying Hooke's Law, the applied force is proportional to the resulting displacement, the proportionality constant being the spring constant. For an ideal fluid, obeying Newton's Laws, the stress is proportional to the rate of strain, the proportionality constant being the fluid viscosity.

Colloidal systems, such as montmorillonite dispersions, may show viscoelastic behaviour (223, 19, 195, 194) which may be described by various combinations of the above ideal elastic and viscous models (225, 226). By correct choice of the experimental technique used the appropriate elastic and viscous elements of a viscoelastic material may be studied (223).

3.2.4.1 Compression studies

The bulk modulus B is the elastic modulus applied to a body with uniform stress over the whole surface of the body (fig. 11), and is defined by (196)

$$B = -V \frac{dp}{dV} \qquad (36)$$

Fig.11 : Definitions of elastic moduli

a: Shear modulus, G

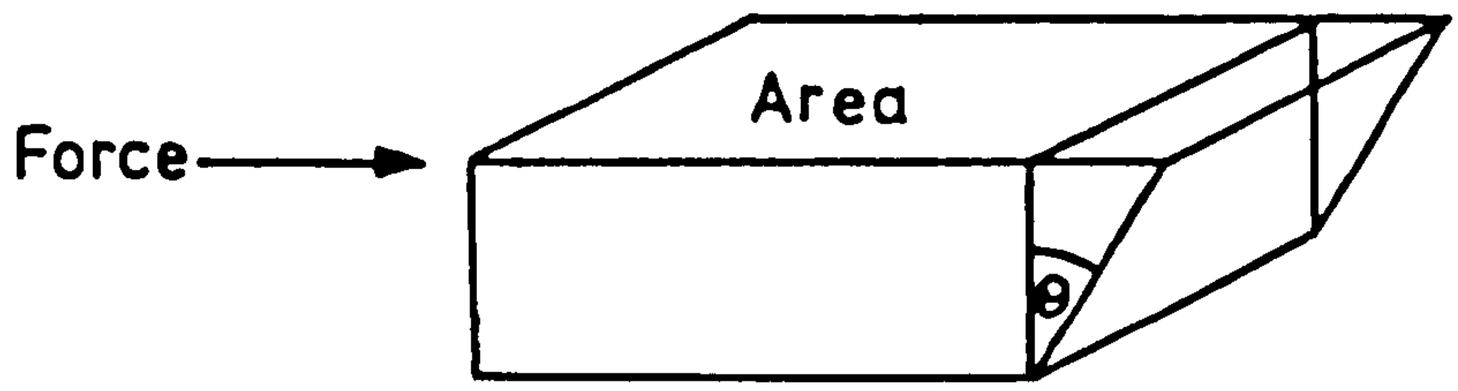

Force / Area = θG

b: Bulk modulus , K

$$\text{Pressure} = -\frac{(\text{Volume change})K}{\text{Volume}}$$

c: Young's modulus , Y

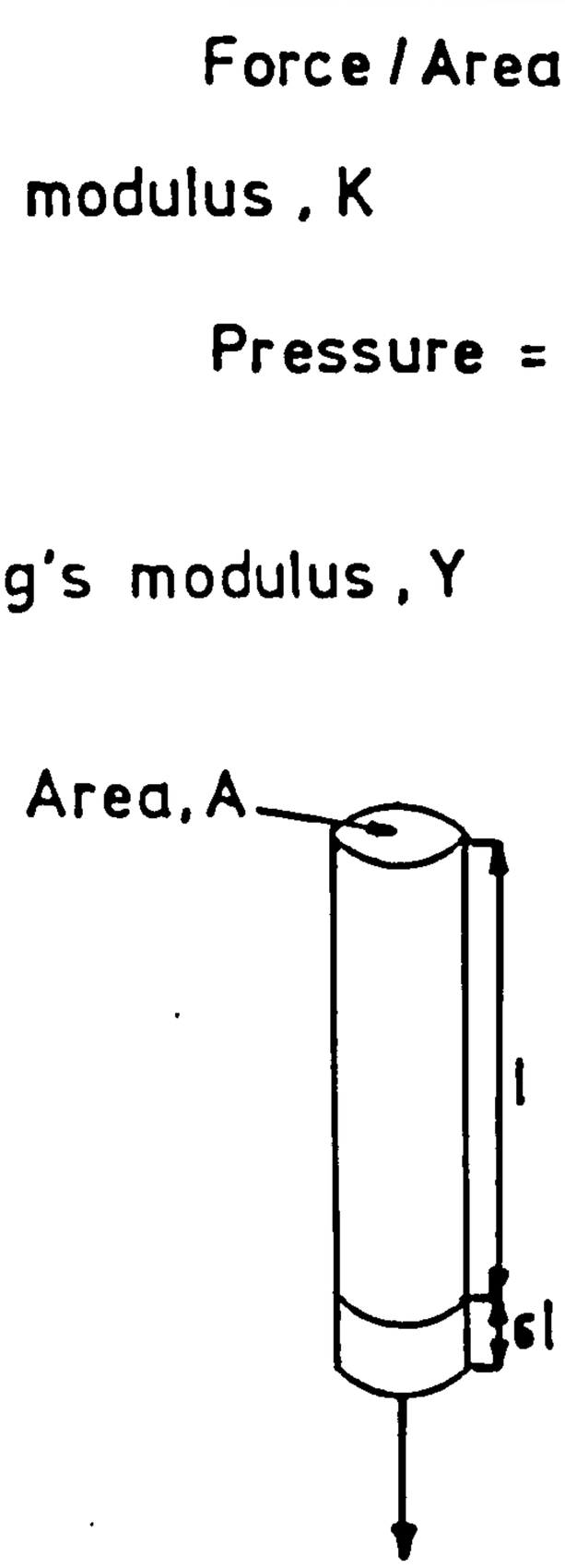

$$\frac{mg}{A} = \frac{-\delta l\, Y}{l}$$

where p = pressure and V volume. The reciprocal of bulk modulus is the coefficient of compressibility (228).

For a system of constant area (196)

$$B = -H_o \left(\frac{dp}{dH_o}\right)_A \qquad (37)$$

The change in interparticle separation H_o with applied pressure p may be calculated from compression cell studies (145, 146, 196, 191, 144, 192, 172, 173). Here a sample of clay dispersion may be compressed and its resulting change in volume may be related to Ho (145, 146, 196, 191, 144, 192, 173) or H_o may be measured directly by X-ray diffraction (172, 202). The results of these compression studies indicate that upon initial compression of a montmorillonite dispersion the montmorillonite layers or tactoids become oriented in a parallel array. Subsequent decompression and compression cycles follow the same p as H_o curve which is in good agreement with theoretical calculations, using equation 26 or the differential of equation 29 with respect to H_o, at relatively large separations and if allowance is made for the amount of electrolyte in the system (192, 145) and the formation of tactoids (145, 146, 202). This behaviour of montmorillonite dispersions also suggests that, having ordered the particles, the particles remain in a face-face orientation upon subsequent decompression and there is little tendency for edge-face orientation as seen with kaolinite dispersions (192, 19, 227, 195).

By differentiation of the p against H_o curves obtained from compression studies, it is possible to calculate the bulk modulus for the dispersion, using equation 37 (196).

3.2.4.2 Shear Modulus measurement

The shear modulus G of a body is given by

$$G = \frac{\tau l_2}{l_1} \qquad (38)$$

where τ = shear stress = force F/area A and l_1 and l_2 are the distance as shown in fig. 11.

G is related to B by the relationship

$$G = \frac{3}{2} \frac{B(1 - 2\mu)}{(1 + \mu)} \qquad (39)$$

where μ = Poisson's ratio, that is the ratio of the axial strain to the longitudinal strain.

The value of μ for a montmorillonite dispersion is difficult to ascertain, although it would be expected that G would have a similar magnitude to B, as for example with Cauchy's identity (229)

$$G = \frac{3B}{5} \qquad (40)$$

and it has been shown that experimental values of B are in reasonable agreement with experimental G values (196).

The shear modulus (G) of viscoelastic dispersions may be measured using a "pulse shearometer" (chapter 8). This apparatus applies a high frequency (~200Hz) shear stress to a dispersion, on which time-scale viscoelastic dispersions may have an elastic response (i.e. viscous contributions to the rheological behaviour are small) (223, 229).

The pulse shearometer has been used to study montmorillonite dispersions previously (194, 230, 231, 232).

Although theoretical treatments for the prediction of the behaviour of a highly ordered system of montmorillonite particles have had some success (section 3.2.4.1), no theory has been found to adequately describe the behaviour of natural (disordered) montmorillonite dispersions that could be used to explain pulse shearometer results or the first compression curve in compression studies.

3.2.4.3 Viscosity measurements

Montmorillonite dispersions often exhibit so-called Bingham plastic flow (233), where the shear stress τ against shear rate curves show a Bingham yield stress τ_B, which is the value of τ at which flow starts (ideally abruptly). The value of τ_B has been used as a measure of the structure in the system (i.e. elastic behaviour) (231, 198, 227, 194, 19, 195, 234), although such results cannot be compared

directly with shear modulus determinations because of perturbation of the system during flow.

The flow behaviour of colloidal dispersions is dependent upon factors such as electroviscous effects, particle size, shape and aggregation (227, 318).

3.3 PROPERTIES OF OTHER BENTONITE MINERALS

It would be expected that the properties of a given bentonite may be affected by variations within the montmorillonite mineral present (e.g. particle size, surface charge density and degree of heterogeneity) and, also, the amount and type of any other minerals (chapter 2) present in the clay.

3.3.1 Clay Minerals

The clay minerals most often present in bentonites, apart from montmorillonite, are beidellite, illite and kaolinite (section 2.2). These minerals have different surface charge density and particle size and shape characteristics to montmorillonite which might modify the bentonite properties.

3.3.2 Associated minerals

Non-clay minerals (section 2.3) may also affect a bentonite's properties, for similar reasons to those given above (section 3.3.1). It may also be possible for interactions between

minerals or mineral components to occur e.g. multimineral aggregates (6), interstratifications (section 2.2.6) (235) or dissolution and precipitation reactions.

C H A P T E R F O U R

PREVIOUS STUDIES ON TEXAS BENTONITES

PREVIOUS STUDIES ON TEXAS BENTONITES

4.1 GEOLOGY OF GONZALES BENTONITES

The geology and mineralogy of the white bentonite occurring in Gonzales county, Texas has been studied by Chem (10). Chen proposed that this bentonite was formed by the following processes:-

During upper Eocene time (~40 million years ago) there was widespread volcanic activity in West Texas (236). During this time large amounts of volcanic dust were ejected and carried some distance by wind before settling. Most of the dust particles that were transported the 400 miles or so to Gonzales county, by the prevailing west winds (237, 238, 239), had a small size. Some of this fine ash fell into brackish or salt water basins where, as it settled slowly through the water, it was initially hydrolysed and then altered to montmorillonite. This alteration of the ash to montmorillonite was brought about by removal of alkali metals (K, Na) and excess silica from the volcanic glass by the alkaline water, followed by adsorption and fixing of alkaline earth metals (Mg, Ca) into the glass from the seawater. This material settled to the bottom of the water basin in the form of a volcanic mud where montmorillonitisation probably continued. The few larger particles in the dust fall remained as largely unaltered glass shards. Jonas (240), however, thinks that conversion took place when subterranean brines rose up fault planes and infused the volcanic ash, since the ash beds tend to be altered where faults intersect them.

Chen (10) suggests that the free silica in solution, from the alteration of the volcanic ash, was then precipitated as colloidal silica due to changing conditions such as supersaturation of the silica, or evaporation of the restricted sea-water. Some of this silica may have been co-precipitated with some newly formed montmorillonite (241). Henderson et al (16), however, suggest that the dissolved silica was utilised by plankton (diatoms, radiolaria) to form skeletons of opal-cristobalite which have been broken up during the 40 million years since original crystallisation. From oxygen isotope analysis Henderson et al (16) indicate that the Helms montmorillonite was formed at ~25°C in sea-water, the Helms opal-cristobalite was formed at ~25°C in meteoric waters and the quartz present in the Helms pit originates from mixture of high and low temperature sources, and was detritally added to the ash or bentonite bed.

The bentonite in the Clark pit was formed from a separate and later ash-fall from that which formed the Helms bentonite (10). At some later stage tectonic uplift of east Texas removed the bentonite beds from the marine environment (10).

Weathering of the montmorillonite then caused the formation of kaolinite minerals on the exposed bentonite faces or in fissures (10). The weathering of montmorillonite to form halloysite has also been suggested, by Yoshimora and Kohyama (242), for a white bentonite occurring in Japan. It is possible that this process has continued further, producing large amounts of kaolinite, in an older formation in Texas (243). During the weathering of the Helms

bentonite colloidal hydrated manganese oxides were precipitated as wad (10).

4.2 MINERALOGY OF GONZALES BENTONITES

The mineral constituents reported in Gonzales bentonites are shown in table 5.

TABLE 5 - MINERALOGY OF GONZALES BENTONITES

A Mineralogy of Helms bentonite

	Mineral	reference
a)	montmorillonite	6, 10, 11
b)	opal cristobalite	10, 16
c)	cristobalite	6, 245
d)	tridymite	6
e)	unaltered volcanic glass	6, 10
f)	quartz	6, 10, 11, 16, 245
g)	kaolinite	6, 10
h)	halloysite	10
i)	mica	6
j)	feldspars	6, 10
k)	gypsum	10
l)	calcite	10, 245
m)	jarosite	10
n)	pyrite, marcasite	10
o)	wad	10

B Mineralogy of other Gonzales bentonites

	Mineral	reference
a)	montmorillonite	12, 13, 244
b)	beidelite-like	12, 13
c)	cristobalite	6, 12, 13
d)	opal	244
e)	unaltered volcanic glass	6, 244, 12, 13
f)	quartz	12, 13, 244
g)	kaolinite	12, 13, 244
h)	halloysite	244
i)	mica, illite, muscovite, glauconite	12, 13, 10, 244
j)	feldspars	12, 13, 244
k)	limonite	244
l)	calcite	12, 13
m)	zeolites	244, 10
n)	allophane	244
o)	diatoms	10, 244
p)	interstratified clay minerals	10
q)	nontronite-like	10

Grim and Güven (6) reported the presence of montmorillonite-tridymite intergrowths in Helms bentonite. Chen (10) suggested that some of the opal-cristobalite cemented montmorillonite layers together by means of silica "pillars", similar material has been prepared synthetically (67, 68).

4.3 OTHER STUDIES ON HELMS BENTONITE

The results of other studies on samples of Helms bentonite are given below. It should be noted that this data may not be representative of the samples studied in this work (section 5.1.1) because of the variability in the properties of the bentonite from different areas of the Helms deposit (6, 12, 13, 10).

4.3.1 Electron microscopy

Samples of Helms bentonite were studied by Grim and Güven (6), these were found to consist of Cheto-type (mossy) or foliated aggregates (sect. 3.1.1) and, also, H- and S- type lamellae. These samples also contained occasional euhedral kaolinite crystals and lath-shaped crystals which were thought to be mica (6). Occasional E-type particles were observed in the Helms and Clark-Yenna bentonites (6).

4.3.2 Cation exchange studies

The cation exchange capacity (C.E.C.) of a sample of Helms bentonite (STx-1) was determined by Worthington, Granquist and Clemency who found values of 80, 85·2 and 88 meq/100g respectively (11). The exchangeable cation composition was found to be 54·5 meq/100g Ca^{2+}, 18·0 meq/100g Mg^{2+}, 0·5 meq/100g K^{+} and 9·9 meq/100g Na^{+} (11). That is, the Helms bentonite is composed of mainly Ca

montmorillonite, as found by other workers (10, 12, 13).

4.3.3 Thermal analysis

Thermal analysis techniques (differential thermal analysis (DTA), thermogravimetry (TG) and derivative thermogravimetry (DTG)) were used to study the above Helms bentonite sample (STx-1) (11). The dehydroxylation peak for the Helms bentonite occurs at a lower temperature (720°C) than that of the Wyoming montmorillonite tested (755°C), however this does not seem low enough to indicate the presence of beidellite in the Helms bentonite (246).

4.3.4 Infrared spectroscopy

The Helms bentonite sample (STx-1) was studied using infrared (ir) spectroscopy by Farmer (11). This sample was found to have a low iron content and an absorption band at 797 cm^{-1} was attributed to the presence of a "clay-size platy disordered tridymite" phase (11, 252). The ir spectra for the Helms bentonite are similar to those of other montmorillonites (11, 253), there being little evidence of beidellite from the Al-O stretching frequencies (253, 254, 255).

4.3.5 Electron spin resonance

Electron spin resonance (esr) studies of the Helms bentonite sample (STx-1), by Pinnavaia (11), indicate the presence of Fe^{3+} and

resonances attributed to paramagnetic lattice defects associated with Mg substitution and, possibly, an adsorbed organic free radical impurity.

C H A P T E R F I V E

STUDIES ON CRUDE BENTONITES

STUDIES ON CRUDE BENTONITES

5.1 INTRODUCTION

This chapter describes studies on the crude supplied bentonite samples. The natural (untreated) samples were studied using X-ray fluorescence spectroscopy, X-ray diffraction, electron microscopy and electron probe micro analysis in order to assess their chemical and mineralogical compositions. The composition of bentonite samples can have a bearing on their properties (5, 6, 11, 14, 19, 61, 71, 195). The composition of the Texas samples is discussed in relation to their geological formation and history.

A simple dispersion test was used to compare the dispersion behaviour of the bentonite samples in water and the effect of different treatments on the dispersion of a Texas bentonite.

5.2 EXPERIMENTAL

5.2.1 Samples supplied

i) Upton, Wyoming bentonite - API sample no. 25 (48W 1250) (256).

ii) Beidellite, Unterupsroth - sample VII as provided by Prof. A. Weiss (145).

The samples below were all supplied by English Clays, Lovering, Pochin and Co. Ltd:-

iii) Wyoming Blackhills standard bentonite - milled, coloured pale green.

iv) Full face Helms bentonite, Texas - Untreated hard Helms bentonite. This sample consisted of pieces of hard white rock coated with red/brown and purple/black staining (fig. 12).

v) Hard Helms bentonite, Texas - milled hard Helms bentonite, coloured red/brown.

vi) "Bentolite L" - milled, cobbed hard Helms bentonite, coloured white.

vii) Soft Helms bentonite, Texas - milled soft Helms bentonite, coloured red/brown.

viii) Cobbed soft Helms bentonite, Texas - milled, cobbed soft Helms bentonite, coloured white.

ix) Soft Clark bentonite, Texas - milled Clark bentonite, coloured red/brown.

x) Milos bentonite, Greece - milled, coloured red/brown.

xi) Halloysite - sample of hard white rock.

xii) European bentonite - milled, coloured grey.

5.2.2 Chemical analysis

The chemical analyses of the clay samples were obtained. by English Clays, Lovering, Pochin & Co. Ltd. (ECLP), using X-ray fluorescence analysis (XRF). With this technique, the specimen is irradiated with an X-ray beam and from the wavelength and intensity

Fig. 12 : Photograph of full face Helms bentonite rock, Gonzales, Texas

of the lines in the resulting X-ray fluorescence spectrum the elements present in the specimen and their concentration may be determined respectively. The amount of associated minerals were also estimated from X-ray diffraction (XRD), by ECLP.

The structural formulae of the montmorillonite in the bentonites were calculated (see appendix 4) from the XRF data making allowance for the presence of impurities estimated from XRD. In some cases the amount of estimated free silica was too low, giving tetrahedral Si>4, possibly because XRD could not 'see' amorphous silica (opal) phases. The minimum amount of silica impurity needed to give tetrahedral Si$\leq$4·00 was calculated iteratively (appendix 4).

5.2.3 X-ray diffraction (XRD)

Samples of clay were slurried in water, spread onto a glass slide and heated at $\sim$200°C for 48 hours, in an oven. The samples were then kept in an evacuated desiccator, with dried silica gel, until they were studied using XRD. The XRD patterns were obtained, using a Philips TW2233/20 X-ray diffractometer with Ni-filtered CuKα radiation (wavelength = 0·77092Å), by Dr. D. Robinson, Dept. of Geology, University of Bristol.

5.2.4 Scanning electron microscopy (SEM)

Samples of full face Helms bentonite were cleaved to give small ($\sim$1cm) pieces of rock. These were then glued to SEM studs,

using electrically conducting adhesive, and sputter coated with gold. They were then studied using a Cambridge Stereoscan scanning electron microscope.

5.2.5 Transmission electron microscopy (TEM)

A dispersion of full face Helms bentonite was prepared by dispersing the cobbed material in water with the aid of ultrasonic treatment. This dispersion was then put on carbon microscope grids, coated with cytochrome c (method b, section 6.1.4) and studied using a Jeol 100CX electron microscope.

Carbon replicae were made of the cleaved full face Helms bentonite surface by coating thin chips of the rock with carbon, dissolving the clay with hydrofluoric acid, washing with water and mounting on copper microscope grids. The replicae were then studied using an Hitachi HS7s transmission electron microscope.

5.2.6 Electron probe microanalysis (EPMA)

The particles in the full face Helms bentonite dispersion studied by TEM (sect. 5.2.5) were analysed using EPMA. With this technique the characteristic X-rays emitted as a result of the electrons focussed on a given particle or specimen area in the electron microscope are analysed to provide quantitative and qualitative information on the elemental composition of the exposed area.

5.2.7 Dispersion tests

The degree of dispersion of the clays upon different treatments was measured using a simple dispersion test. A known weight (∿50g) of dry clay was added to 2dm^3 of water, together with a known amount of dispersing agent, stirred for 30 minutes and then left to sediment for a further 30 minutes. A 50 cm^3 sample of the dispersion was taken from 2 cm below the liquid surface and its dry weight determined. The degree of dispersion of the clay was then calculated, and corresponded to the proportion of the clay dispersed to a Stoke's spherical diameter of less than ∿6μm.

5.3 RESULTS AND DISCUSSION

5.3.1 Chemical analysis

The results of the chemical analysis, by X-ray fluorescence analysis (sect. 5.2.2) are given in appendix 3. The chemical formulae calculated from this data (appendix 4) are given in Table 6.

There is a significant difference between the chemical formulae calculated for Wyoming Blackhills bentonite by the two different methods (table 6); this is due to the presence of impurities in the sample. There are problems with the calculation of the amount of Fe in the lattice and the cec seems high; again these effects are due to impurities in the sample (probably mainly Ca CO_3 and $CaSO_4$).

TABLE 6: Chemical Formulae of Crude Bentonites

Sample	Method	Tetrahedral Cations		Octahedral Cations					Interlayer Cations			cec/ meq/ 100g	Anions (O=10)	Impurity Silica	
		Si	Al	Al	Fe^{3+}	Fe^{2+}	Mg	Total	Ca^{2+}	Na^{+}	K^{+}		OH_1F	XRD	Calc.
Wyoming Blackhills	1	3·99	0·01	1·52	-0·16	0·36	0·16	1·83	0·14	0·20	0·05	149	2	9	18
	2	4	0	1·61	-0·17	0·39	0·17	2	0·15	0·21	0·05	155	2·39	9	21
Wyoming Upton	1												2	7	
	2							2						7	
Bentolite L	1	3·98	0·02	1·55	0·03	0·03	0·37	1·99	0·18	0·05	0·01	121	2	30	35
	2	3·99	0·01	1·56	0·02	0·04	0·37	2	0·18	0·05	0·01	121	2·04	30	35
Cobbed Soft Helms	1	3·99	0·01	1·59	0·04	0·02	0·35	1·99	0·16	0·04	0·02	106	2	6	12
	2	4	0	1·59	0·04	0·02	0·35	2	0·16	0·04	0·02	106	2·02	6	12
Soft Clark	1	3·99	0·01	1·61	-0·26	0·31	0·23	1·90	0·09	0·18	0·20	155	2	1	18
	2	3·98	0·02	1·70	-0·26	0·32	0·25	2	0·09	0·19	0·21	162	2·32	1	21
Milos	1	3·81	0·19	1·49	0·55	-0·40	0·49	2·13	0·11	0·05	0·02	79	2	2	2
	2	3·73	0·27	1·37	0·63	-0·47	0·47	2	0·10	0·05	0·02	79	1·53	2	2

The structural formulae calculated for the Bentolite L and cobbed soft Helms bentonites by each of the two methods are in very good agreement (table 6). This is probably due to the smaller amount of calcium salt impurities as compared to Wyoming Blackhills bentonite; the major impurity being silica.

The chemical formulae of Bentolite L and cobbed soft Helms are also similar to each other. The main differences between the Texas and Wyoming bentonites are that the former has less Fe substitution and the major exchangeable cation is Ca rather than Na. These results are in general agreement with previous work (10, 11, 6). Also the "hard" bentonite (Bentolite L) contains more silica impurity (~35%) than the "soft" bentonite (cobbed soft Helms) (~12%).

5.3.2 X-ray diffraction

The X-ray diffraction (XRD) patterns obtained for the heated, crude samples of Wyoming Blackhills, Bentolite L and cobbed soft Helms bentonites are given in appendix 7. The corresponding d-spacings and band assignments (259) are given in tables 7, 8 and 9 respectively.

Most of the peaks in these XRD spectra can be assigned to minerals known to occur in the bentonite samples.

All three samples give broad basal (001) reflections. This may be due to "pillaring" of interlayer silica in the Texas samples as suggested by Chem (10), however the Wyoming Blackhills sample also shows this effect. It is possible that some rehydration of the samples had occurred before/during the XRD measurement, although the procedures used (sect. 5.2.3) were considered to reduce this effect to a minimum (264).

Table 7: X-ray diffraction results for crude Wyoming Blackhills bentonite

20/°	d-spacing/Å	Band assignment
6•4 - 9	13•8 - 9•8	Smectite (expanded - "collapsed")
19•6 - 20•2	4•53 - 4•40	Dioctahedral smectite
20•8	4•27	Low quarts
21•9	4•06	Feldspar
23•5	3•79	Feldspar
25•5	3•49	Anatase, anhydrite
26•6	3•35	Low quartz
27•8	3•21	Smectite, feldspar
29•4	3•04	Smectite, calcite
35•0	2•56	Smectite
35•8	2•51	High quartz
36•0	2•49	-
36•5	2•46	Low quartz
39•4	2•29	Calcite
40•3	2•24	-
42•4	2•13	-
43•2	2•09	Anhydrite
45•7	1•985	-
46•8	1•941	-
47•6	1•910	Calcite
48•5	1•877	-
48•6	1•873	Calcite
50•1	1•821	Low quartz
50•6	1•804	-
50•8	1•797	-
54•8	1•675	Smectite
60•0	1•542	Quartz
62•0	1•497	Smectite

Table 8: X-ray diffraction results for crude Bentolite L

20/°	d-spacing/Å	Band assignment
5 - 9·4	17·7 - 9·4	smectite (expanded - "collapsed")
18·8	4·72	-
19·8	4·48	dioctahedral smectite
21·8	4·08	opal-CT, low cristobalite, low tridymite
28·2	3·16	smectite
35 - 36	2·56 - 2·49	opal-CT, cristobalite, smectite
48·0	1·895	anatase
48·2	1·888	low cristobalite
54·2	1·692	smectite
54·8	1·675	smectite
54·9	1·672	smectite
56·1	1·639	high cristobalite
56·8	1·621	kaolinite
61·8	1·501	smectite
64·0	1·455	high cristobalite, kaolinite

Table 9: X-ray diffraction results for crude cobbed soft Helms bentonite

20/°	d-spacing/1Å	Band assignment
6·6 - 9·2	13·4 - 9·6	smectite (expanded - "collapsed")
12·4	7·14	7Å-halloysite, kaolinite
18·8	4·72	-
19·0	4·67	smectite
20·0	4·44	smectite, halloysite, kaolinite
20·8	4·27	low-quartz
21·8	4·08	opal-CT, low-tridymite, low-cristobalite
26·8	3·33	low-quartz
27·8	3·21	smectite
28·2	3·16	smectite
35·4	2·54	opas-CT, cristobalite, smectite
54·2	1·692	smectite
62·2	1·492	smectite, kaolinite, halloysite

5.3.3 Scanning electron microscopy (SEM)

Most of the cleaved surface of the full face Helms bentonite samples, studied by SEM, was found to consist of leaf-like clay plates, although the individual plates varied from being relatively "smooth" (fig. 13) to "granular" (fig. 14) in appearance. This granular appearance may be due to the presence of opaline silica coatings. Some areas of the rock, close to the weathered surface were found to consist of areas of (presumably halloysite) rods (fig. 15, 16). SEM of the halloysite rock sample surface showed similar rod-like particles (fig. 17). This is in agreement with the results of Chem (10) (sect. 4.1). Occasional inclusions of volcanic glass or quartz surrounded by a "nest" of halloysite rods were found (frontispiece, fig. 18, 19). The presence of halloysite may be due to weathering of the montmorillonite as meteoric water passed through pores in the material (8, 265, 323).

5.3.4 Transmission electron microscopy (TEM)

Transmission electron micrographs of the full face Helms sample are shown in figs. 20 to 23. A general view of the sample is shown in fig. 20, this shows the sample to consist mainly of (S-type) thin irregular montmorillonite sheets (fig. 23). Also seen were tubular halloysite particles (fig. 21) and "amorphous" particles of silica (fig. 22). A cobbed sample of full face Helms bentonite shows little evidence of halloysite (fig. 23). This is probably

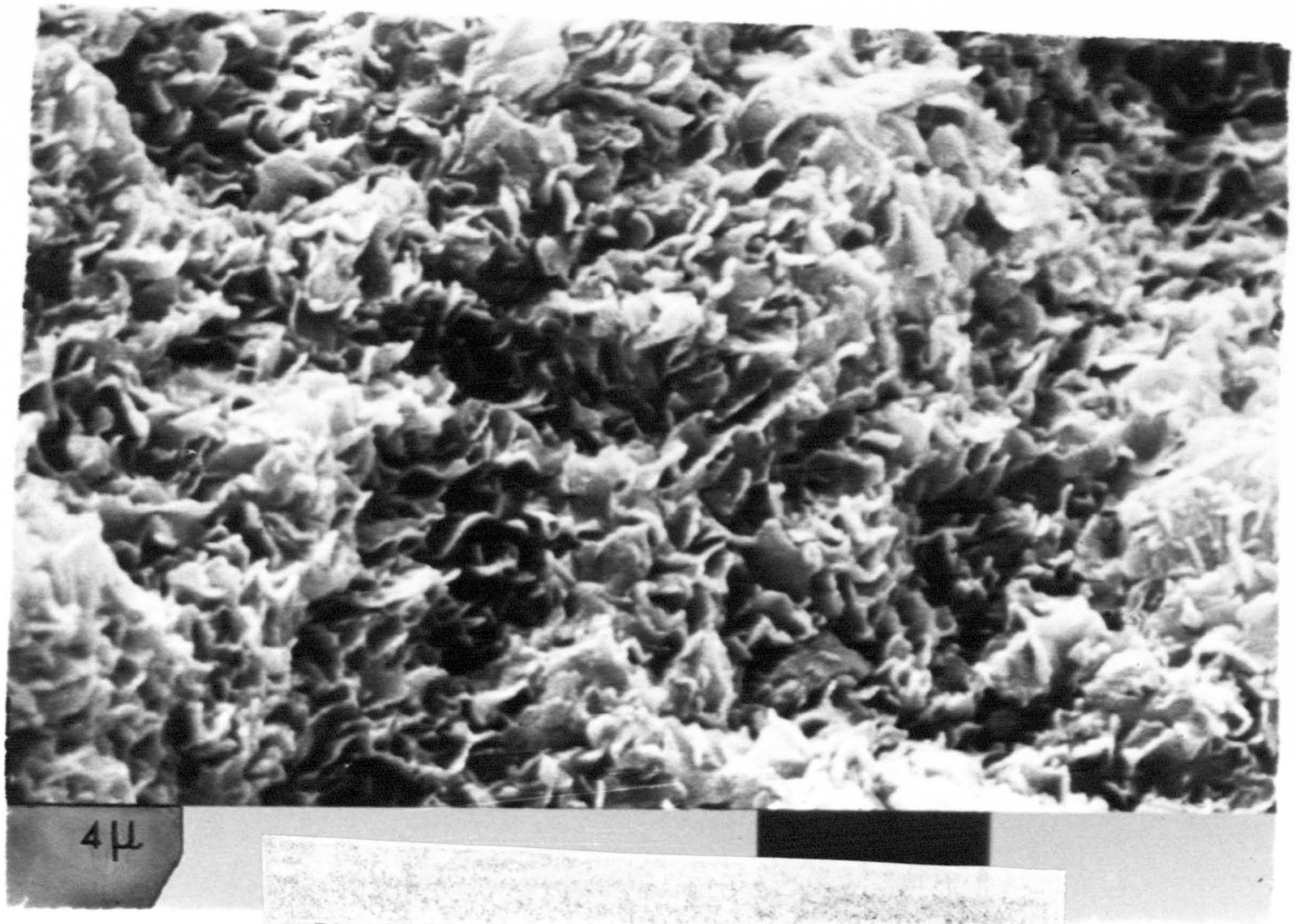

Fig. 13 : Scanning electron micrograph of cleaved surface of full face Helms bentonite

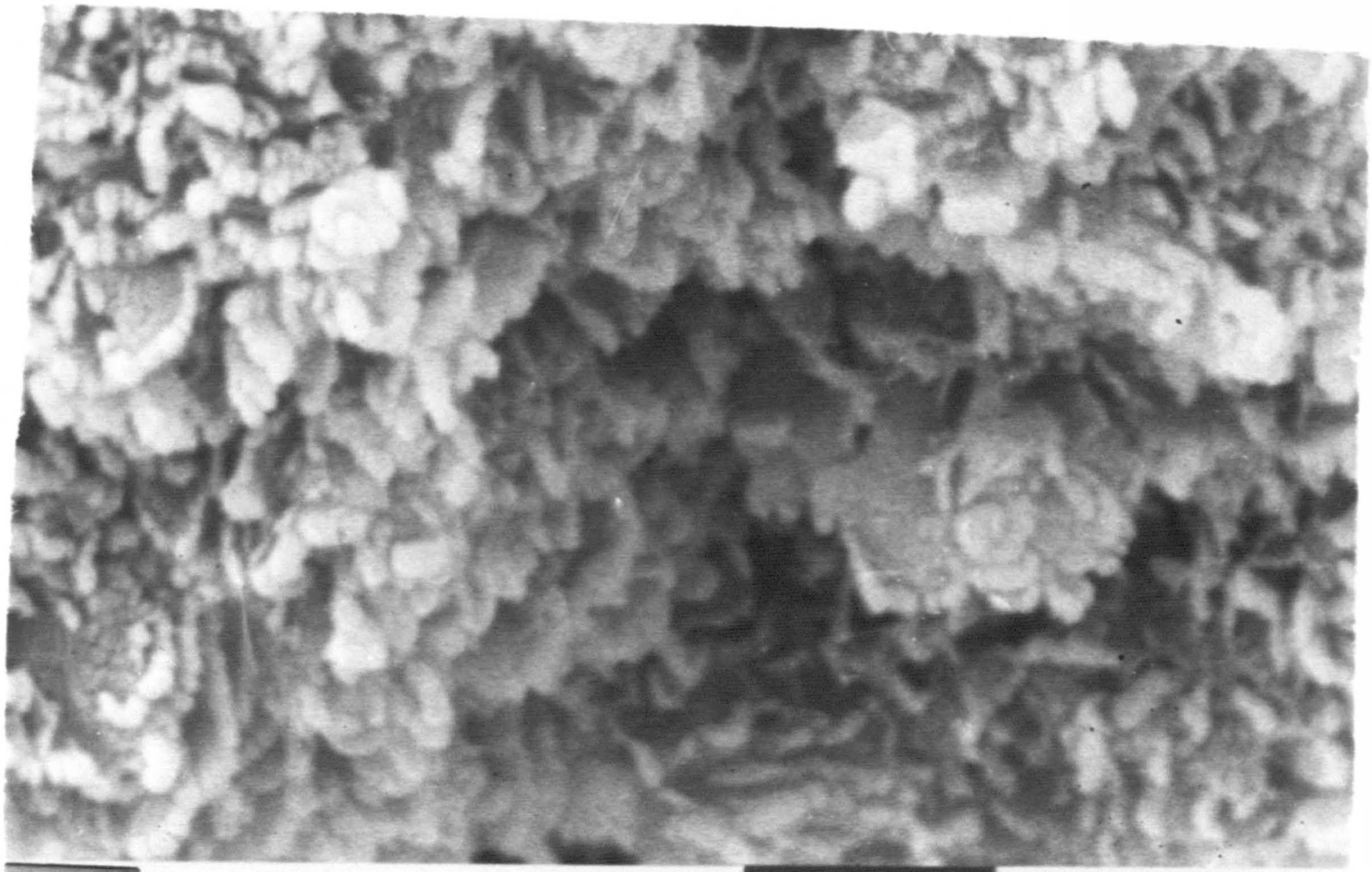

Fig. 14 : Scanning electron micrograph of cleaved surface of full face Helms bentonite

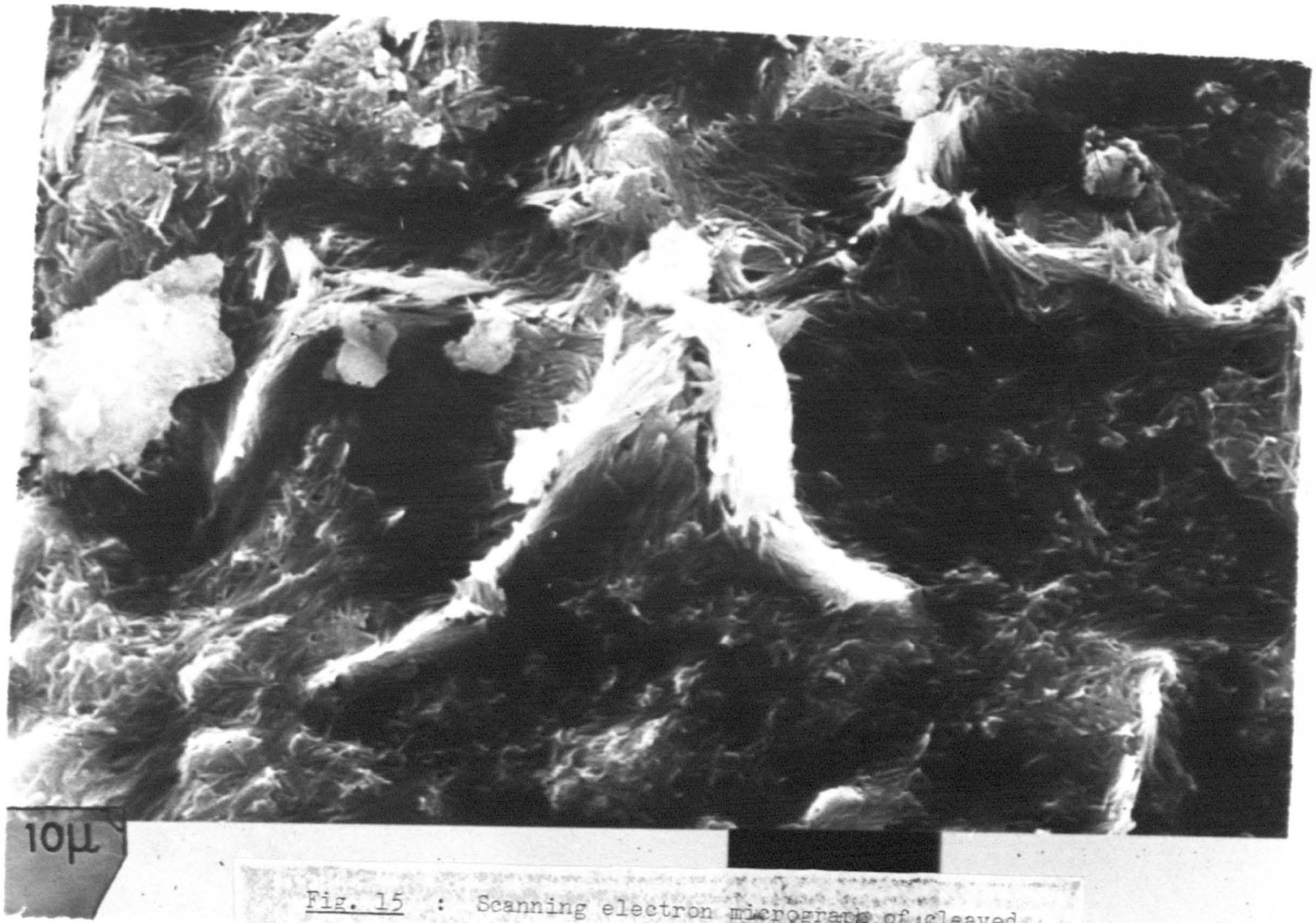

Fig. 15 : Scanning electron micrograph of cleaved surface of full face Helms bentonite

Fig. 16 : Scanning electron micrograph of cleaved surface of full face Helms bentonite

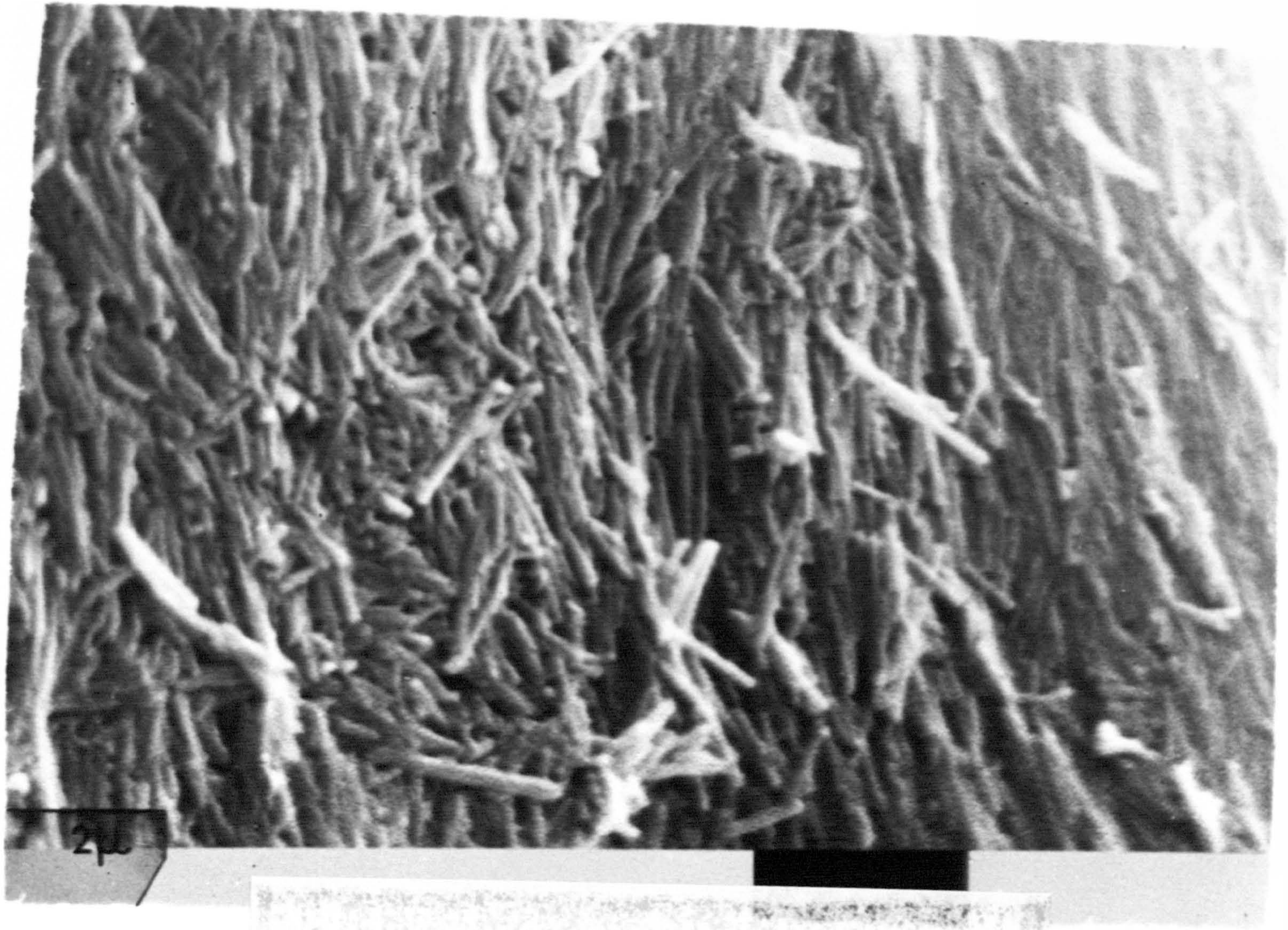

Fig. 17 : Scanning electron micrograph of cleaved surface of halloysite rock sample

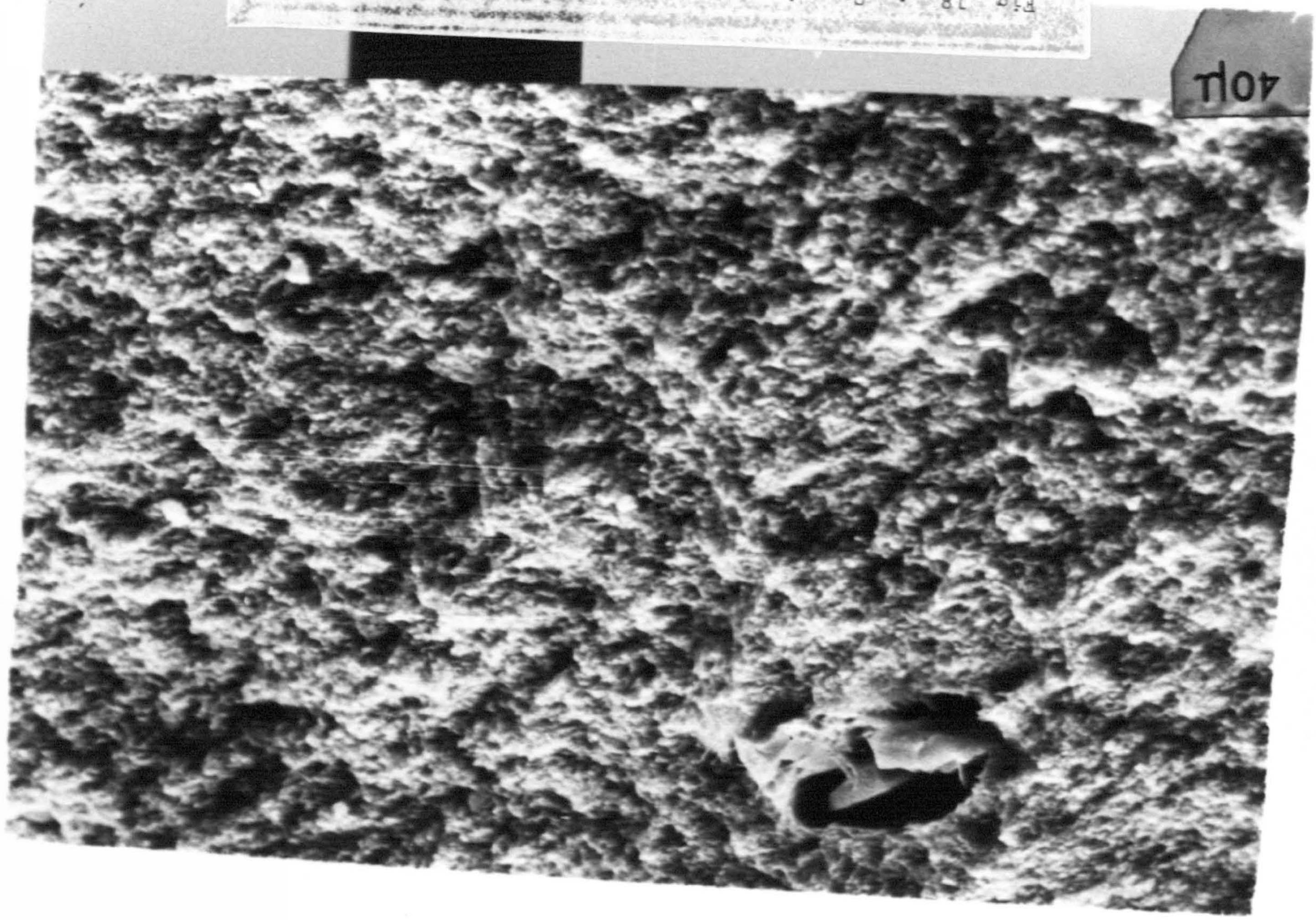

Fig. 18 : Scanning electron micrograph of cleaved surface of full face Helms bentonite

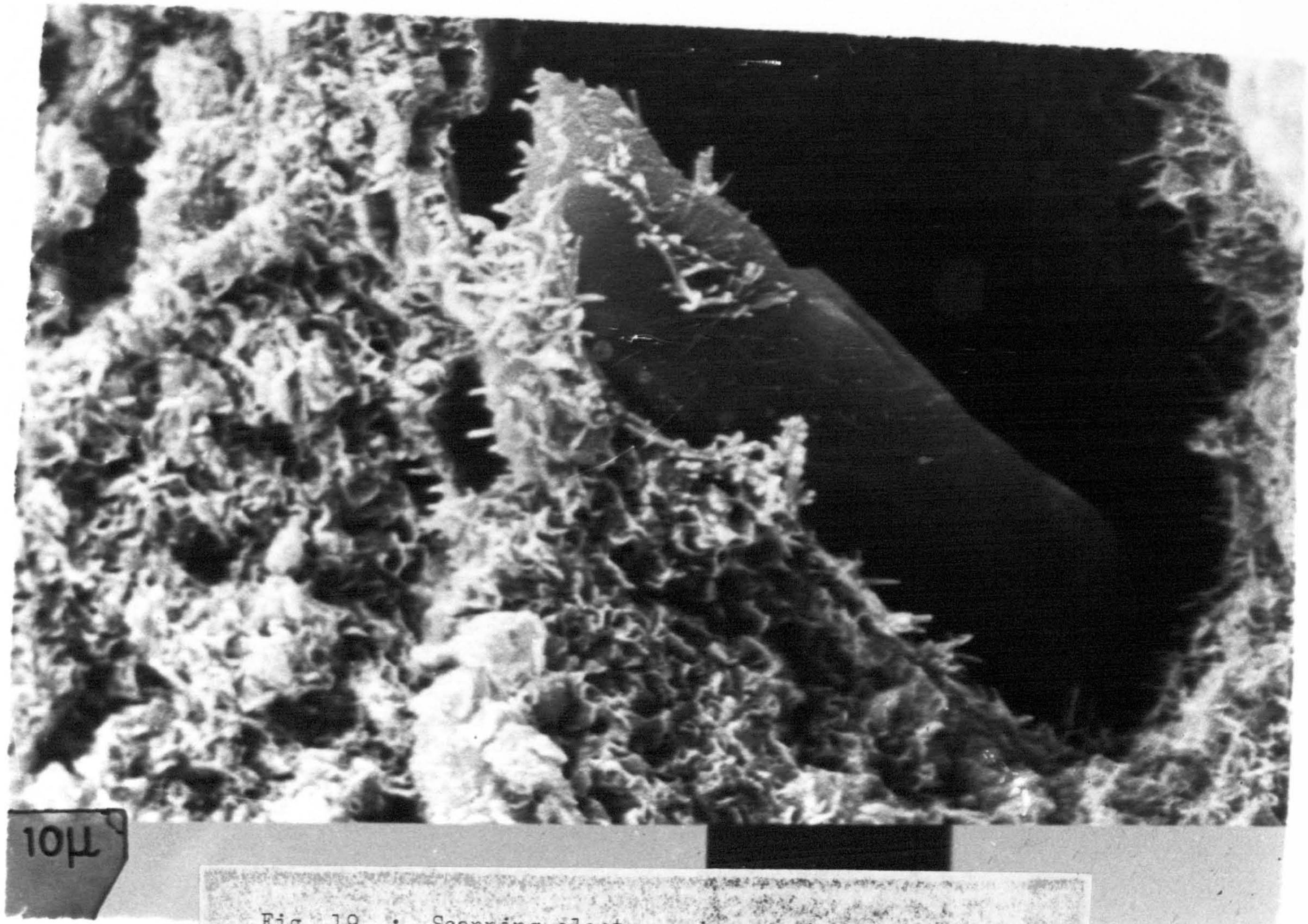

Fig. 19 : Scanning electron micrograph of cleaved surface of full face Helms bentonite

1µm

Fig. 20 : Transmission electron micrograph of full face Helms dispersion

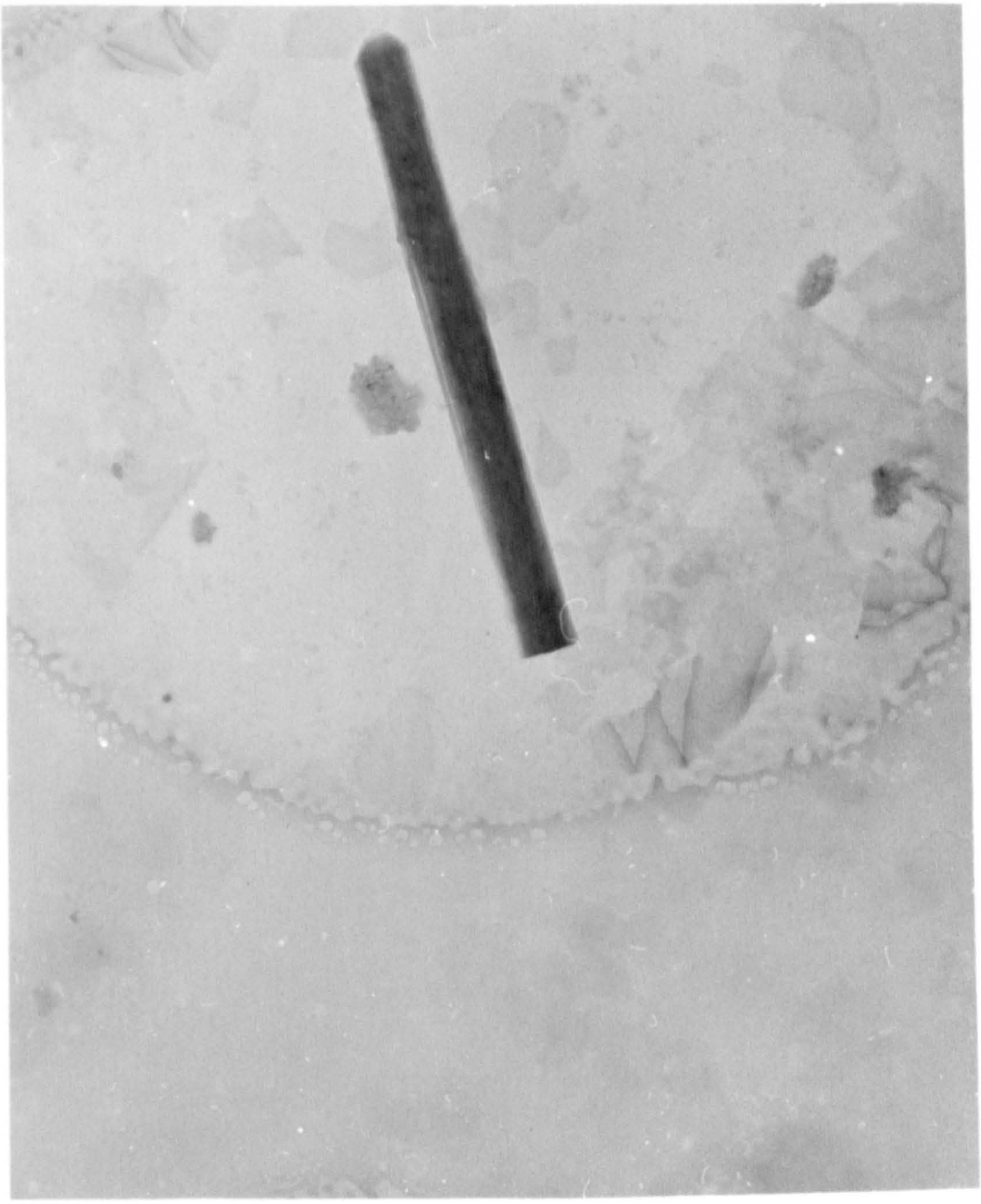

1µm

Fig. 21 : Transmission electron micrograph of full face Helms dispersion

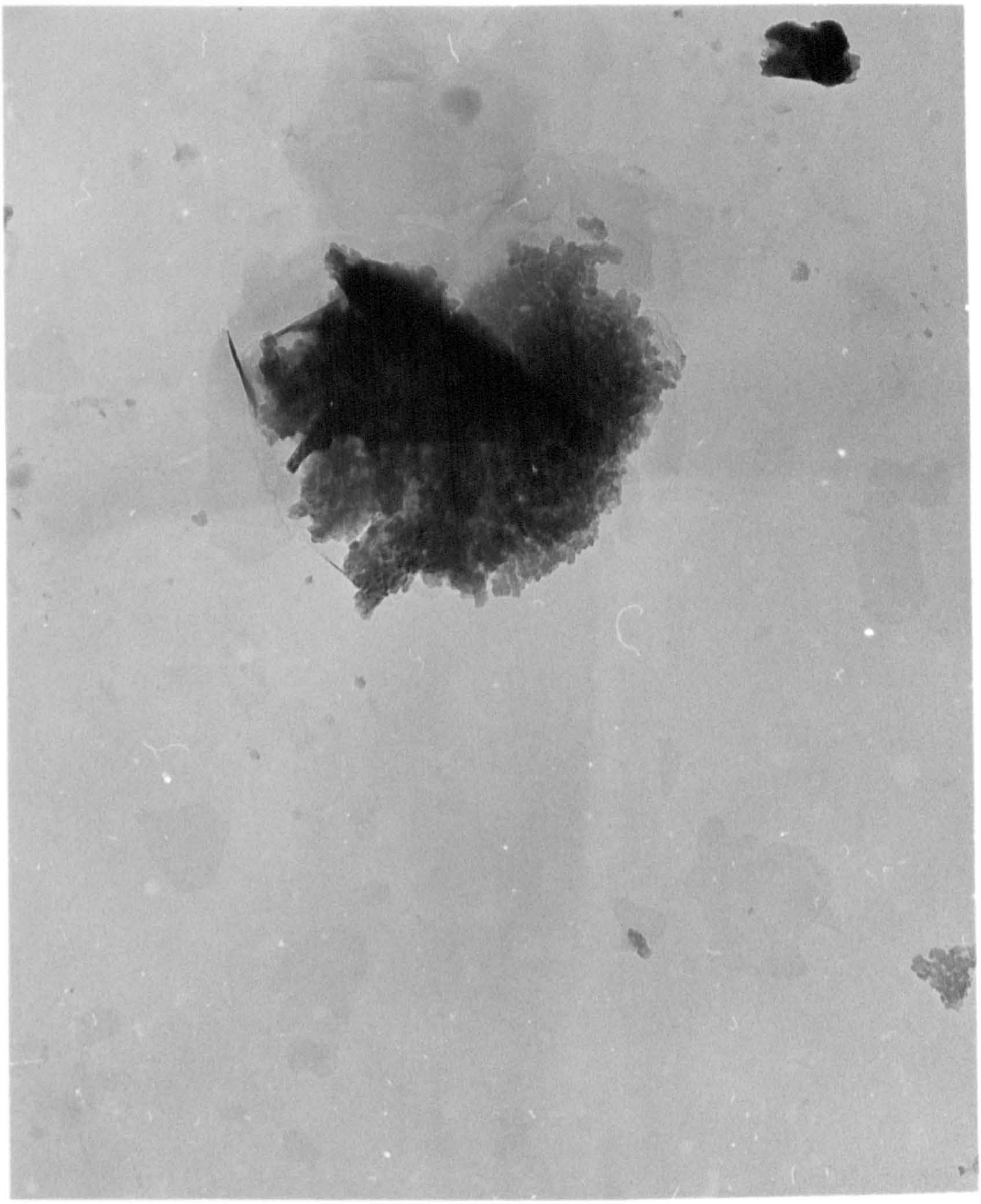

1µm

Fig. 22 : Transmission electron micrograph of full face Helms dispersion

1µm

Fig. 23 : Transmission electron micrograph of "cobbed" full face Helms dispersion

because cobbing removes most of the halloysite which occurs at the surfaces of the rock (sect. 5.3.3).

TEM of the full face Helms bentonite carbon replica revealed areas having the appearance of large undulating sheets with curled edges (fig. 24, 25), similar in appearance to previously published electron micrographs of carbon replicas of Wyoming and Montmorillon montmorillonites (5, 263). There were also areas, as shown in fig. 21, having coatings similar in appearance to the silica material observed directly (i.e. fig. 26). This suggests that some, at least, of the opaline silica present in the hard Helms material occurs as surface coatings on the montmorillonite, rather than interculated between the montmorillonite layers, as suggested by Chen (10).

5.3.5 Electron probe microanalysis (EPMA)

There was found to be some variation in the composition of the individual montmorillonite particles observed in full face Helms bentonite (figs. 20, 23); a representative electron probe micro-analysis (EPMA) spectrum is shown in fig. 27a, Al, Si, Mg, Ca and Fe were detected. This variation may be due to variations in the counter-ion composition and/or the occupancy of the octahedral and tetrahedral substitution sites, as suggested by Roberson (12, 13). The tubular particles observed (fig. 21) were found to contain similar amounts of Si and Al. This is consistent with them being halloysite (fig. 60). The "amorphous" particles observed (fig. 22)

1µm

Fig. 24 : Transmission electron micrograph of carbon replica of cleaved full face Helms bentonite rock surface

1µm

Fig. 25 : Transmission electron micrograph of carbon replica of cleaved full face Helms bentonite rock surface

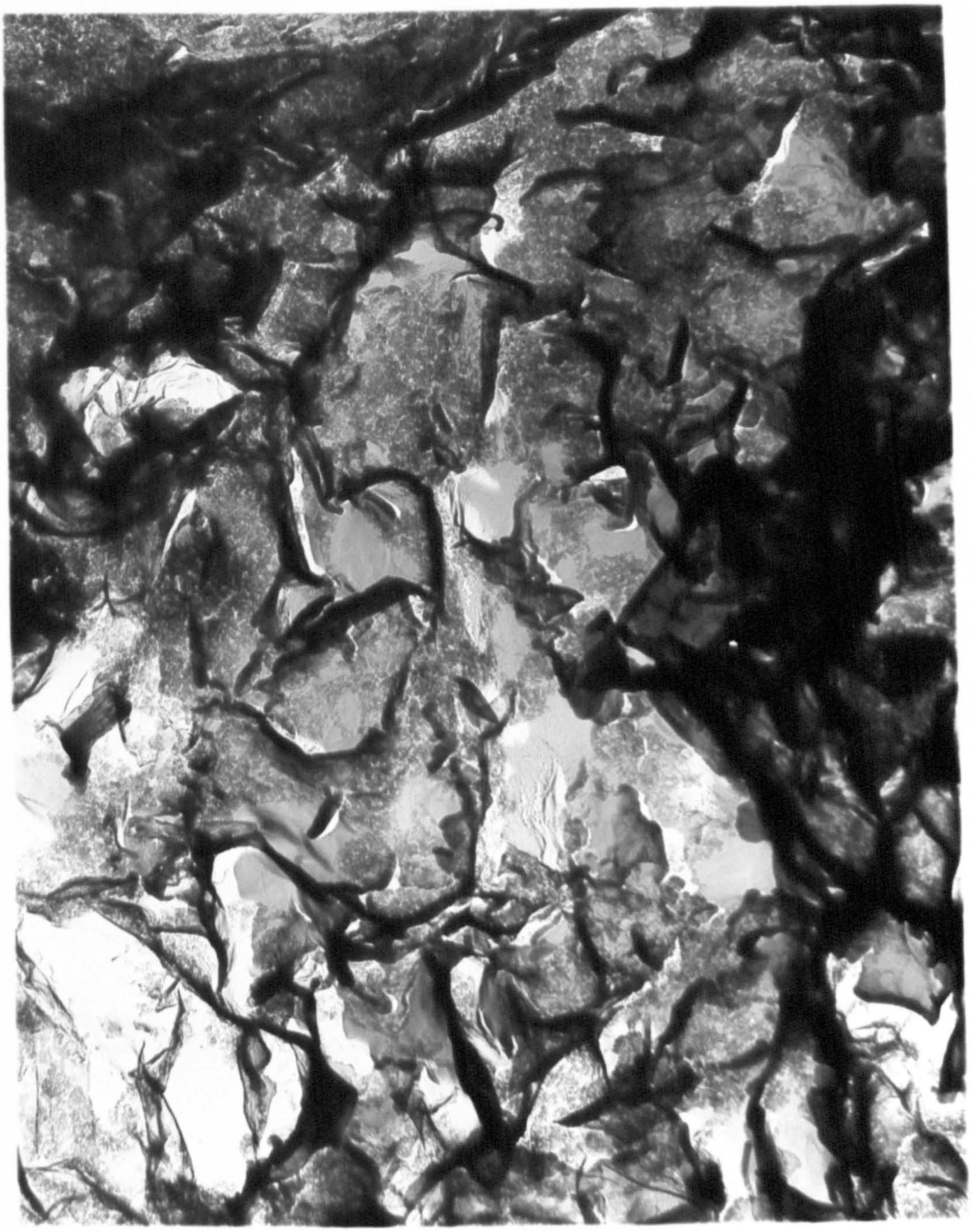

1µm

Fig. 26 : Transmission electron micrograph of carbon replica of cleaved full face Helms bentonite rock surface

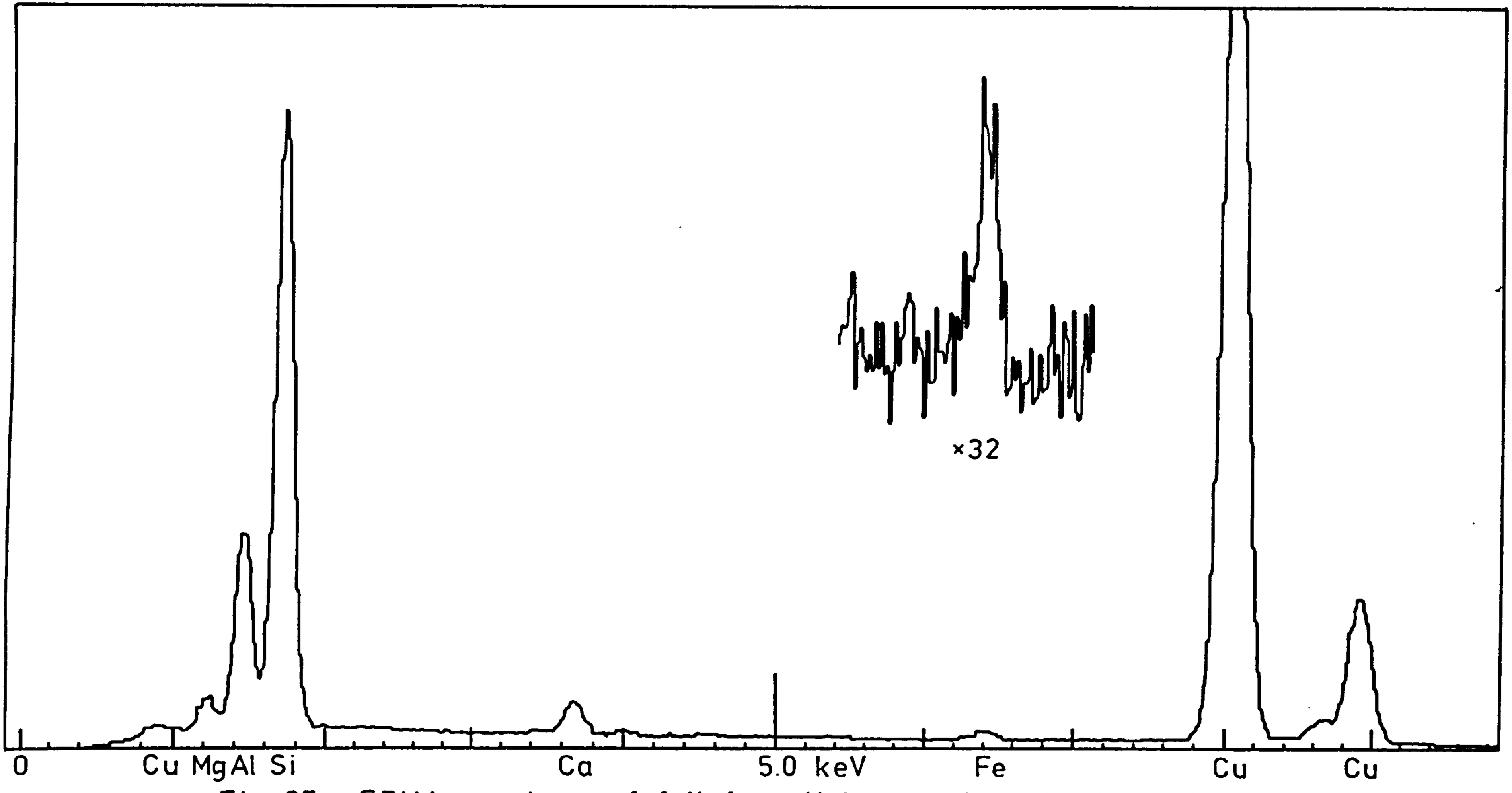

Fig. 27a: EPMA spectrum of full face Helms montmorillonite particle

were found to contain Si only, and probably make up the "opal-cristobalite" phase present in the Gonzales bentonites (sect. 4.2). The X-ray diffraction results (sect. 5.3.2) and the particle morphology observed by transmission electron microscopy (sect. 5.3.4) suggest that this silica phase is largely made up of Opal-CT (sect. 2.3.1.3).

Some of the surface coloured material on the full face Helms rock was suspended in water, put on a carbon coated grid and studied using EPMA. This material was found to be very variable in appearance and composition; the elements Al, Si, Mg, Cl, K, Ca, Ti, Fe and P were found (see for example fig. 27b).

5.3.6 Dispersion tests

The results of the dispersion tests are shown in table 10.

In view of the inaccuracies involved in the dispersion test, conclusions are only drawn where there is a large (~10%) difference in the degree of dispersion.

The dispersion tests show that the Wyoming bentonite disperses much more readily, in water, than the Texas, and other, bentonites (Table 10a-h). Also it seems that the hard Texas clays (Table 10e, f) disperse more readily than the soft clays (Table 10a, b, d) in water.

The results show that treatments which tend to convert the Texas clay (Bentolite L) into the Na or Li forms increase the degree of dispersion (Table 10i-m, s, t). This is also shown in fig. 28.

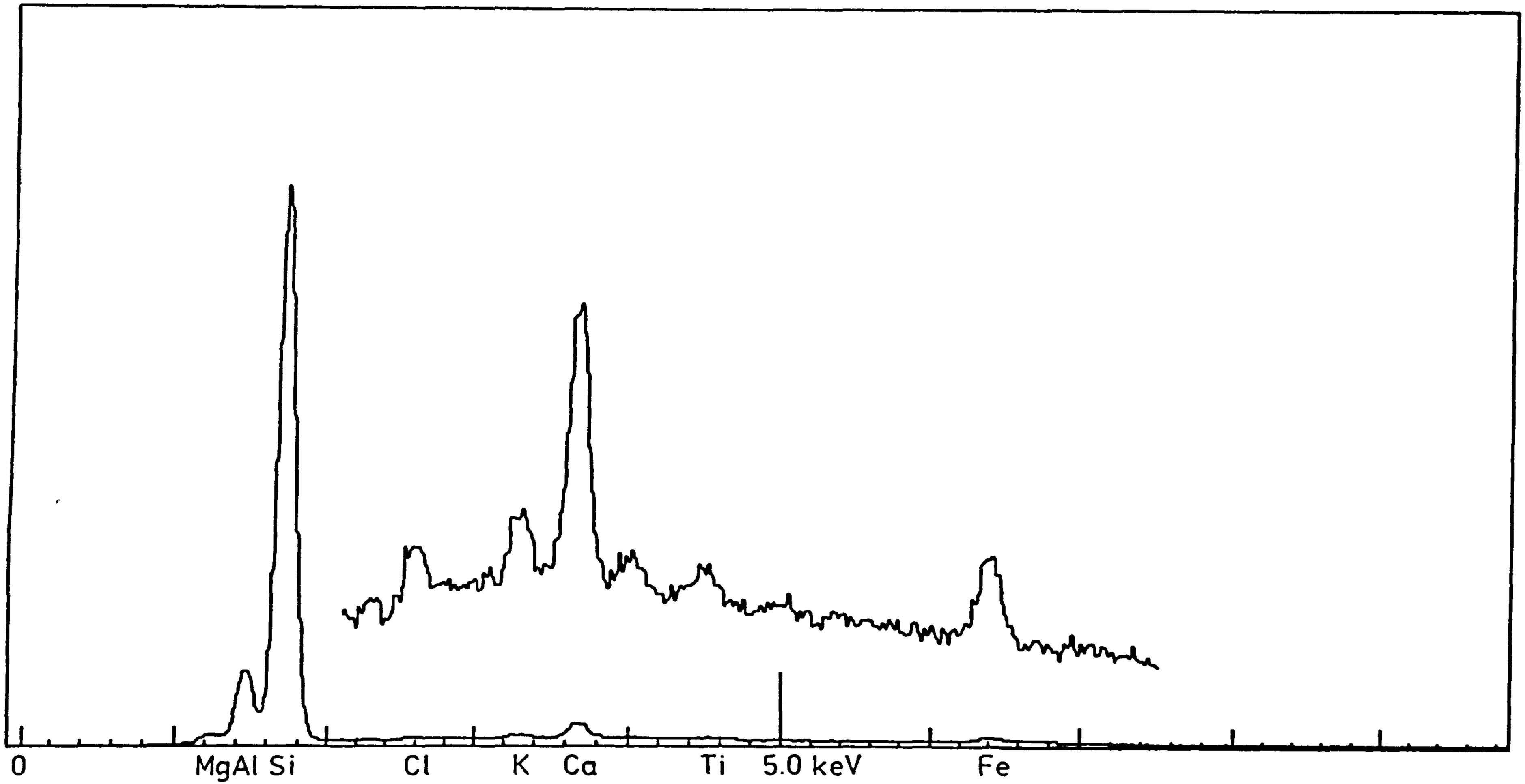

Fig. 27b: EPMA spectrum of full face Helms coloured surface material

Table 10: Dispersion test results

	Clay sample	Dispersion treatment	Stirring Time	Degree of Dispersion* 1%
a	Soft Clark	Water (natural pH)	30 minutes	18
b	Soft Helms	"	"	21
c	European	"	"	21
d	Cobbed soft Helms	"	"	29
e	Hard Helms	"	"	34
f	Bentolite L	"	"	36
g	Milos	"	"	48
h	Wyoming Blackhills	"	"	86
i	Bentolite L	1 mol dm^{-3} NaCl	"	66
j	"	6 mol dm^{-3} NaCl	"	(61+)
k	"	1 mol dm^{-3} NaCl	7 days	67
l	"	6 mol dm^{-3} NaCl	11 days	86
m	"	"	35 days	(103)
n	"	1 $3x10^{-3}$mol dm^{-3}EDTA(pH1·5)	30 minutes	-1
o	"	" (pH5·8)	"	57
p	"	" (pH10·5)	"	48
q	"	1 mol dm^{-3}NaCl+10^{-2}mol dm^{-3} EDTA(pH10·3)	"	74
r	"	1 mol $dm^{-3}NH_4Cl$	"	4
s	"	0·5 mol $dm^{-3}Na_2SO_4$	"	78
t	"	1 mol dm^{-3}LiCl	"	95
u	"	5 mol dm^{-3} Urea	"	59
v	"	~5% w/w Sodium hexameta phosphate	"	(109)

* - for $\gtrsim$6μm traction

Fig.28: Effect of Na-exchange of bentolite L on degree of dispersion

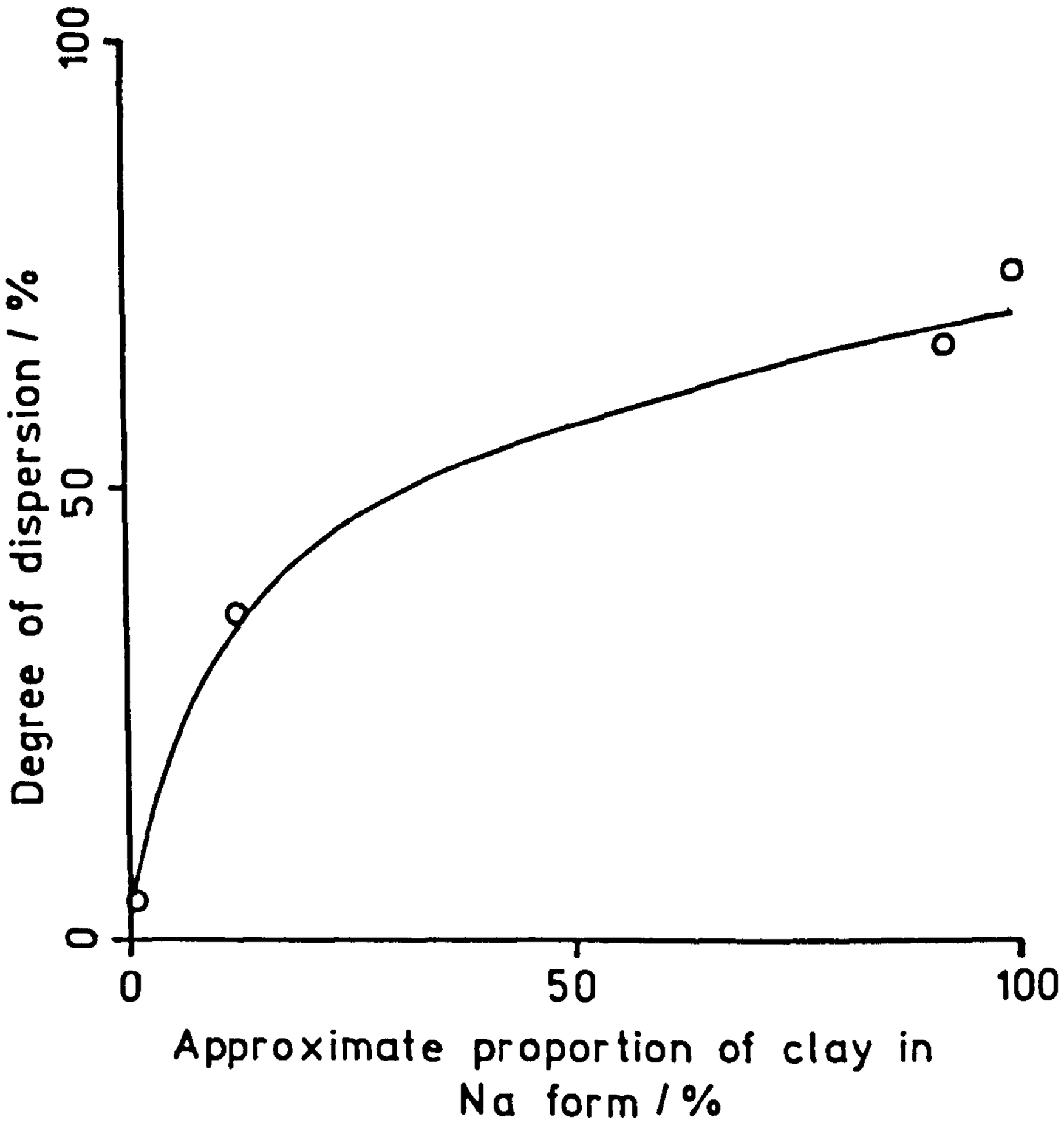

The use of ethylenediaminetetraacetic acid (EDTA) salts at medium to high pH tends to promote clay dispersion (table 10 o, p) since under these conditions it may remove calcium and other divalent ions from solution by complexation reactions (306). At low pH the clay is flocculated and does not disperse (Table 10n); this is probably due to "hydrolysis" of the clay (sect. 3.1.10) under the acid conditions.

The use of NaCl and EDTA in conjunction seems to be more effective than the use of either reagent on its own (table 10q). This is probably because the Na^+ for Ca^{2+} exchange equilibrium

$$\text{clay} - \text{Ca} + 2\text{Na}^+_{aq} \rightleftharpoons \text{clay} - \text{Na}_2 + \text{Ca}^{2+}_{aq}$$

proceeds further to the right hand side as aqueous Ca^{2+} ions are chelated by the EDTA. The use of Na_2SO_4 gives a similar result (Table 10s), possibly because, in this case, Ca^{2+} is removed from solution by precipitation of solid $CaSO_4$. It is also possible that the sulphate ions may remove any interlayer aluminium species present (307, 308, 309). The use of a sodium ion exchange resin in the presence of NaCl has also been shown to be effective in removing Ca^{2+} from Texas bentonites (310).

C H A P T E R S I X

PREPARATION OF CLAY DISPERSIONS

PREPARATION OF CLAY DISPERSIONS

6.1 INTRODUCTION

The preparation of well-defined clay dispersions is desirable in order to study the clay minerals behaviour. This chapter described the preparation of such clay dispersions.

Smectite particles normally have an 'equivalent spherical diameter' of less than 1 - 2μm and these size tractions may be obtained by sedimentation and/or centrifugation, having previously dispersed the material, usually in aqueous solution (19, 259).

The clay may be dispersed with the aid of physical and possibly chemical procedures (19, 334, 335, 336, 337). Although such treatments are best kept to a minimum since clay minerals may be easily damaged by (even apparently mild) mechanical processes or chemical treatments (259).

If the sample is suspected of containing organic material it may be subjected to a hydrogen peroxide treatment (19).

Having dispersed the clay mineral, the separation of particles >1μm in size by sedimentation in water under gravity or by centrifugation will often remove, or greatly reduce, the quantity of coarse non-clay minerals such as quartz, feldspars, coarse-particle micas and carbonates (259). Mineral impurities having similar particle sizes as that of the clay minerals are difficult to remove (19).

It is then usually desirable to convert the clay dispersion into the desired ion form, by ion exchange. This may be achieved by several treatments with an excess of 1 or 2 mol dm^{-3} solution of the

chloride of the chosen cation (19). This is best carried out at pH ≃ 7 (since H^+ is a cation also). Cation exchange may also be achieved with the aid of cation exchange resin (19).

After conversion of the clay into the desired ion form the dispersion must be washed free of excess electrolyte. This may be achieved by repeated decanting of the supernatant salt solution after settling and replacement with distilled water. Initially, while the clay is flocculated, the dispersion will sediment rapidly under gravity. In the later stages, when the clay becomes dispersed, high speed centrifugation and/or dialysis must be used (19, 145).

A diagrammatic representation of the preparation procedure is shown in fig. 29.

6.2 PREPARATION OF DISPERSIONS

6.2.1 Dispersion of samples

Various procedures were used to disperse the different bentonite samples. As already noted, the Texas (sect. 5.3.6) do not disperse as readily in water as the Wyoming bentonites. Hence the Texas bentonites were dispersed in a 1 mol dm^{-3} NaCl or LiCl solution (method B), rather than water (method A), in an attempt to exchange the clay into Na or Li form and hence increase the degree of dispersion.

Once the samples had been dispersed, the subsequent treatment given to each material was similar.

Fig. 29: Dispersion preparation procedure

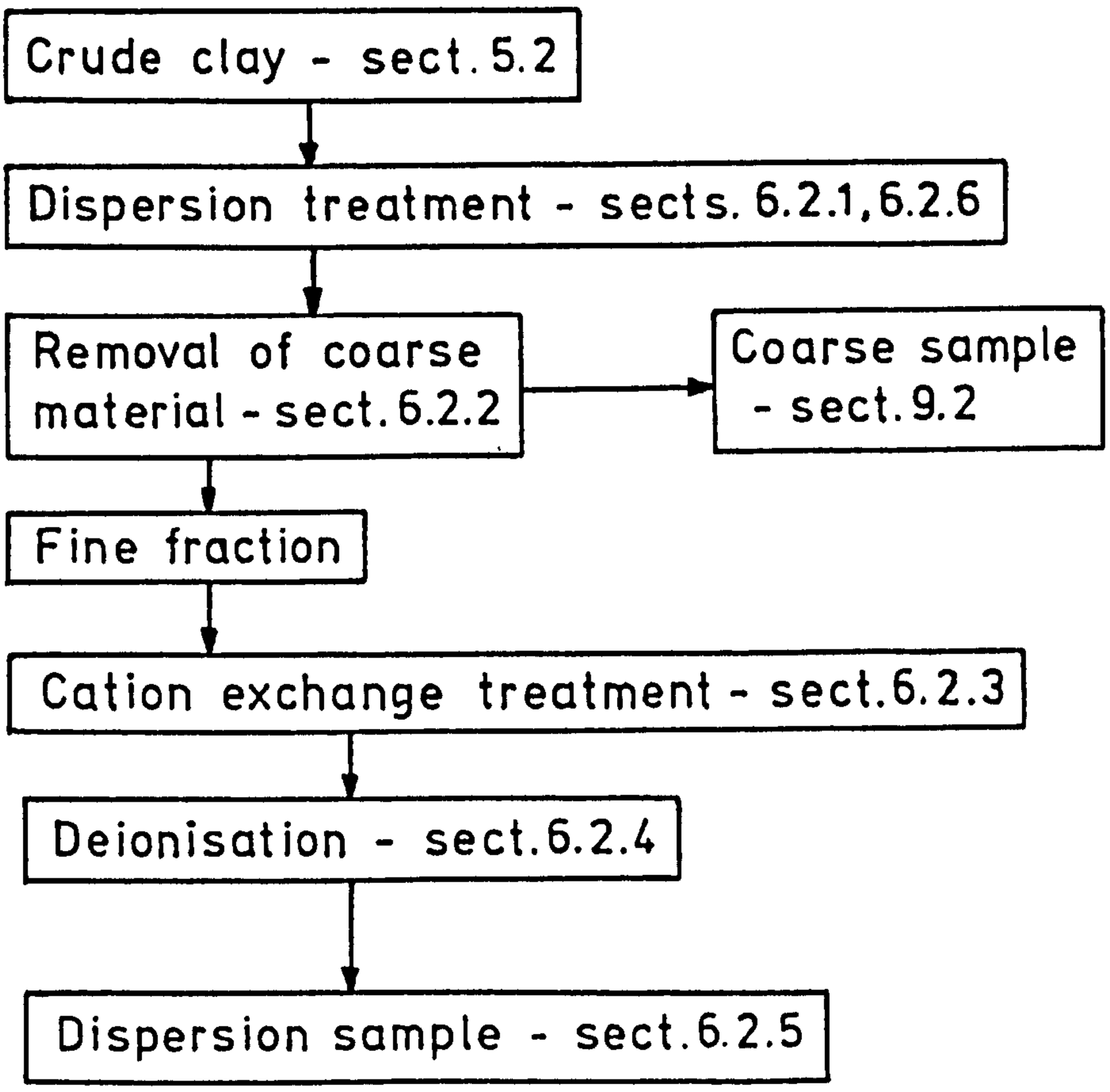

The dispersion methods were:-

i) Method A: This preparation was based on that of Barclay and Ottewill (173) and was found to be most effective for the more easily "water-dispersable", Wyoming bentonites. 200g of dry Wyoming Blackhills, or 50g of Wyoming Upton, bentonite was stirred in 2dm^3 of distilled water for 24 hours. This treatment results in the swelling and then dispersion of the smectite mineral as described in sect. 3.1.11.

This preparation method was also used to prepare samples of hard Helms, soft Helms, soft Clark and Milos bentonites, although the low degree of water-dispersion of these samples (sect. 5.3.6) resulted in only small quantities of dispersion being prepared.

ii) Method B: This preparation was used for the less readily "water-dispersable", Texas bentonites. 200g of dry Bentolite L or cobbed soft Helms was stirred in 2dm^3 of 1 mol dm^{-3} NaCl or LiCl solution for 24 hours. This procedure was found to result in the partial conversion of the, mainly Ca, clay into the Na or Li form, hence resulting in a better dispersion of the clay mineral (sect. 5.3.6).

This method was also used to disperse the samples of halloysite and beidellite.

iii) Method C: This preparation was used for samples that were found to contain large amounts of "free iron oxides" and is based on the method of Mehon and Jackson (266). This treatment would also remove most of any manganese oxide present (11). This treatment has been shown to have almost no effect on the clay mineral structure, but may increase the Fe^{2+}:Fe^{3+} ratio in the minerals (279).

200g of dry soft Clark or Milos bentonite was added to 400 cm^3 of water in a 1 dm^3 round-bottom reaction flask, 70·6g of tri-sodium citrate and 8·4g of sodium hydrogen carbonate were added. The mixture was stirred and its temperature brought to 80°C by heating in a water bath. 20g of solid sodium dithionite was then added and the stirring continued for 15 minutes. (It was noticed that there was a colour change, from red/brown to green, of the mixture upon addition of the sodium dithionite - indicating reduction of the iron oxides). 200cm^3 of water and 58g of of sodium chloride were added to the mixture, followed by the slow addition of 200cm^3 of acetone. The mixture was allowed to cool and was then transferred to a 3dm^3 beaker and made up to a volume of 2dm^3 using 1 mol dm^{-3}NaCl, stirred and allowed to stand for 48 hours. The supernatant liquid was decanted from the flocculated clay sediment and discarded, 1mol dm^{-3} NaCl solution was added to the clay to bring the volume to 2dm^3, the mixture was then stirred to redisperse the clay and allowed to stand for a further 48 hours. This

procedure was repeated several times until there was no longer any green colouration visible in the supernatant liquid.

iv) Method D: This method was used in an attempt to achieve a more complete exchange of Ca^{2+} ions from the Bentolite L clay (sect. 5.3.3). $2dm^3$ of a 5mol dm^{-3}LiCl and 0·1 mol dm^{-3} of ethylenediaminetetra-acetic acid (EDTA) was prepared and its pH adjusted to 6·6 using LiOH. 200g of Bentolite L was added to this solution and stirred for 3 days. The mixture was allowed to stand for 48 hours, the supernatant was removed and discarded, a further $1dm^3$ of 5mol dm^{-3}LiCl, 0 1mol dm^{-3} EDTA, pH6·5 solution was added to the clay sediment and stirred for a further 7 days. The dispersion was allowed to stand for 3 days and the supernatant was discarded.

The flocculated dispersions produced by methods B, C and D were de-flocculated by washing free of salt. This was achieved by allowing the dispersion to sediment for 24 hours, decanting off the supernatant liquid, adding water to give a volume of 2 - 2·5 dm^3 and stirring for 30 minutes. This was repeated several times until the dispersion was no longer appreciably flocculated. The salt concentration at which this de-flocculation occurred was calculated to be of the order of 10^{-2}mol dm^{-3}LiCl or NaCl.

6.2.2 Removal of coarse material

The dispersion was allowed to stand for at least 5 days, after

which the dispersion was decanted from any coarse sediment. This coarse material was retained for further study (chapter 9).

The dispersed clay was then centrifuged at 18,000rpm for one hour to bring all the clay to the bottom of the tube as a gel. The supernatant liquid was poured off and the fine (upper) fraction of the gel was separated from any coarse material at the bottom of the centrifuge tube and retained. Any coarse material was discarded. The retained material was anticipated to be <2μm in size.

6.2.3 Ion exchange

The fine clay fraction obtained above was dispersed in 1 mol dm^{-3} salt and stirred for at least 24 hours. The clay was centrifuged at 16,000rpm for 40 minutes (methods A and B) or sedimented for 24 hours (methods C and D), the supernatant discarded and the clay redispersed in 1mol dm^{-3} salt solution. This procedure was repeated a further 3 times, the clay being redispersed in water after the final centrifugation/sedimentation. By using LiCl, NaCl, KCl, CsCl or $CaCl_2$ solution to wash the clay it was possible to prepare the clays in the Li^+, Na^+, K^+, Cs^+ or Ca^{2+} forms respectively.

6.2.4 Deionisation

The clay dispersion was dialysed against water for at least 7 days, with daily changes of dialysate, after which the salt concentration was estimated to be of the order 10^{-3}mol dm^{-3}. The dispersion

was then further deionised using mixed bed ion exchange resin.

The resins used were 'analytical grade' resins supplied by Bio-Rad Ltd. (AG50W-X4 cation exchange resin and AG1-X4 anion exchange resin). The resins were further cleaned by the method of Vanderhoff et al (267, 268, 269). The resins were washed with an 85% water : 15% methanol solution until no more colour was removed. The resins were then washed with an excess of 3 mol dm^{-3}NaOH, hot water, methanol, cold water, 3 mol dm^{-3}HCl, hot water, methanol and cold water. This was repeated a further 3 times. The anion and cation exchange resins were then washed with an excess of 3 mol dm^{-3} NaOH or 3 mol dm^{-3}HCl respectively. The resins were then washed frequently (3 or 4 times a day) for at least 14 days with double distilled water. The resins were washed 5 times with double distilled water immediately before use. Vanderhoff et al (267) claim that resins prepared in this way can be used in experiments of large surface area without introducing an appreciable amount of contamination.

The dispersion to be deionised was stirred in a beaker, whilst its pH was monitored using a pH electrode (Radiometer G202B glass electrode and K401 calomel reference electrode). The concentration of the dispersion at this stage was approximately 2% by weight. Small amounts ($\sim$1cm^3) of resin were then added to the dispersion, whilst observing the resulting pH changes. Upon addition of OH^--resin the pH increased because of exchange of OH^- ions for any co-ions present in the system. Addition of H^+-resin gave a decrease in pH as H^+ ions were exchanged for counter-ions

present. OH^--resin and H^+-resin were added to the mixture alternately such that the pH remained within the range 4 to 10 at all times, in order to reduce "hydrolysis" of the clay to a minimum (19, 270). This was repeated until the pH no longer increased upon addition of OH^--resin i.e. all co-ions had been exchanged for OH^- ions. It was noticed that further addition of OH^--resin at this stage would actually cause a slight decrease in pH). H^+-resin was then added to change the pH to 6 (±0·5). If the pH dropped below ~6 LiOH or NaOH was added to return the pH to the desired value.

The resin was then removed from the dispersion by vacuum filtration through a no.1 size glass sinter funnel, the de-ionised clay dispersion being collected in a Buchner flask. The used resin was removed from the funnel, washed free of clay particles with water and retained for later regeneration.

If an excess of H^+-resin was added to the dispersion it was found that the pH dropped to very low values (typically <3) and the dispersion became very viscous and very difficult to filter. This treatment would have presumably exchanged most of the counter ions for H^+ and then the clay lattice would be attacked under the acid condition causing dissolution of Al^{3+} and Mg^{2+} etc. from the clay (19, 119, 271, 272, 273).

It would be expected that the pH drop upon addition of excess H^+-resin would be dependent on the surface charge density and the volume fraction concentration of the clay, i.e. the suspension effect.

The used (mixed bed) ion exchange resin was regenerated by

adding 3 mol dm^{-3} NaOH to the resin and separating the two resins by decanting off the (now less dense) OH resin. Both resins were then treated with one cleaning cycle as described above before re-use.

6.2.5 Final sample preparation

A known volume of 1 mol dm^{-3} salt solution or a known weight of solid salt (for higher electrolyte concentration) was added to the deionised dispersion, to give the required electrolyte concentration, and the dispersion was shaken.

The dispersion was centrifuged at 16,000 rpm for 2 hours and different amounts of the sedimented gel were redispersed by stirring or occasional shaking in either uncentrifugal dispersion or the supernatant liquid from the centrifuge tubes to give dispersions having a range of clay concentration.

The dispersions so prepared were studied by pulse shearometry within 3 days of preparation, in order to reduce any significant ageing effects, which could have occurred slowly in dispersions at low ($<10^{-3}$ mol dm^{-3}) ionic strength (152).

Double distilled water and AnalaR reagents were used for all processes subsequent to de-ionisation.

6.2.6 Other preparations

i) Method E: A sample of Li Bentolite L (prep. B) was subjected to a very high shear homogenisation treatment (310), after which the

dispersion was washed once with 1 mol dm^{-3} LiCl solution and then deionised and prepared as described above. This sample was referred to as homogenised Li Bentolite L. This treatment was found to reduce the mean particle size (as measured by light scattering) from 0·65μm (Li Bentolite L) to 0·45μm (homogenised Li Bentolite L) (276).

ii) Method F: 10g of dry Bentolite L or cobbed soft Helms was added to 200cm^3 of 10·5mol kg^{-1}LiCl solution (∿13·5mol dm^{-3}) (almost saturated) and stirred, using a magnetic stirrer, for 28 days. The dispersion was washed several times with water in order to reduce the salt concentration. The coarse material was removed by sedimentation and retained.

iii) Method G: The method of Fey + Le Roux (277) was used in an attempt to remove the free silica from Bentolite L. 0·2g of dry Bentolite L was added to 20cm^3 of 0·3 mol dm^{-3} ammonium oxalate solution at pH3 and shaken for 5 hours. Study of the dispersion by transmission electron microscopy (section 7.3.3) indicated that there was still free silica present in the sample. No further work was carried out with this technique.

C H A P T E R S E V E N

CHARACTERISATION OF CLAY DISPERSIONS

CHARACTERISATION OF CLAY DISPERSIONS

7.1 INTRODUCTION

The clay dispersions, prepared as described in chapter 6, were characterised by X-ray fluorescence, X-ray diffraction, electron microscopy and other techniques. These studies are described in this chapter.

7.2 EXPERIMENTAL

7.2.1 Chemical analysis

A sample of dispersion was dried at 120°C to give ∿5g of dry clay. The chemical composition of this sample was obtained using X-ray fluorescence analysis (sect. 5.2.2) by English Clays, Lovering, Pochin and Co. Ltd. The chemical formulae of the montmorillonites were then calculated (appendix 4).

7.2.2 X-ray diffraction

The (powder) X-ray diffraction (XRD) patterns were also obtained for the above samples, as prepared for X-ray fluorescence analysis by English Clays, Lovering, Pochin and Co. Ltd.

The Hofman-Klemen (127) and Greene-Kelley (278) test was used in an attempt to distinguish montmorillonite and beidellite in the bentonite samples. A Li-clay sample was heated at 200°C, in an oven, for 48 hours, saturated with glycerol for at least 7 days and an XRD pattern was obtained. The Li^+ ions migrate into the clay lattice upon heating and if the layer charge is due to octahedral substitution (montmorillonite) the layer charge is neutralised and the mineral does not re-expand with the glycerol treatment giving a d-spacing of ~9·5Å. If the layer charge is due to tetrahedral substitution (beidellite) the clay re-expands with glycerol treatment giving a 17·7Å d-spacing.

7.2.3 Transmission electron microscopy

Specimen preparation

Samples of clay dispersed in $\lesssim 10^{-3}$ mol dm^{-3} electrolyte were diluted with water, before mounting onto microscope grids.

Two preparative methods were used.

i) Method a: A cytochrome c film was formed on top of a carbon coated microscope grid. This was achieved by coating a glass microscope slide with carbon, in a vacuum evaporator, floating the carbon film off the slide onto the surface of some water in a petri-dish. Copper electron microscope grids were then lifted through the carbon film. This resulted in a carbon film being spread across the grids. A few

crystals of cytochrome c were then dissolved in some water in a petri-dish. A dried carbon coated grid was then placed, carbon film downwards, on the liquid surface. This resulted in the carbon becoming coated with a thin film of the cytochrome c protein. The grid was then allowed to dry. The grid was then placed, protein film downwards, on top of the dilute clay dispersion. The grid was removed, washed with water, and dried. Clay particles which had adhered to the protein film were then studied in the electron microscope. This procedure was found to result in the individual clay particles being well spread out across the grid, although the fine fraction of the clay dispersion would tend to be collected.

ii) Method b: A drop of diluted clay dispersion was spotted onto a cytochrome c coated carbon grid, prepared as above, using a platinum wire loop, and dried. This procedure should give a more representative picture of the sample than method a, but it would be difficult to distinguish aggregates from individual clay particles which had aggregated upon drying.

These specimens were then studied using either a Hitachi H57, H57s or Joel 100CX transmission electron microscope.

7.2.4 Electron probe microanalysis

Particles in some of the specimens prepared for transmission electron microscopy (sect. 7.2.3) were analysed using electron probe microanalysis, as described in sect. 5.2.6.

7.2.5 Cation exchange capacity determinations

A known amount (∿0·1g) of Na-clay, in dispersion, was stirred in 100cm^3 of 1 mol dm^{-3} ammonium acetate solution for 4 days, a small amount (∿5mg) of calcium hydroxide was added to the dispersion, stirred and the Na^+ concentration measured using a calibrated (in 1 mol dm^{-3} ammonium acetate) sodium ion selective electrode (Radiometer G50Na sodium selectrode and a K401 calomel reference electrode). The Na^+ concentration in the Na-clay dispersion, added to the ammonium acetate solution was also measured using the sodium electrode (calibrated in water). From the results, assuming the NH_4^+ ions expelled all of the Na^+ ions from the clay surface, and that all the clay counterions were Na^+, the cation exchange capacity (CEC) of the clay could be calculated, using equation 41.

$$CEC = \frac{\text{amount of } Na^+ \text{ expelled/molx10}^5}{\text{weight of clay added/g}} \quad \text{meq/100g} \qquad (41)$$

Calibration plots for a Na^+ electrode are shown in fig. 1 appendix 8. The same stirring conditions were used for calibration and measurement using the Na^+ electrode, and in both cases 4 minutes were allowed for the electrode to reach equilibrium before the readings were noted.

The cation exchange capacities were also determined by stirring a known amount of Li-clay in 100cm^3 of 1 mol dm^{-3} ammonium acetate or 2 mol dm^{-3} ammonium acetate for 5 days and allowing the flocculated clay to sediment. Samples of the clear supernatant were removed, diluted by a factor of 100 and analysed for Li^+ using atomic emmission spectroscopy (at wavelength = 670·7nm) by Dr. D.J. Roberts. A

calibration plot is shown in fig. 126 appendix 8. The CEC was calculated by the method described above.

7.2.6 Transient Electric Birefringence

The particle size distribution of Li Bentolite L and Li Wyoming Blackhills dispersions were measured using a transient electric birefringence technique in the laboratory of Prof. B.R. Jennings. Transient birefringence is induced in the dispersion by applying a pulsed electric field. The rate of decay of birefringence, after termination of the field, is measured, analysed and the rotary diffusion coefficient, and size, of the particles calculated (280, 281).

7.2.7 Calcium analysis

The amount of calcium present in some of the dispersions was measured using a procedure similar to that used to measure the cation exchange capacities (sect. 7.2.5). A known amount of clay was dispersed in 1 mol dm^{-3} ammonium acetate solution and the Ca^{2+} concentration in solution then measured using a calibrated Ca^{2+} selective electrode (Radiometer F211Ca calcium Selectrode and a K401 calomel reference electrode). A calibration plot is shown in fig. 125, appendix 8.

7.2.8 Scanning Electron Microscopy (SEM)

Specimen preparation

Two preparative methods were used.

i) Cytochrome c method: A cytochrome c film was spread onto a SEM stud. This was achieved by dissolving a few crystals of cytochrome c in some water in a petri-dish. The flat surface of an aluminium SEM stud was then placed on the liquid surface, removed and dried. This resulted in the stud surface being coated with a thin film of the cytochrome c protein. Some of the sample dispersion was then placed on the stud, which was then washed with water, dried and sputter coated with gold. The specimen was then examined by SEM using a Cambridge Stereoscan scanning electron microscope.

ii) Freeze-drying method: Some specimens were prepared by a freeze-drying technique, currently under development (311). The following procedure was carried out by Dr. D.W. Thompson. A thin film of the dispersion (10 - 20μm thick) was formed on the surface of freshly cleaved muscovite mica by immersing a small piece of mica (5 x 5mm square) in the dispersion and subsequently syphoning off most of the adhering dispersion by touching the edge of the mica square, on absorbent paper. The dispersion film was then frozen rapidly by immersion in liquid isopentane at -150°C. The frozen film on the mica support was clamped to a large block of copper which had previously been cooled to -196°C by immersion in liquid nitrogen. The cold copper block together with the frozen dispersion sample was placed in the chamber of a vacuum coating unit and pumped using a single stage rotary pump for a period of 12 hours. During this time, complete sublimation of the dispersion medium occurred leaving the dry particles supported on the mica surface. The mica support was

glued to a metal specimen holder using graphite paste, sputter-coated with a thin layer of gold and examined by SEM using a Jeol 100CX TEM-SCAN electron microscope.

This technique may give a better representation of the structure of particles in dispersion (313), although there is disagreement as to whether such techniques can give meaningful results or not (52, 263, 311, 315, 316).

7.2.9 Electrophoresis

The electrophoretic mobilities of particles in clay dispersions were measured using the Pen-Kem system 3000 equipment (282, 283). This is a micro-electrophoresis apparatus in which the particles, in a dispersion, are viewed in a ~1mm diameter cylindrical silica cell. The particles are illuminated by a helium-neon laser, with associated optics, such that only the particles at the focal plane of the microscope system are illuminated. An image of these particles is projected onto the surface of a rotating glass disc containing a precision radial grating. Upon application of a potential across the two palladium electrodes at each end of the cell, if the particles move electrophoretically, then the frequency shift with respect to the grating movement, is detected and converted into the electrophoretic mobility distribution by a fast Fourier transform analyser and microcomputer.

7.3 RESULTS AND DISCUSSION

7.3.1 Chemical Analysis

The results of chemical analyses by X-ray fluorescence analysis (sect. 7.2.1) are given in appendix 3, table 33. The chemical formulae calculated (appendix 4) from this data are given in table 11.

These results show that the preparation methods A and B do not seem to have been completely successful at obtaining homoionic clays. This is indicated by the CaO_1K_2O and Na_2O analyses for Li Wyoming Blackhills, Li Bentolite L and Li cobbed soft Helms, and the CaO and K_2O analyses for these clays in the Na form shown in table 33, appendix 3. The results (table 11) indicate degrees of exchange from 90 to 97% for the Na clays and 89% for Li soft Clark bentonite.

The samples prepared by methods C (Li soft Clark and Li Milos) and D (Li Bentolite L), appear to be more completely exchanged (ie$>\sim$85%). It is possible that the application of heat, during preparation method C, has increased the rate and/or degree of exchange of the clay into the Na form which is then more easily exchanged into the Li^+ form, than a Ca^{2+} clay would be (sect. 3.1.10). The use of EDTA in conjunction with LiCl solution is probably more effective at exchanging Ca^{2+}, and other ions, from the clay surface by the mechanism described in sect. 5.3.6.

TABLE 11: Chemical formulae of bentonite preparations

Sample	Method	Tetrahedral Cations		Octahedral Cations					Interlayer Cations				CEC/ neq/	Anions (O=10)	Impurity Silica	
		Si	Al	Al	Fe^{3+}	Fe^{2+}	Mg	Total	Ca^{2+}	Na^{+}	K^{+}	Li^{+}	100g	OH_1F	XRD	Calc
Na Wyoming	1	3·97	0·03	1·57	0·18	0·05	0·18	1·98	0·01	0·25	0	0	76	2·00	3	0
Blackhills	2	3·98	0·02	1·59	0·16	0·07	0·18	2	0·01	0·25	0	0	76	2·07	3	0
Na Bentolite L	1	4	0	1·61	-0·04	0·10	0·31	1·97	0·01	0·37	0·01	0	116	2	15	8
	2	3·99	0·01	1·63	-0·04	0·09	0·31	2	0·01	0·38	0·02	0	117	2·09	15	9
Na cobbed	1	3·99	0·01	1·58	0·04	0·02	0·35	1·99	0	0·37	0·01	0	109	2	4	29
soft Helms	2	3·99	0·01	1·59	0·03	0·03	0·35	2	0	0·37	0·01	0	109	2·03	4	29
Li soft Clark	1	3·83	0·17	1·64	0·20-0·15		0·36	2·05	0	0·04	0	0·33	108	2	-	0
	2	3·80	0·20	1·59	0·24-0·18		0·35	2	0	0·04	0	0·33	108	1·83	-	0

The prepared colloidal dispersions contain similar amounts of TiO_2 to the crude materials, which is surprising since the amounts of associated minerals present have been reduced in these samples (sect. 7.3.2). This suggests that the TiO_2 is present either as a constituent of the clay mineral or as associated mineral (e.g. anatase (sect. 2.3.7)) particles that have a similar size to the clay mineral particles, possibly rendering them difficult to separate by centrifugation (19). However, since there is a density difference between anatase and montmorillonite of $\sim 3 g cm^{-3}$ the latter possibility seems unreasonable.

The chemical analysis results for the Li and Na Wyoming Blackhills are very similar to each other (except for the Na_2O results) (table 33, appendix 3).

The calculated chemical formulae for Na Wyoming Blackhills bentonite (table 11) suggest that this sample is purer than the crude materials, since these were not the problems in the calculation of octahedral Fe found with the latter material (table 6). The values for total octahedral cations and OH,F are also closer to the ideal value of 2, for methods 1 and 2 respectively.

The negative octahedral Fe^{2+} values for Na Bentolite L (table 11) are probably due to excess NaCl in the sample, c.f. soluble impurities in crude Wyoming Blackhills bentonite (sect. 5.3.1).

The negative octahedral Fe^{2+} values for Li soft Clark bentonite (table 11) suggest that there may be interlayer cations present other than Ca^{2+}, Na^{+}, K^{+} and Li^{+}. These may be Al, Mg^{2+} or H^{+} ions, possibly due to clay mineral damage due to heating during preparation (method C, sect. 6.2.1).

7.3.2 X-ray diffraction

The X-ray diffraction (XRD) results for Li Wyoming Blackhills, Li Bentolite L, Li Bentolite L (prep. D), Li cobbed soft Helms, Na Wyoming Blackhills, Na Bentolite L and Na cobbed soft Helms shown in appendix 7 and in table 12 indicate that the amounts of coarse impurities (mica, quartz and feldspars) have been much reduced in the colloidal dispersions with respect to the crude bentonites. There seems to have been a significant reduction in the amount of opal-CT in the samples, although reasonable amounts are still present in the Bentolite L samples.

The Greene-Kelly test results (figs. 30 - 35) indicate that all the samples, except Li Bentolite L and the fine fraction of Li Bentolite L, give only one peak at $2\theta \approx 9{\cdot}6$A, indicating the presence of montmorillonite only. The occurrence of a second peak at $\sim 17{\cdot}7$A in the patterns for Li Bentolite L (fig. 31) and the Li Bentolite L fine fraction (fig. 35), could be interpreted as due to the presence of beidellite in the samples. However, it seems more likely that this is an artifact due, at least in part, to the presence of Ca montmorillonite in the samples (sect. 7.3.7). This is because Ca montmorillonite would not lose its cation exchange capacity upon heating, as does Li montmorillonite (sect. 7.2.2), and would swell in the normal manner upon treatment with glycerol (sect. 3.1.11).

It is interesting to note that, if this is the case, the Ca montmorillonite seems to be present in the fine fraction rather than the coarse fraction of Li Bentolite L (fig. 34) and this seems to be

TABLE 12: X-ray diffraction results

Sample	2θ/°	d-spacing/Å	Band assignment
Li Wyoming Blackhills	8·0	11·1	smectite
	19·9	4·46	smectite-dioctahedral
	21·0	4·23	low quartz
	22·1	4·02	feldspar
	26·8	3·33	low quartz
	28·6	3·12	smectite
	35·0	2·56	smectite
Na Wyoming Blackhills	8·0	11·1	smectite
	18·8	4·72	smectite
	20·8	4·27	low quartz
	22·0	4·04	feldspar
	26·6	3·35	low quartz
	28·2	3·16	smectite
	36·0	2·49	low quartz
Li Bentolite L	7·6	11·6	smectite
	19·8	4·48	dioctahedral smectite
	21·8	4·08	opal-CT, low tridymite
	28·8	3·10	smectite
	35·0	2·56	smectite
Li Bentolite L (preparation method D)	7·4	11·9	smectite
	19·8	4·48	dioctahedral smectite
	21·8	4·08	opal-CT, low tridymite
	28·6	3·12	smectite
	35·0	2·56	smectite

TABLE 12 (continued)

Sample	2θ/°	d-spacing/Å	Band assignment
Na Bentolite L	7·0	12·6	smectite
	14·0	6·33	-
	19·8	4·48	dioctahedral smectite
	21·6	4·11	opal-CT, low tridymite
	28·6	3·12	smectite
	35·4	2·54	smectite
Li cobbed soft Helms	7·6	11·6	smectite
	12·3	7·2	7Å-halloysite
	19·8	4·48	dioctahedral smectite
	21·6	4·11	opal-CT, low tridymite
	28·4	3·14	smectite
	35·0	2·56	smectite
Na cobbed soft Helms	7·0	12·6	smectite
	14·0	6·33	-
	19·6	4·53	smectite
	21·6	4·11	opal-CT, low tridymite
	26·5	3·36	low quartz
	28·4	3·14	smectite
	35·4	2·54	smectite

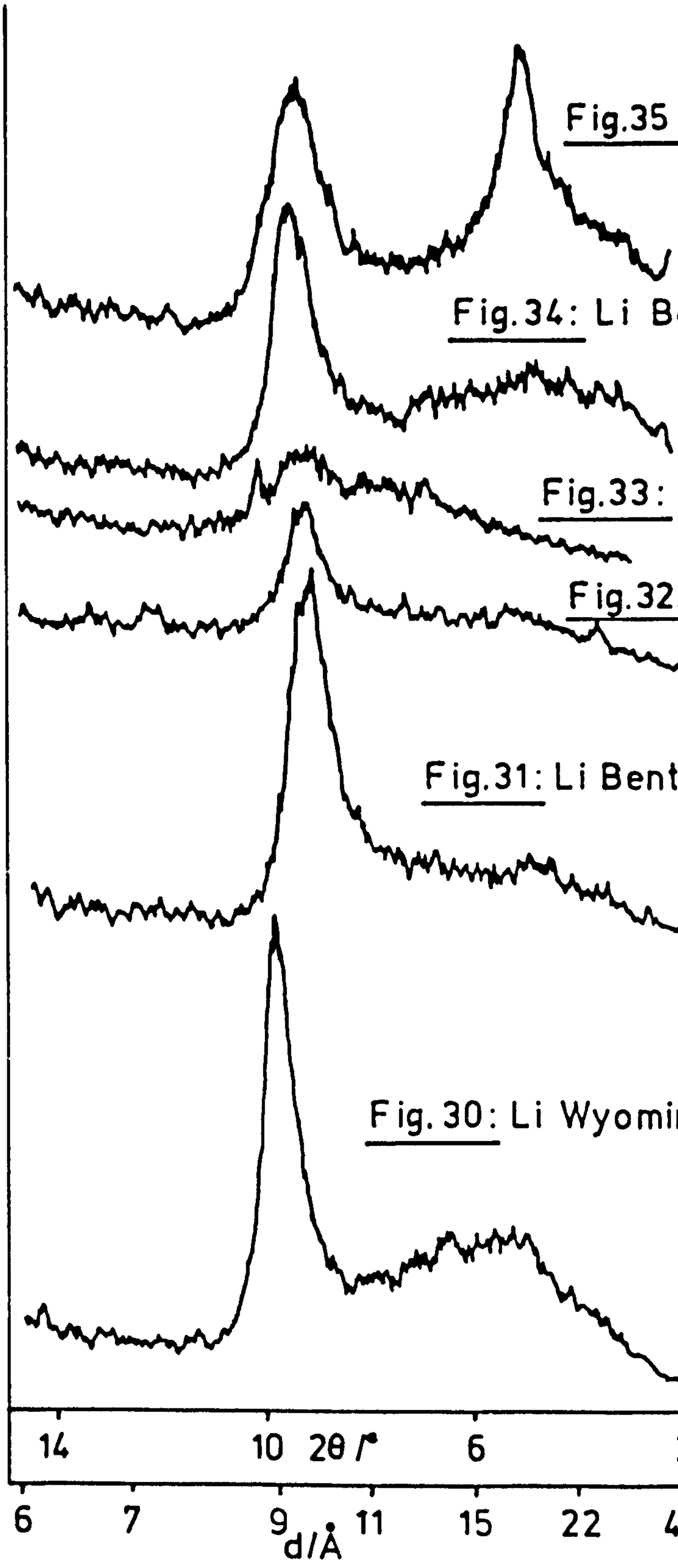

Fig.35 : Li Bentolite L
- prep.
- fine fraction

Fig.34: Li Bentolite L - prep.
- coarse fraction

Fig.33: Li beidellite

Fig.32: Li cobbed soft Helms

Fig.31: Li Bentolite L

Fig.30: Li Wyoming Blackhills

X-Ray diffraction - Greene-Kelly test results

confirmed by electron probe microanalysis measurements (sect. 7.3.5). This suggests that the incomplete dispersion of the coarse fraction of Li Bentolite L is <u>not</u> due to the presence of Ca montmorillonite or beidellite.

7.3.3 <u>Transmission electron microscopy</u>

Transmission electron microscopy (TEM) of the Wyoming bentonite (Wyoming Blackhills and Wyoming Upton) dispersion samples (figs. 36 - 47) suggests that they both consist mainly of thin irregularly shaped montmorillonite particles, some of which are ~1μm in length, as shown in figs. 36 and 37. These particles in Li Wyoming Upton seem to show a greater tendency to aggregation and curling (figs. 37 and 38) than those in Li Wyoming, Blackhills (fig. 36). These samples contain few impurities.

Na Wyoming Upton and Na Wyoming Blackhills are similar in appearance to the Li clays as shown in figs. 39 to 41. Some montmorillonite aggregates present in NaWB (fig. 40) were observed, under higher magnification, to show regions indicating a repeating layer structure of ~1μm, as shown in fig. 42. It seems that these layers correspond to the individual smectite 2:1 layers (sect. 2.2 and 2.2.4.2).

K, Cs and Ca Wyoming Blackhills montmorillonite particles, as shown in figs. 43, 45 and 47 respectively, seem to show a greater tendency to aggregate that the Li or Na clays. This has previously been ascribed (145) to tactoid formation (sect. 3.2.2).

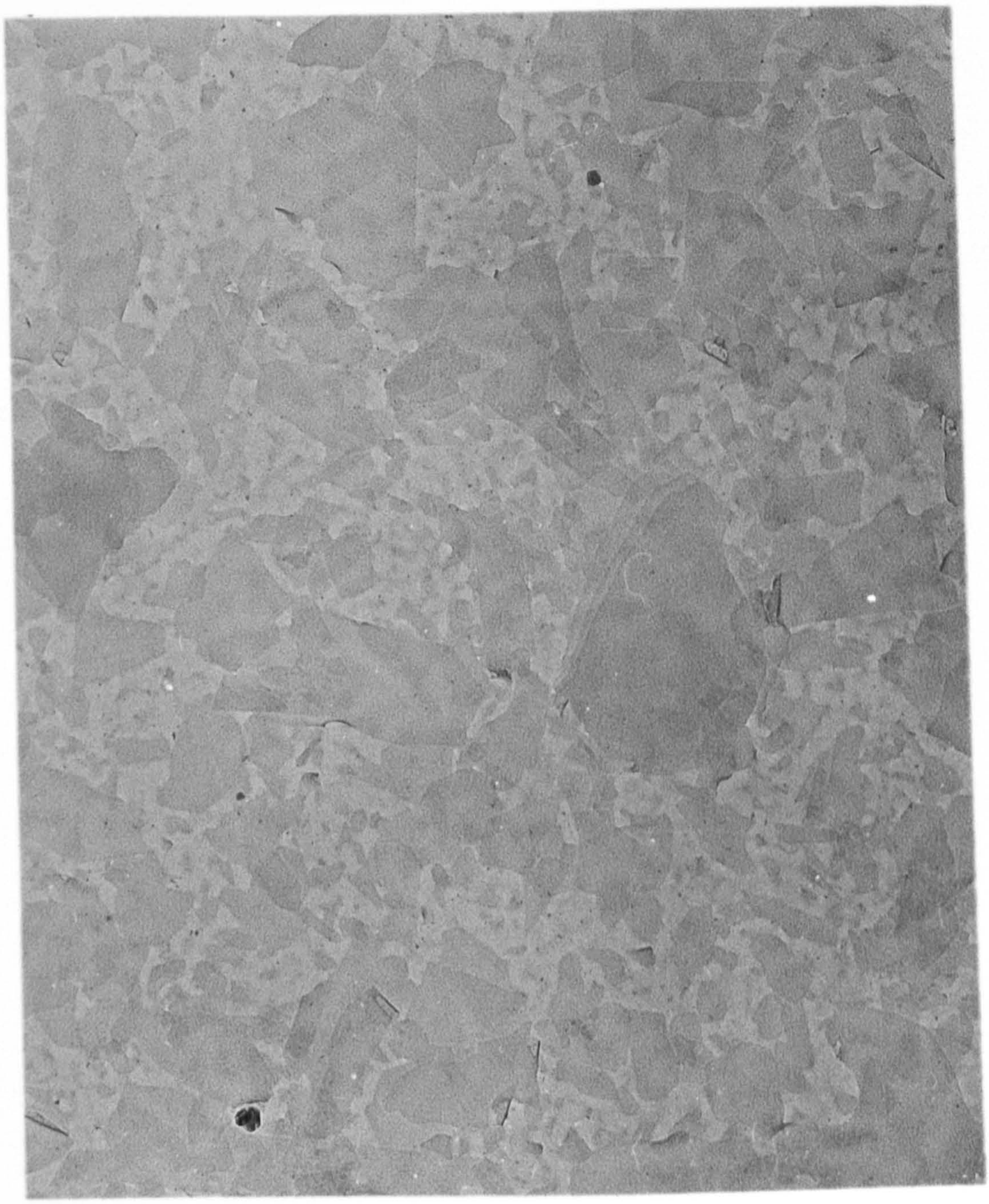

1µm

Fig. 36 : Transmission electron micrograph of Li Wyoming Blackhills dispersion (method a)

1µm

Fig. 37 : Transmission electron micrograph of Li Wyoming Upton dispersion (method a)

1µm

Fig. 38 : Transmission electron micrograph of Li Wyoming Upton dispersion (method a)

1µm

Fig 39 : Transmission electron micrograph of Na Wyoming Upton dispersion (method a)

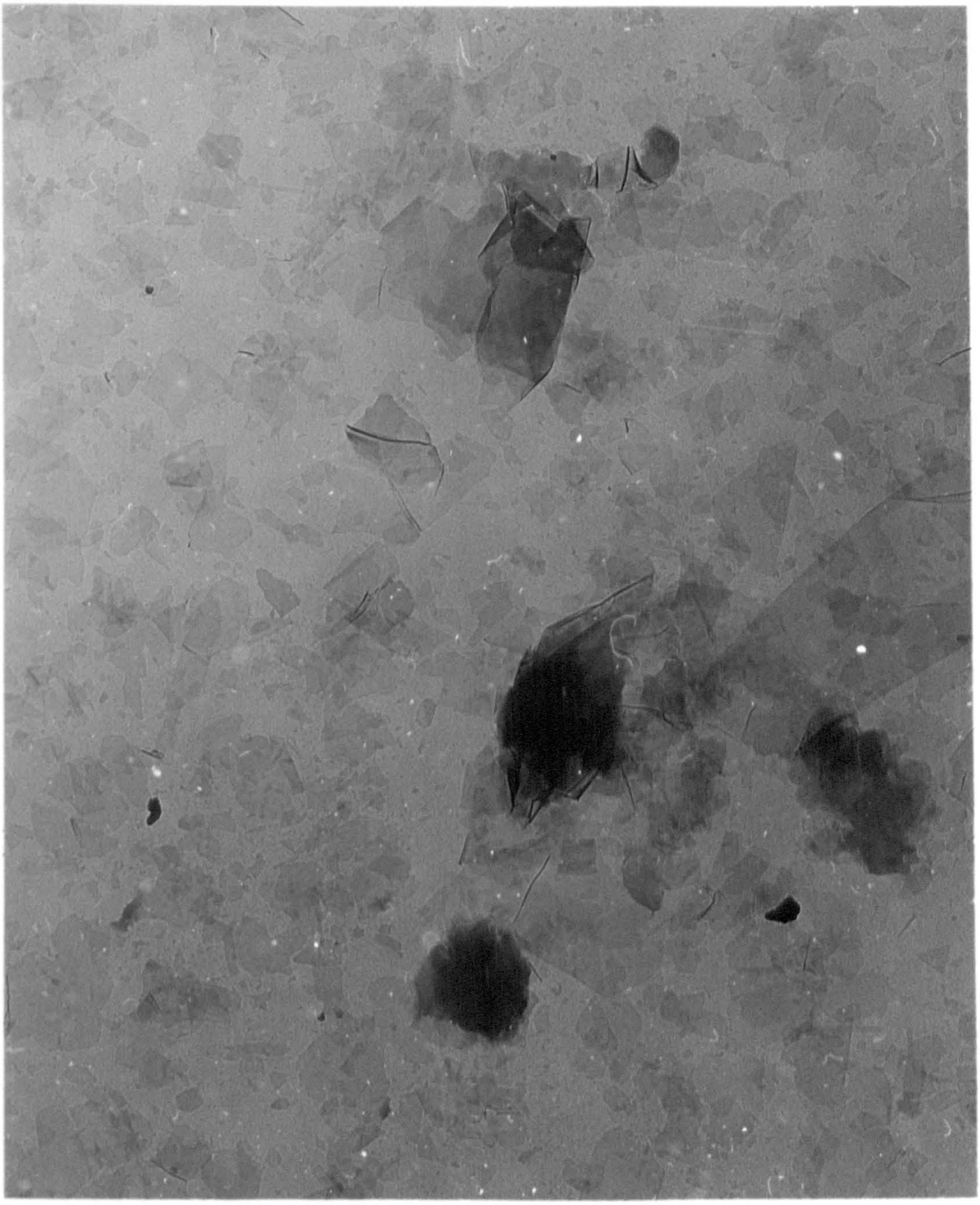

1µm

Fig. 40 : Transmission electron micrograph of
Na Wyoming Blackhills dispersion (method a)

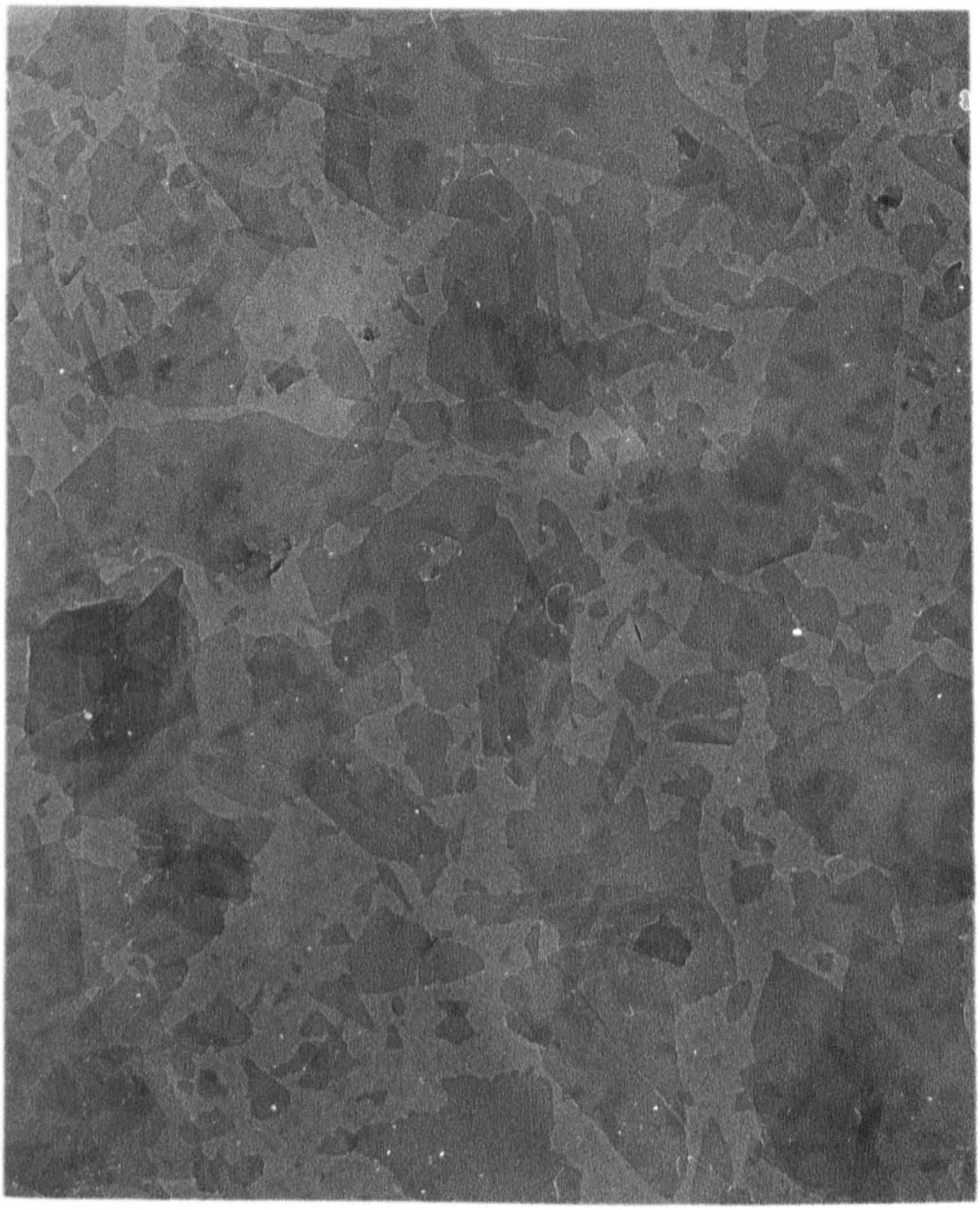

1µm

Fig. 41 : Transmission electron micrograph of Na Wyoming Blackhills dispersion (method a)

0•1µm

Fig. 42 : Transmission electron micrograph of Na Wyoming Blackhills dispersion (method a)

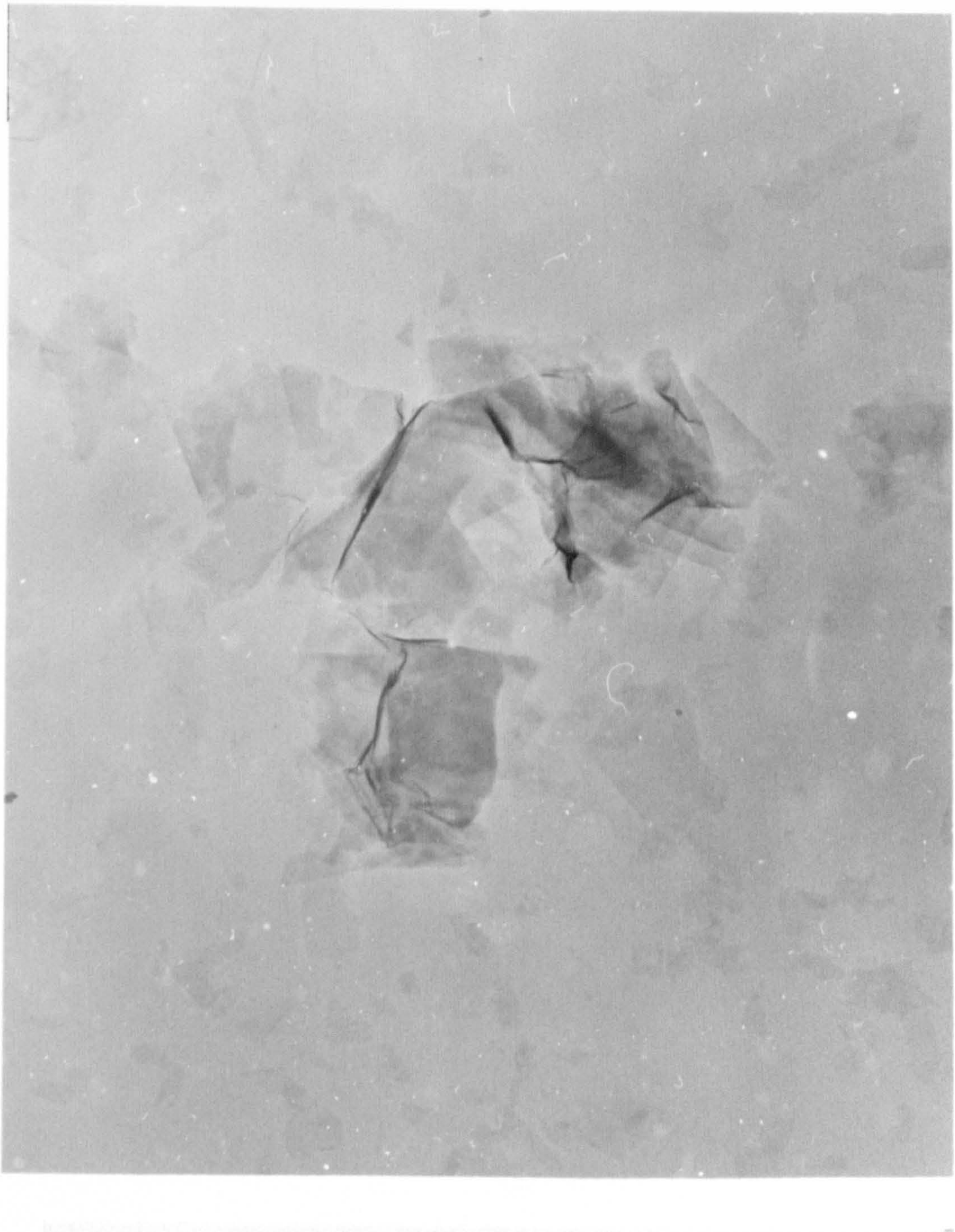

1µm

Fig. 43 : Transmission electron micrograph of K Wyoming Blackhills dispersion (method a)

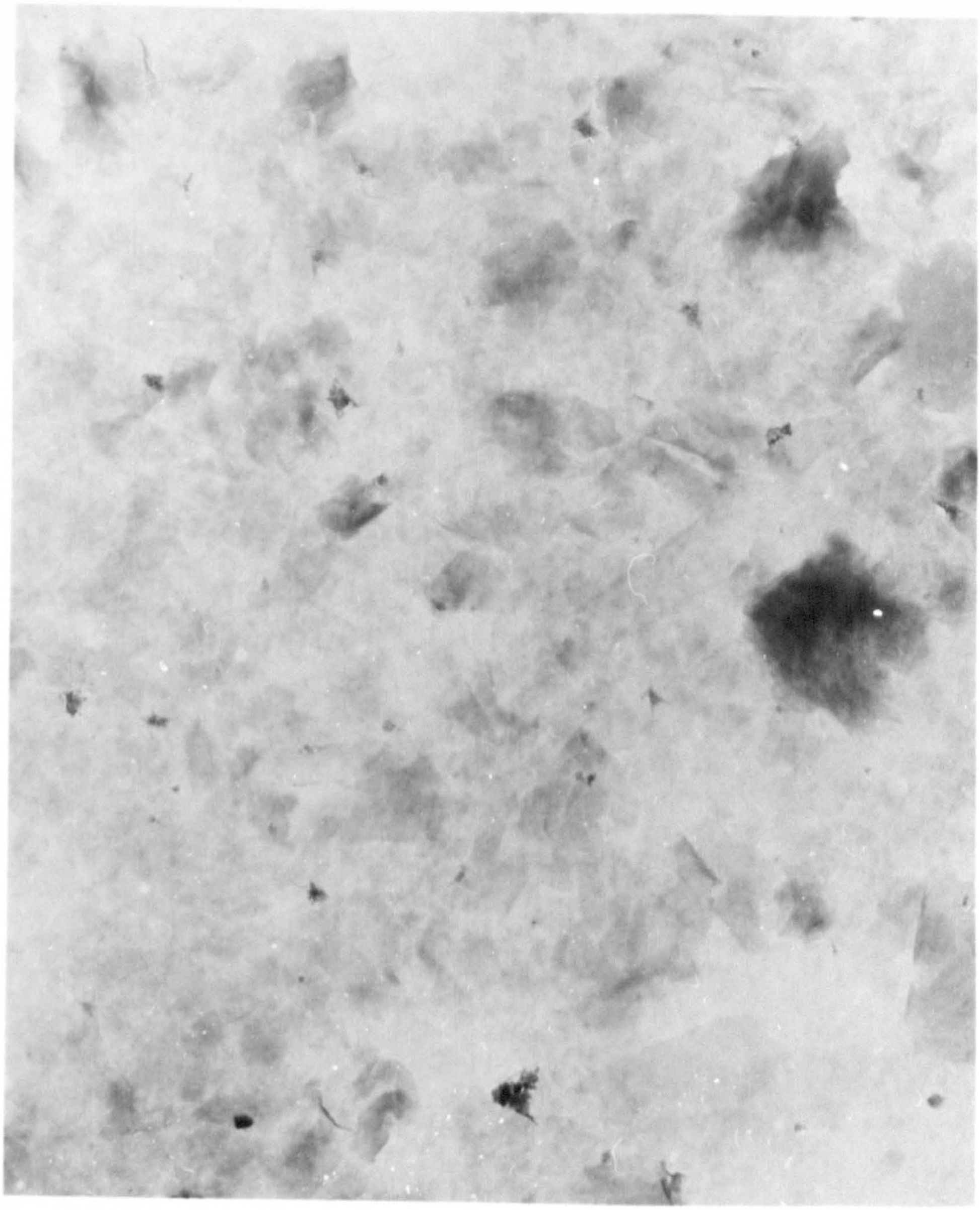

1µm

Fig. 44 : Transmission electron micrograph of
K Wyoming Blackhills dispersion (method b)

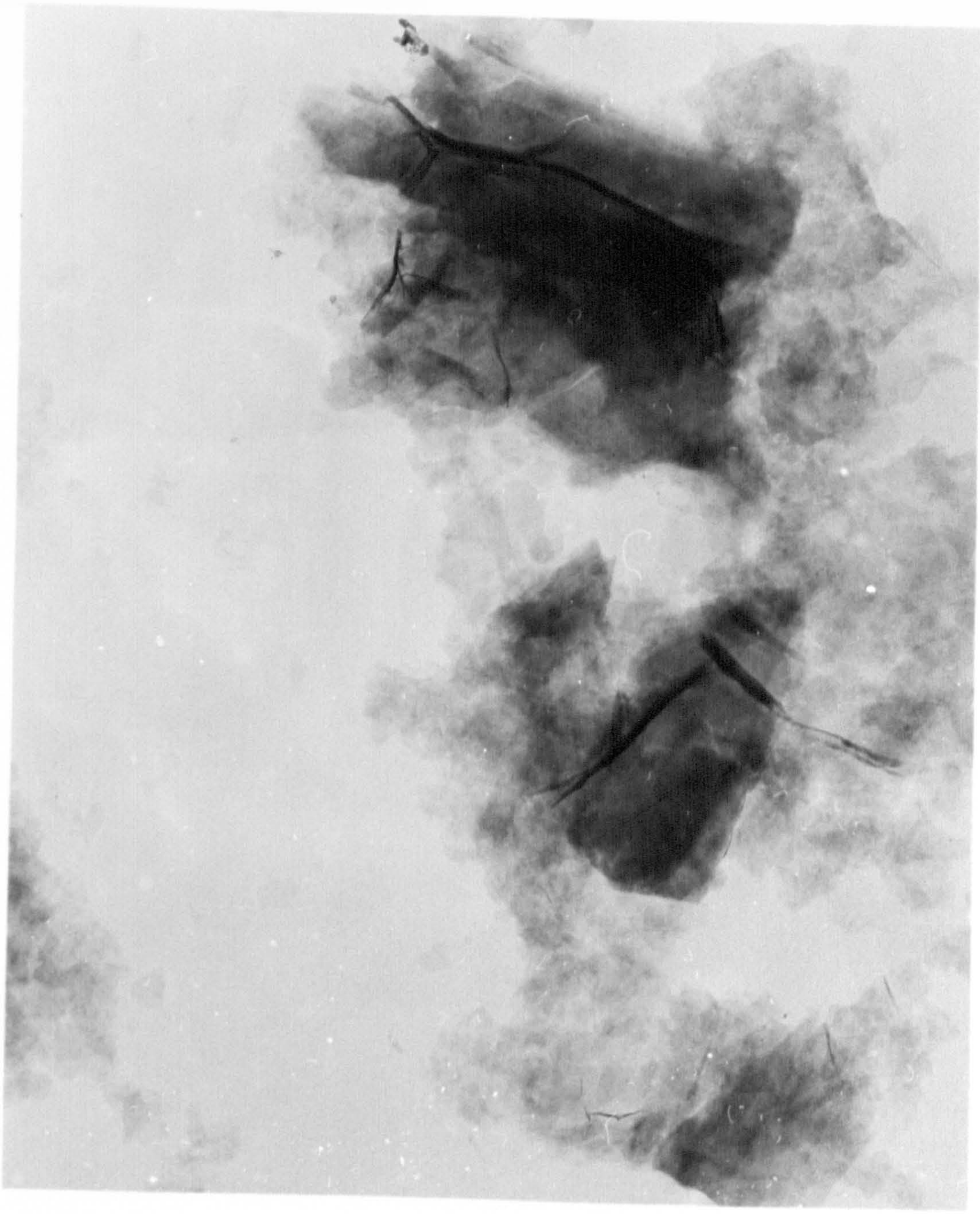

1µm

Fig. 45 : Transmission electron micrograph of Cs Wyoming Blackhills dispersion (method a)

1µm

Fig. 46 : Transmission electron micrograph of Cs Wyoming Blackhills dispersion (method b)

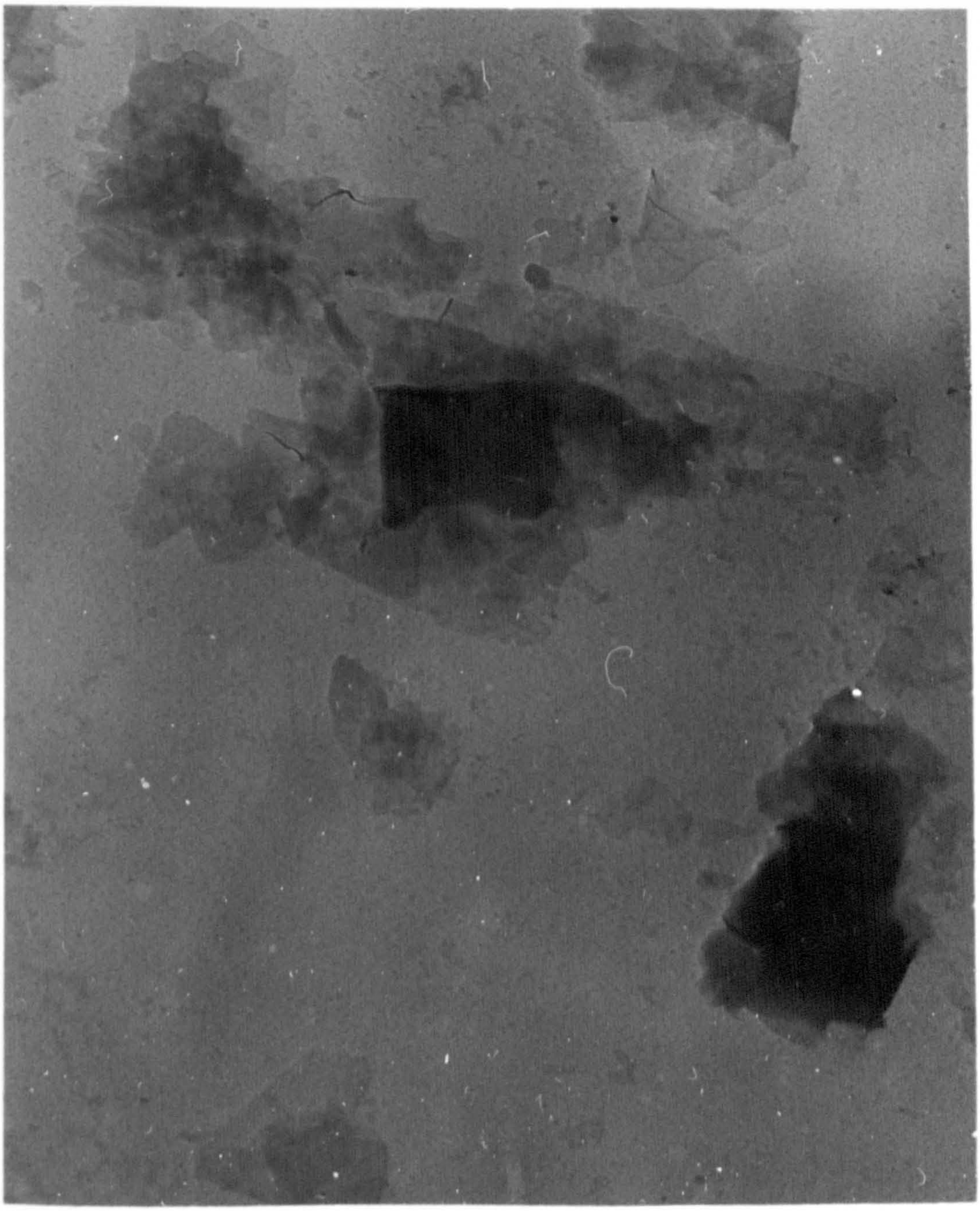

1µm

Fig. 47 : Transmission electron micrograph of Ca Wyoming Blackhills dispersion (method a)

Uncobbed Texas bentonites contain quite large amounts of accessory minerals.- even after purification. This is shown by TEM of the Na hard Helms sample (fig. 48), which gives similar micrographs to crude full face Helms bentonite (figs. 20 - 22)., containing halloysite (fig. 49) and opal-CT (fig. 50) particles. Na soft Helms (fig. 51) and Na soft Clark (fig. 52) also contain impurities, the latter sample consisting of large amounts of halloysite (fig. 52).

TEM of Li Bentolite L indicates that this sample consists mainly of small thin montmorillonite particles (fig. 53) along with some halloysite and opal-CT particles (fig. 54). This sample seems to contain much less halloysite than the uncobbed hard Texas bentonites, Na hard Helms (fig. 48) and crude full face Helms (figs. 20 - 22). This is probably because cobbing removes the surface weathered phases of the rock which seem to contain concentrations of halloysite (sect. 5.3.3). None of the thin montmorillonite particles present in Li Bentolite L (fig. 53) seem to be as large as some of those, up to ~1μm in length (figs. 36 and 37), present in the Wyoming samples, although some aggregates of montmorillonite particles are present in the coarse size fraction of Li Bentolite L (obtained by sedimentation) (fig. 55). Na Bentolite L is similar in appearance to Li Bentolite L, containing thin montmorillonite particles, opal-CT particles (figs. 56 and 57), montmorillonite aggregates and occasional kaolinite particles (fig. 57).

TEM indicates that Li cobbed soft Helms is similar to Li Bentolite L although the former seems to contain more halloysite (fig. 58). Li soft Clark (fig. 59) is similar in appearance to Li cobbed

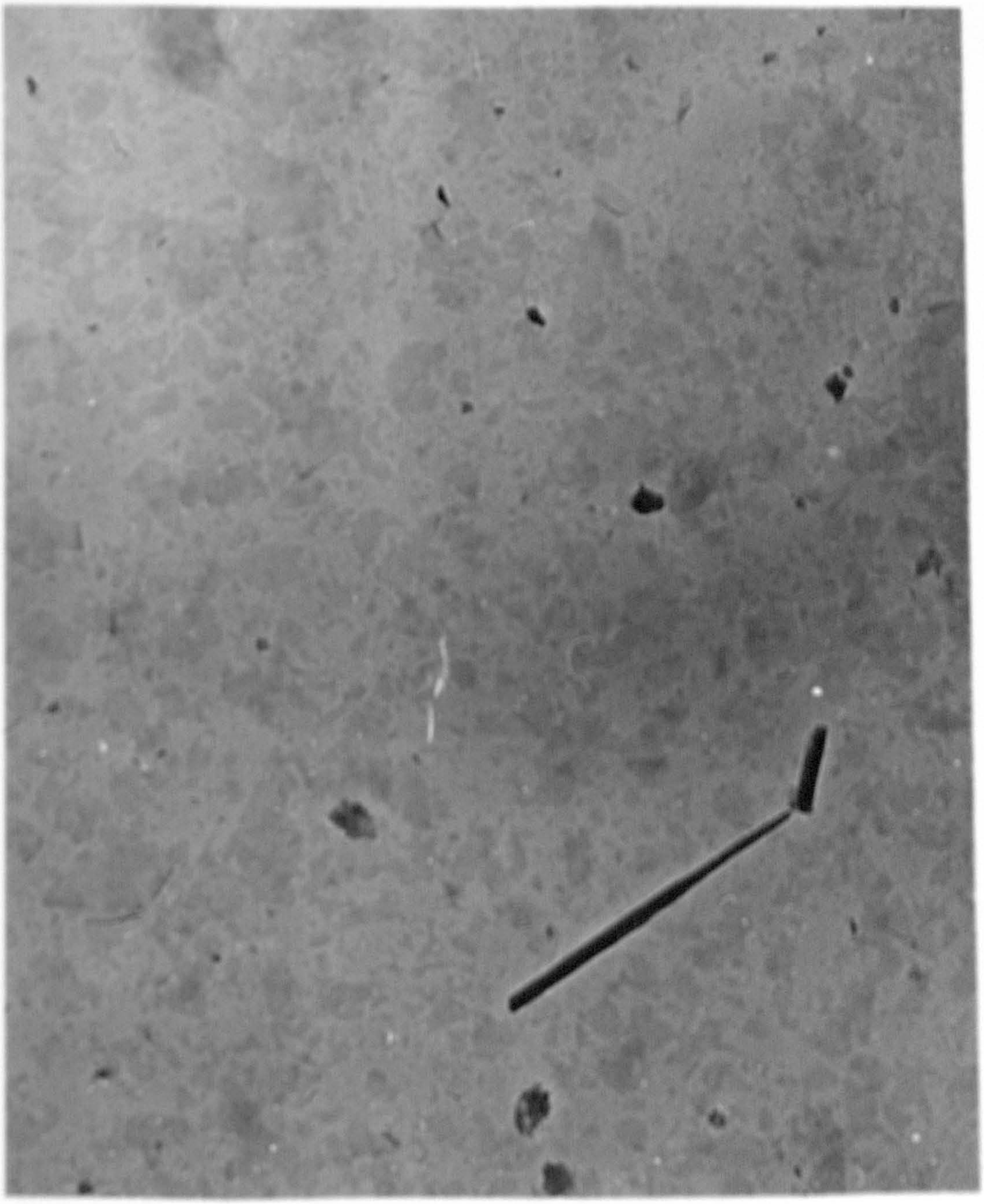

Fig. 48 : Transmission electron micrograph of Na hard Helms dispersion (method a)

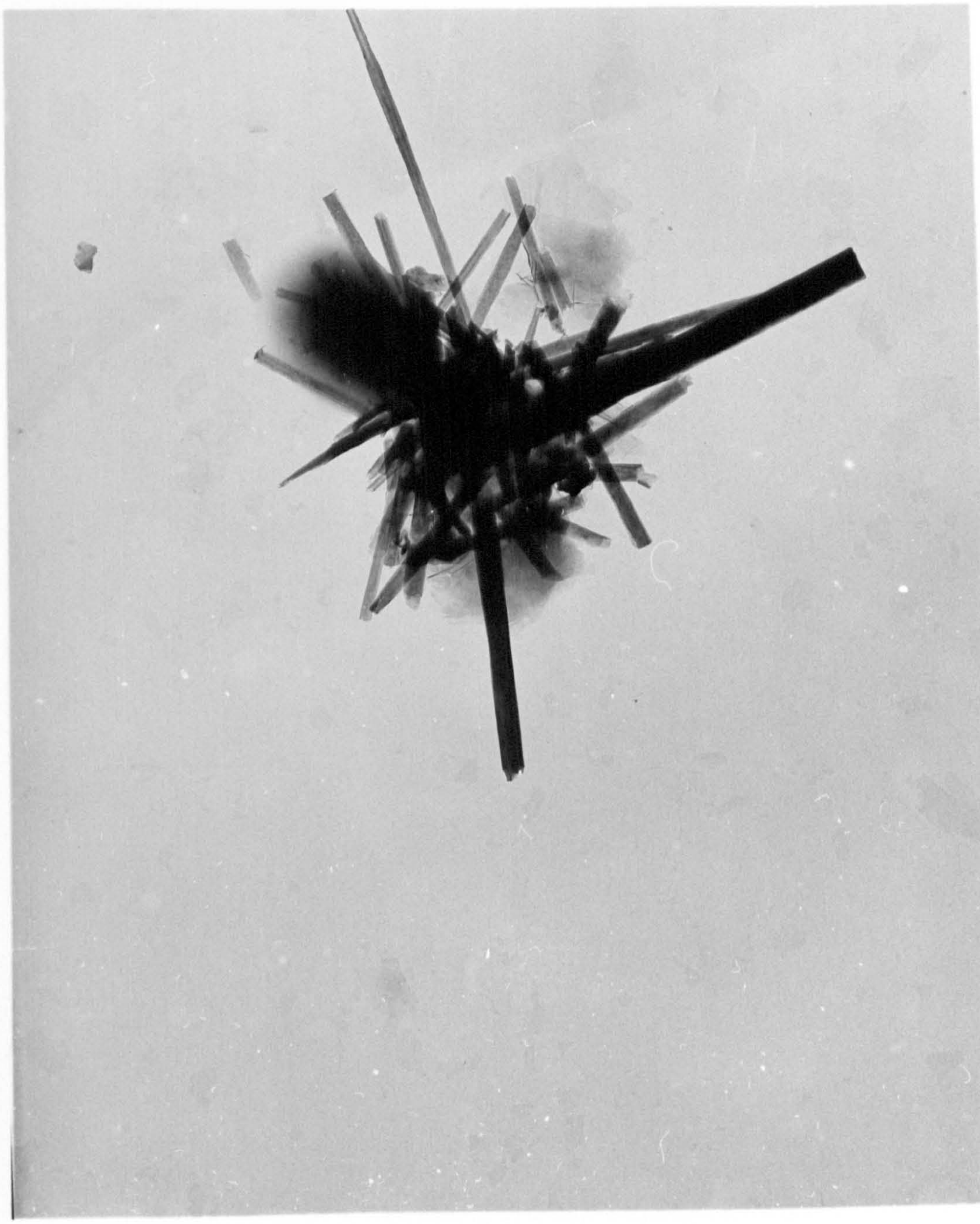

1µm

Fig. 49 : Transmission electron micrograph of Na hard Helms dispersion (method a)

0·1µm

Fig. 50 : Transmission electron micrograph of Na hard Helms dispersion (method a)

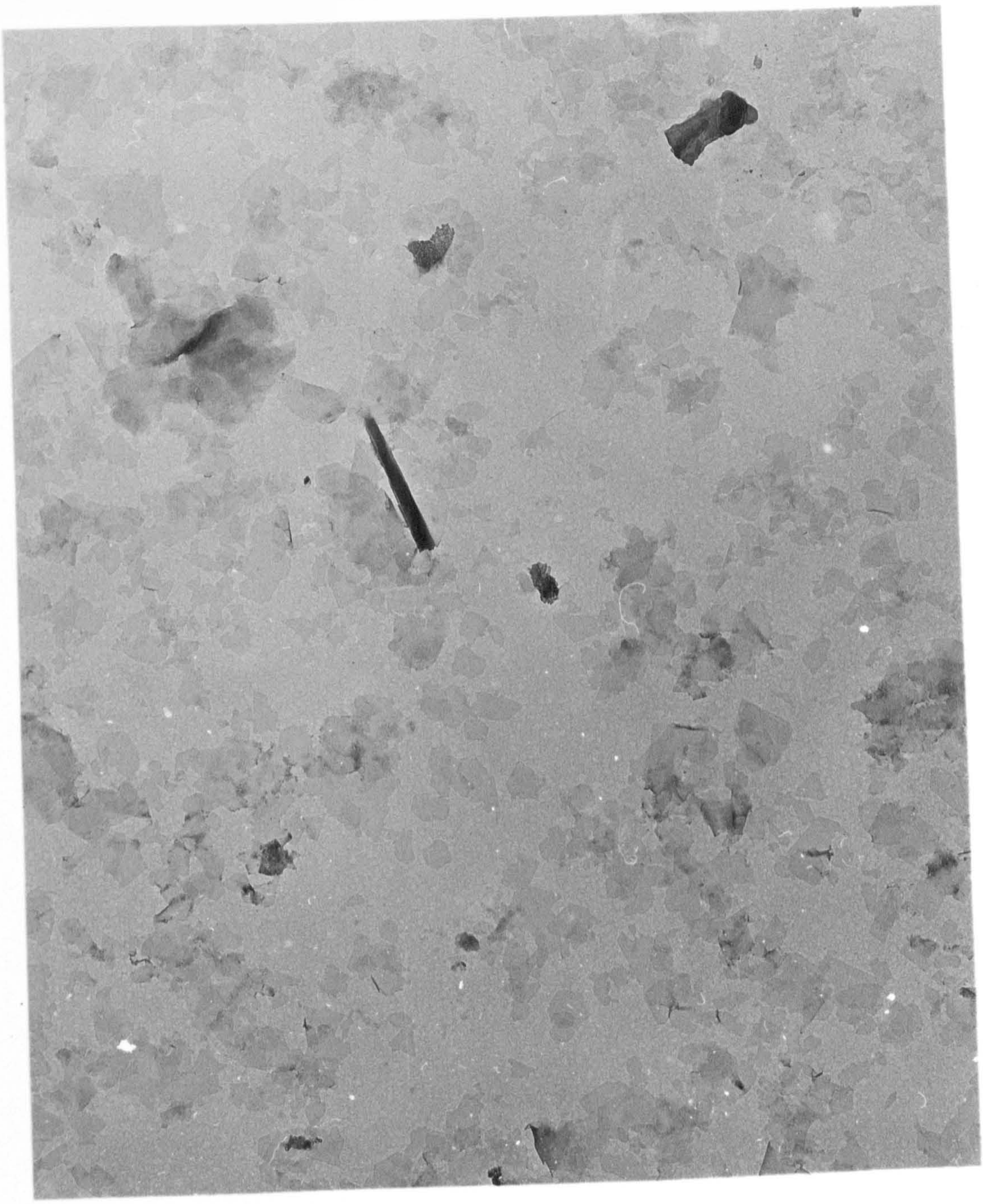

1µm

Fig. 51 : Transmission electron micrograph of Na soft Helms dispersion (method a)

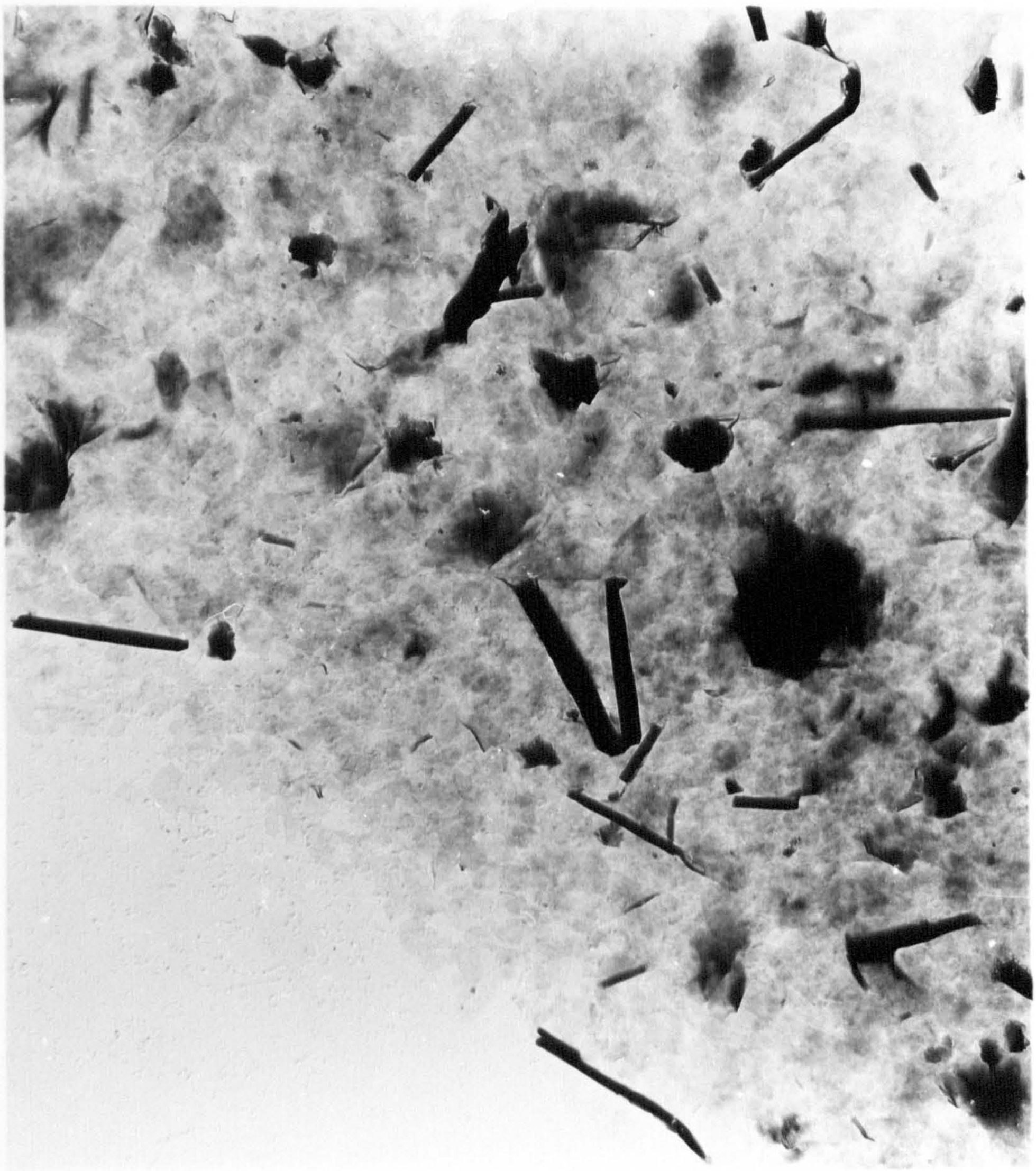

1µm

Fig. 52 : Transmission electron micrograph of Na soft Clark dispersion (method b)

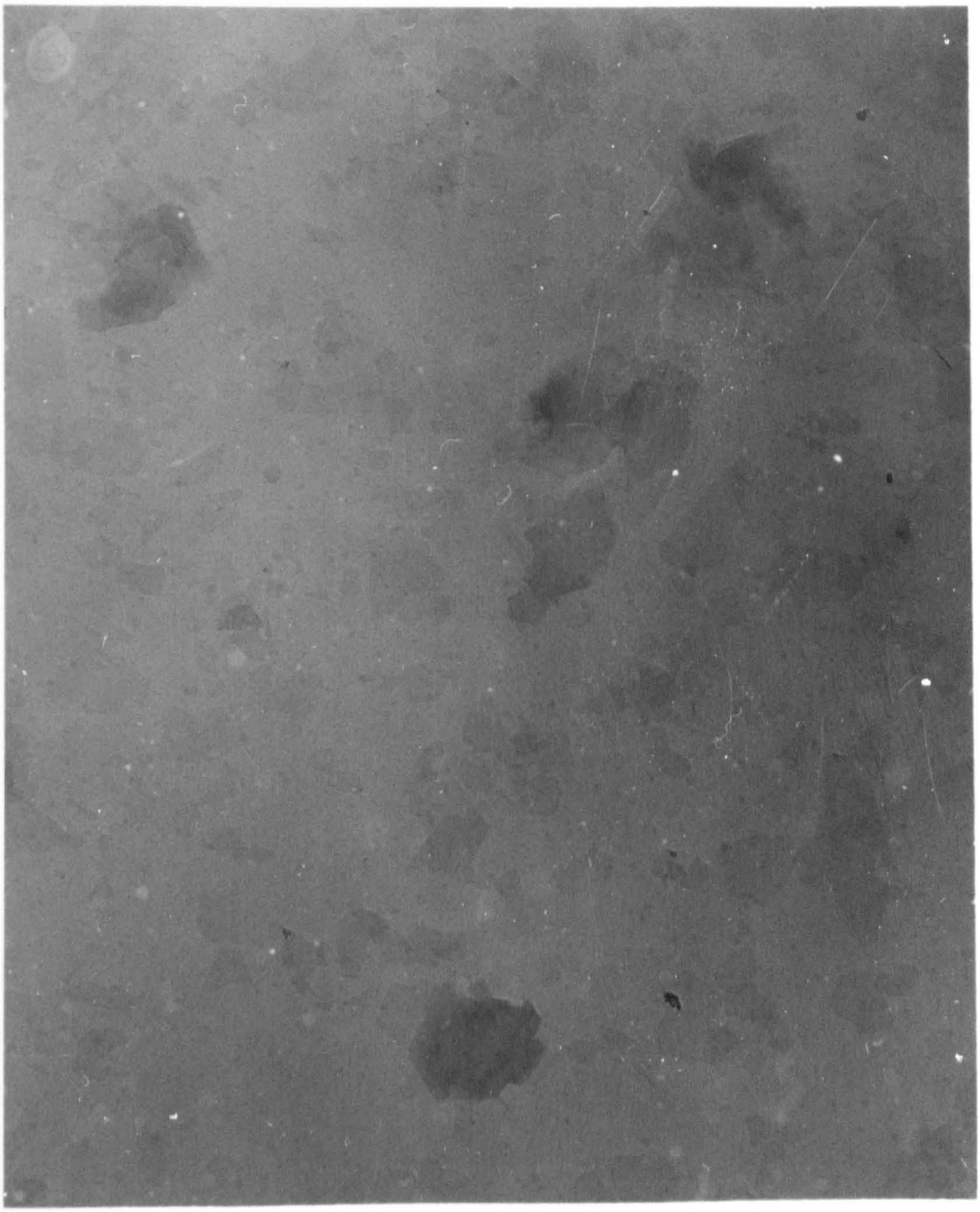

1µm

Fig. 53 : Transmission electron micrograph of Li Bentolite L dispersion (method a)

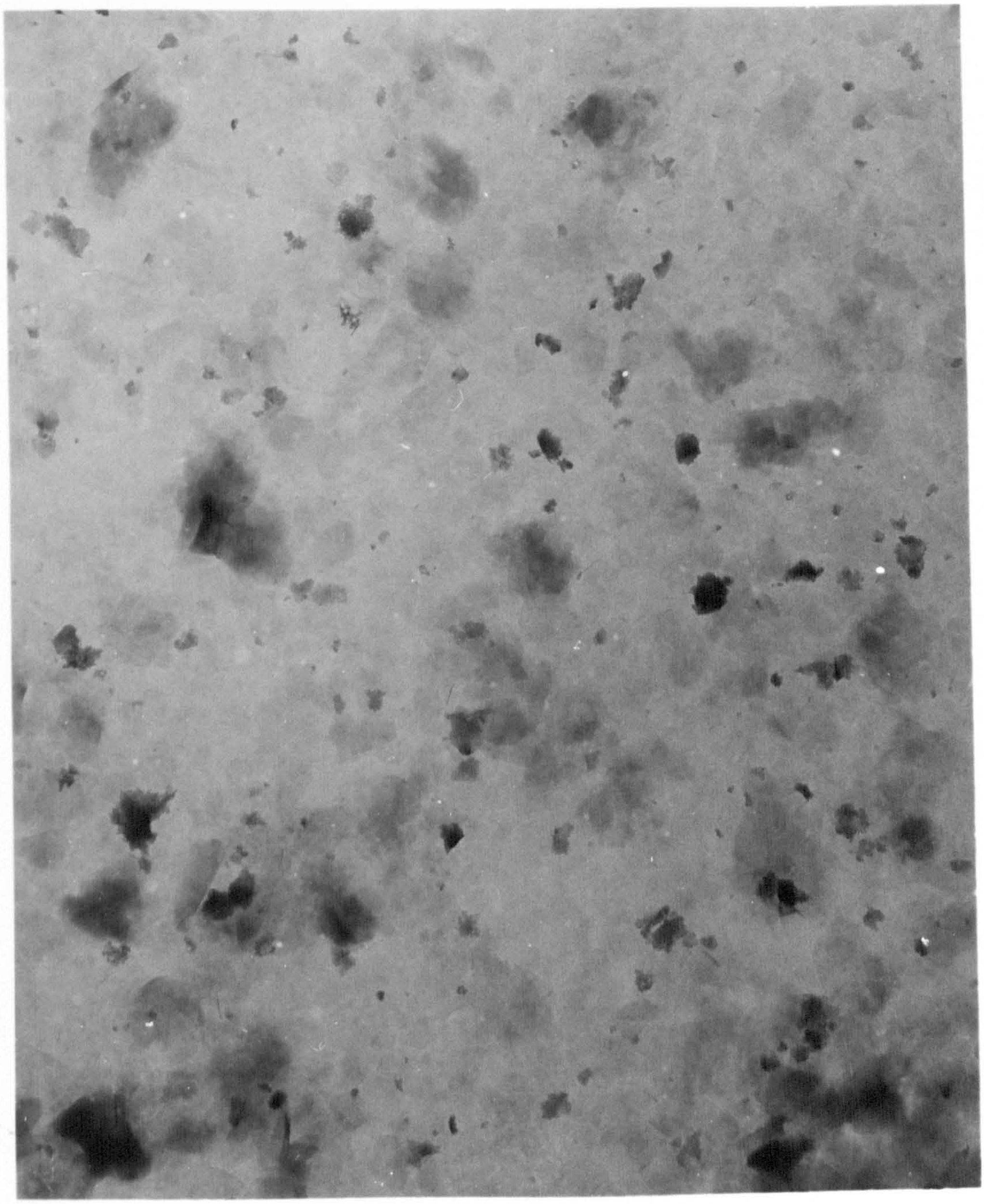

1µm

Fig. 54 : Transmission electron micrograph of Li Bentolite L dispersion (method b)

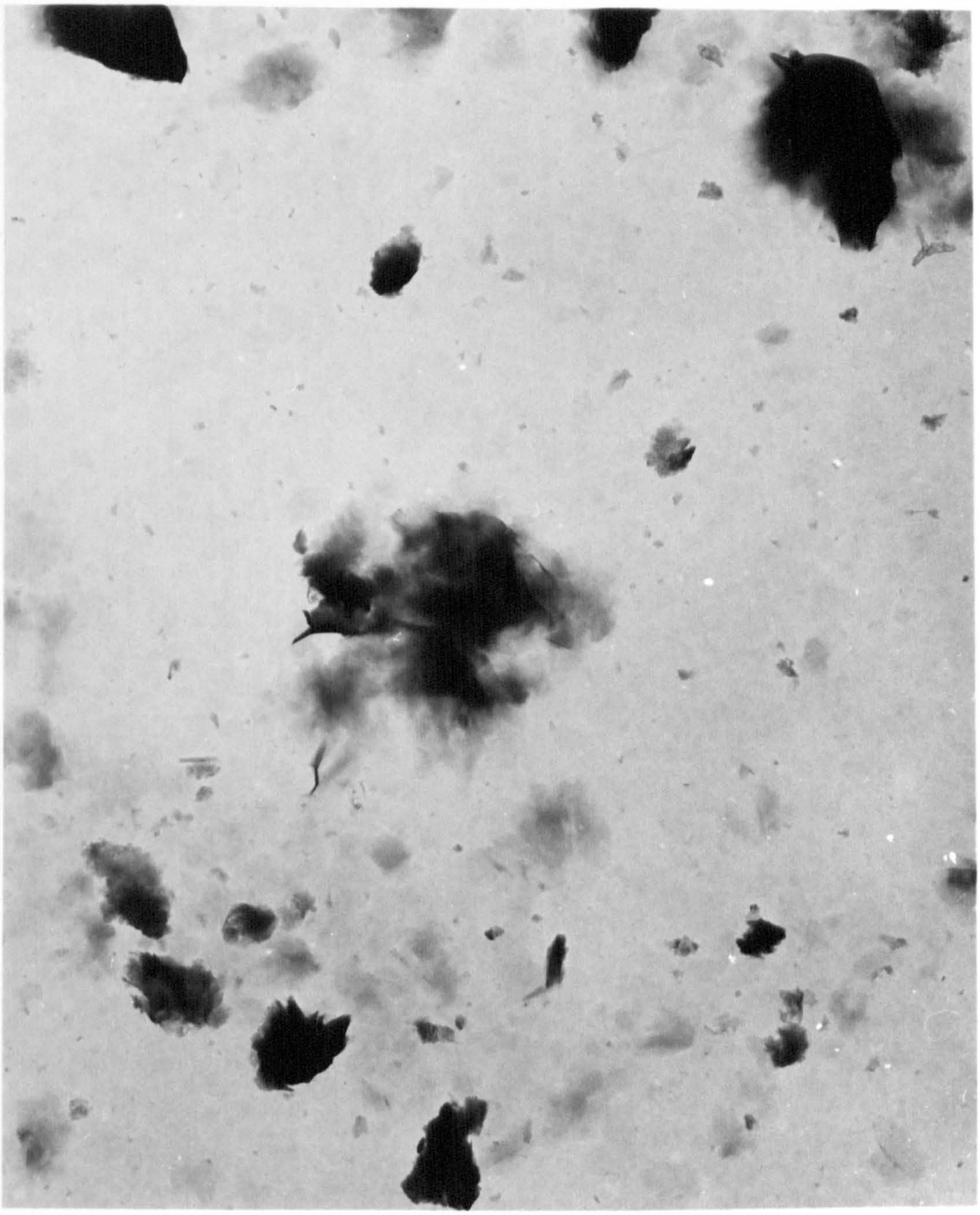

1µm

Fig. 55 : Transmission electron micrograph of Li Bentolite L - prep. D - coarse fraction (method b)

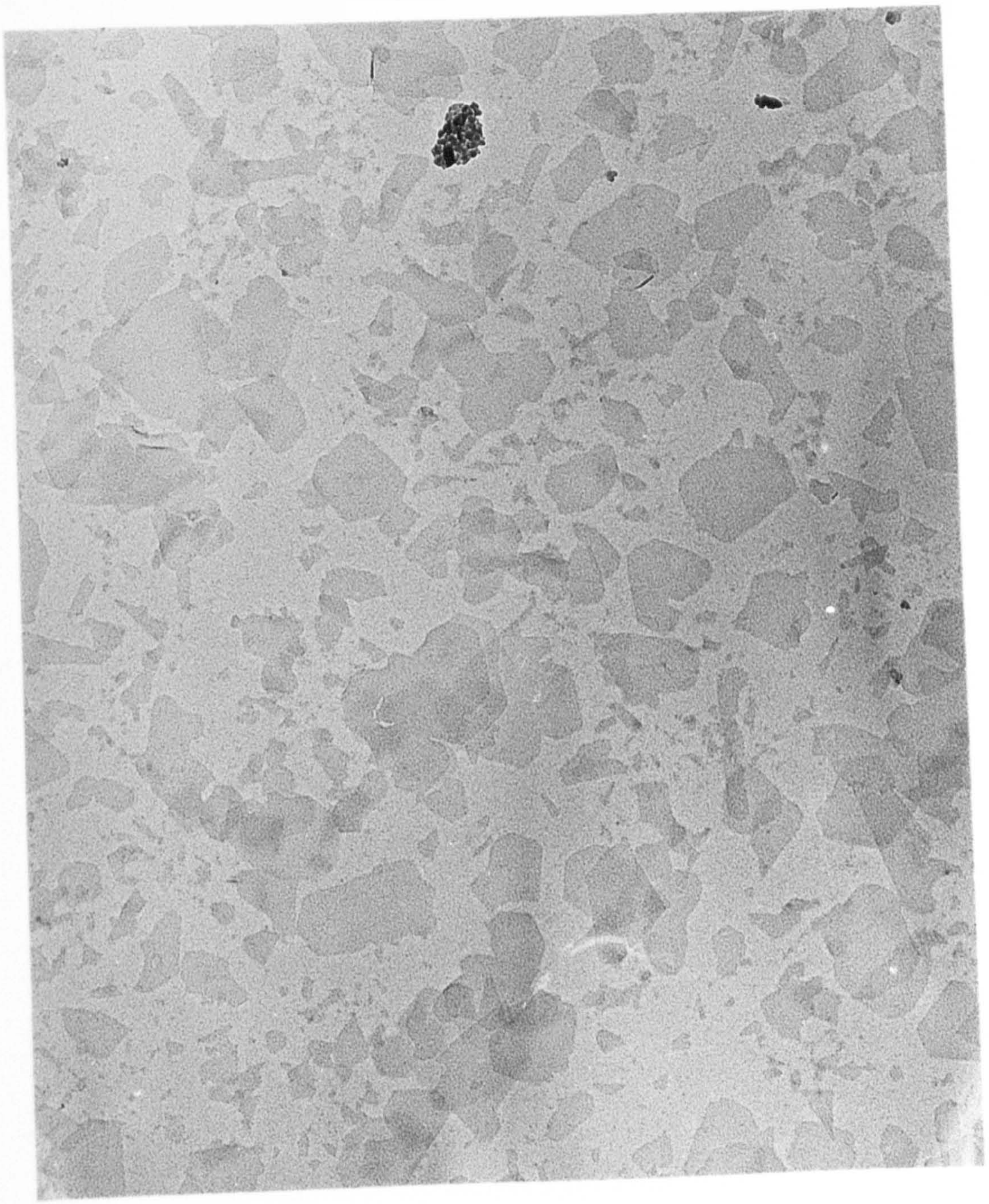

1µm

Fig. 56 : Transmission electron micrograph of Na Bentolite L dispersion (method a)

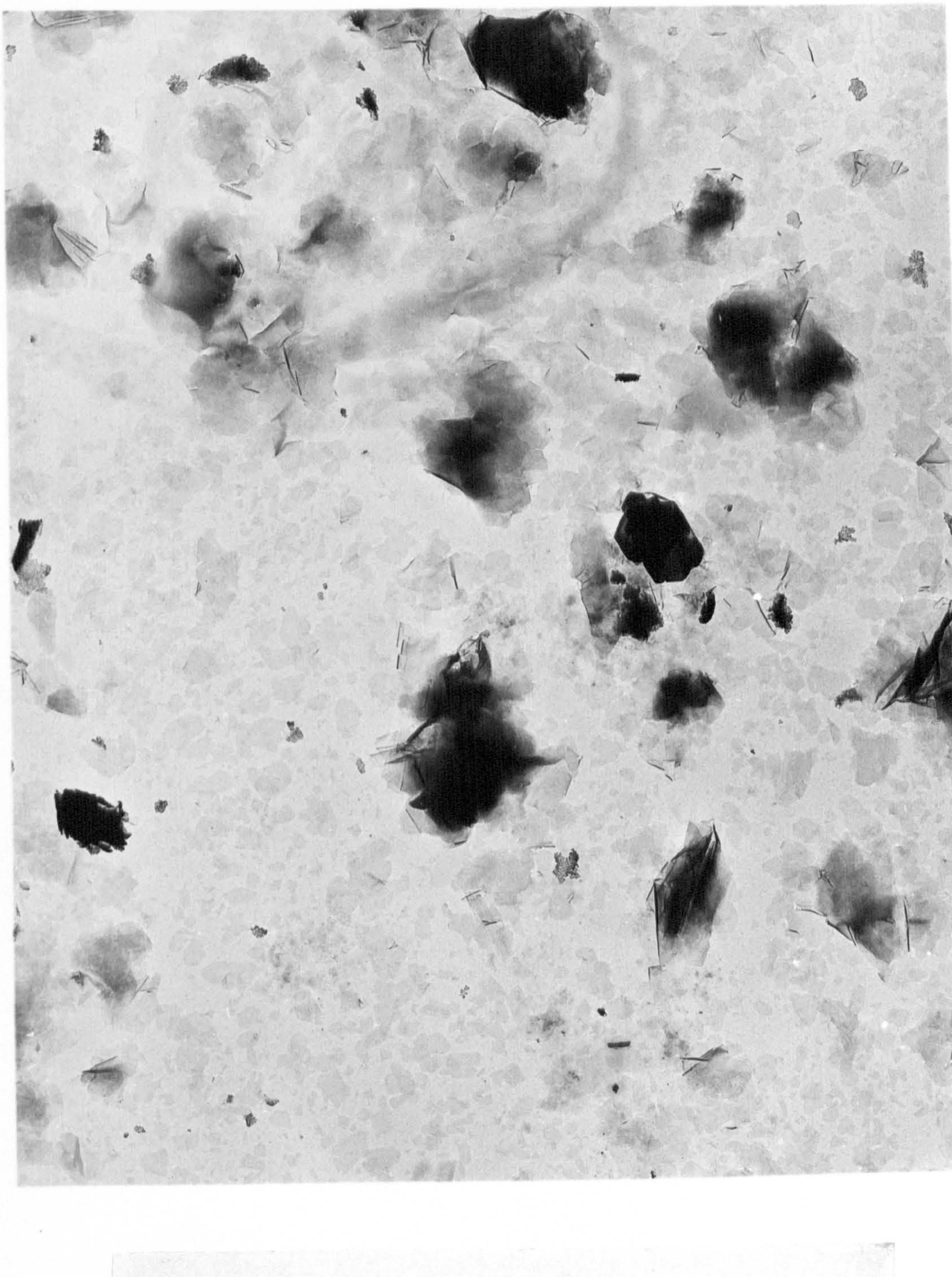

1µm

Fig. 57 : Transmission electron micrograph of Na Bentolite L dispersion (method a)

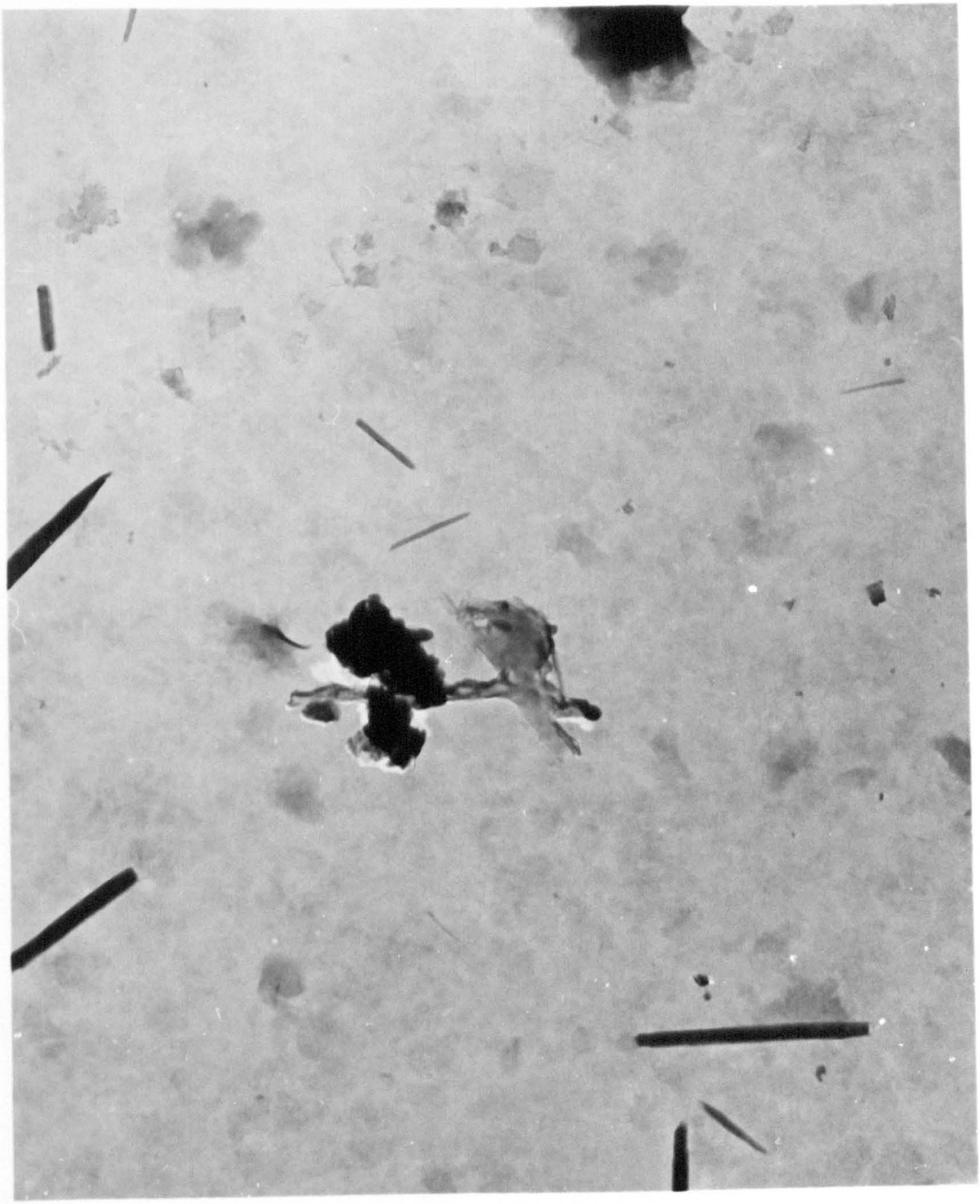

1µm

Fig. 58 : Transmission electron micrograph of Li cobbed soft Helms dispersion (method b)

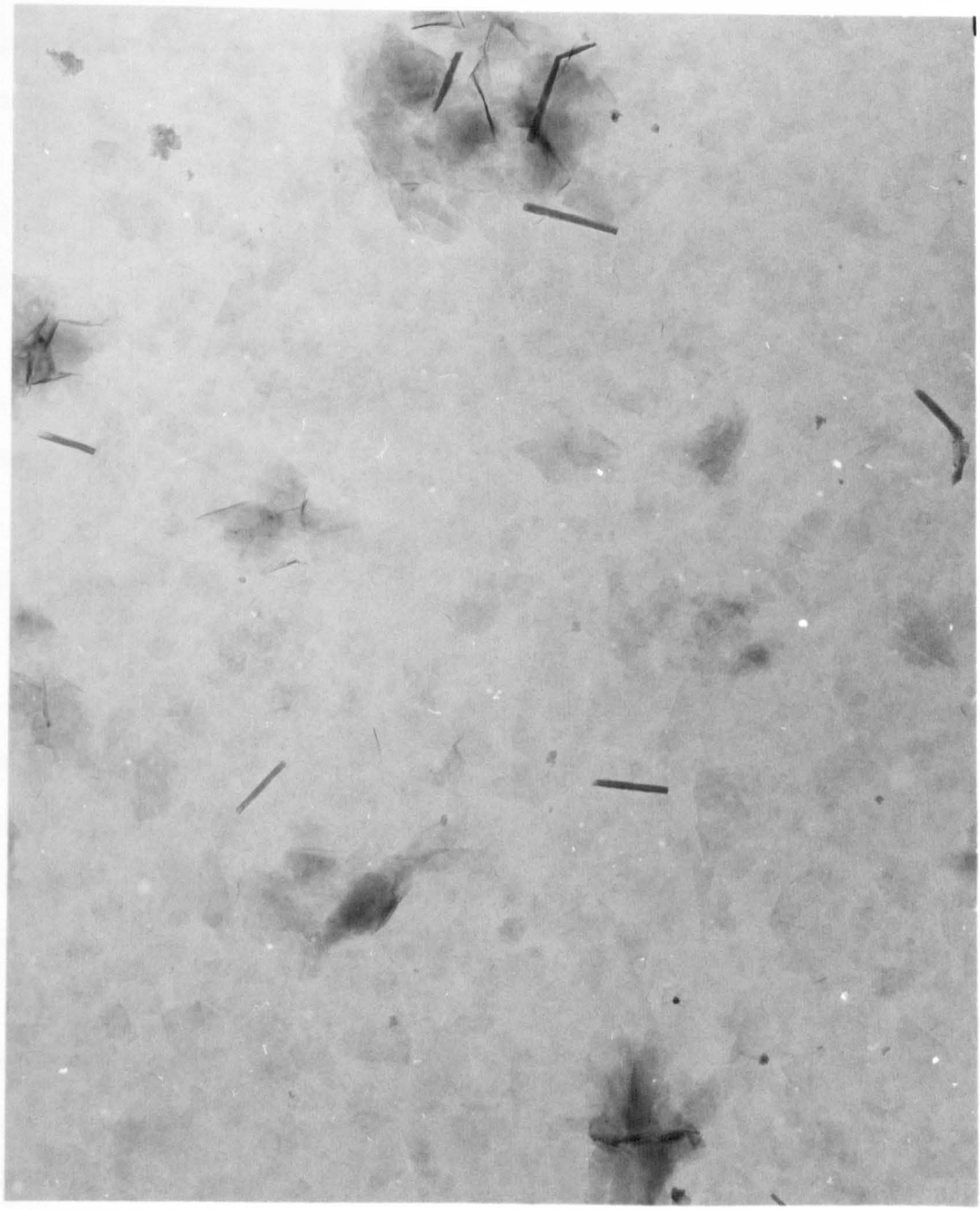

1µm

Fig. 59 : Transmission electron micrograph of Li soft Clark dispersion (method b)

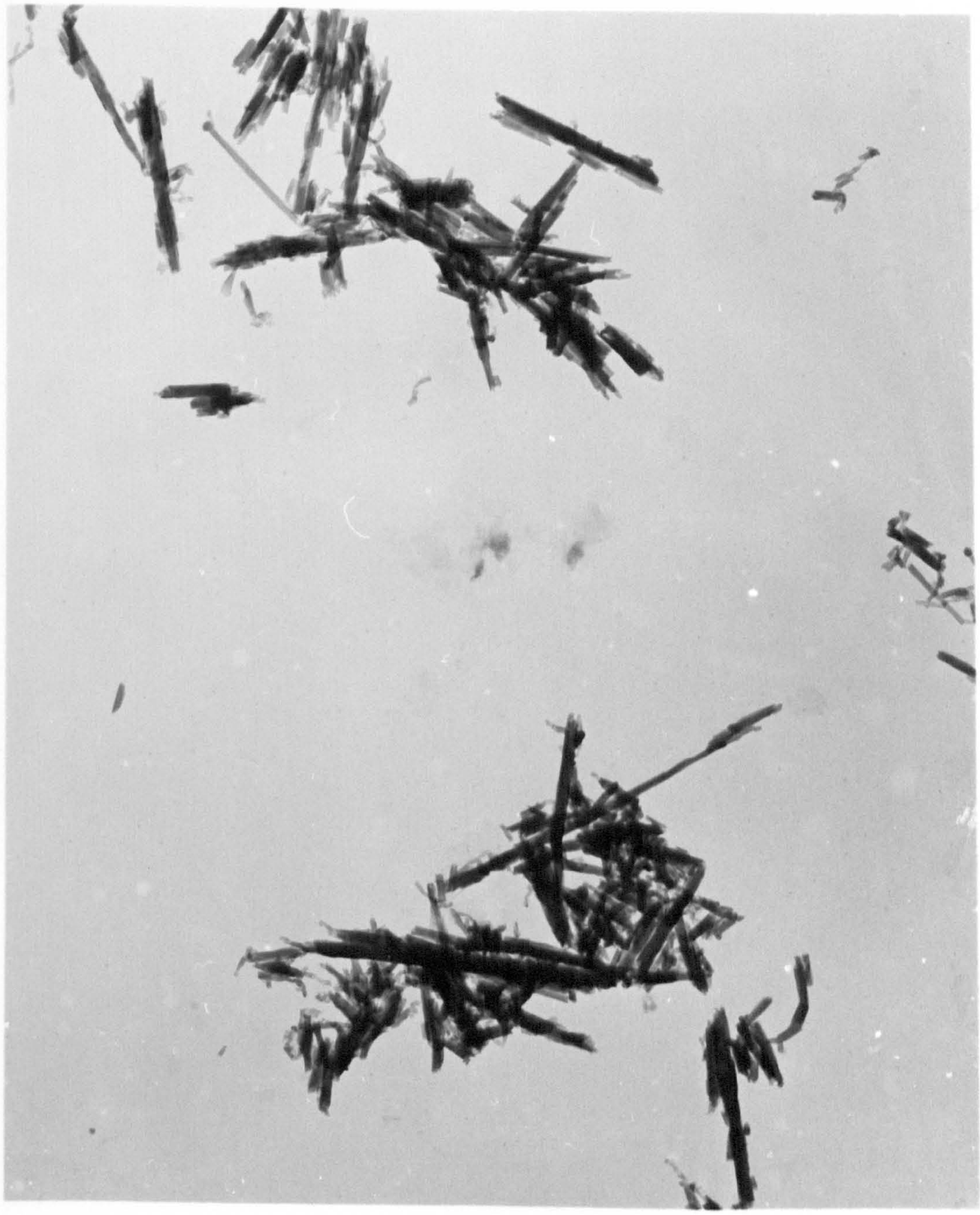

1µm

Fig. 60 : Transmission electron micrograph of Li halloysite dispersion (method a)

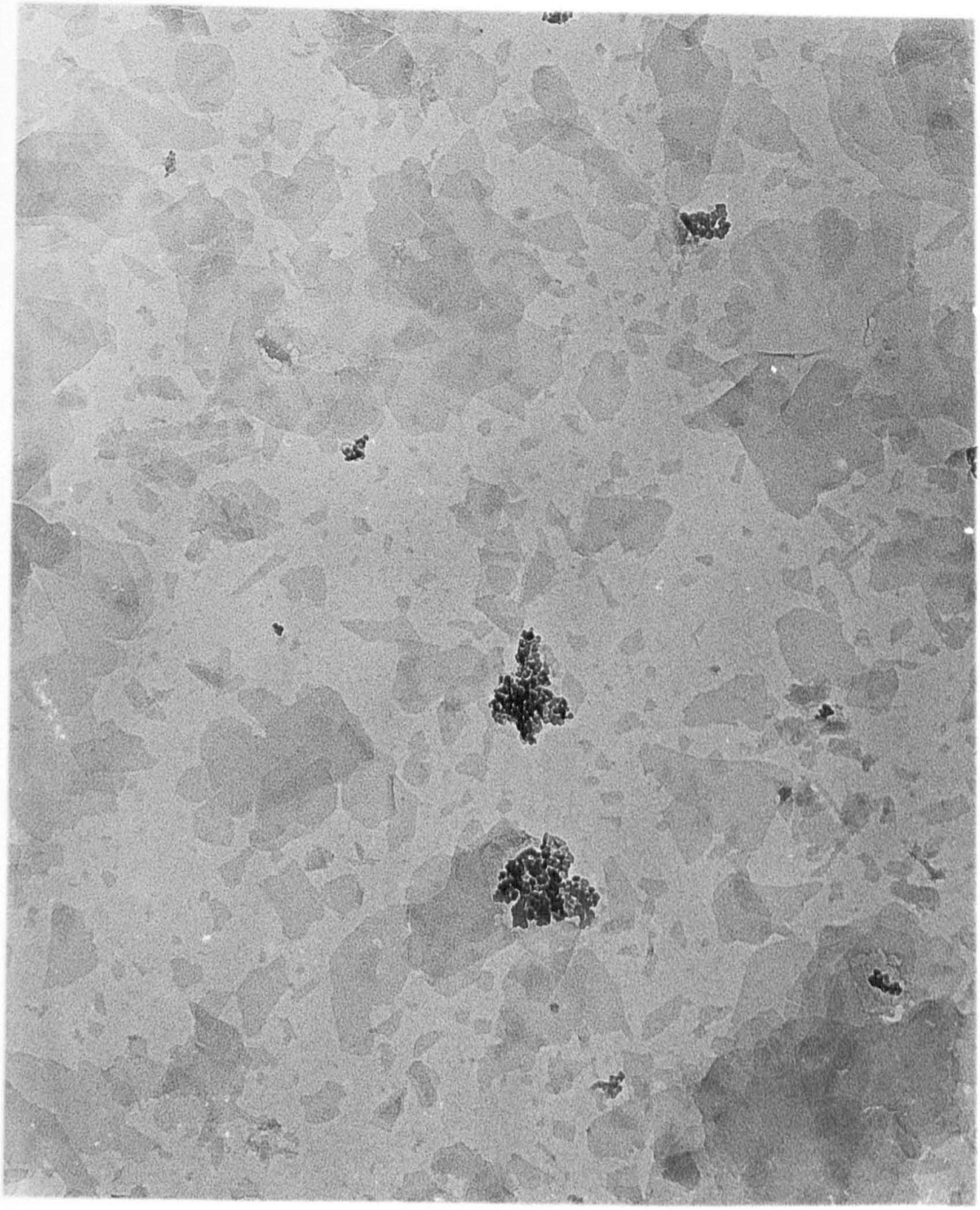

Fig. 61 : Transmission electron micrograph of Bentolite L dispersion prepared by method G (method a)

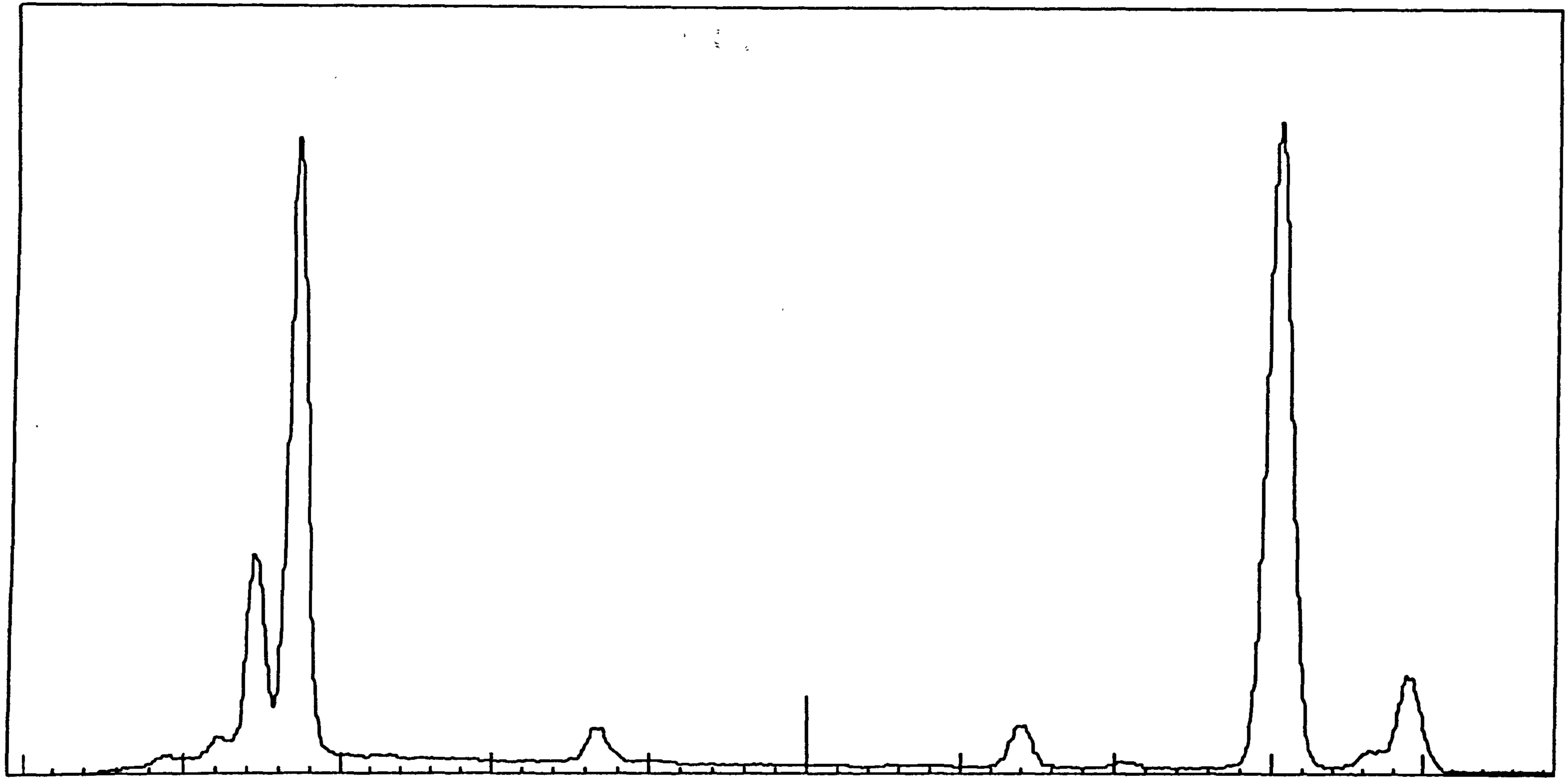

Fig.62: EPMA spectrum of Li Wyoming Upton montmorillonite

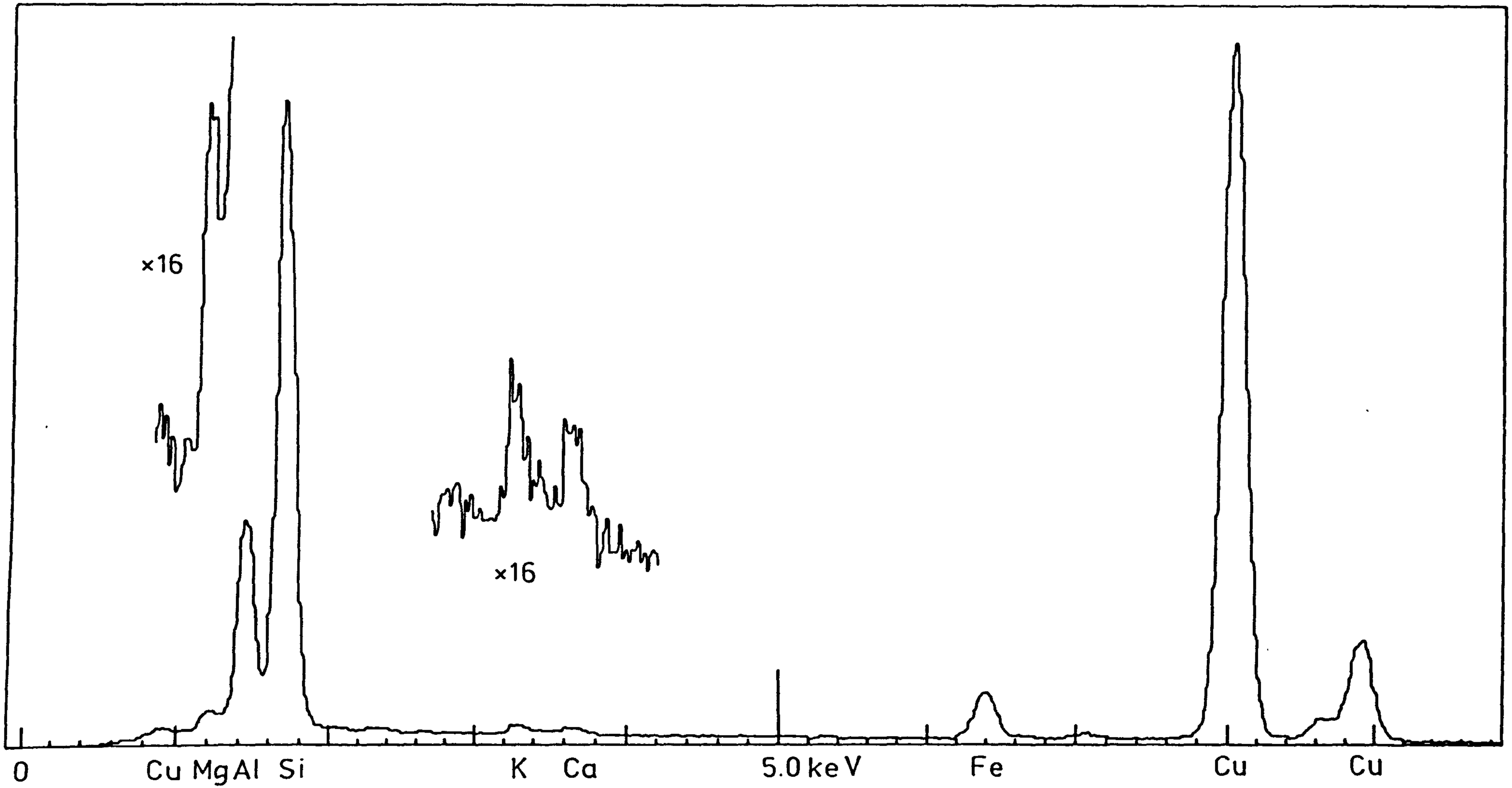

Fig.63: EPMA spectrum of Na Wyoming Upton montmorillonite

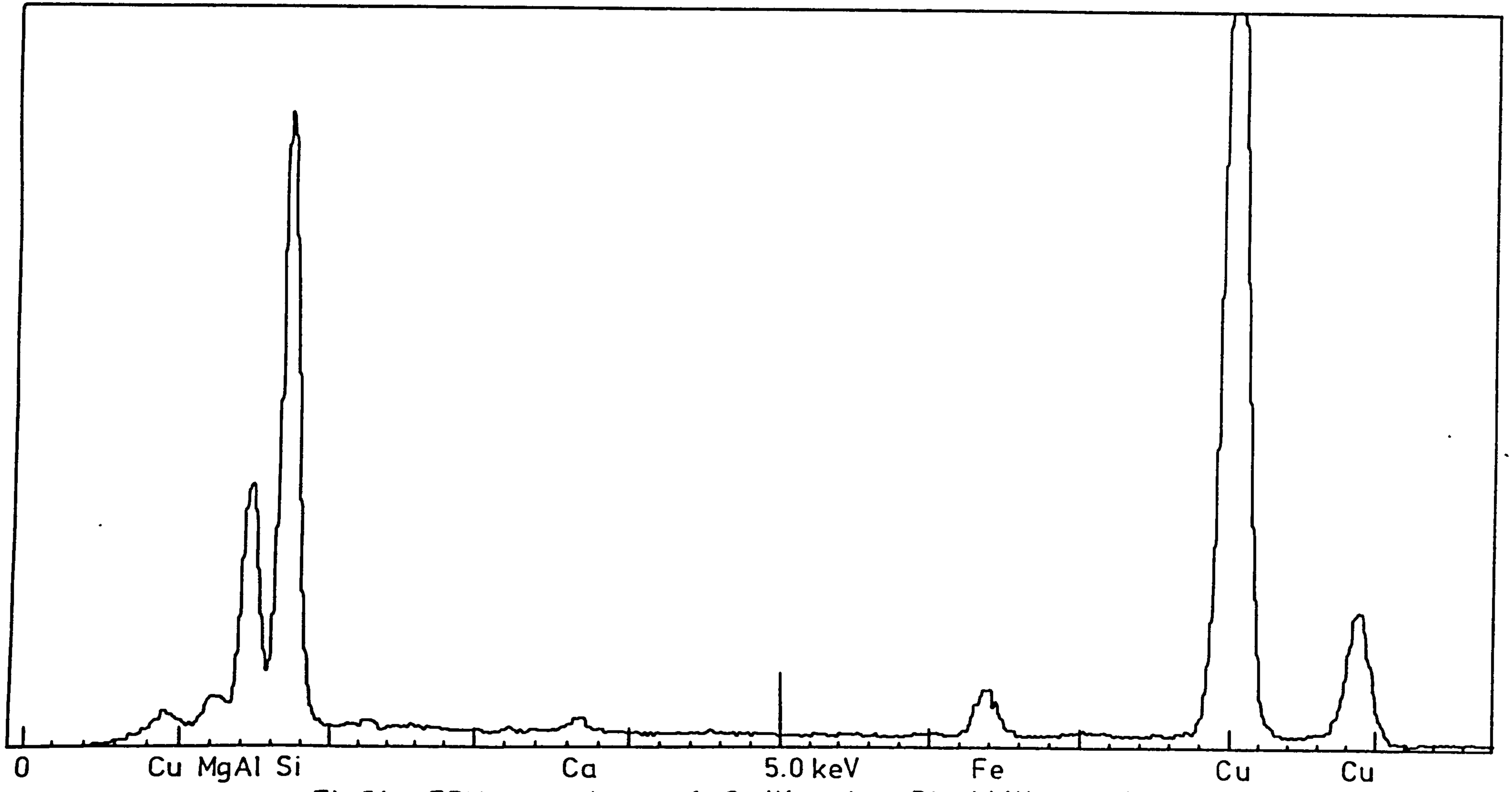

Fig.64 : EPMA spectrum of Ca Wyoming Blackhills montmorillonite

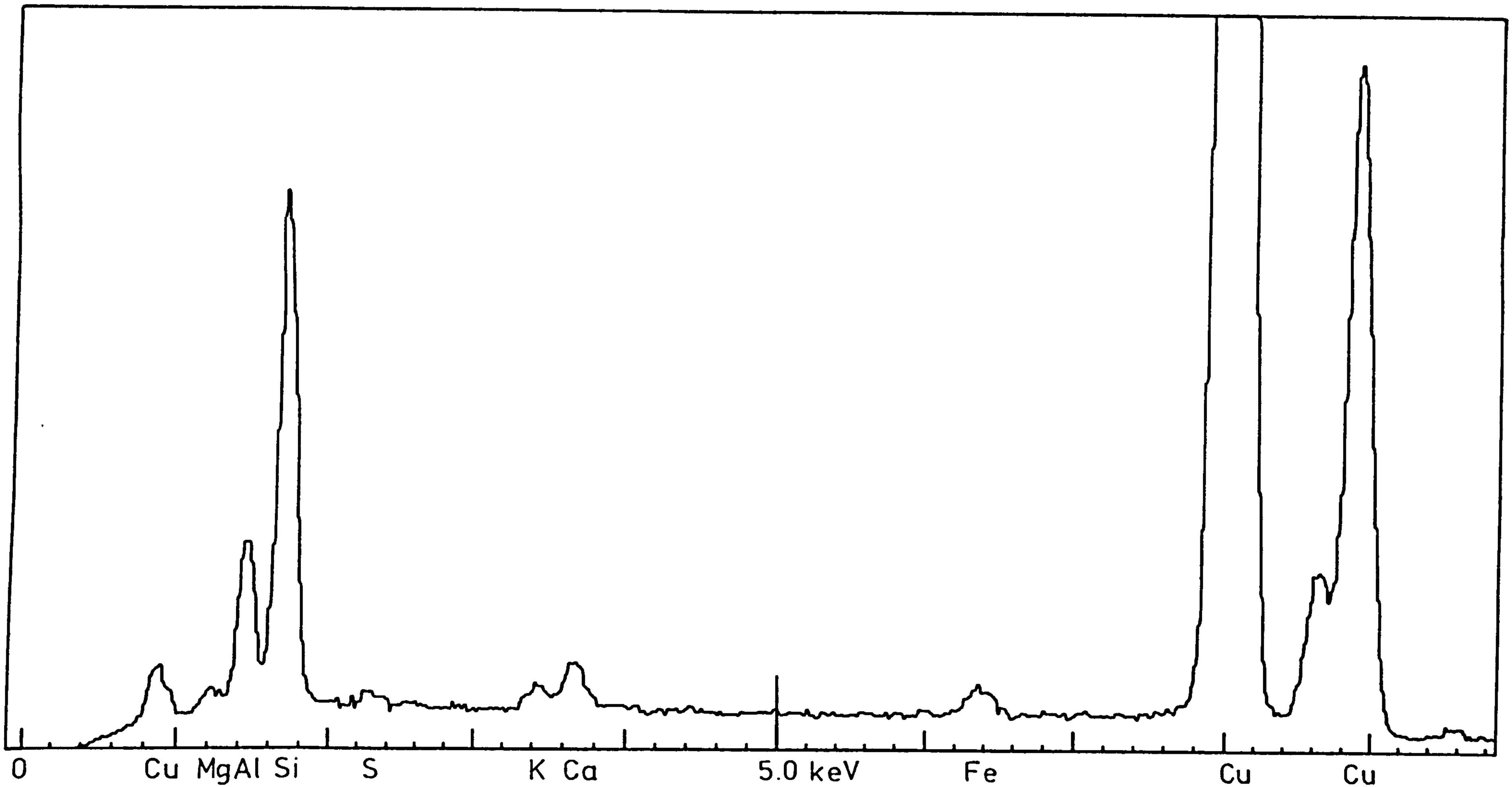

Fig.65: EPMA spectrum of Na hard Helms montmorillonite

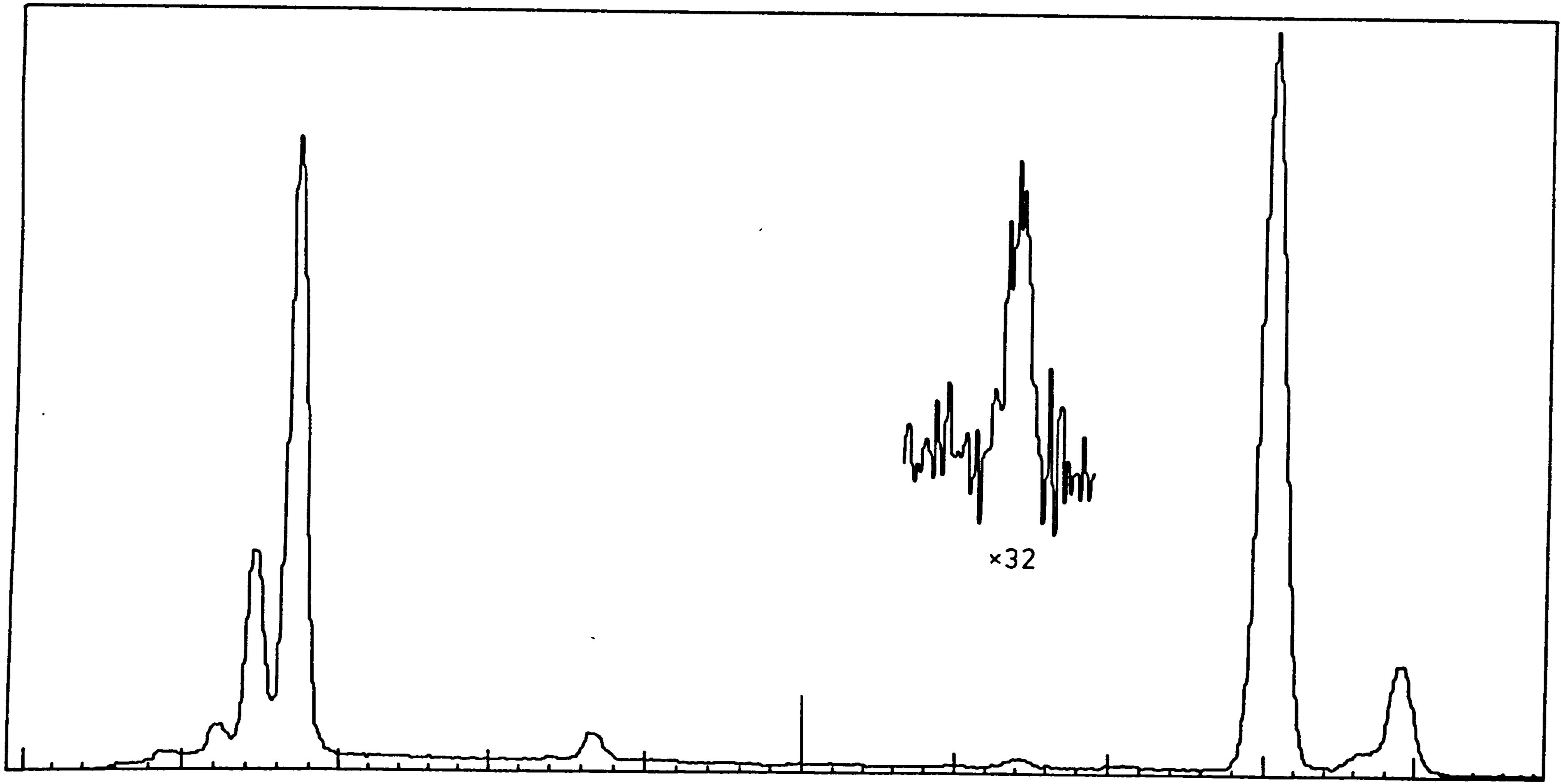

Fig.66: EPMA spectrum of Na soft Clark montmorillonite

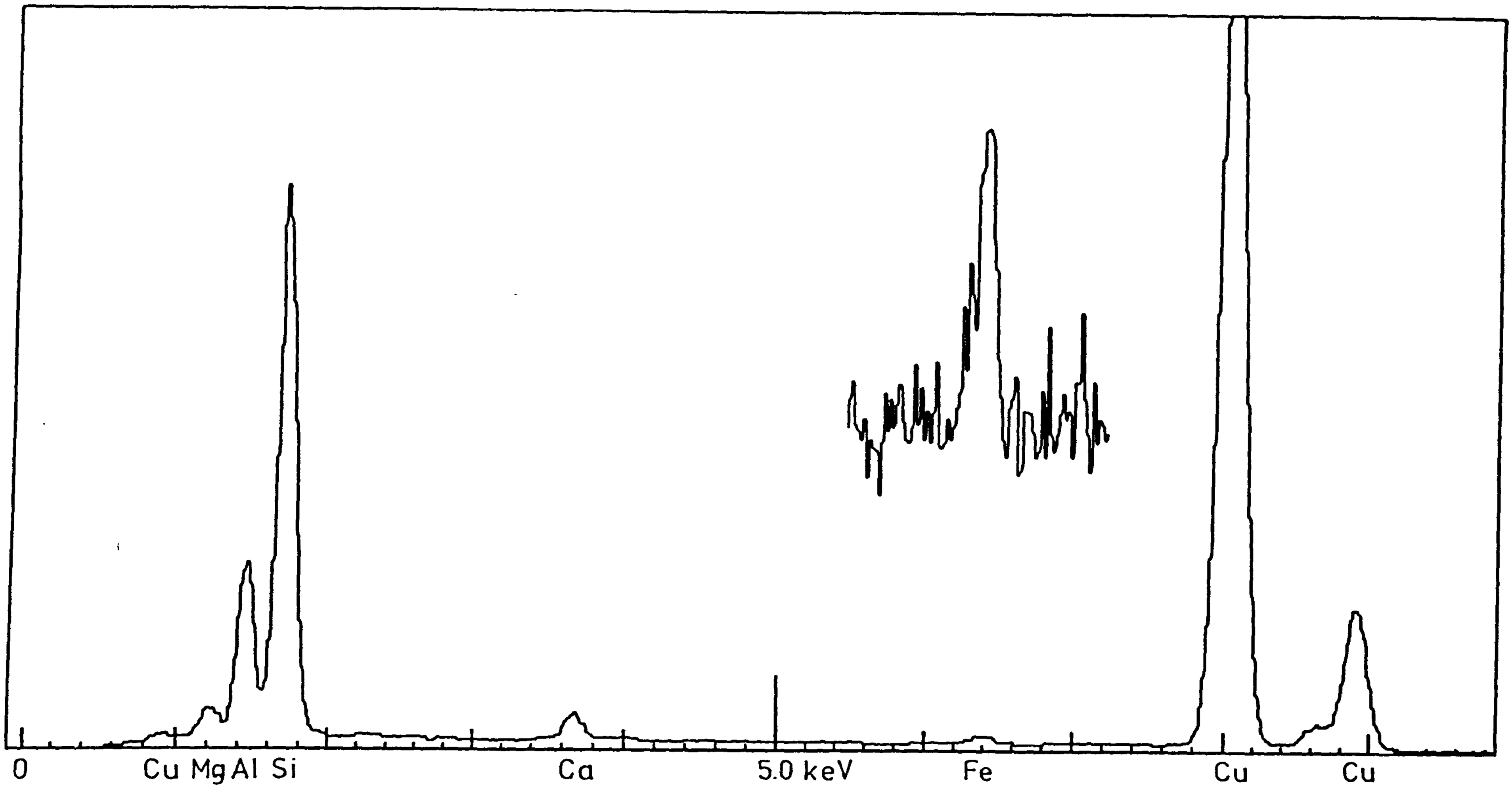

Fig.67: EPMA spectrum of Na Bentolite L montmorillonite

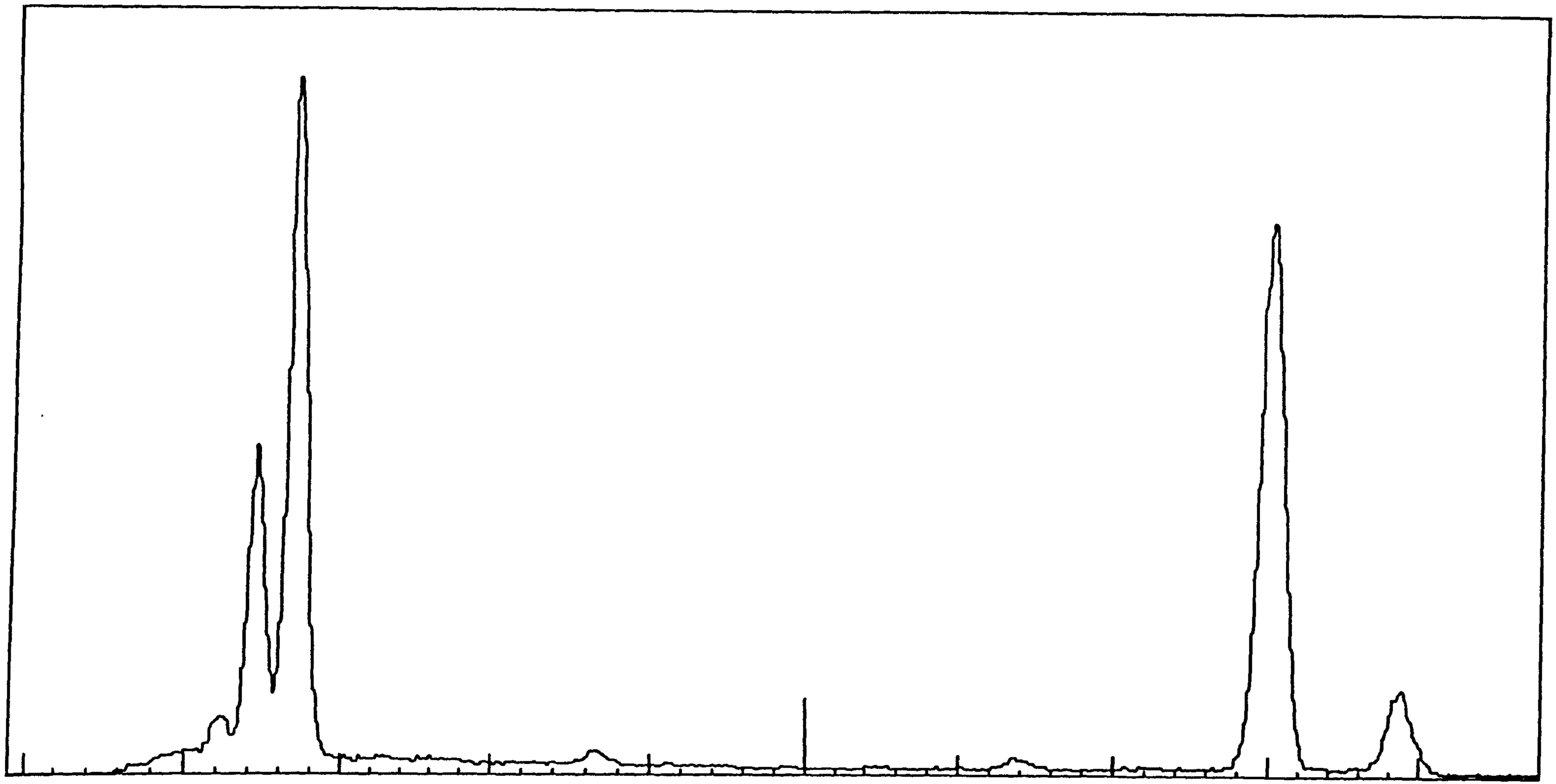

Fig.68: EPMA spectrum of Li soft Clark montmorillonite

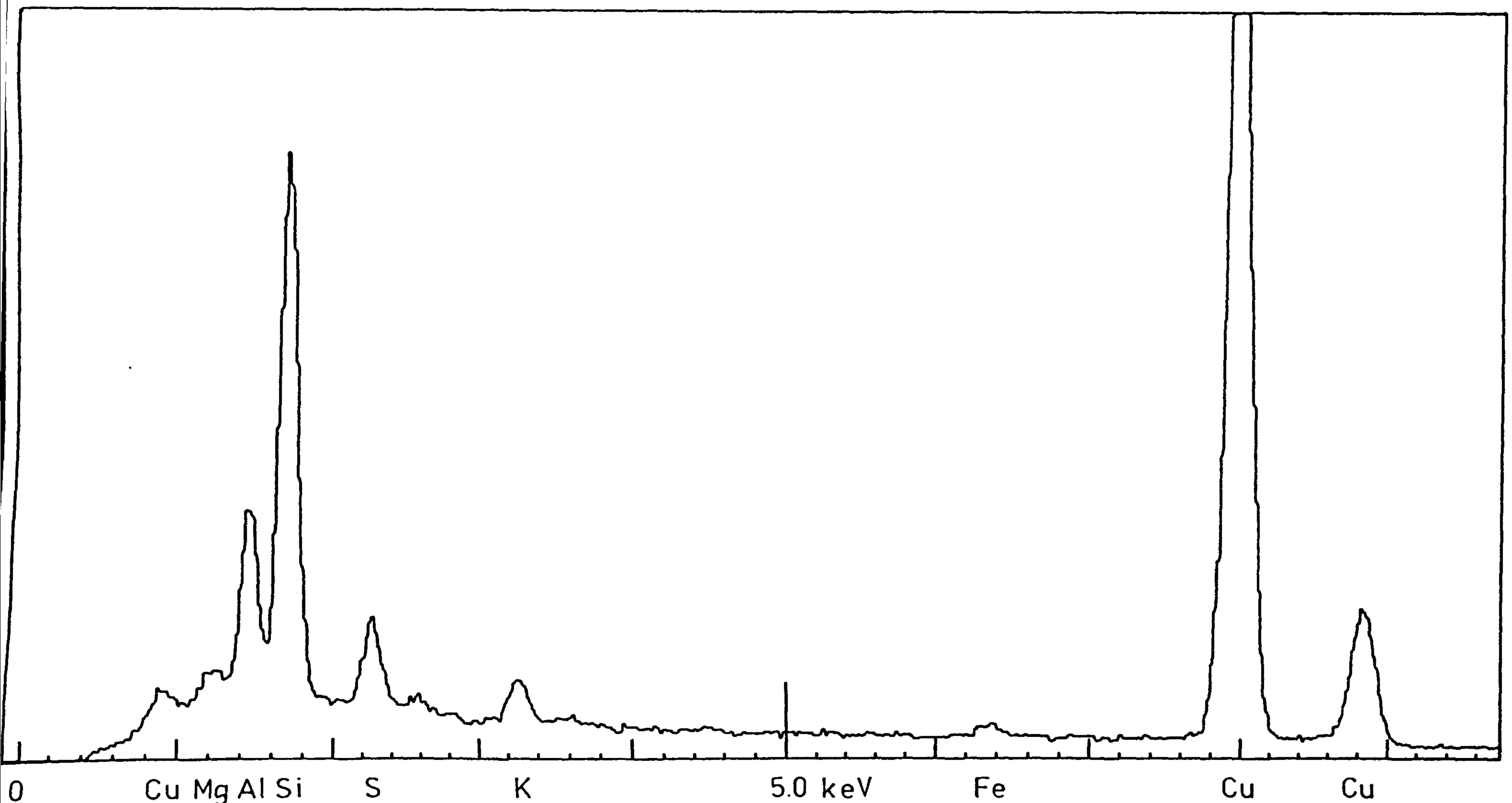

Fig.69: EPMA spectrum of Li Bentolite L - coarse fraction montmorillonite

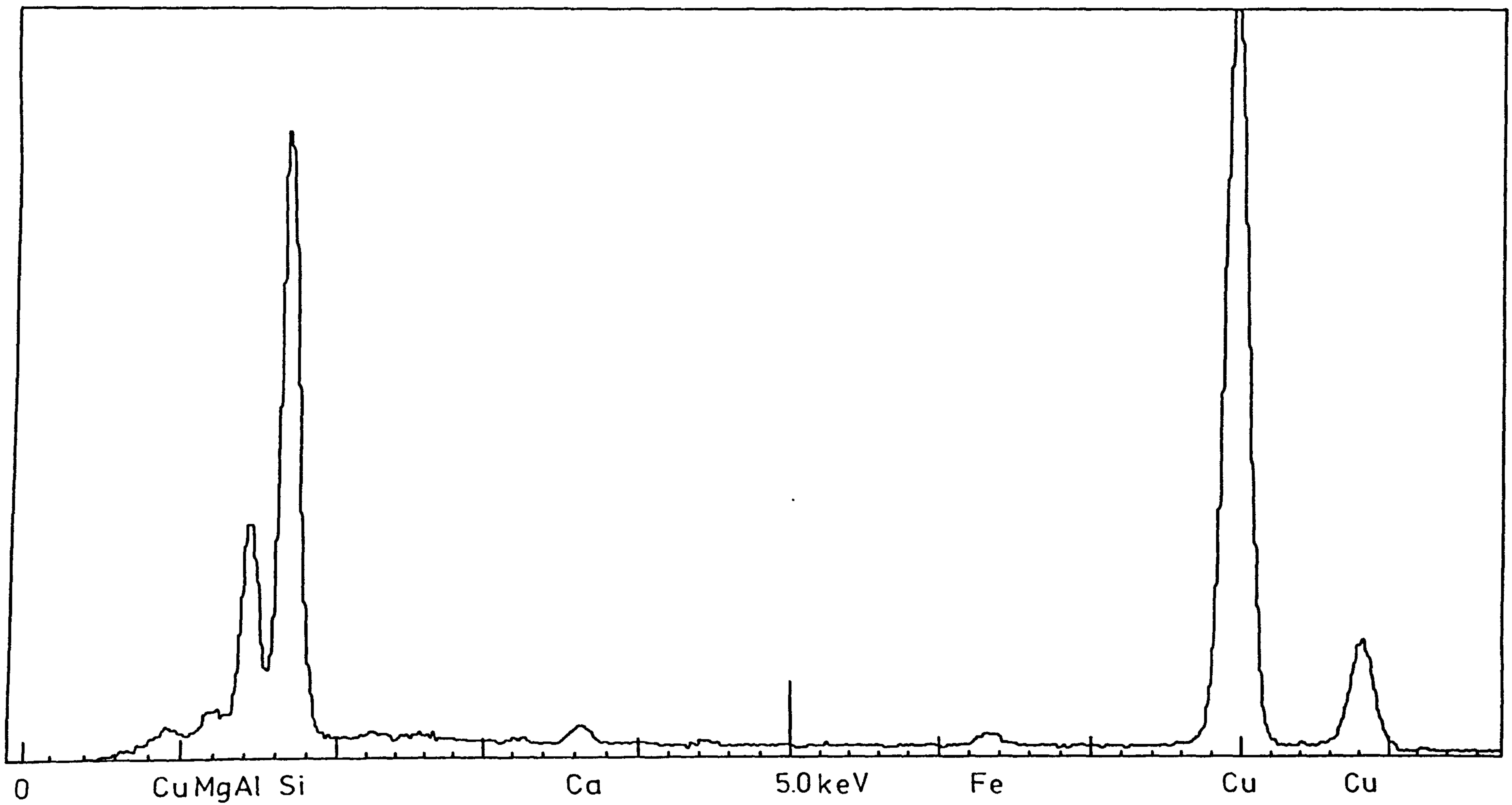

Fig.70 : EPMA spectrum of Li Bentolite L - fine fraction montmorillonite

can be used to help explain the Greene-Kelly results (sect. 7.3.2).

The electron probe microanalysis trace for the Li halloysite particles, shown in fig. 71 indicates the presence of Al and Si only.

It was noted with all samples that the electron probe microanalysis patterns obtained were similar for different individual montmorillonite particles in a given specimen.

.3.5 Cation exchange capacities

The measured cation exchange capacities for clay preparations are given in table 13.

TABLE 13: Cation exchange capacities

a. Analysis for Na^+ using ion selective electrode after exchange with 1 mol dm^{-3} ammonium acetate

Sample	CEC/meq/100g
Na Bentolite L	82•9±3•7
Na hard Helms	79•5±5•3
Na soft Clark	90•4±11•6

b. Analysis for Li^+ after exchange with

	1mol dm^{-3} CH_3COONH_4	2mol dm^{-3} CH_3COONH_4
Li Bentolite L	66•1	60•7
homogenised Li Bentolite L	66•3	72•2
Li soft Clark	87•7	76•5
Li cobbed soft Helms	57•5	60•2
Li Wyoming Blackhills	74•5	87•4

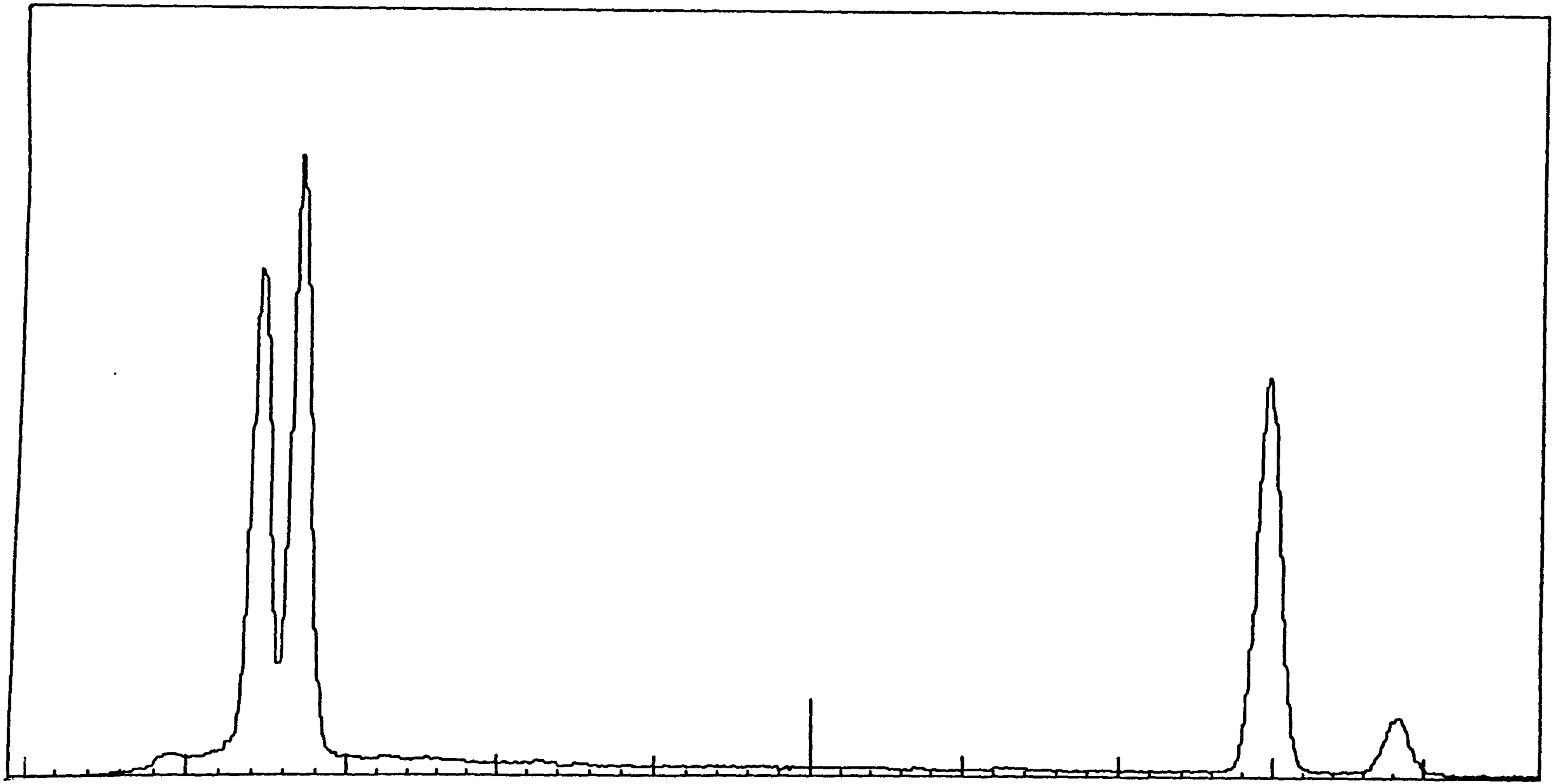

Fig.71 : EPMA spectrum of Li halloysite

7.3.6 Transient electric birefringence

The transient electric birefringence results, shown in fig. 72, obtained in the laboratory of Prof. B.R. Jennings, indicate that the Li Bentolite L and Li Wyoming Blackhills samples both have a very broad distribution of disc diameters. The two samples are very similar to each other (317), the mean disc diameters for Li Bentolite L and Li Wyoming Blackhills being 187 and 177nm respectively.

7.3.7 Calcium analysis

The amount of Ca^{2+} expelled by clay preparations, upon treatment with 1 mol dm^{-3} ammonium acetate, are given in table 14.

TABLE 14: Ca^{2+} analysis results

Sample	Measured Ca^{2+}/meq/100g
Li Wyoming Blackhills	5·0±2·2
Na Wyoming Blackhills	3·3±1·9
Li Bentolite L	11·3±0·2

These results (table 14) indicate that the Li Bentolite L sample contains significant amounts of calcium. The amounts of calcium in the Wyoming Blackhills samples are lower. These results are confirmed by the chemical analysis results (table 33, appendix 3).

Fig.72: Transient electric birefringence results - Disc diameter distributions

a: Li Bentolite L

mean diameter = 187 nm
mean (weight average) diameter = 3.5 µm

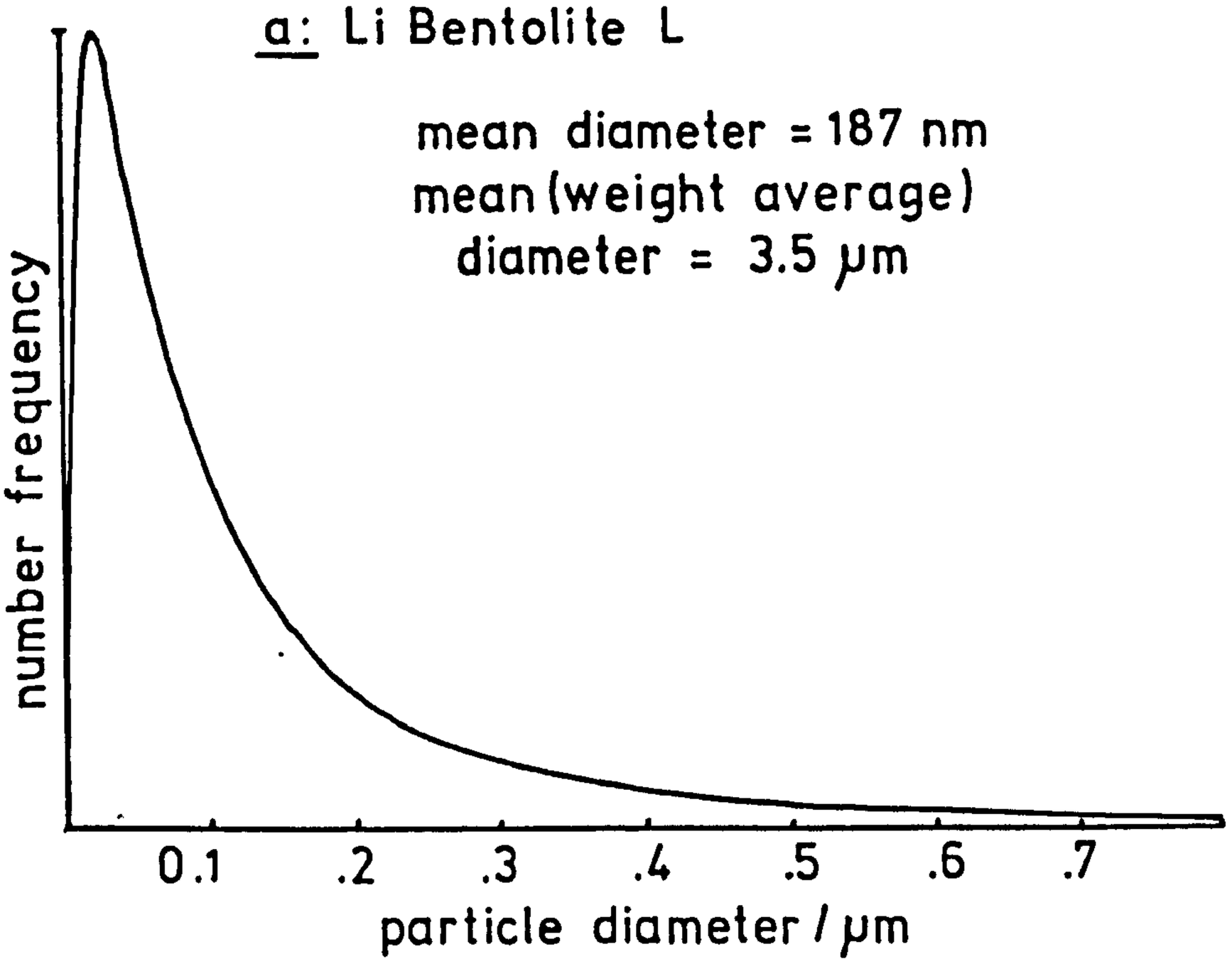

b: Li Wyoming Blackhills

mean diameter = 177 nm
mean (weight average) diameter = 3.9 µm

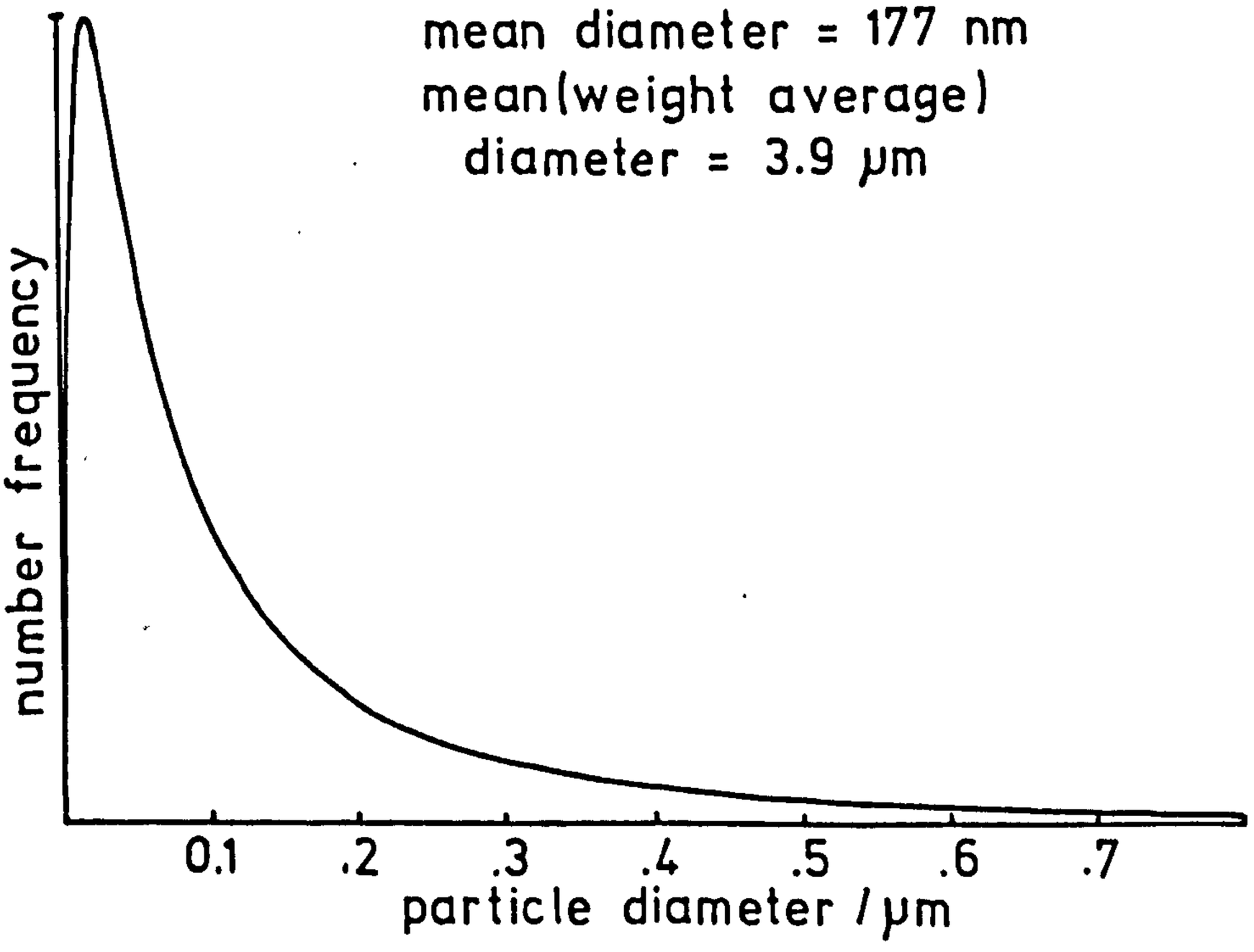

7.3.8 Scanning electron microscopy

The use of the freeze-drying technique for the preparation of specimens for scanning electron microscopy (sect. 7.2.8) has given electron micrographs which suggest that the coarse fraction of Li Bentolite L contains aggregates of large folded sheets incorporating regions of thicker/denser material (possibly silica or unaltered volcanic glass) (fig. 73) which are not present in the fine fraction of the sample (fig. 74). However the results obtained from this (or indeed any other) technique of specimen preparation must be interpreted with great caution because of the possibility of artifacts introduced during the procedure (sect. 7.2.8).

Scanning electron microscopy of the Li Bentolite L coarse fraction, prepared using a cytochrome c coated stud (sect. 7.2.8), showed aggregates (fig. 75) similar in appearance to those prepared by the freeze-drying technique (fig. 73). Some of these aggregates had a similar surface appearance to smectite in the crude material (sect. 5.3.3) and clay particles in the coarse samples (sect. 9.3) suggesting that they are composed of non-dispersed smectite particles. However, as with the freeze-drying method, these aggregates may be artifacts caused by aggregation of individual montmorillonite particles upon drying the sample, although it was hoped that the use of cytochrome c may have prevented this.

7.3.9 Electrophoresis

The electrophoretic mobilities of the particles in the clay

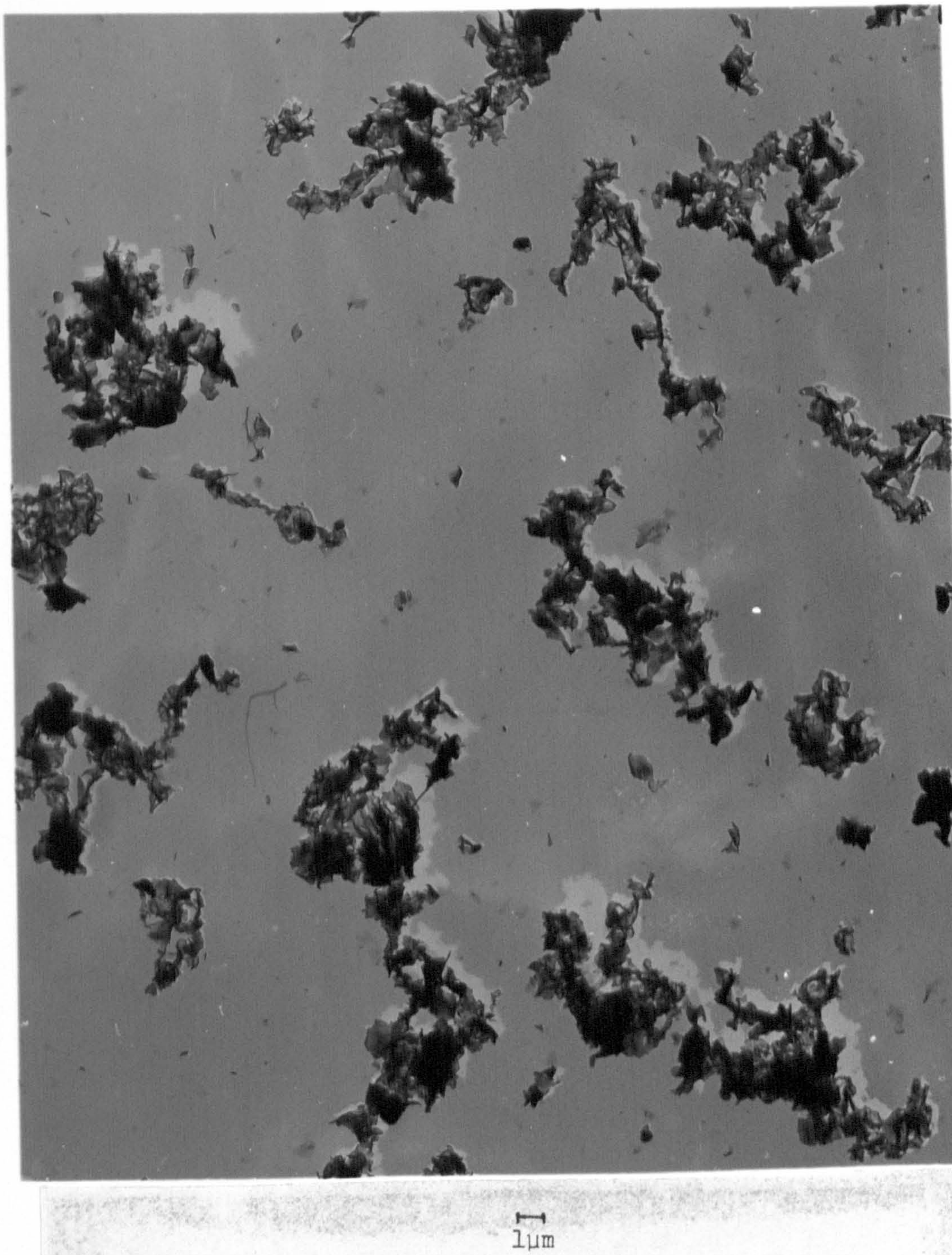

Fig. 73a : Transmission electron micrograph of Li Bentolite L - coarse fraction (method c)

Fig. 73b : Transmission electron micrograph of Li Bentolite L - coarse fraction (method c)

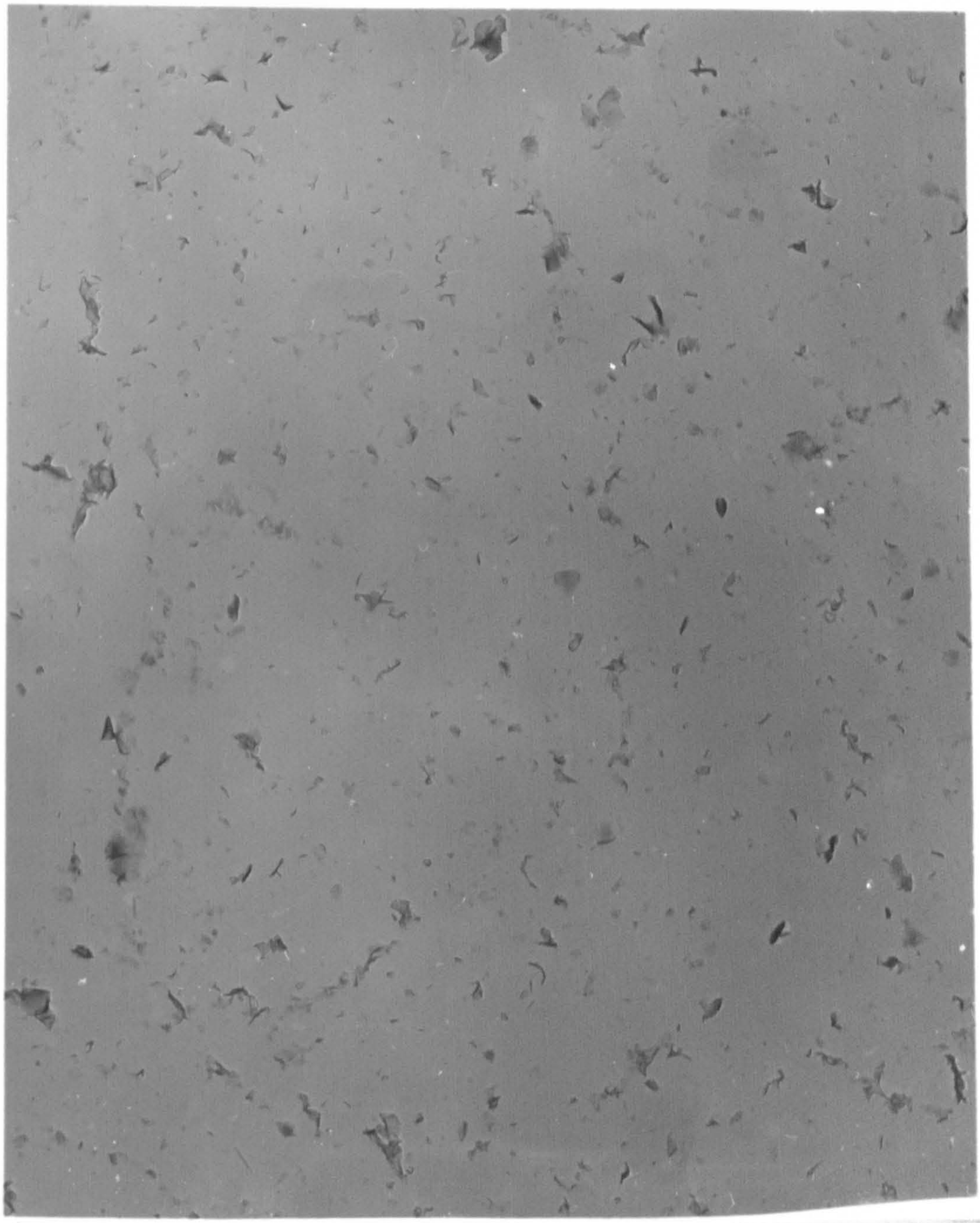

Fig. 74a : Transmission electron micrograph of Li Bentolite L - fine fraction (method c)

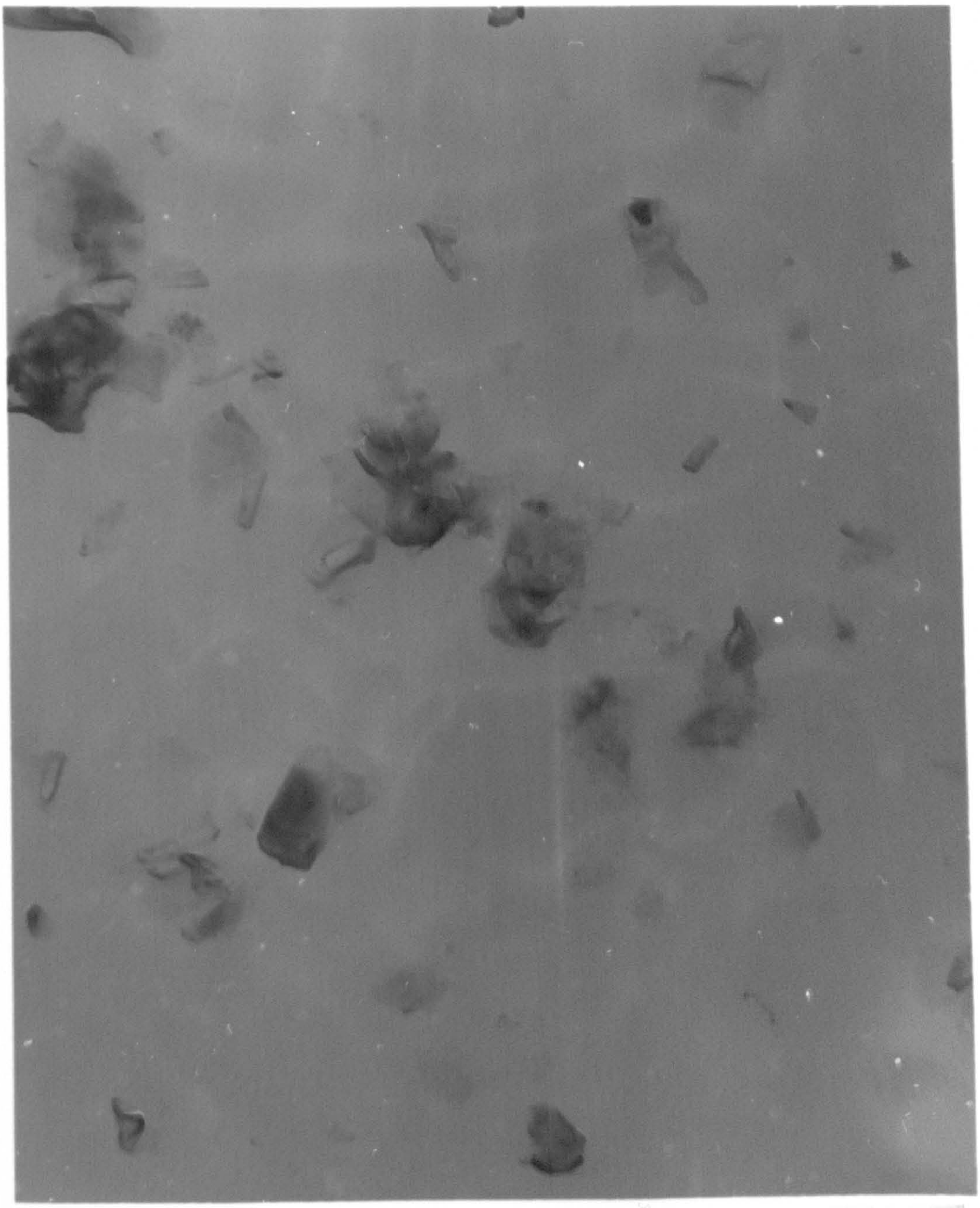

Fig. 74b : Transmission electron micrograph of Li Bentolite L - fine fraction (method c)

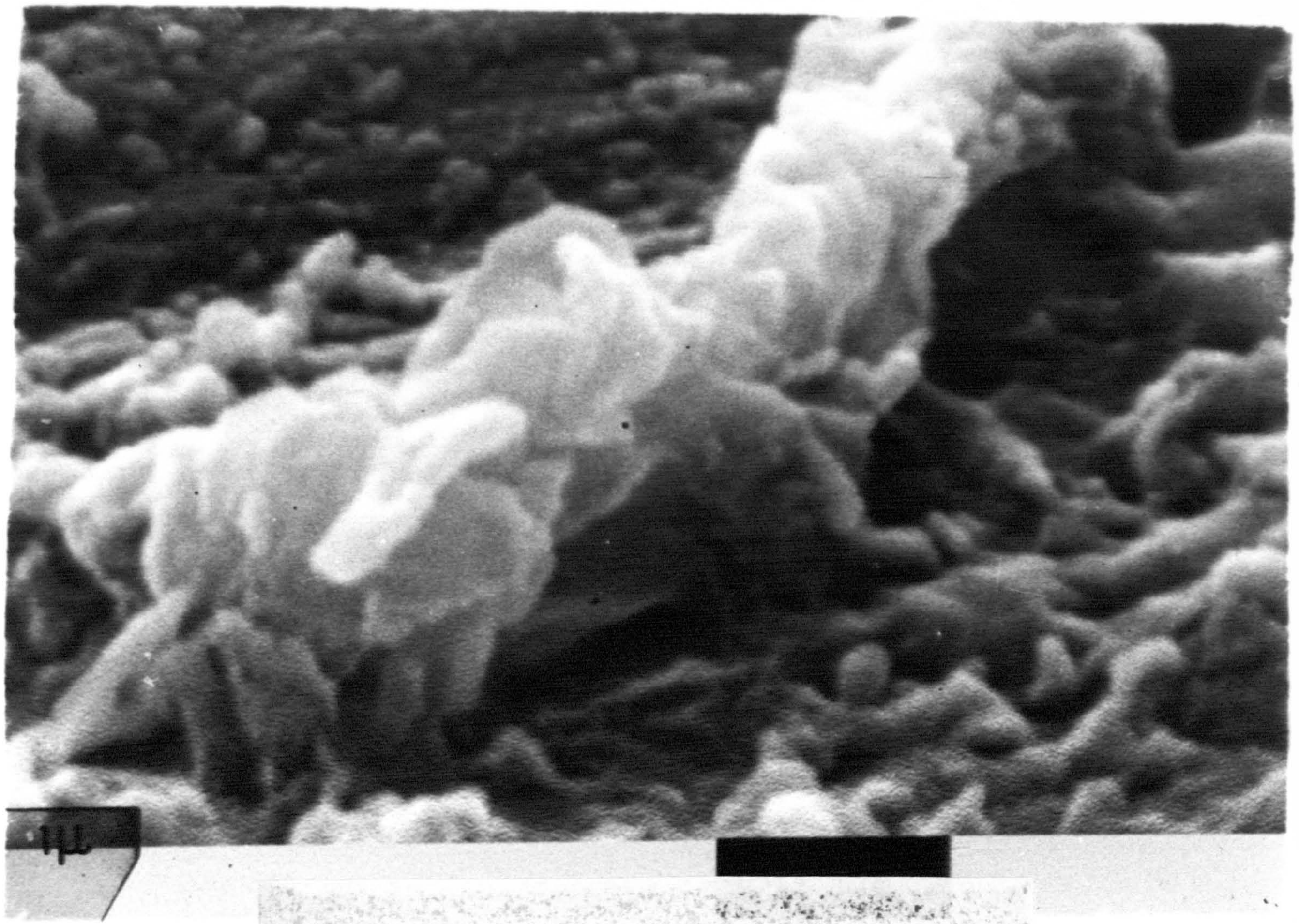

Fig. 75 : Scanning electron micrograph of Li Bentolite L - coarse fraction (on cytochrome c coated stud)

dispersions, shown in fig. 76, were found to be independent of pH in the range 3 - 11 and had similar mean values of 2·3 and $2 \cdot 1 \times 10^{-8} m^2 V^{-1} s^{-1}$ for Na Wyoming Upton and Na Bentolite L respectively. The occasional occurrence of particles having higher pH dependent mobilities in Na Bentolite L may be due to the presence of large impurity particles, e.g. quartz. The electrophoretic behaviour of the montmorillonite particles has a similar pH dependence to the results of Callaghan and Ottewill (196).

Fig.76: Effect of pH on electrophoretic mobilities of bentonite dispersions

● - NaBL , o - NaWU in 10^{-3} mol dm^{-3} NaCl solution

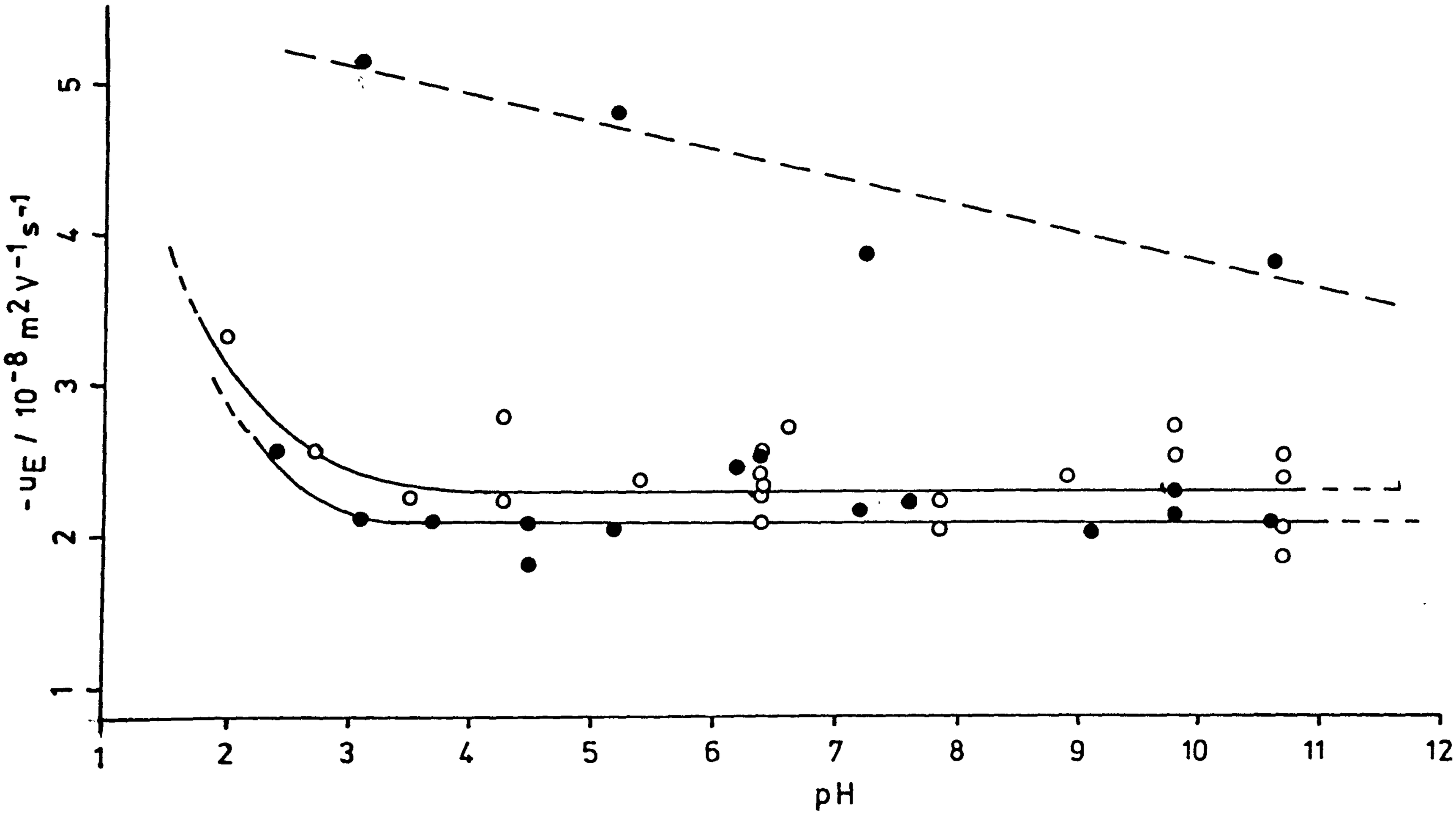

CHAPTER EIGHT

PULSE SHEAROMETRY

PULSE SHEAROMETRY

8.1 INTRODUCTION

Montmorillonite dispersions, if sufficiently concentrated, usually show viscoelastic behaviour (sect. 3.2.4), with the elastic component becoming progressively more dominant as the degree of interparticle interaction is increased (194, 338). Under appropriate conditions the rigidity of a bentonite dispersion will be such that it exists as a gel. The shear modulus (sect. 3.2.4.2) may be used as a measure of the stiffness of such a gel (194, 230, 231, 232, 338).

This chapter describes the measurement of the shear moduli of the clay dispersions prepared as described in chapter 6. The shear modulus of each dispersion sample was measured using a Rank Brothers pulse shearometer (284). In this way it was possible to study the effects of variations in sample preparation procedure, sample conditions (e.g. clay volume fraction, electrolyte concentration, counter-ion type) and source of sample upon the rigidity of the gels. The main aim of the work being to compare the gelling properties of the Wyoming and Texas bentonites (chapter 1).

8.2 ESTIMATION OF SHEAR MODULUS

The response of a linear viscoelastic fluid to an oscillatory shearing strain may be described in terms of a complex modulus G* (W),

(223, 338). This has two components defined by equation 42

$$G^* (\omega) = G'(\omega) - i\omega\eta'(\omega) \qquad (42)$$

where $G'(\omega)$ and $\eta'(\omega)$ are the dynamic rigidity and the dynamic viscosity, respectively. ω is the angular frequency of deformation and $i = \sqrt{-1}$. Under steady flow conditions ($\omega=0$) $G'=0$ and purely viscous (Newtonian) behaviour is observed.

Under non-steady shear conditions ($\omega>0$) both energy dissipation and storage occur in varying degrees, and at high frequencies G' approaches a limiting value given by

$$G_0 = \lim_{\omega\to\infty} G' \qquad (43)$$

The components of the dynamic modulus are related to the velocity of the wave, v_p, and the density of the sample, ρ, by

$$G' = \frac{v_p^2\rho(1-r^2)}{(1+r^2)^2} \qquad (44)$$

and

$$\eta' = \frac{2\rho v_p^2}{\omega(1+r^2)^2} \qquad (45)$$

where $r = \Lambda/2x_0$,

Λ = wavelength of the shear-wave

and x_0 = critical damping length.

If damping is small (i.e. r<0•1), then the approximation

$$G' \simeq v_p^2 \rho \qquad (46)$$

may be made (338). The pulse shearometer may be used to measure the velocity of propagation of a shear-wave through a gel sample and the shear modulus G obtained from equation 47, (284, 338).

$$G = v_p^2 \rho \qquad (47)$$

8.3 EXPERIMENTAL

8.3.1 Introduction - The Pulse Shearometer

The shear moduli of the clay dispersions were measured using a Rank Brothers pulse shearometer (284). The apparatus used consisted of a shearometer cell connected to a signal processing unit which was interfaced with an Acorn Atom microcomputer and TV monitor.

A diagram of the pulse shearometer cell is shown in fig. 77. The cell consists of two parallel stainless steel discs, each mounted, via an axial perspex rod, on a piezo-electric crystal. The separation of the discs may be altered by means of an adjustment screw and measured with a dial gauge.

8.3.2 Principle of operation

A potential pulse applied to the (lower) piezo-electric crystal

Fig.77 : Diagram of pulse shearometer cell

Not to scale

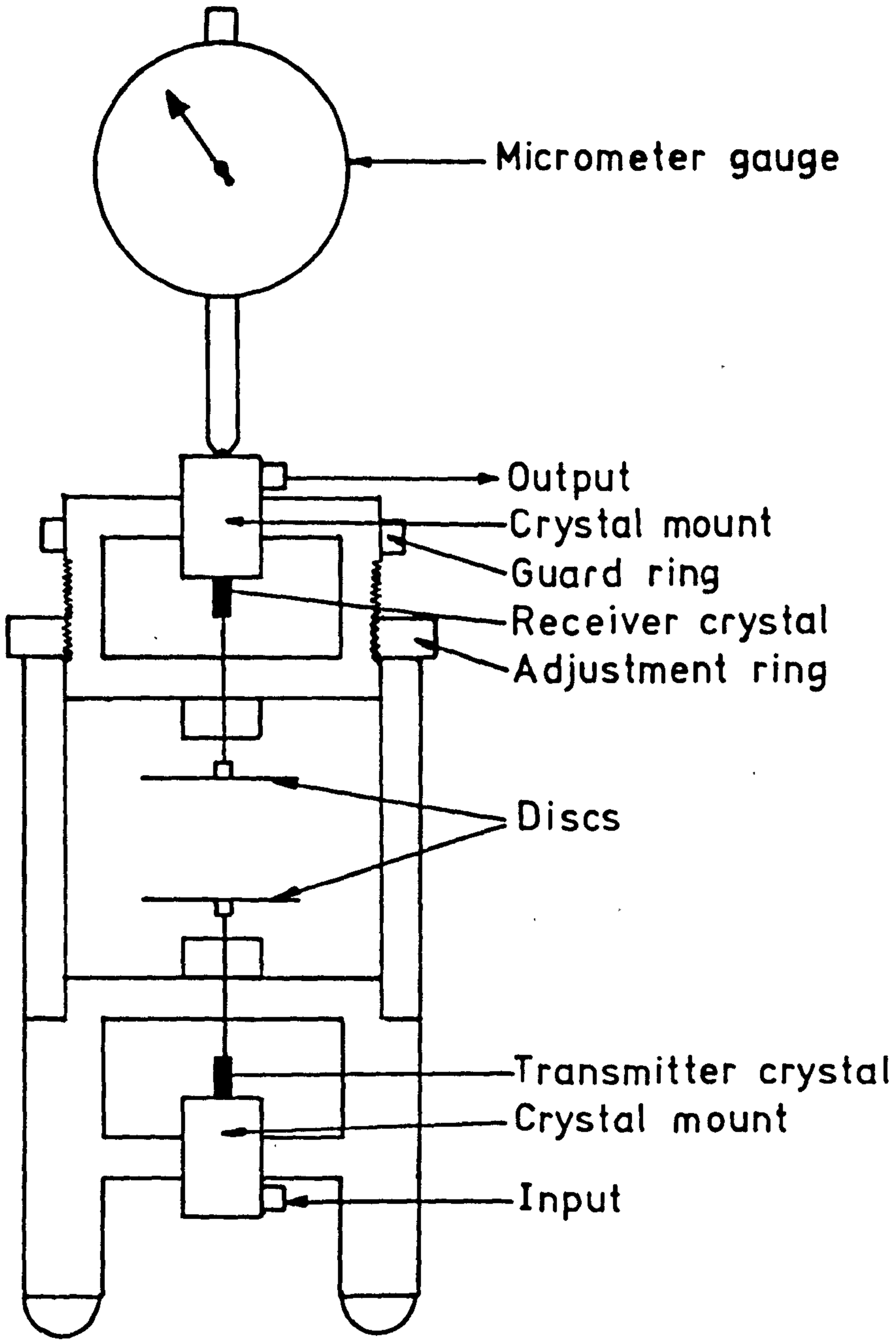

causes the transmitter disc to twist. A torsional shear wave is propagated through the medium contained between the discs, causing motion of the (upper) receiver disc. This displacement is converted into electrical signals, by the second piezo-electric crystal, which are amplified by the signal processor unit and monitored by the computer.

The voltage of the potential pulse applied to the transmitter crystal and the amount of amplification of the detected signal could be altered, using the sensitivity and gain controls on the signal processing units respectively, until a satisfactory signal was obtained. An ideal signal, consisting of a horizontal line ending with an exponentially damped sine wave, is shown in fig. 78. The propagation time, t_p, of the shear wave was measured.

8.3.3 Measurement Procedure

The zero separation position was set by assembling the shearometer with an empty cell and connected to the signal processing unit and computer. The discs were adjusted to a separation of ∿2mm. The discs were slowly moved together, ∿100μm at a time, pulsing the transmitter crystal with the signal processing unit between each adjustment, until a wave form was first seen on the computer display. The discs were then separated, in ∿10μm steps, until the wave form just disappeared. The guard ring (see fig. 77) was now pushed down into contact with the adjustment screw and locked into place. The dial gauge height (fig. 77) was now adjusted until the gauge read zero, with the measuring tip in

Fig.78: Pulse shearometer trace

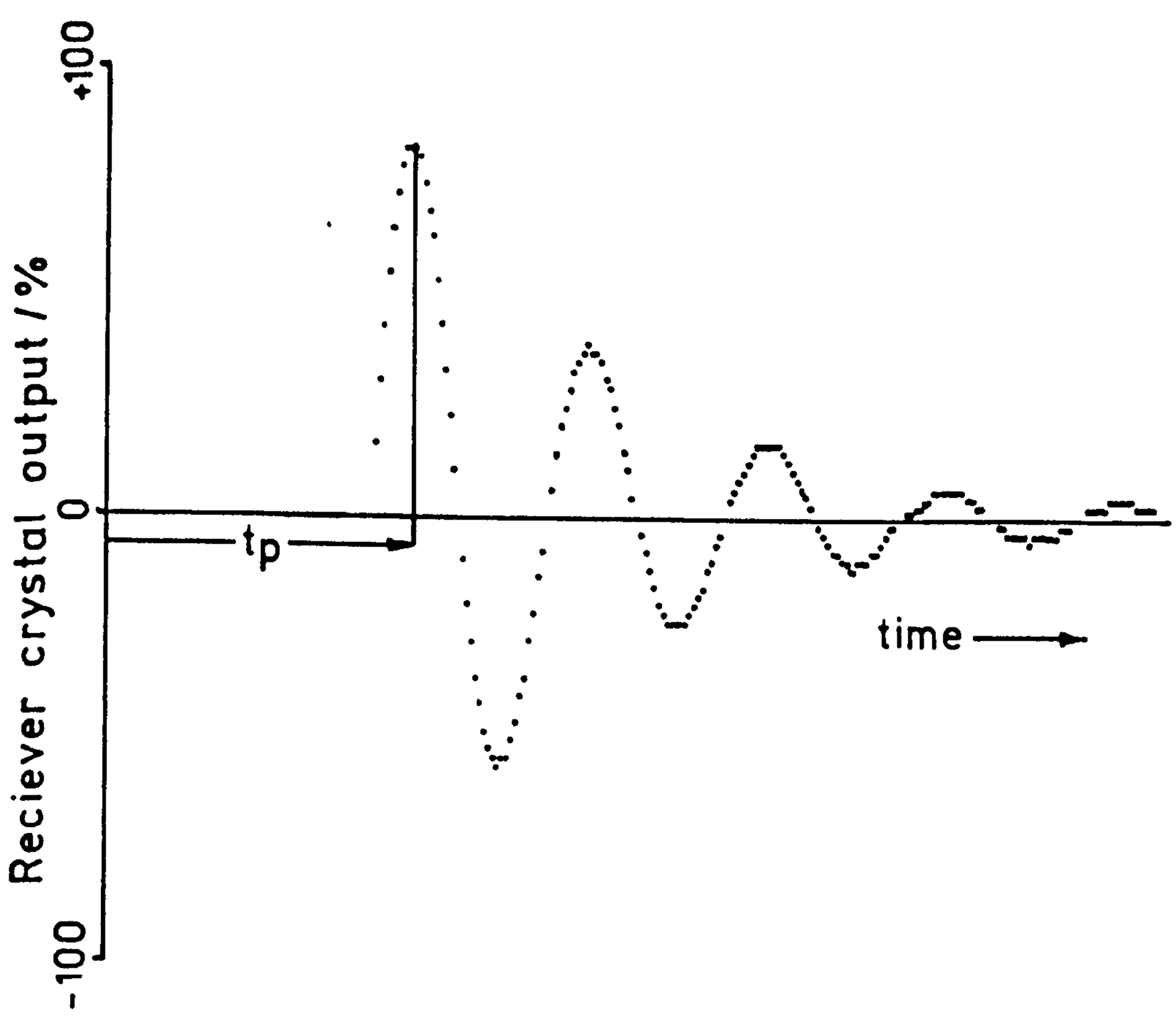

contact with the centre of the top of the receiver crystal mount.

The shearometer cell was filled with ~50cm^3 of dispersion and the propagation times were measured for a series of disc separations. A graph of disc separation against t_p was plotted and the velocity of propagation, v_p, 'e.g. fig. 30) was found from the slope of the line, which was calculated by the computer using the least squares method. The shear modulus, G, can then be calculated from

$$G = v_p^2 \rho \qquad (47)$$

where ρ is the density of the dispersion, as given in sect. 8.2, ρ was calculated using the equation

$$\rho = \frac{100\rho_c\phi}{\omega} \qquad (48)$$

where ω and ϕ are the weight (/%) and volume fractions of clay in dispersion respectively and ϕ was calculated from

$$\phi = \frac{1}{\left[1+\rho_c(100/\omega-1)/\rho_\omega\right]} \qquad (49)$$

where ρ_c = density of clay and ρ_ω = density of water. ρ_ω was set equal to 1·0 gcm^{-3} and ρ_c was assumed to be 2·5 gcm^{-3} (285), although the actual value may vary with differing degree and type of isomorphous substitution (5).

The shear modulus measurements were carried out at ambient temperature.

8.3.4 Accuracy

The error in G due to the calculation of the slope of the disc separation against t_p plots (fig. 79) was usually very small (<< 0·1% - by least squares or least distance). The reproducubility between measurements of G was typically ∿3%, for non time dependent gels of high G (>100Nm^{-2}). For thixotropic or weak gels reproducibility could be much worse because of the variation of G with time, significant damping (hence equation 46 being invalid) or poor signal:noise ratios. Artifacts also occurred due to the close spacing of the discs (225). Variations in G of ∿100% were possible with very weak gels (G<50Nm^{-2}).

Under ideal conditions, for a gel having an easily measurable shear modulus, it was considered that the experimental procedure was sufficiently good that the shearometer could measure differences due to the methods of sample preparation.

8.4 RESULTS* AND DISCUSSION

Figs. 80 to 87 show plots of log G against weight fraction (w/w) of clay. Figs. 80 and 81 compare the results for the Li and Na Wyoming bentonites respectively, in 10^{-3} mol dm^{-3} electrolyte solution. These indicate that the two Wyoming bentonite samples, Wyoming Blackhills (WB) and Wyoming Upton (WU), have similar shear moduli at a given

* see footnote on p.123

Fig.79: Example of pulse shearometer results

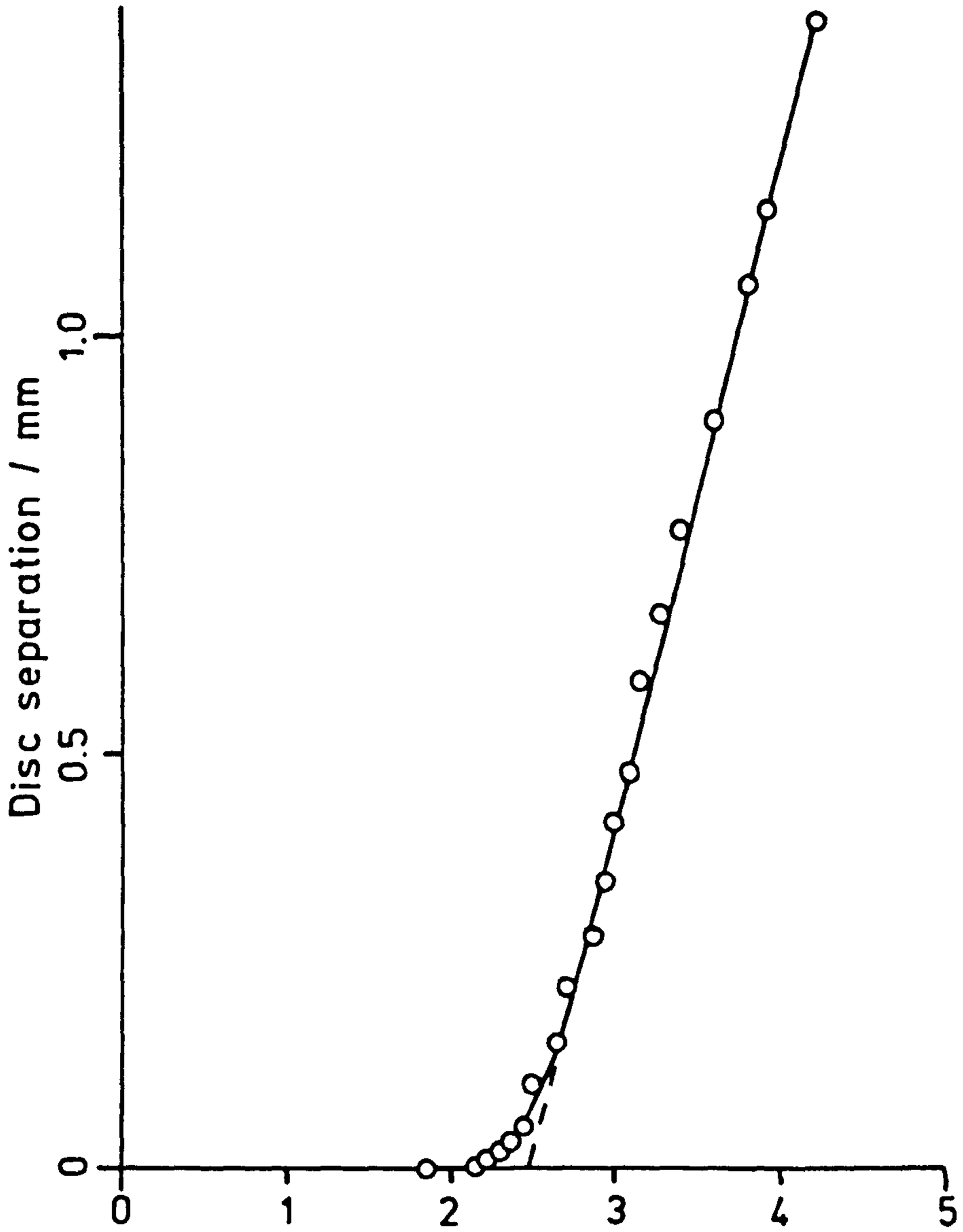

Fig.80: Pulse shearometer results for Li Wyoming bentonite dispersions

● - LiWB , o - LiWU in 10^{-3} mol dm^{-3} LiCl solution

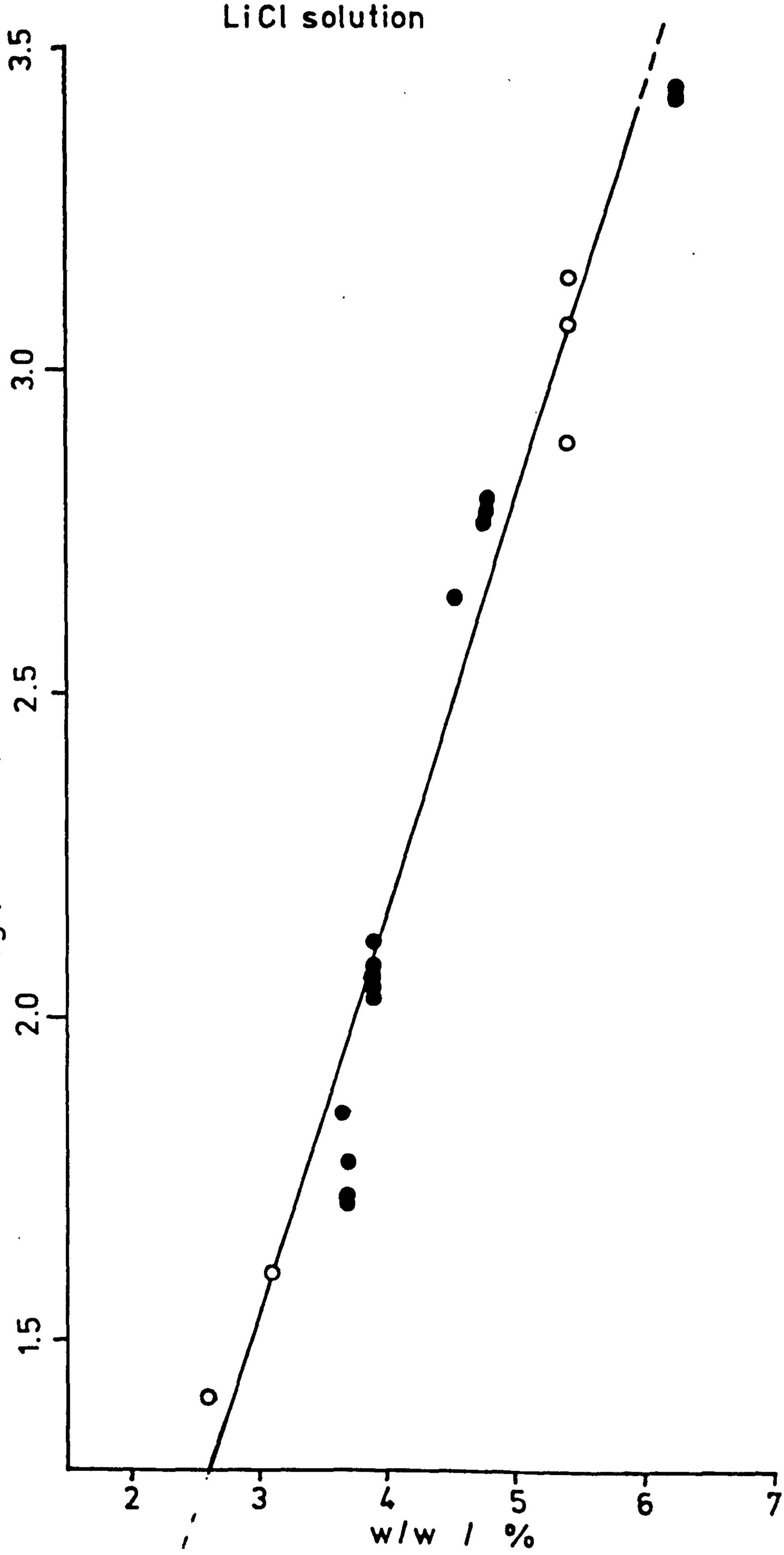

Fig.81 : Pulse shearometry results

× - NaWB in 10^{-4} mol dm^{-3} NaCl
○ - NaWB in 10^{-3} mol dm^{-3} NaCl
● - NaWU in 10^{-3} mol dm^{-3} NaCl

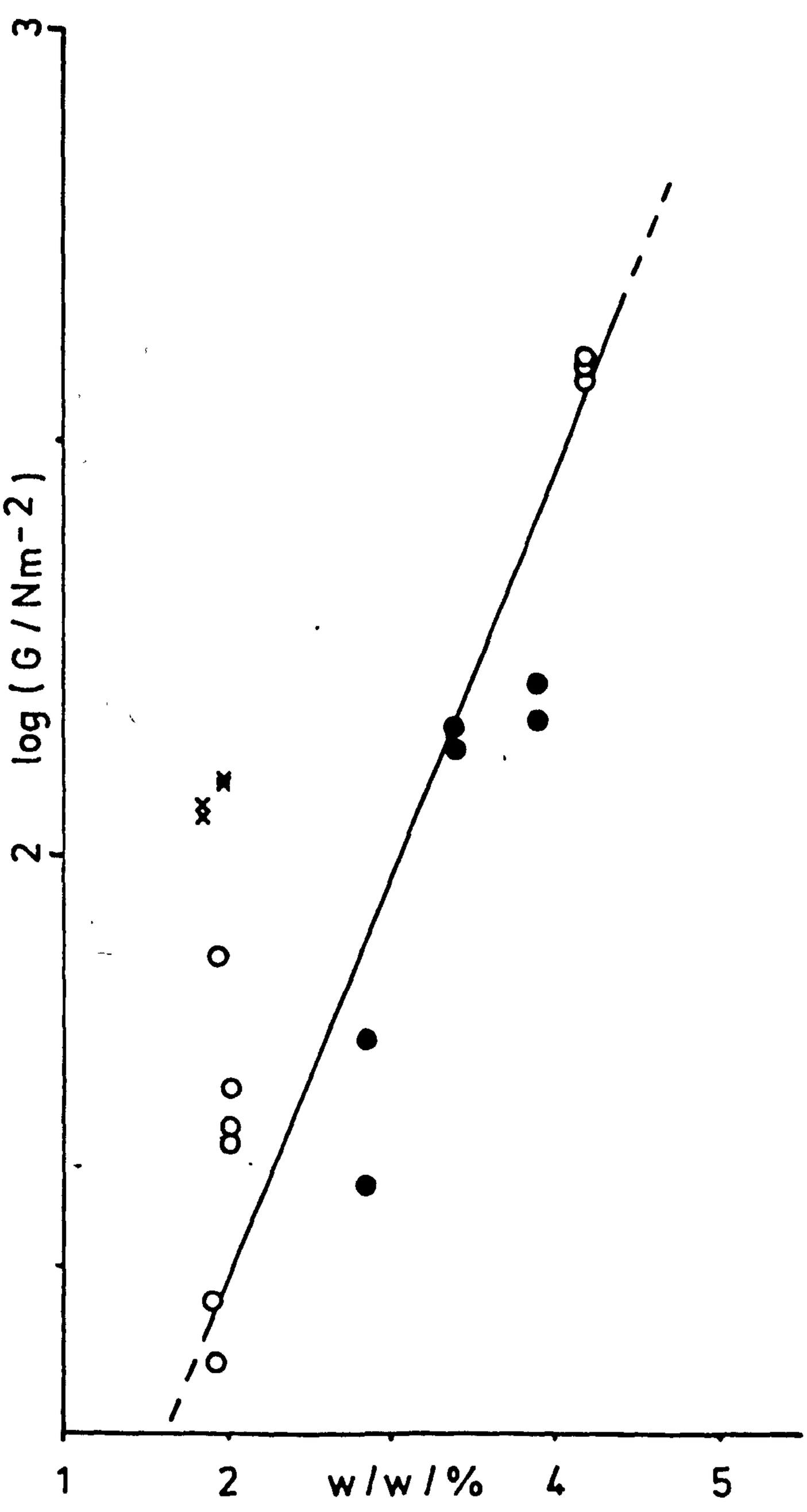

volume fraction, in either the Li (fig. 80) or Na (fig. 81) forms.

The results for Li Wyoming Blackhills bentonite at different LiCl concentrations are shown in fig. 82. The results at 10^{-4} and $5x10^{-4}$ mol dm^{-3} LiCl seem similar to each other. However it is not possible to discuss comparisons of the results obtained at $5x10^{-4}$ mol dm^{-3} LiCl with the others in fig. 82 since different batches of Wyoming Blackhills bentonite and different preparation procedures involved repeated high speed centrifugation and redispersion of the clay in $5x10^{-4}$ mol dm^{-3} LiCl rather than the use of ion exchange resins (sect. 6.2.3) used for the results of 10^{-4}, 10^{-3} and 10^{-2} mol dm^{-3} LiCl. The preparation of the sample in $5x10^{-4}$ mol dm^{-3} LiCl were used to prepare these samples. The results obtained at 10^{-4}, 10^{-3} and 10^{-2} mol dm^{-3} LiCl show that G decreases, at a given w/w, as the electrolyte concentration is increased. This also occurs

---

* - Note on presentation of results

It was noted that some of the plots of log G against w/w (figs. 80 - 87 and 96) showed apparently linear relationships (e.g. fig. 80). The results of Rand et al (194) indicated that there was such a linear relationship for Na Wyoming bentonite dispersed in $4{\cdot}6x10^{-4}$ mol dm^{-3}NaCl. Hence a least squares analysis was carried out to fit the data to log G = M(w/w/%) + C. The results of these least squares analyses are given in table 15 and the corresponding straight lines are shown on some of the plots. It is not being suggested here that there is a linear relationship between log G and w/w, indeed some of the results (e.g. fig. 85) and the theoretical calculations (chapter 10) indicate that there is some slight curvature to the plots. The least squares parameters were only used to compare general trends in the results. Possibly unreliable results for data with $G<50 Nm^{-2}$ (sect. 8.3.4) (log $G<1{\cdot}7$) were generally ignored in the analyses.

Fig.82: Pulse shearometer results for Li Wyoming Blackhills dispersions

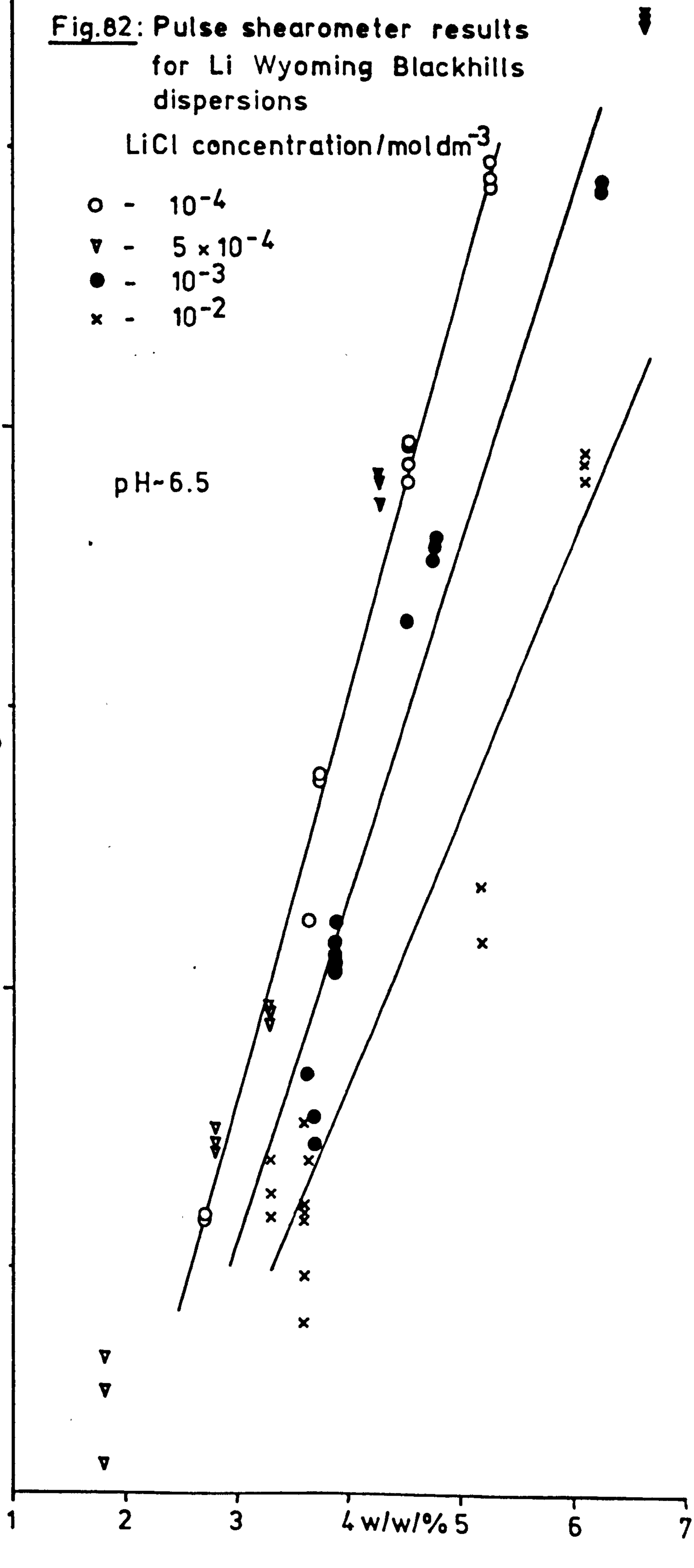

Table 15: Least squares parameters for Log G against w/w data

	Clay	electrolyte concentration/ mol dm^{-3}	slope (m)	intercept (c)
a)	Na Wyoming Blackhills(pH3)	10^{-3}	0•64±0•76	0•14±3•47
b)	Na Wyoming Blackhills	10^{-4}	0•35±0•05	0•41±0•01
c)	Na Wyoming Blackhills	10^{-3}	2•23±1•90	-2•76±13•78
d)	Na Wyoming Blackhills	10^{-2}	0•55±0•03	0•75±0•06
e)	Li Wyoming Blackhills	$5x10^{-4}$	0•53±0•02	0•29±0•01
f)	Li Wyoming Blackhills	10^{-4}	0•76±0•02	-0•55±0•01
g)	Li Wyoming Blackhills	10^{-3}	0•63±0•03	-0•40±0•02
h)	Li Wyoming Blackhills	10^{-2}	0•43±0•03	0•12±0•02
i)	Li Wyoming Blackhills	∿1	0•24±0•06	1•61±0•06
j)	K Wyoming Blackhills	10^{-3}	0•58±0•03	-0•05±0•01
k)	Cs Wyoming Blackhills	10^{-3}	0•20±0•07	1•98±0•06
l)	Li Wyoming Upton	10^{-3}	0•65±0•05	-0•49±0•05
m)	Na Wyoming Upton	10^{-3}	0•75±0•22	-0•61±0•54
n)	Na Bentolite L	10^{-2}	0•24±0•05	0•89±0•10
o)	Li Bentolite L	10^{-4}	0•43±0•04	-0•38±0•04
p)	Li Bentolite L	10^{-3}	0•40±0•03	-0•33±0•04
q)	Li Bentolite L	10^{-2}	0•25±0•02	0•23±0•02
r)	Li Bentolite L-prep D	10^{-3}	0•42±0•01	-1•03±0•01
s)	Li Bentolite L-prep D fine fraction	10^{-3}	0•30±0•11	1•00±0•43
t)	Li Bentolite L-homogenised	10^{-3}	0•40±0•07	0•29±0•09
u)	Li cobbed soft Helms	10^{-4}	0•28±0•03	1•11±0•03
v)	Li cobbed soft Helms	10^{-3}	0•44±0•04	-0•36±0•06
w)	Li soft Clark	10^{-3}	0•52±0•08	-0•32±0•11
x)	Li Halloysite	10^{-3}	0•15±0•03	1•60±0•10

for Na Wyoming Blackhills bentonite as the NaCl concentration is increased from 10^{-4} to 10^{-3} mol dm^{-3} (NaWB in fig. 81). This trend may be explained by a reduction of the range of the electric double layer repulsions as the electrolyte concentration is increased (chapter 10). There also seems to be a reduction in the general slope of the plots as the electrolyte concentration is increased (table 15f, g, h), this trend is also shown by simple theoretical calculations (chapter 10).

Fig. 83 shows the results for the Li, Na, K and Cs forms of Wyoming Blackhills bentonite, in 10^{-3} mol dm^{-3} solutions of the appropriate chloride. Fig. 83 and table 15g, c, j, k, show that the slope of the plot for Cs Wyoming Blackhills bentonite is much lower than that of the other forms in 10^{-3} mol dm^{-3} electrolyte. This is probably due to differences in the rheological behaviour of the samples at this electrolyte concentration (see also fig. 93), ranging from the anti-thixotropic* Li Wyoming blackhills bentonite (LiWB) (see fig. 90) to the thixotropic* Cs form. It was noted that the gels of the Li and Na forms of the Wyoming Blackhills bentonite

---

* - A thixotropic system is defined here as one which having been shaken and poured into the shearometer cell exhibits an increase in structure (G) with time. With an anti-thixotropic system G decreases with time after disrupting the system. Rheopexy is the phenomenon where the rate of increase in G (or viscosity of a thixotropic system is increased by the application of gentle shearing to the system. The rheopectic properties of bentonite dispersions (340, 341) were not studied in this work.

Fig.83 : Pulse shearometry results

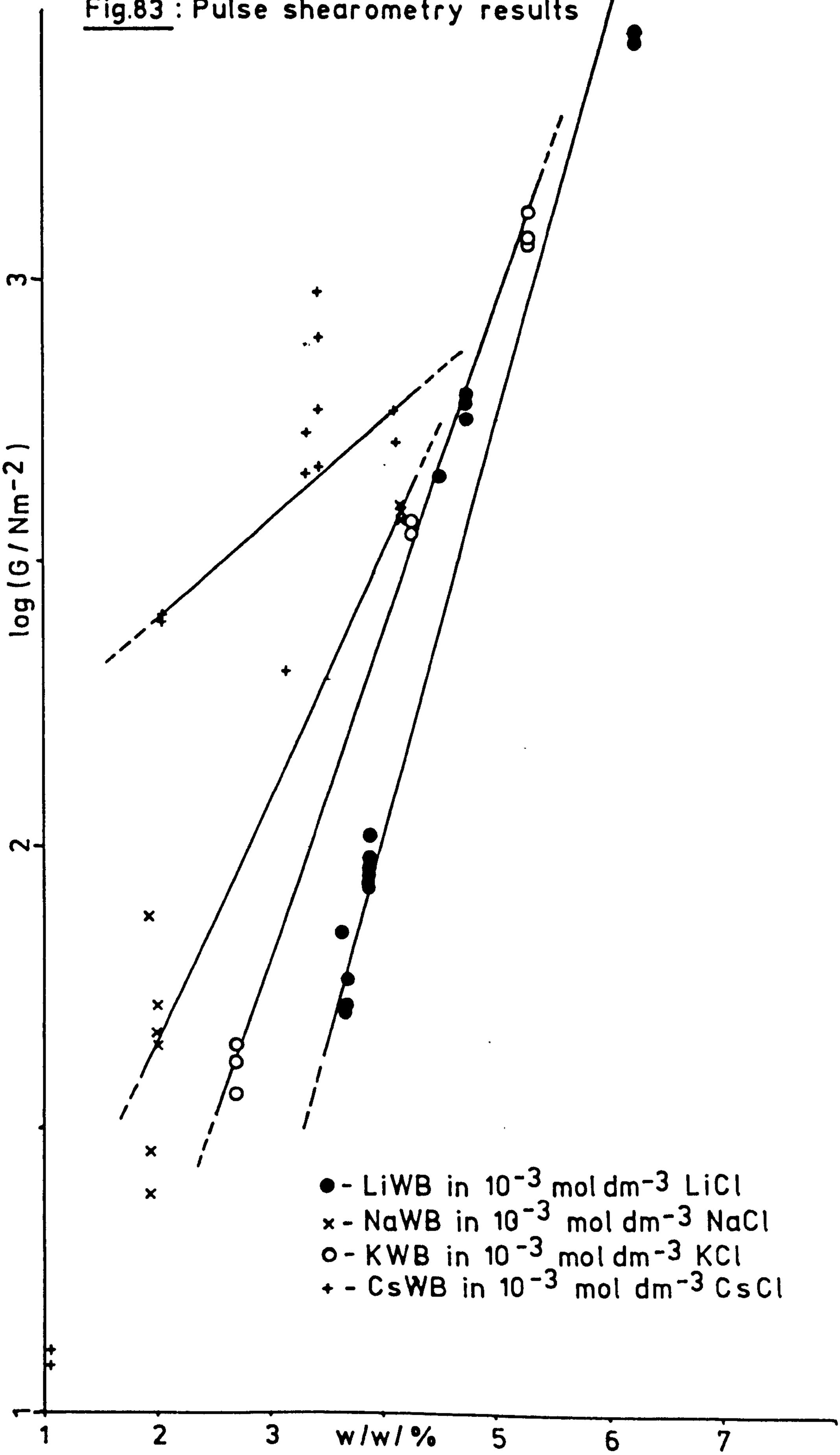

were quite dark green in appearance. The K form was slightly paler green than the Li and Na forms, while the Cs form was much paler than the other forms. This change in appearance has been noted previously (145) and has been attributed to increased light scattering as the tactoid (sect. 3.2.2) size increases (145) as the counter-ion is changed from Li to Na, K and then Cs. A sample of Ca Wyoming Blackhills bentonite prepared was found to be almost white in appearance 10^{-3} mol dm^{-3} $CaCl_2$, which would seem to be in agreement with the above trend (145) (table 4).

Fig. 84 shows the effects of changing LiCl concentration on the pulse shearometry results for Li Bentolite L dispersions. As the LiCl concentration is increased, in the range 10^{-4}, 10^{-3} to 10^{-2} mol dm^{-3}, G decreases for a given w/w, as with the Wyoming bentonites already described, also the slope of the plots tends to decrease (table 15o, p, q).

The results for Li cobbed soft Helms bentonite, shown in fig. 85, also indicate that G decreases as LiCl concentration is increased from 10^{-4} to 10^{-3} and then 10^{-2} mol dm^{-3}. The results for this clay in 10^{-3} mol dm^{-3} LiCl indicate that the results of a given clay sample batch (i.e. same particle size distribution) are reproducible with the sample preparation technique used (chapter 6).

The results in fig. 84 do not, however, show the trend of decreasing slope with increasing electrolyte concentration (table 15u, v) shown by most of the other results (table 15) and the theoretical calculations (chapter 10).

The pulse shearometry results of different Li clays dispersed in

Fig.84: Pulse shearomtry results for Li bentolite L dispersions

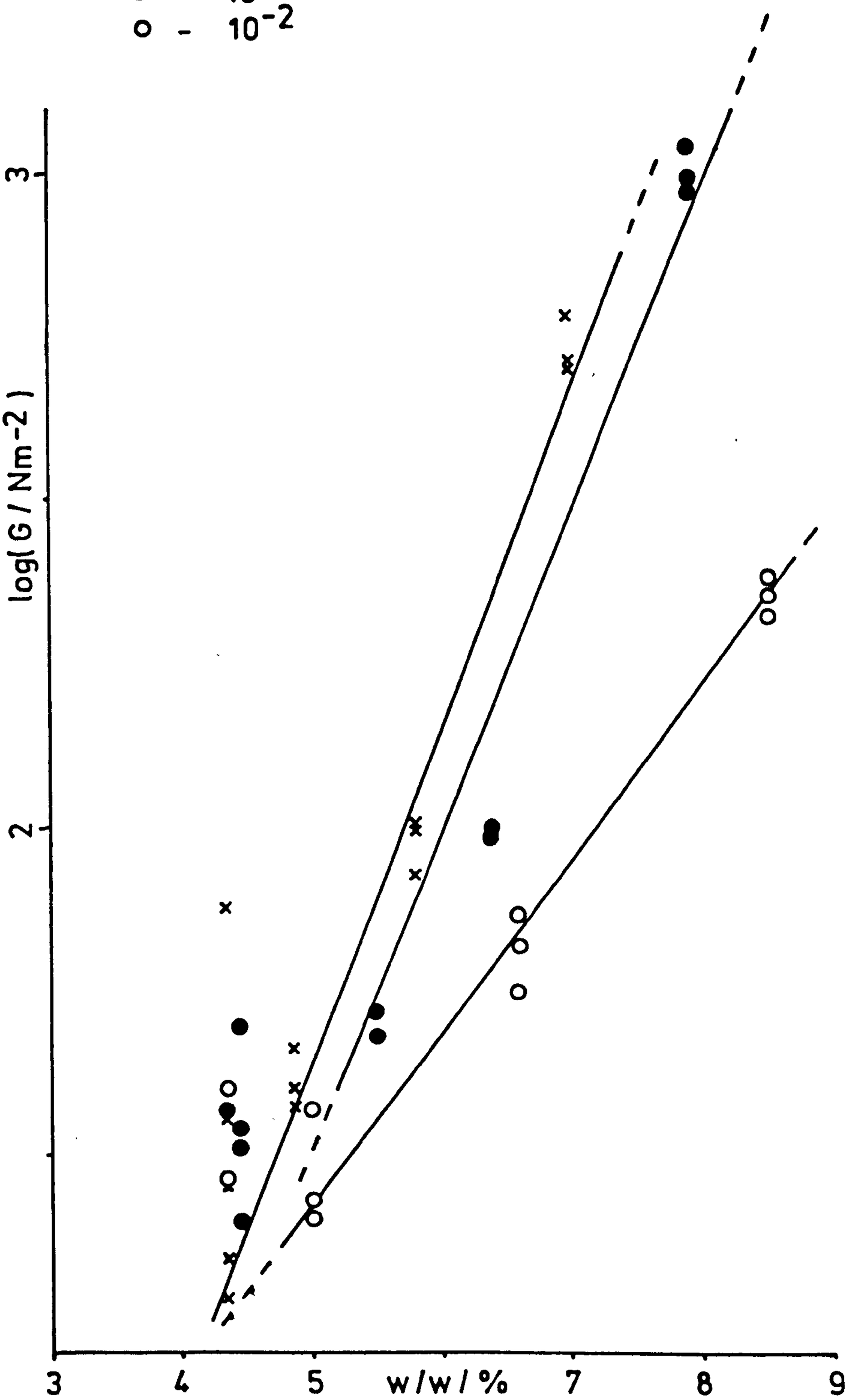

Fig.85 : Pulse shearometry results for Li cobbed soft Helms dispersions

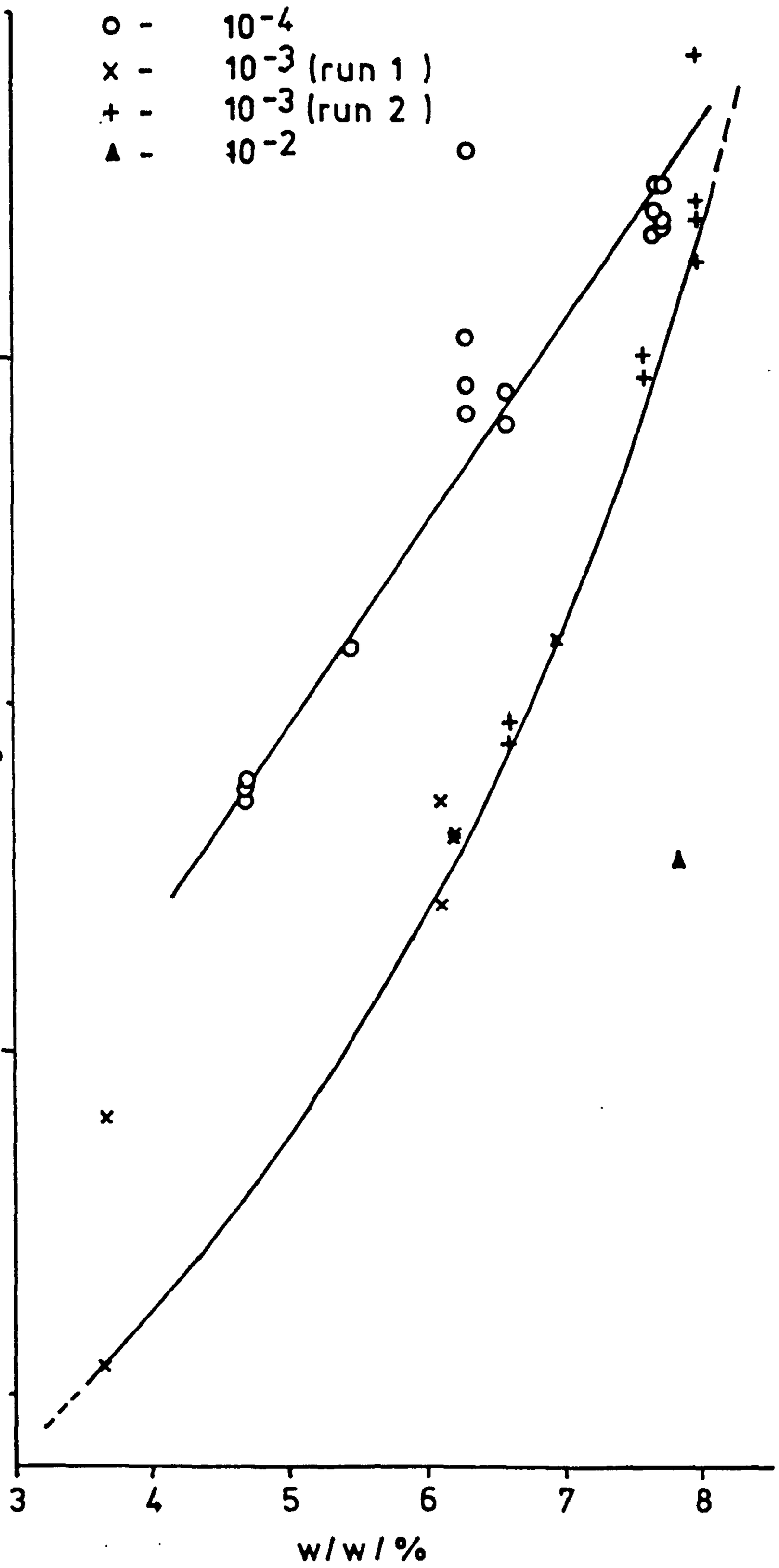

10^{-3} mol dm^{-3} LiCl are compared in fig. 86. Fig. 86 indicates that, at a given w/w of clay, the value of G decreases along the series

Li beidellite ≃ Li Wyoming Blackhills (WB) fine fraction

> Li Wyoming Blackhills ≃ Li Milos (Mi)> Li soft Clark (SC)

> Li cobbed soft Helms (CSH) >Li Bentolite L (BL)

> Li Wyoming Blackhills coarse fraction (not shown on plot - 2.38% w/w% - unmeasureable)

i.e. the Texas clays are less effective gelling agents than the Wyoming bentonites and the soft Texas bentonites (Li cobbed soft Helms and Li soft Clark) are more effective than the hard clay (Li Bentolite L). This trend is also shown at 10^{-4} and 10^{-2} mol dm^{-3} LiCl concentrations as shown by figs. 82, 84 and 85. The results for the Li Wyoming Blackhills fine fraction sample (obtained by high speed centrifugation of the Li Wyoming Blackhills sample) indicate that the particle size of the particles in the dispersion is important, with G increasing as the mean particle size is reduced. This is also indicated by the results for Li Bentolite L (BL) fine fraction and homogenised Li Bentolite L (LiBL/h) (sect. 6.2.6.i) shown in fig. 87. This improvement in "gelling ability" upon reducing particle size may be explained on the basis of an increased particle number concentration giving greater interparticle interactions. This trend is also shown by a simple theoretical cell model (appendix 9). The Li beidellite sample also seemed to have a small mean particle size (since it formed a semi-transparent gel, as did the other fine fraction bentonite samples) which may, at least in part, explain its gelling properties (fig. 86).

Fig.86: Pulse shearometry results

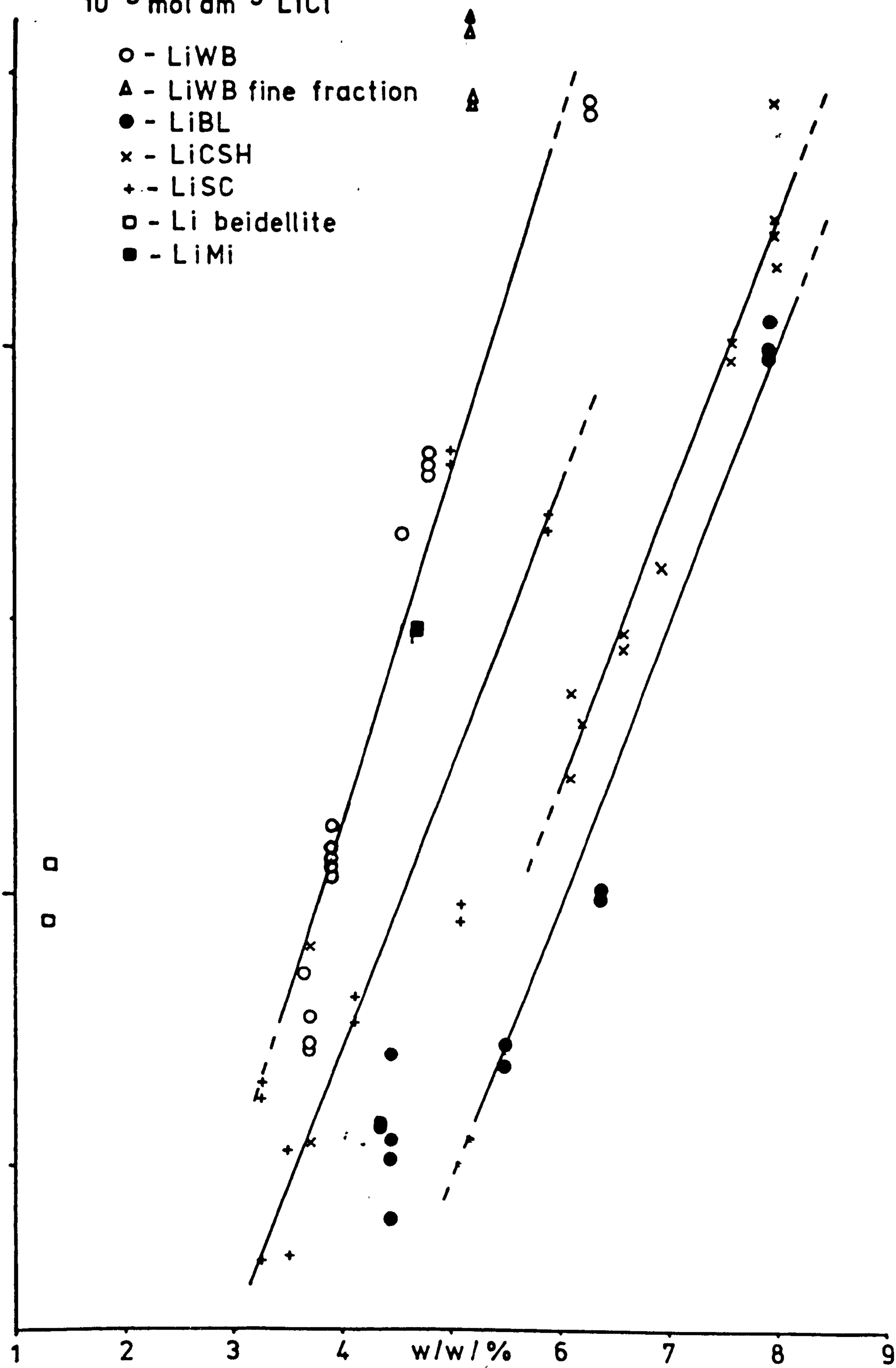

Fig.87: Pulse shearometry results

10^{-3} mol dm^{-3} LiCl

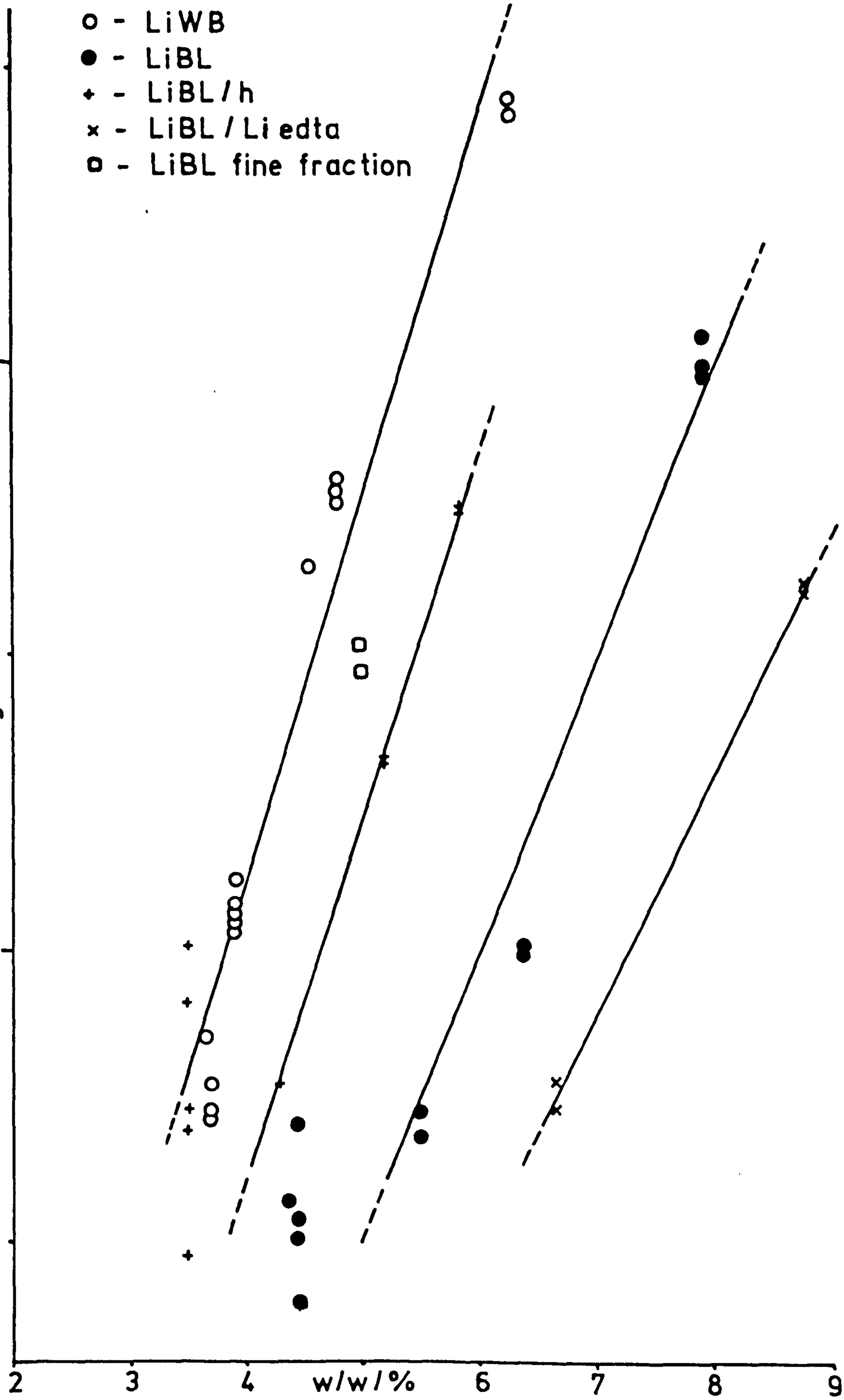

Fig. 87 compares the results for Li Wyoming Blackhills bentonite (WB) and samples of Li Bentolite L (BL) having received different treatments. These results indicate the trend of decreasing 'gelling ability'

Li Wyoming Blackhills > Li Bentolite L fine fraction
> homogenised Li Bentolite L (LiBL/h) > Li Bentolite L
> Li Bentolite L (method D) (LiBL/Li edta) > Li Bentolite L coarse fraction (not shown on plot - 11·55%w/w unmeasurably small G).

The slopes of all the plots for the Texas clays are generally similar to each other, but slightly lower than those for the Wyoming bentonites (table 15g, l, p, t, r, s, v, w) (figs. 86, 87) in 10^{-3} mol dm^{-3}LiCl. The results at other ionic strengths show a similar trend (figs. 82, 84, 85, table 15f, o, u, h, q, d, n).

These results suggest that the 'gelling effectiveness' of the Li Bentolite L may be improved by decreasing the mean particle size, possibly by some mechanical comminution treatment (homogenised Li Bentolite L), this seems to be confirmed by previous studies on Texas bentonites (198, 234). The trend of increasing G with decreasing particle size is also shown by polystyrene latices (fig. 105).

On this basis, the results for Li Bentolite L (method D) (LiBL/Li edta), in fig. 87, may be explained by this sample having a different (larger) particle size distribution (to Li Bentolite L) caused by differences in the preparation procedures.

Fig. 88 compares, schematically, the results for Li clay dispersions, already discussed, Li halloysite, crude bentonite samples

Fig.88: Pulse shearometry results

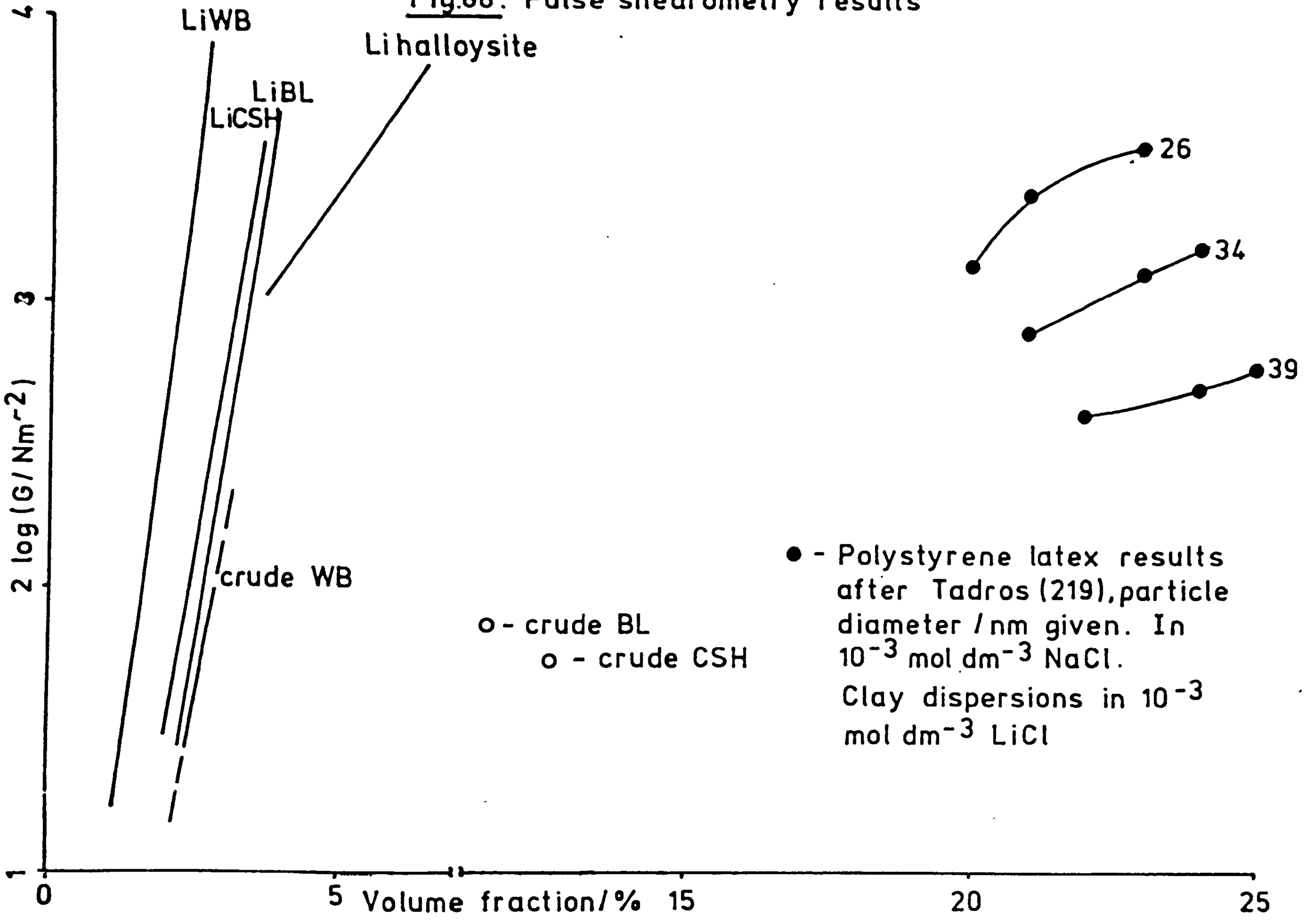

in 10^{-3} mol dm^{-3}LiCl and previously published data for polystyrene latices (219, 322). These results indicate the improvement in 'gelling ability' upon treating crude Wyoming Blackhills bentonite (WB) (to obtain Li Wyoming Blackhills) is much less than the corresponding improvement for the crude Texas bentonites; Bentolite L (BL) and cobbed soft Helms (CSH). The crude Texas bentonites also have lower 'gelling abilities' than the crude Wyoming Blackhills bentonite. This is probably because the crude Wyoming and Texas bentonites are mainly in the Na and Ca forms respectively (sect. 5.3.1). Crude Bentolite L also gives a higher G value than crude cobbed soft Helms bentonite, at a lower volume fraction. This may be because the crude Bentolite L initially disperses to a greater extent than the crude cobbed soft Helms bentonite as indicated by the dispersion tests (sect. 5.3.6). Fig. 88 also shows that the slopes of the bentonite curves are much steeper than those for other colloidal systems (latices in this case) as noted previously (194), and the (thixotropic) Li Halloysite (table 15x).

Figs. 93 and 94 show plots of Log G against electrolyte concentration (c_e) for various clay samples.

As mentioned previously, the shear modulus of Li Wyoming Blackhills bentonites decreases as the LiCl concentration is increased up to 10^{-2} mol dm^{-3}. As the LiCl concentration is increased further above 10^{-2} mol dm^{-3} the shear modulus increases (figs. 93, 94). This trend has been noted previously (7, 19, 169, 194, 319, 320, 321). At low electrolyte concentrations there is possibly some reduction in structure with time (anti-thixotropy)

(figs. 89 - 91). Anti-thixotropy has been noted in Na-montmorillonite dispersions at low NaCl concentrations (194). The rate of relaxation seems to increase as the LiCl concentration is increased (figs. 89 - 91, 106 - 108). This is perhaps because the anti-thixotropy is caused by the relaxation of the disordered dispersion to some more ordered state having a lower free energy (see sect. 3.2.3.1). The co-operative motion of the montmorillonite particles, as they diffuse in such a way to lower the free energy of the system, would be rendered easier as the degree of structure in the system was reduced; the range of the electric double layer repulsions having been decreased by the addition of electrolyte.

In 0•1 mol dm^{-3} LiCl the Li Wyoming Blackhills bentonite dispersion becomes thixotropic (fig. 92), i.e. G increases with time after initial mixing. This behaviour may be explained by the gradual formation of a flocculated network structure (19, 194).

It was also noted that at 10^{-4} and 10^{-3} mol dm^{-3} LiCl the dispersions appeared dark green, while at 10^{-2} mol dm^{-3} LiCl the dispersion was a slightly paler green and significantly paler at 0•1 and 1 mol dm^{-3} LiCl. This may be interpreted as being due to increased aggregation of the particles (145) as the electrolyte concentration is increased.

Fig. 93 also indicates that as the ionic form of the Wyoming Blackhills bentonite is changed there is a shift of the position of the minimum in the log G against c_e curves. The electrolyte concentration at the position of this minimum decreases along the series

$$Li > Na \simeq K > C_s$$

Fig.89 : Effect of time on shear modulus

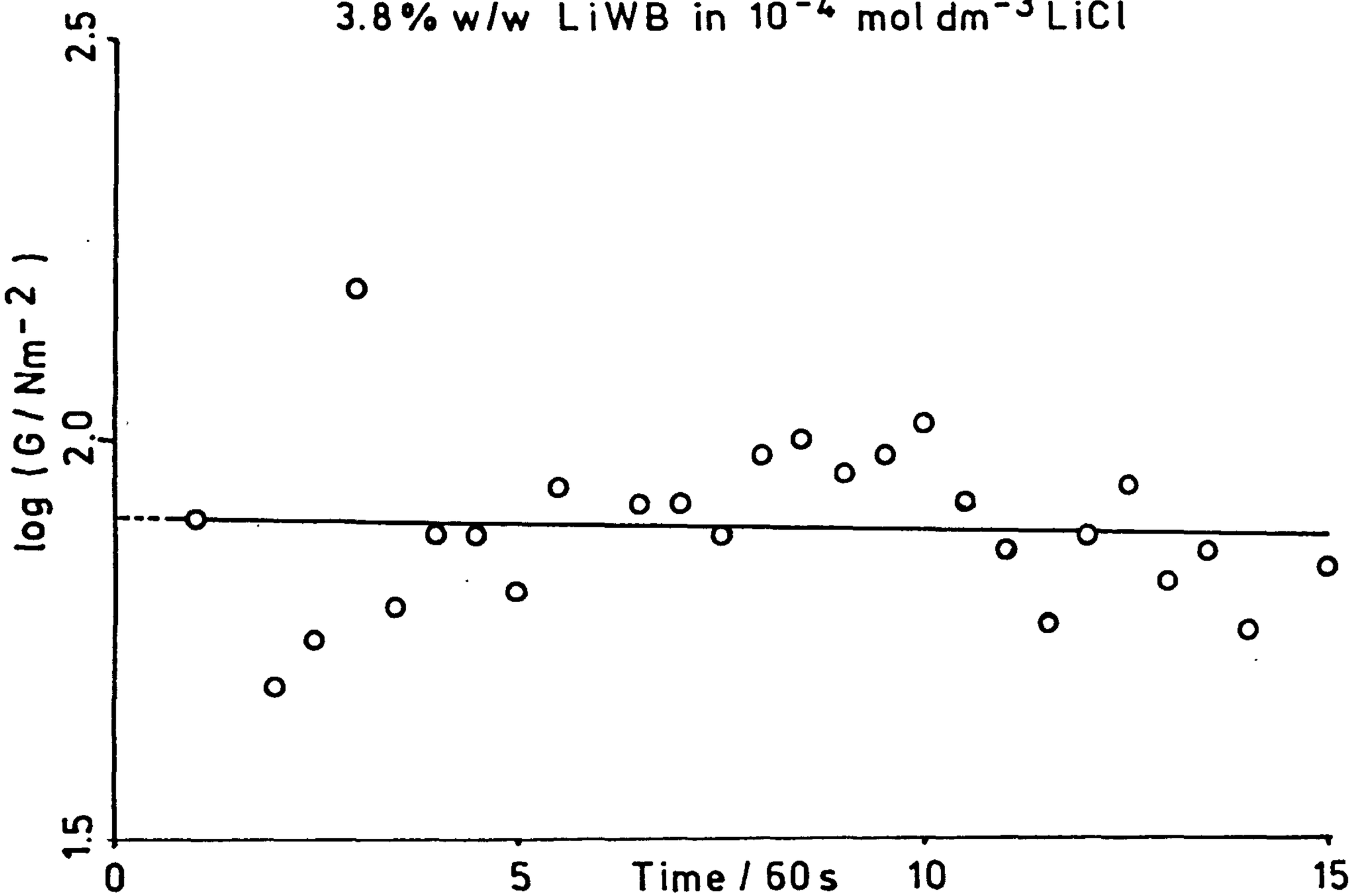

Fig.90 : Effect of time on shear modulus

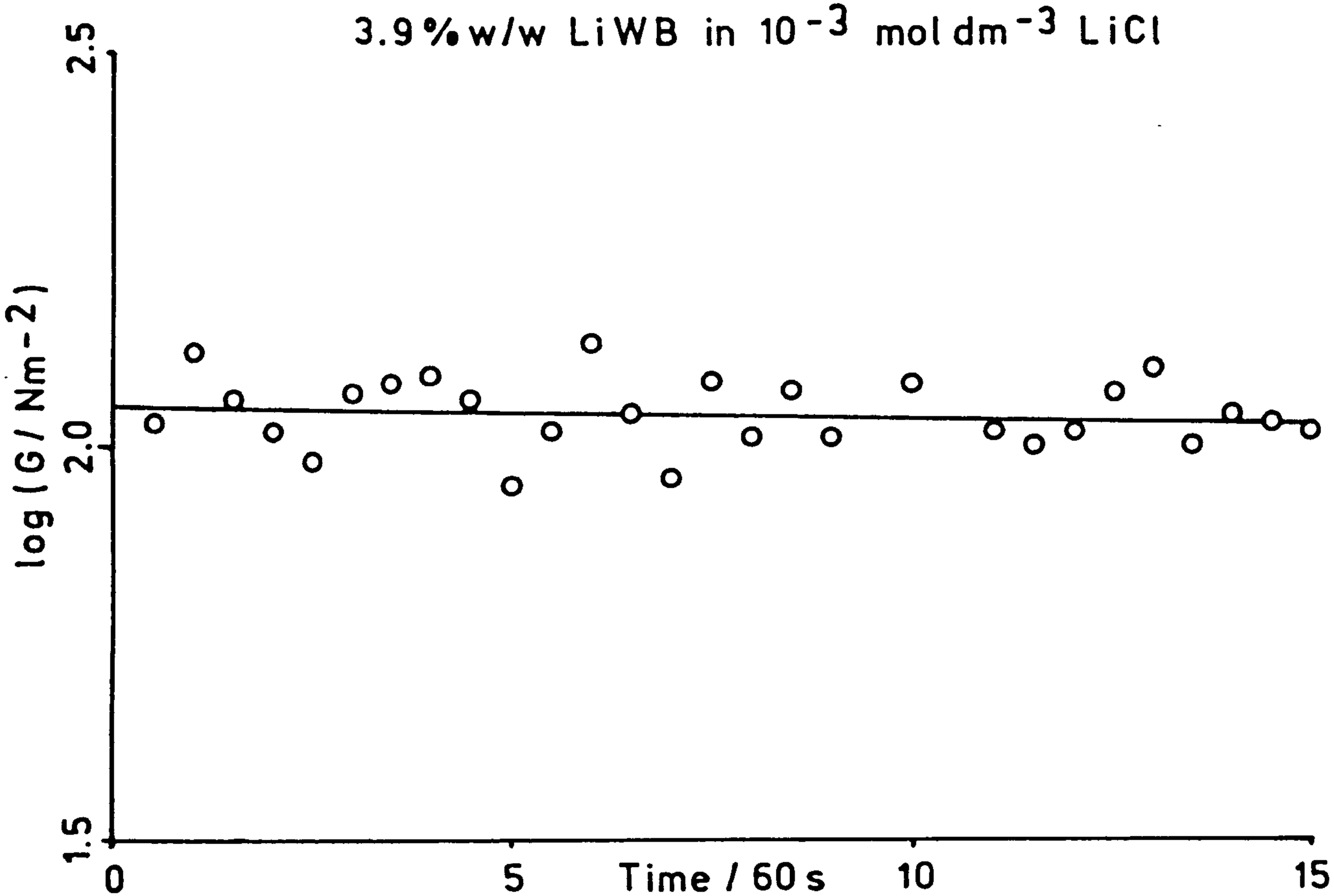

Fig.91: Effect of time on shear modulus

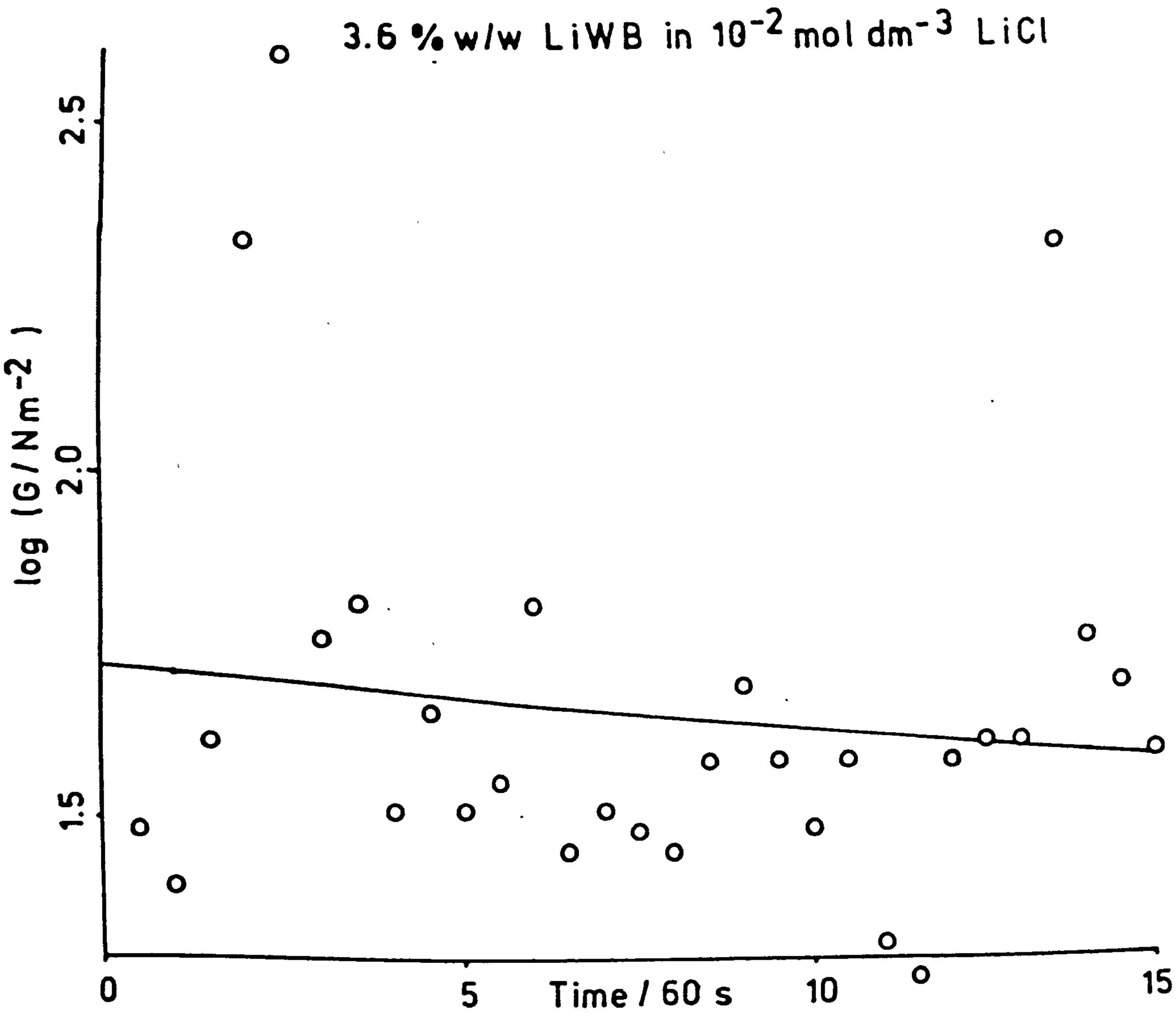

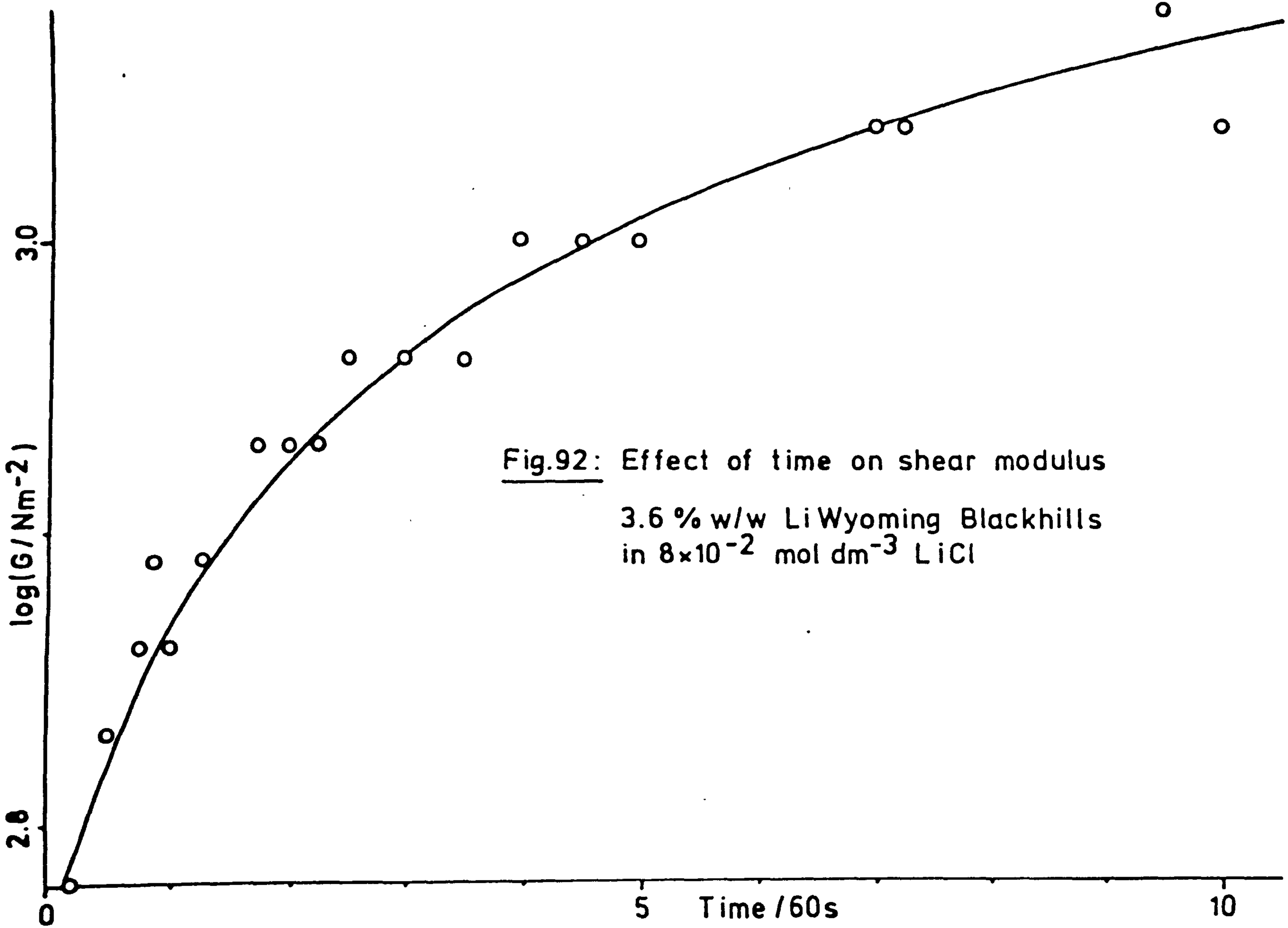

Fig.92: Effect of time on shear modulus

3.6 % w/w Li Wyoming Blackhills
in 8×10^{-2} mol dm^{-3} LiCl

Fig.93: Pulse shearometry results

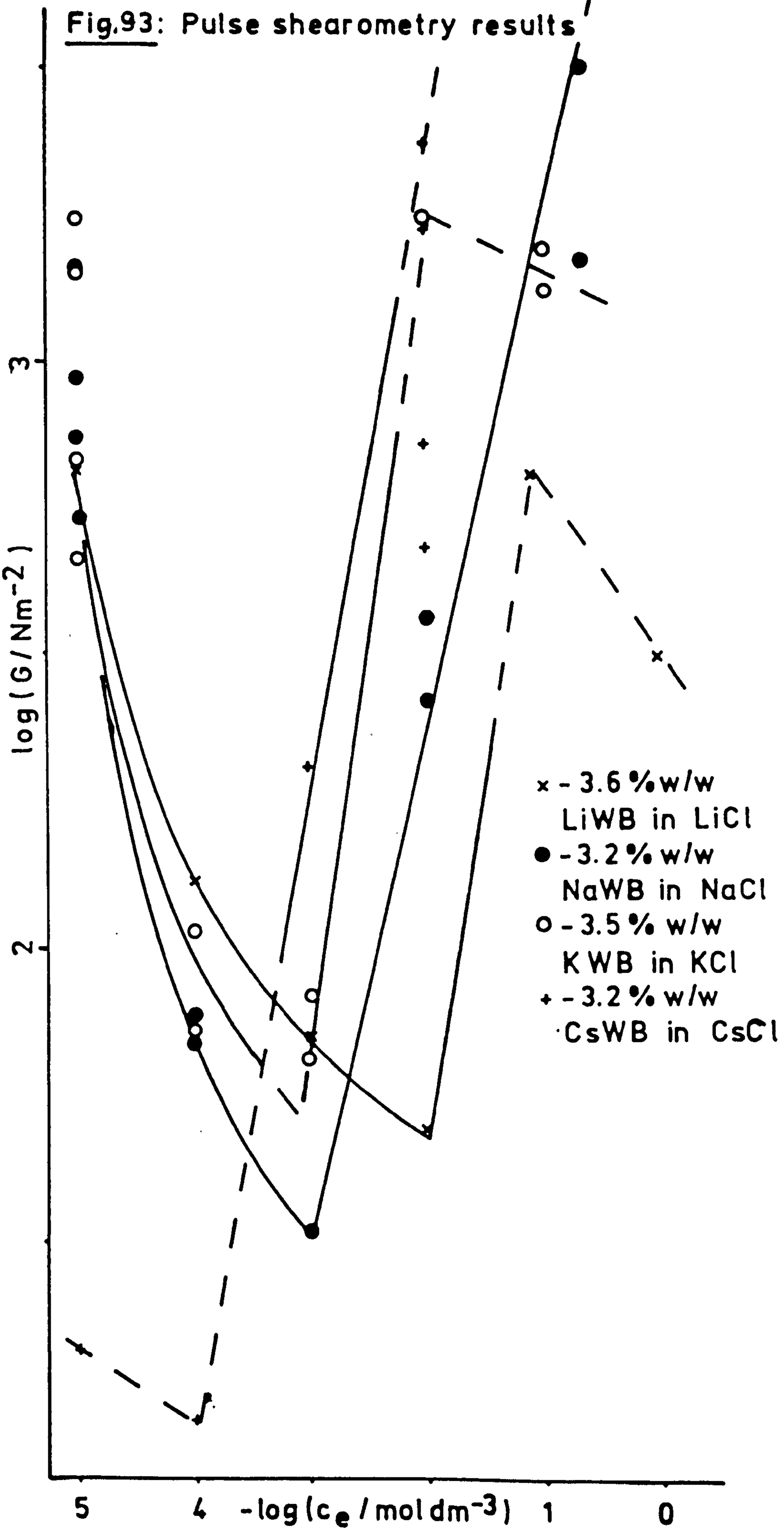

The minimum in the curve for 3•6%w/w Li Wyoming Blackhills bentonite (LiWB) occurs at $\sim 10^{-2}$ mol dm^{-3} LiCl (fig. 93) which is similar to the results for the same clay and Li Bentolite L, at a slightly higher clay concentration, as shown in fig. 94.

The minimum in the curves for 3•2%w/w Na and 3•5%w/w K Wyoming Blackhills bentonite (Na WB + KWB respectively) occur at $\sim 10^{-3}$ mol dm^{-3} electrolyte (fig. 93). This is slightly lower than the NaCl concentration of $\sim 5 \times 10^{-3}$ mol dm^{-3} given by van Olphen (19) and Rand et al (194) for the point of minimum structure in Na Californian and Wyoming montmorillonite dispersions respectively, at similar weight fractions of clay (3•22 and 3•3%w/w, respectively). This difference is probably due to differences in the sample preparation procedures used. In view of the time-dependent nature of these systems (thixotropic/anti-thixotropic) the results obtained may also depend upon the time scale (fig. 94) and the amount of system perturbation (shearing) involved in in the experiment.

The minimum in the curve for 3•2%w/w Cs Wyoming Blackhills bentonite (CsWB) (fig. 93) occurs at $\sim 10^{-4}$ mol dm^{-3} CsCl, although this value may be inaccurate due to the difficulty in measuring the low G values of the samples in this region of CsCl concentrations.

It is likely that the shift in the minima of the plots shown in fig. 93, upon changing the counter-ion type, is due to changes in ψ_δ (sect. 3.1.12.3) or particle size, axial ratio or face:edge potential (293) upon tactoid formation (sect. 3.2.2) or some combination of these effects.

The curves for Li and K Wyoming Blackhills bentonite, shown in

Fig.94 : Pulse shearometry results

	initial value	3 min. value
4.6 % w/w LiWB	●	+
4.3 % w/w LiBL	o	×

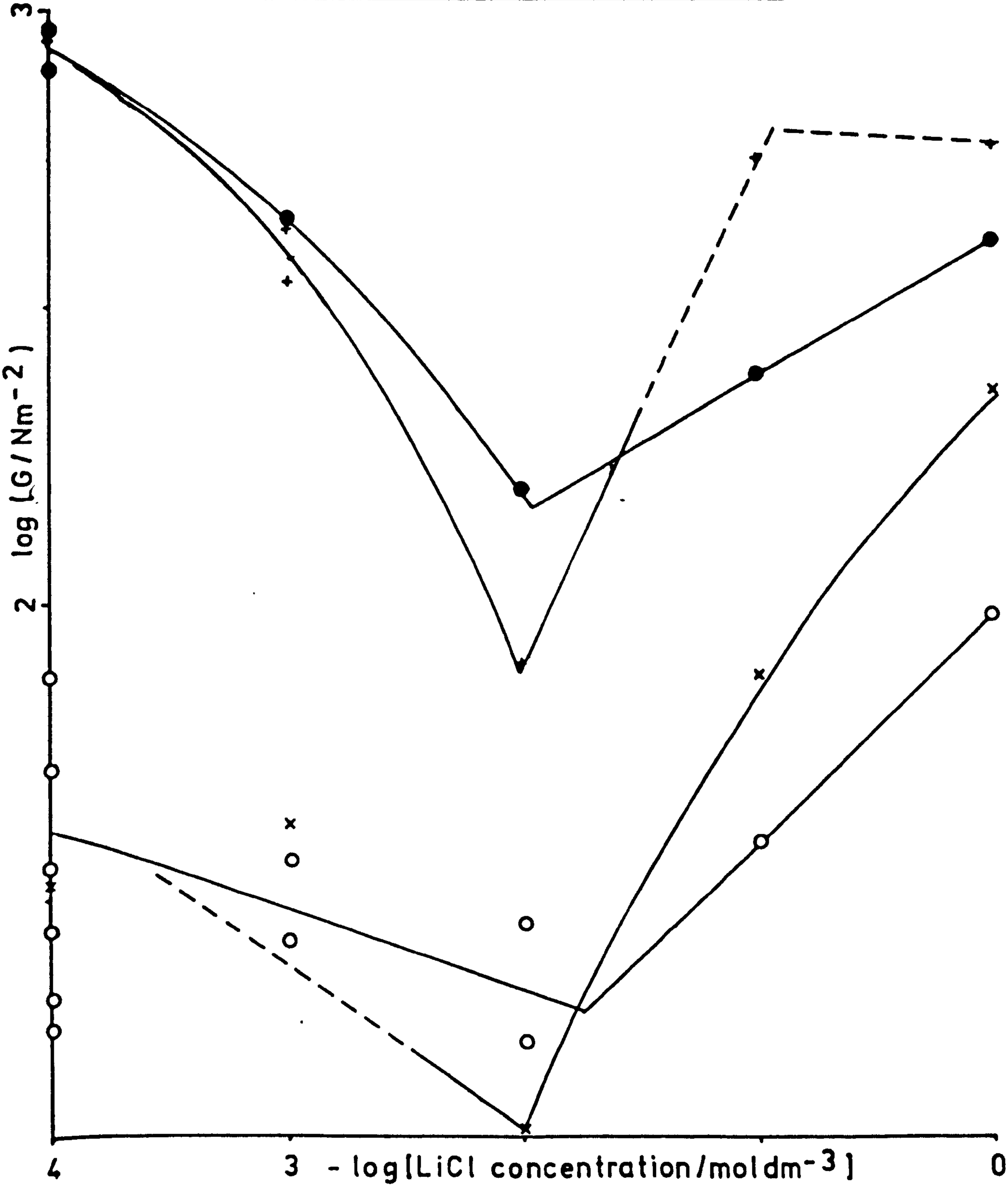

fig. 93, also show a decrease in G at higher electrolyte concentration. This may be experimental error because of significant damping rendering equation 46 invalid. The reduction of structure at very high electrolyte concentration has also been reported by van Olphen (19, 7) and Rand et al (194).

It is generally considered (19, 194) that the rheological behaviour of Li montmorillonite at low ($<10^{-2}$ mol dm^{-3}) LiCl concentrations is due to structuring of the gel due to significant electric double layer repulsive forces at the interparticle distances in the dispersion. This idea seems reasonable in view of the anti-thixotropic nature of the gels and the reduction in G upon increasing electrolyte concentration as qualitatively predicted by a simple theoretical model taking into account electric double layer forces (chapter 10).

At higher ($>10^{-2}$ mol dm^{-3}) LiCl concentrations it has generally been considered that the dispersion becomes flocculated forming some sort of 3-dimensional network of particles (19, 194), e.g. the so-called "house of cards". The apparent "transition concentration" of $\sim 10^{-2}$ mol dm^{-3} LiCl is much lower than that expected (~ 1 mol dm^{-3}) (162, 163, 164, 296) for primary minimum coagulation to occur. Also simple DLVO calculations (sect. 3.2.1) (fig. 9) suggest that the secondary minimum is too shallow for flocculation to occur at 10^{-2} mol dm^{-3} LiCl.

Other possible explanations for this behaviour include:-

i) Flocculation occurs at $\sim 10^{-2}$ mol dm^{-3} LiCl with these samples of bentonite since the presence of small amounts of Ca may render the system more sensitive to changes in electrolyte concentration, due to an effective reduction in ψ_δ. This explanation is supported by the

observation that as the counter-ion is changed from Li^+ to Na^+, K^+ and then Cs^+ there is a reduction in the electrolyte concentration at the minima in the curves (fig. 93) which may be due to a corresponding reduction in ψ_δ (sect. 3.1.12.3).

ii) Flocculation occurs at $\sim 10^{-2}$ mol dm^{-3} LiCl since the effective electrolyte concentration is in fact higher than this due to the presence of counter-ions in the electric double layers of the particles (sect. 10.2.5). Such an effect may result in a significant increase in the effective electrolyte concentration (sect. 10. 2.5) which could explain flocculation of the system. If this was the case then the amount of added electrolyte needed to bring about flocculation would be dependent upon the volume fraction of clay present. Such a relationship was not investigated here.

iii) If flocculation occurs then the electrolyte concentration at the minimum in the curves may not be strictly relevant since it appears that the transition from anti-thixotropic to thixotropic behaviour occurs at a somewhat higher electrolyte concentration (fig. 94). It may be this electrolyte concentration that corresponds to the "critical flocculation concentration".

iv) It is possible that there are changes in the ordering of the systems (sect. 3.2.3) at electrolyte concentrations below that at which flocculation occurs. At low electrolyte concentrations the system would be relatively ordered. As the electrolyte concentration is increased the system becomes more disordered as the effective particle size is reduced with electric double layer range. At some point between the extremes of order and disorder there would be a possible

phase separation of ordered and disordered regions (sect. 3.2.3).

It is possible that when phase separation occurs the overall structure, and hence G, of the system will be at a minimum. This effect would be dependent upon ψ_δ, particle volume fraction, size and axial ratio and hance may be strongly affected by tactoid formation. This explanation may be supported by the observation that the Cs Wyoming Blackhills dispersion in 10^{-4} mol dm^{-3} was noted to have separated into two phases, comprising a lower gel occupying $\sim\frac{3}{4}$ of the volume of the sample and an upper dilute dispersion, approximately 1 month after preparation. However this may have been due to sedimentation, since no such separation was observed with the other forms of bentonite at the clay concentrations given in fig. 93. (Phase separation was noted with more dilute ($\sim$2%w/w) dispersions of Li and Na Wyoming bentonites in $\sim 10^{-3}$ mol dm^{-3} electrolyte).

The rheological behaviour of bentonites upon changing electrolyte concentration may be due to some or all of the factors given above and/or other factors not mentioned. It was not possible to estimate the contribution of each of these factors in this work.

Fig. 94 shows that Li Bentolite L (LiBL) behaves in a similar manner to Li Wyoming Blackhills bentonite upon changing the LiCl concentration.

Fig. 95 shows the effect of pH changes on the shear moduli of freshly prepared LiWB dispersions and indicates that as pH increases G decreases. However, it should be noted that, during this experiment the clay concentration was reduced as pH was increased, because of dilution upon addition of the LiOH solution, and also there would be an increase in ionic strength above pH7.

Fig.95 : Effect of pH on shear modulus

Li Wyoming Blackhills

x - 10^{-3} mol dm^{-3} LiCl, w/w = 6.0 to 3.7 %
o - 0.1 mol dm^{-3} LiCl, w/w = 4.1 to 3.7 %

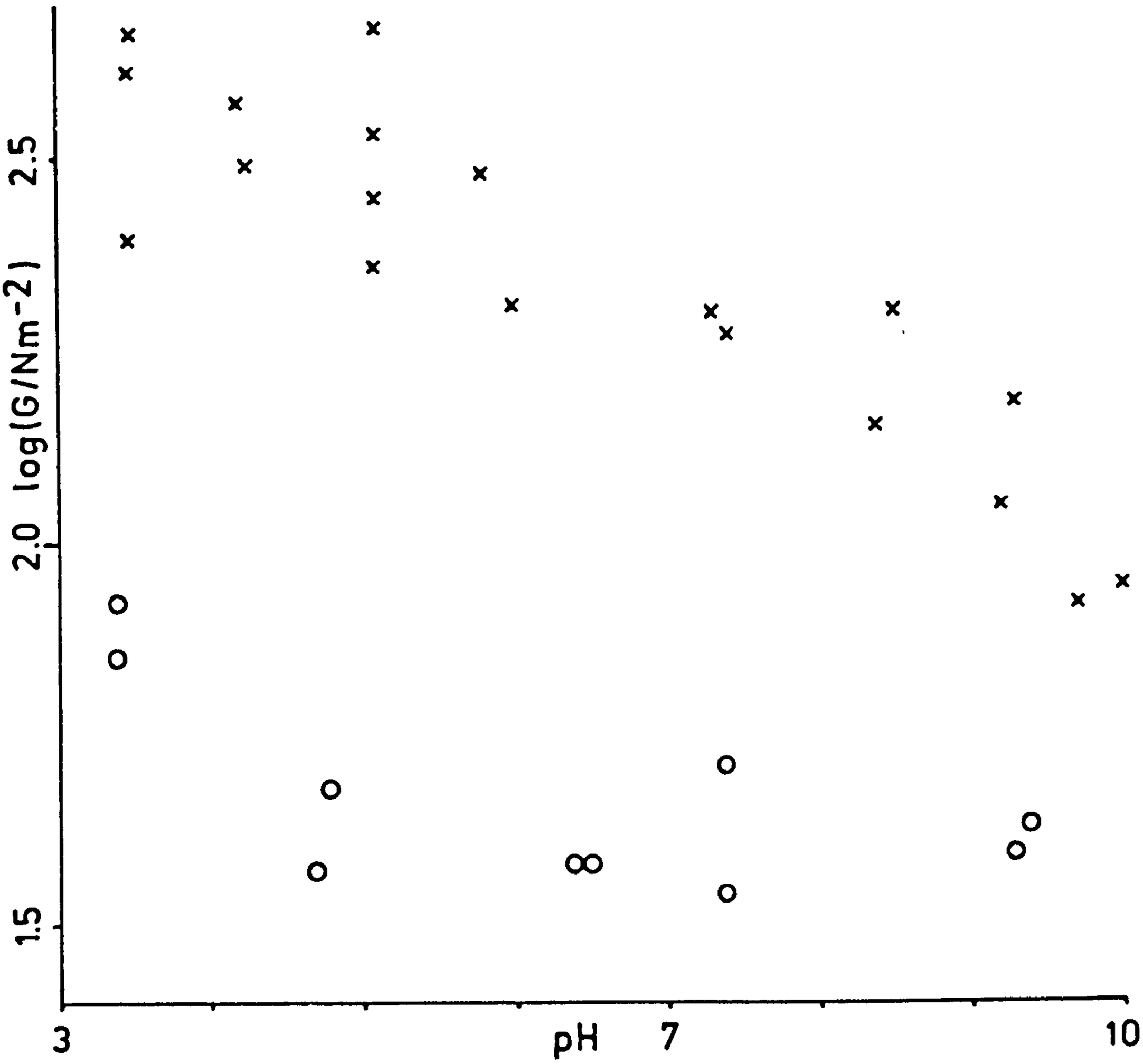

Fig.96 : Pulse shearometry results for Na Wyoming Blackhills

10^{-3} mol dm^{-3} NaCl

o - pH 6.5 ± 0.5

× - pH 3.0 ± 0.1

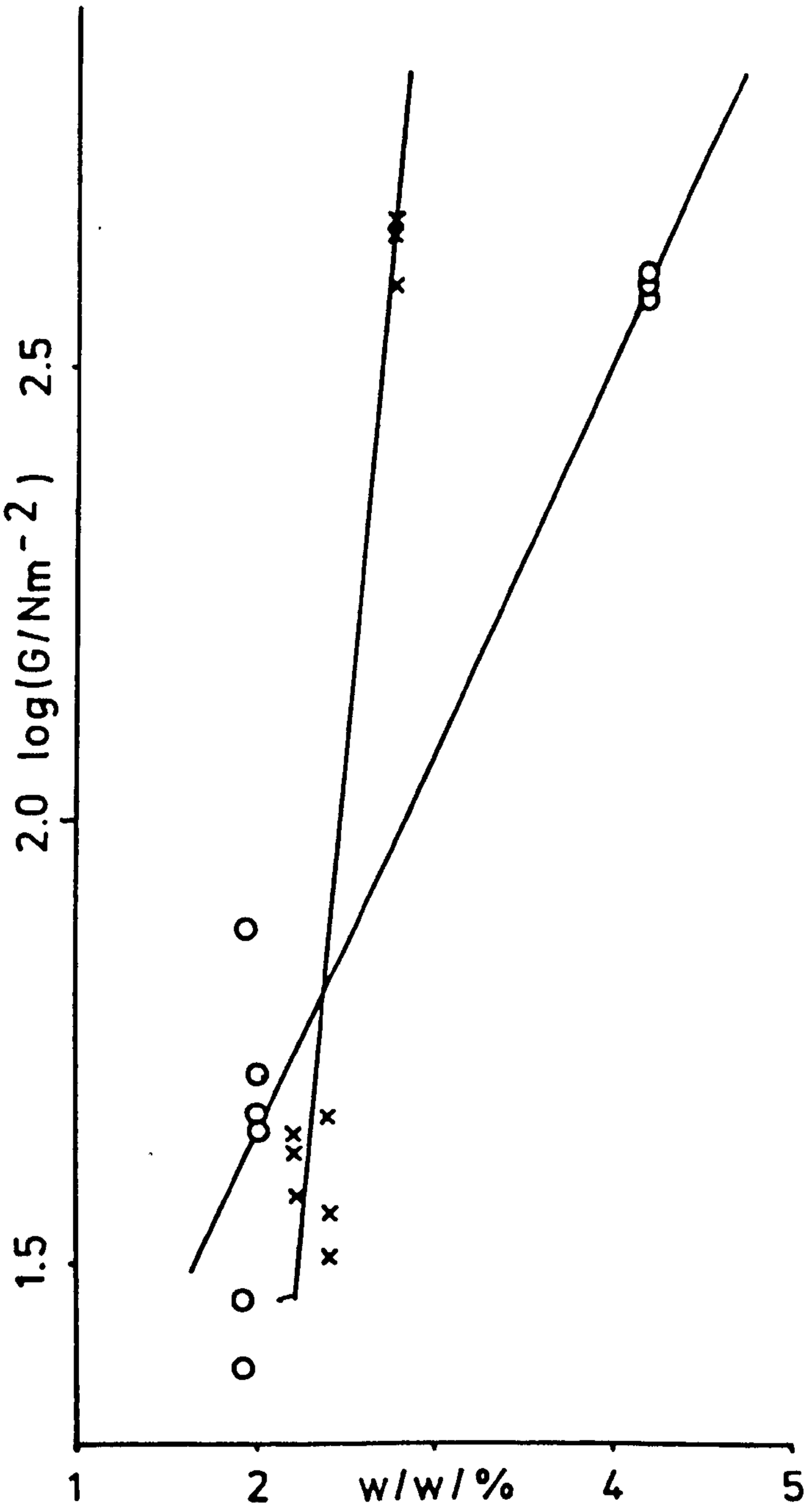

Hence these results may not be strictly valid, however they indicate that the changes in G due to variations in the pH are much less than the changes resulting from variations in electrolyte concentration (figs. 93 and 94). Fig. 96 shows results obtained for Na Wyoming Blackhills bentonite prepared at pH3 by treatment with an excess of H^+-resin (see sect. 6.2.4). These results suggest that G decreases as pH is increased from 3 to 7 in 10^{-3} mol dm^{-3} NaCl.

C H A P T E R N I N E

STUDIES ON COARSE SAMPLES

STUDIES ON COARSE SAMPLES

9.1 INTRODUCTION

In this chapter the study of the coarse material removed from the clay samples, during the preparation of their dispersions (chapter 6), by scanning electron microscopy, is discussed.

9.2 EXPERIMENTAL

9.2.1 Preparation of coarse samples

The coarse material removed from the clay dispersions (section 6.2.2) was washed free of colloidal material using double distilled water.

9.2.2 Scanning electron microscopy

A small amount of sample was placed upon a scanning electron microscope stud, dried and sputter coated with gold. The samples were then studied using a Cambridge Stereoscan scanning electron microscope.

9.3 RESULTS AND DISCUSSION

9.3.1 Scanning electron microscopy

Figs. 97, 98 and 99 show scanning electron micrographs of

Fig. 97 : Scanning electron micrograph of coarse Na hard Helms

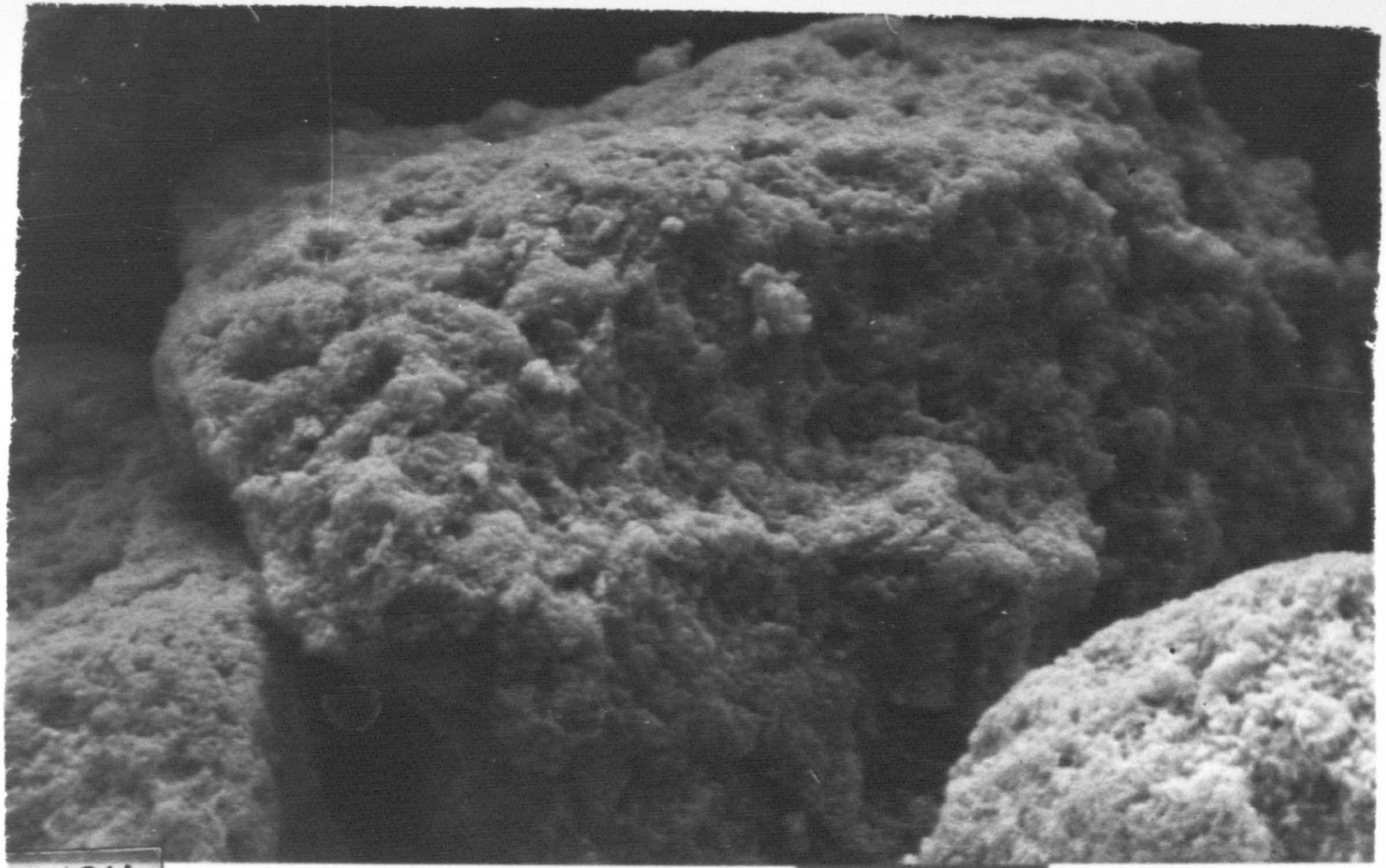

Fig. 98 : Scanning electron micrograph of coarse Na hard Helms

Fig. 99 : Scanning electron micrograph of coarse Na hard Helms

the washed coarse material obtained during the preparation of Na hard Helms. Fig. 100 shows a micrograph of washed coarse material from Na Bentolite L.

These micrographs (figs. 97 - 100) indicate that the coarse fractions of the hard Texas bentonites mainly consist of large, sand-size, (>~50μm) particles having similar surface appearance to the crude smectite (sect. 5.3.3). This indicates that substantial amounts of these samples are not dispersed by treatment with water or 1 mol dm^{-3} NaCl or LiCl. Some of the clay particle surfaces had the "granular" appearance (fig. 99) previously observed (sect. 5.3.3), suggesting that some of the undispersed clay may contain Opal-CT.

Figs. 101 and 102 show coarse material from Na and Li Wyoming Blackhills respectively. This material seems to consist of large abraded particles, probably quartz and feldspars broken up during milling.

Micrographs of the coarse material present in Bentolite L after treatment with 10·5 mol kg^{-1} LiCl solution for 28 days (method F - sect. 6.2.6) are shown in figs. 103 - 105. This treatment seems to have been effective at dispersing large amounts of the clay, with the coarse material containing relatively much more non-clay material. This material seems to consist of irregular particles, which are probably unaltered volcanic glass, and plate-like particles, which may be mica or abraded quartz (sect. 2.3.1.1) (84) particles. Although scanning electron microscopy indicates that this treatment has dispersed the clay to a greater extent than the standard methods, there is no evidence that all the clay material has been dispersed to the ultimate extent (i.e. individual layers in dispersion).

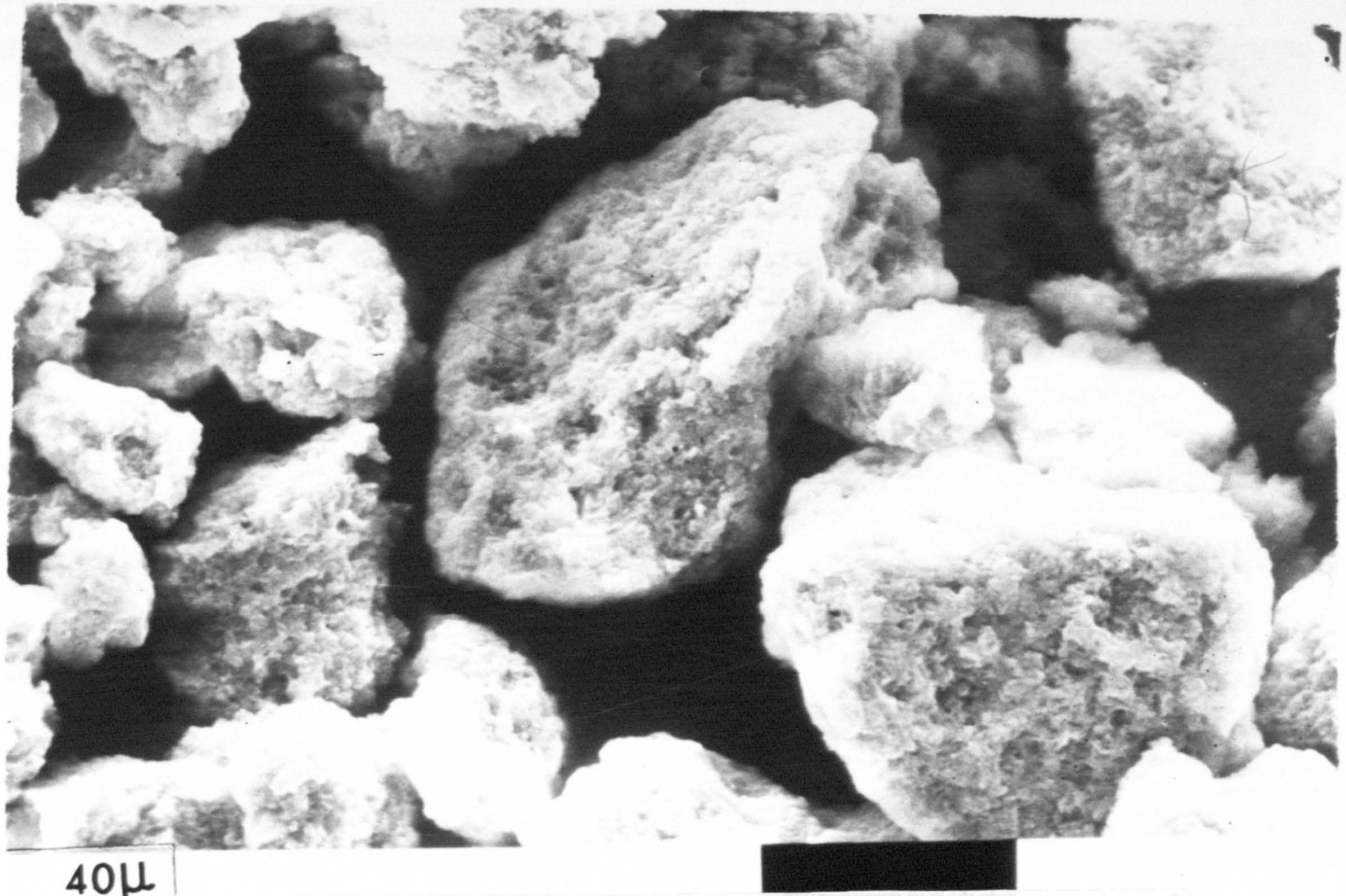

Fig. 100 : Scanning electron micrograph of coarse Na Bentolite L

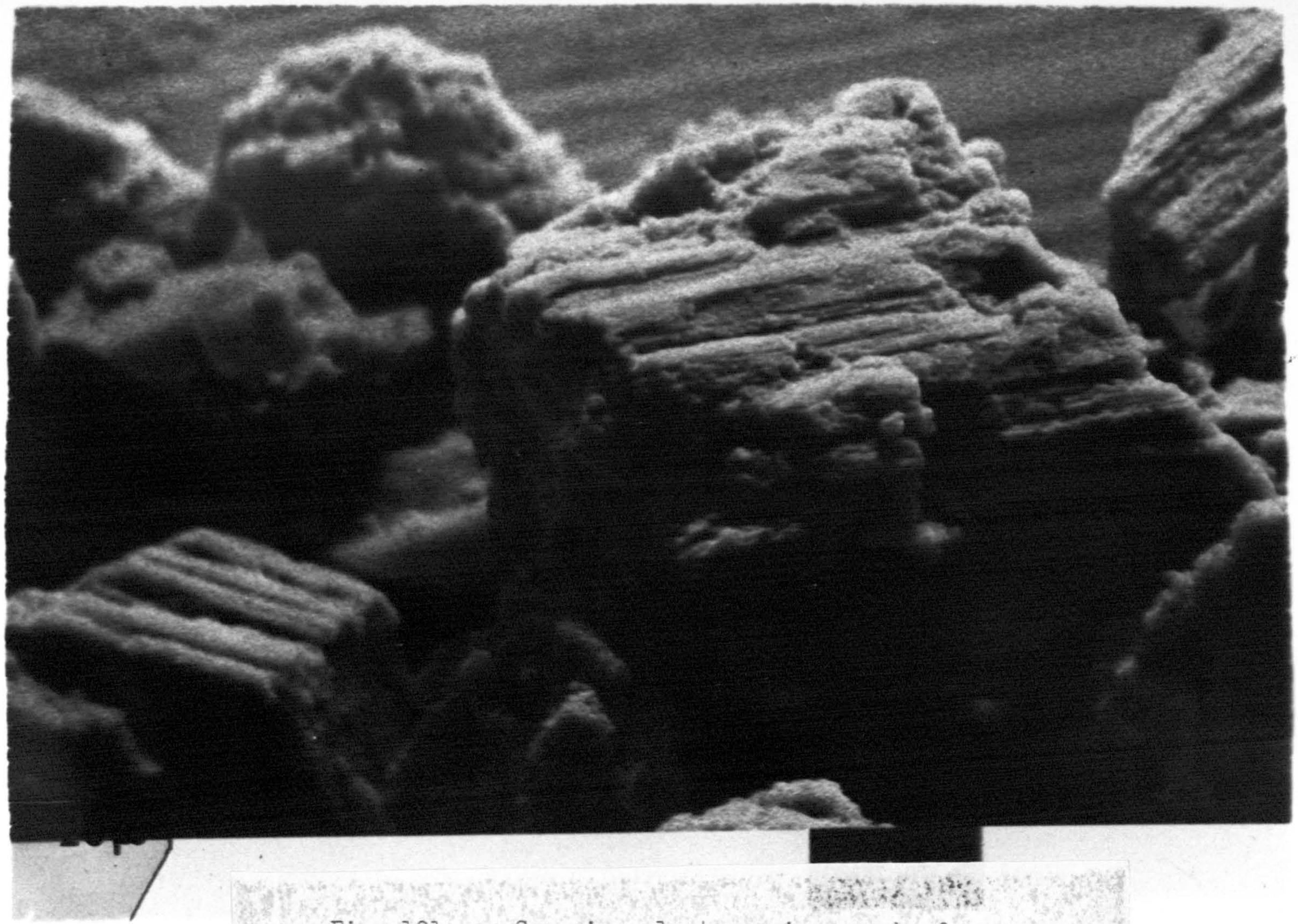

Fig. 101 : Scanning electron micrograph of coarse Na Wyoming Blackhills

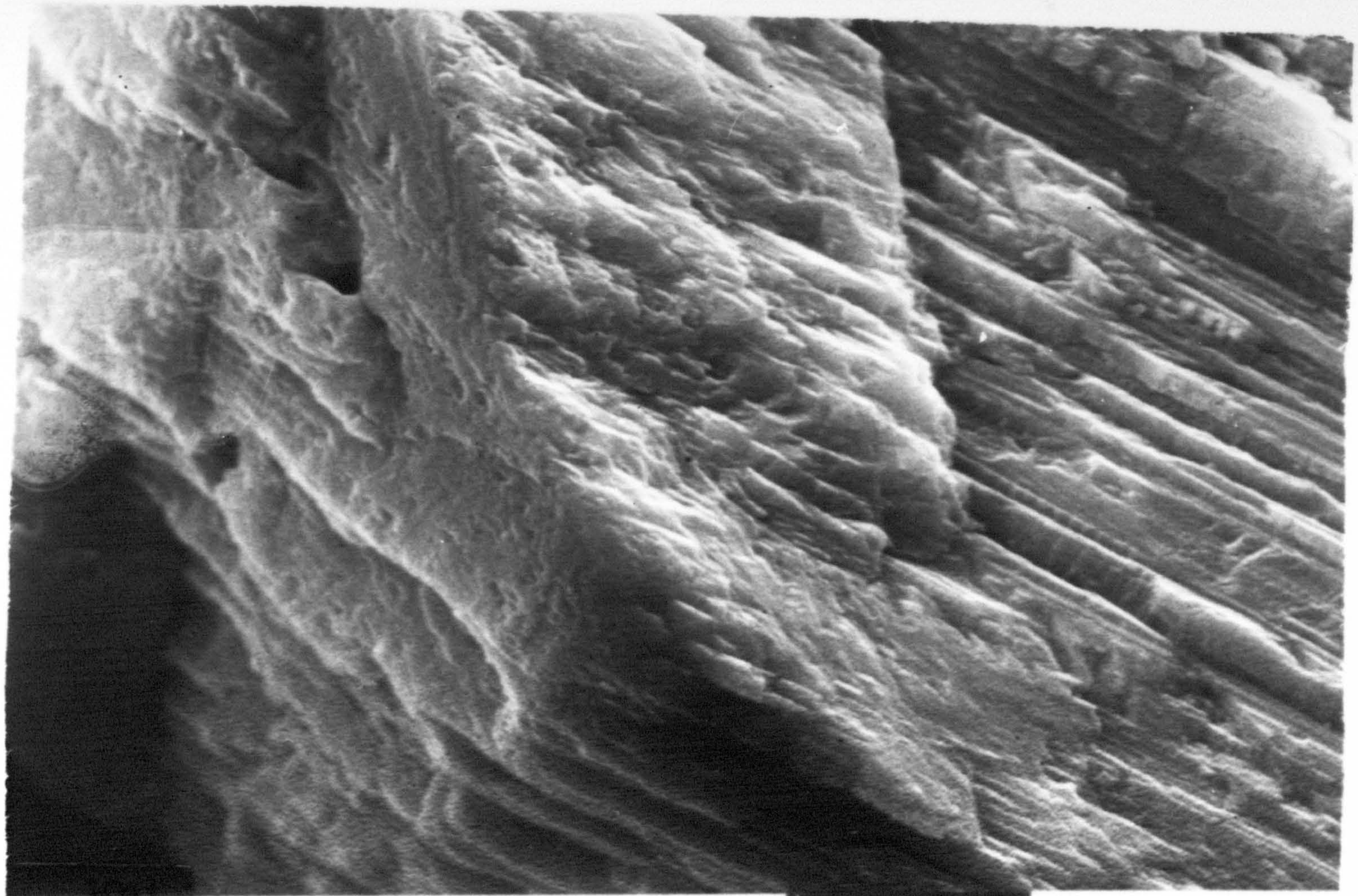

Fig. 102 : Scanning electron micrograph of coarse Li Wyoming Blackhills

Fig. 103 : Scanning electron micrograph of coarse Bentolite L - preparation method F

Fig. 104 : Scanning electron micrograph of coarse Bentolite L - preparation method F

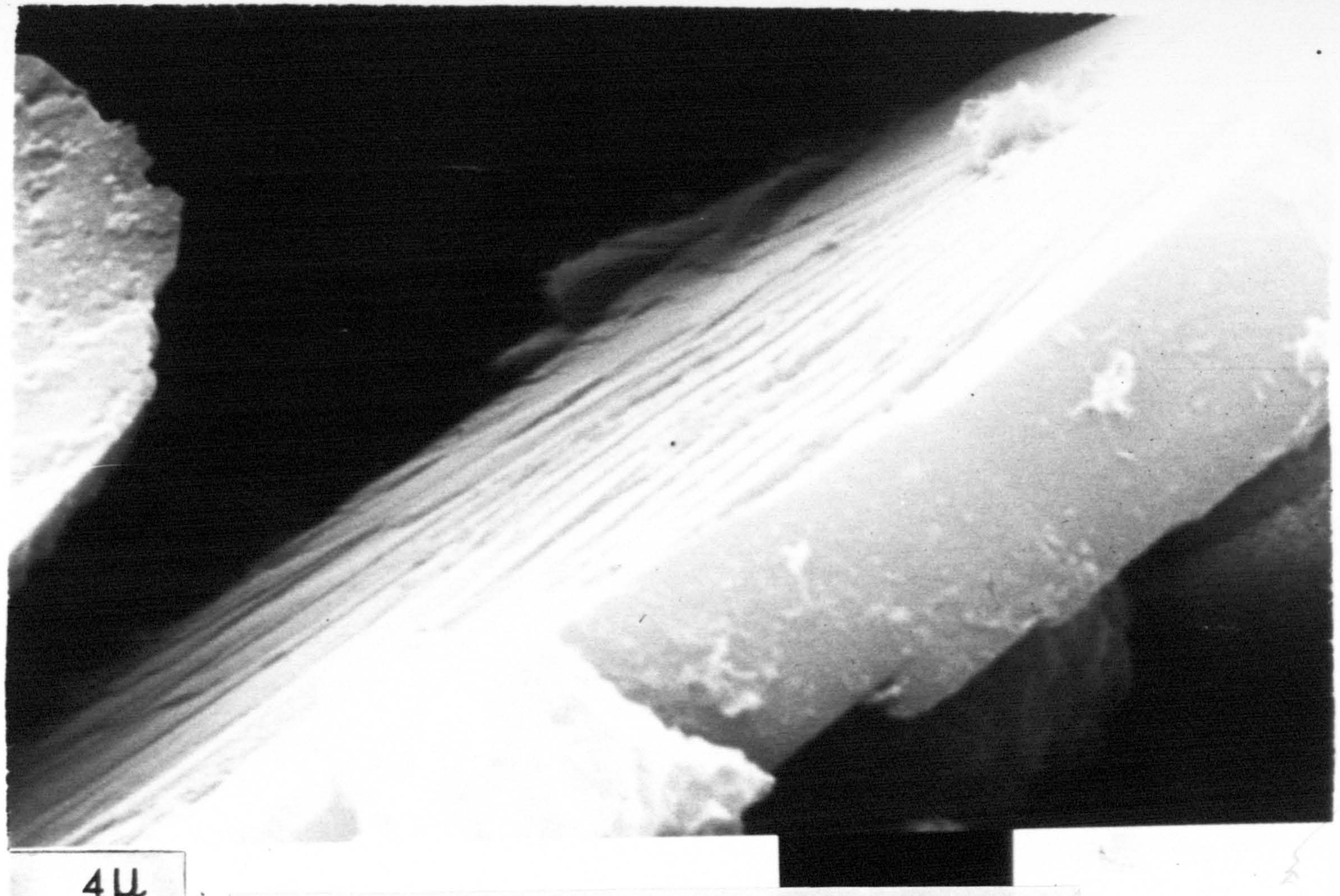

Fig. 105 : Scanning electron micrograph of coarse Bentolite L - preparation method F

C H A P T E R T E N

THEORETICAL PREDICTION OF SHEAR MODULI

THEORETICAL PREDICTION OF SHEAR MODULI

10.1 INTRODUCTION

As mentioned previously (sect. 3.2.4), the shear modulus G would be expected to have a similar magnitude to the bulk modulus B. This chapter describes the theoretical calculation of B for bentonite dispersions and relates these models to the experimental G values.

The bulk modulus is the reciprocal of the coefficient of isothermal compressibility i.e.

$$B = -V\left(\frac{\partial p}{\partial V}\right)_T \qquad (36)$$

or, for a system of unit area and constant distance between the plates H_o

$$B = -H_o\left(\frac{\partial p}{\partial H_o}\right) \qquad (37)$$

or, ignoring attractive interactions (169), since

$$p = -\frac{\partial V_R}{\partial H_o} \qquad (50)$$

$$B = \frac{H_o \partial^2 V_R}{\partial H^2_o} \qquad (51)$$

Therefore, it should be possible to calculate B for a bentonite dispersion, if H_o and the relationship between V_R or P_R and H_o is known. By assuming the dispersion particles are ordered in static lattice positions, H_o may be calculated for given lattice arrangements, and then V_R or P_R calculated from equations 26 or 29 respectively.

10.2 INFINITE PARALLEL PLATE MODEL

The simplest models for the arrangement of montmorillonite particles in dispersion are those assuming the particles are arranged as, in effect, infinitely large parallel plates. These models have been used with some success to explain the behaviour of highly aligned montmorillonite particles in dispersion, obtained by compression of the sample (145, 146).

10.2.1 Calculation of interplate distance

For tactoids consisting of n montmorillonite layers, of thickness 1nm, separated by 0·5nm (203), the tactoid thickness t is given by

$$t = 1 + 1{\cdot}5\ (n-1) \qquad \text{nm} \qquad (52)$$

For a "unit cell" of infinitely large parallel tactoids,

having a distance Ho between the outer tactoid surfaces, the unit cell volume is given by

$$\text{unit cell volume} = (Ho+t) \times \text{tactoid area } nm^3 \qquad (53)$$

and

$$\text{montmorillonite volume in unit cell} = n \times 1 \times \text{tactoid area } nm^3 \qquad (54)$$

Therefore, the volume fraction ϕ of montmorillonite is given by

$$\phi = \frac{nxl}{(Ho+t)} \qquad (55)$$

and, therefore

$$Ho = n/\phi - 5 \quad nm \qquad (56)$$

Plots of the variation in Ho with ϕ, given by eq. 56, are shown in fig. 106

10.2.2 Langmuir theory

As described previously (sect. 3.1.13.1), Langmuir (169) derived the following equation

$$P_R = 2 \times 10^3 c_e N_A kT \, (\cosh u - 1) \qquad (26)$$

where, for $Ho > 2/\kappa$,

$$u = 8\gamma \exp(-\kappa Ho/2) \qquad (28)$$

(A general expression for u is given in equation 27).

Fig.106: Plots of interplate separation against clay concentration for infinite parallel plate model

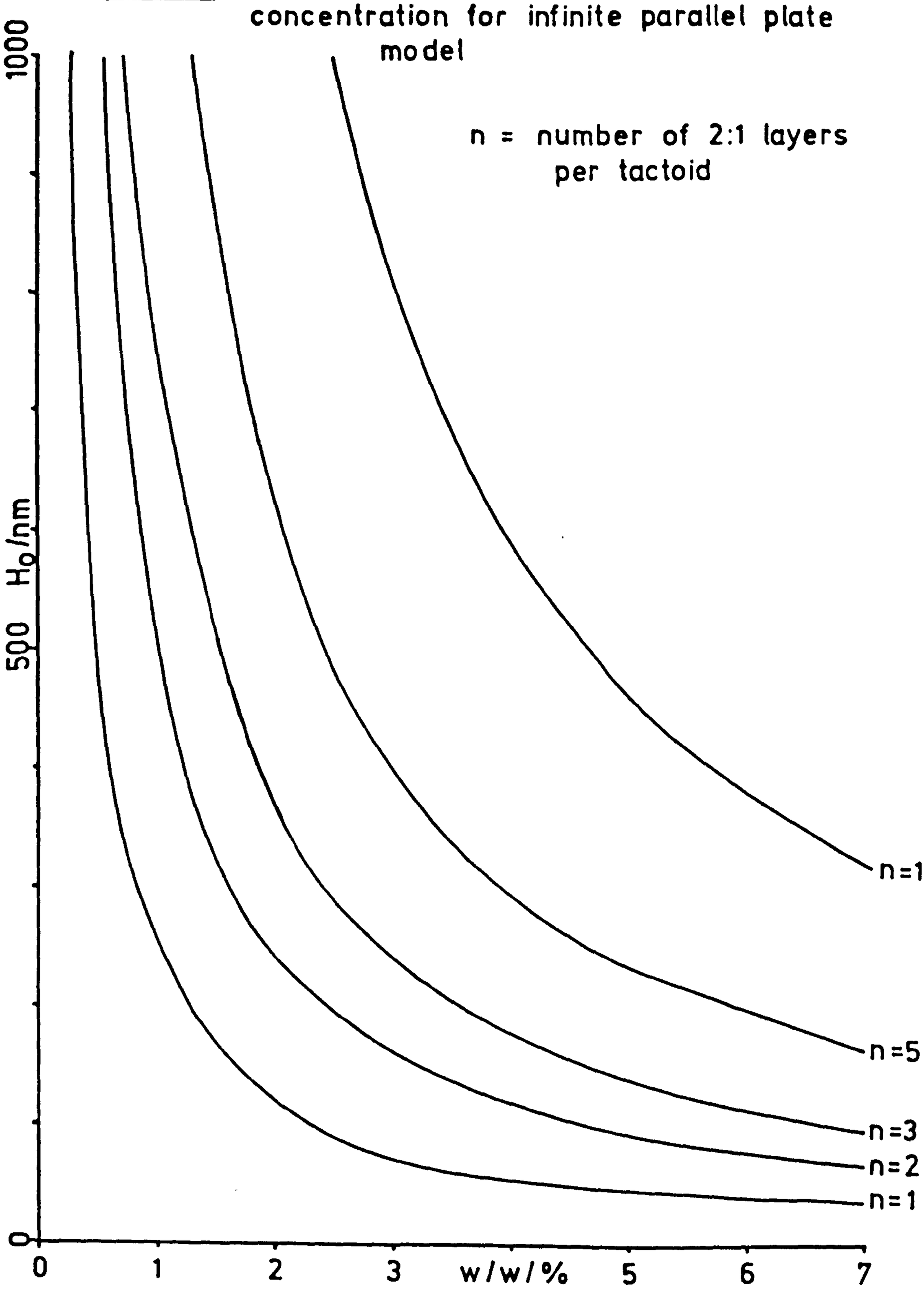

Differentiation of equation 26 with respect to Ho gives

$$\frac{\partial P_R}{\partial H_o} = -8 \times 10^3 \gamma\kappa \, N_A c_e kT \, (\sinh u) \exp(-\kappa Ho/2) \, Nm^{-3} \quad (57)$$

$$\therefore \quad B = \frac{Ho \partial P_R}{\partial H_o} = 10^3 \kappa N_A c_e kTu \, (\sinh u) Ho \quad Nm^{-2} \quad (58)$$

$$\text{or} \quad B = \frac{P_R \kappa u Ho \sinh u}{2(\cosh u - 1)} \quad Nm^{-2} \quad (59)$$

Plots of B, calculated from equation 59, against w/w of clay for different values of c_e are shown in fig. 107.

10.2.3 Verwey and Overbeek theory

Verwey and Overbeek (160) have given the following equation for V_R (sect. 3.1.13.1)

$$V_R = \frac{64 \times 10^3 c_e N_A kT\gamma^2}{\kappa} \exp(-\kappa Ho) \quad Jm^{-2} \quad (29)$$

Therefore,

$$B = Ho \frac{\partial^2 V_R}{\partial Ho^2} = H_o 64 \times 10^3 \kappa c_e N_A kT\gamma^2 \exp(-\kappa Ho) \quad Nm^{-2} \quad (60)$$

$$\text{or} \quad B = V_R \kappa^2 Ho \; Nm^{-2} \quad (60)$$

Plots of B, calculated from equation 60, against w/w of clay, for different values of c_e, in fig. 108.

Fig.107: Langmuir theory results for infinite parallel plates

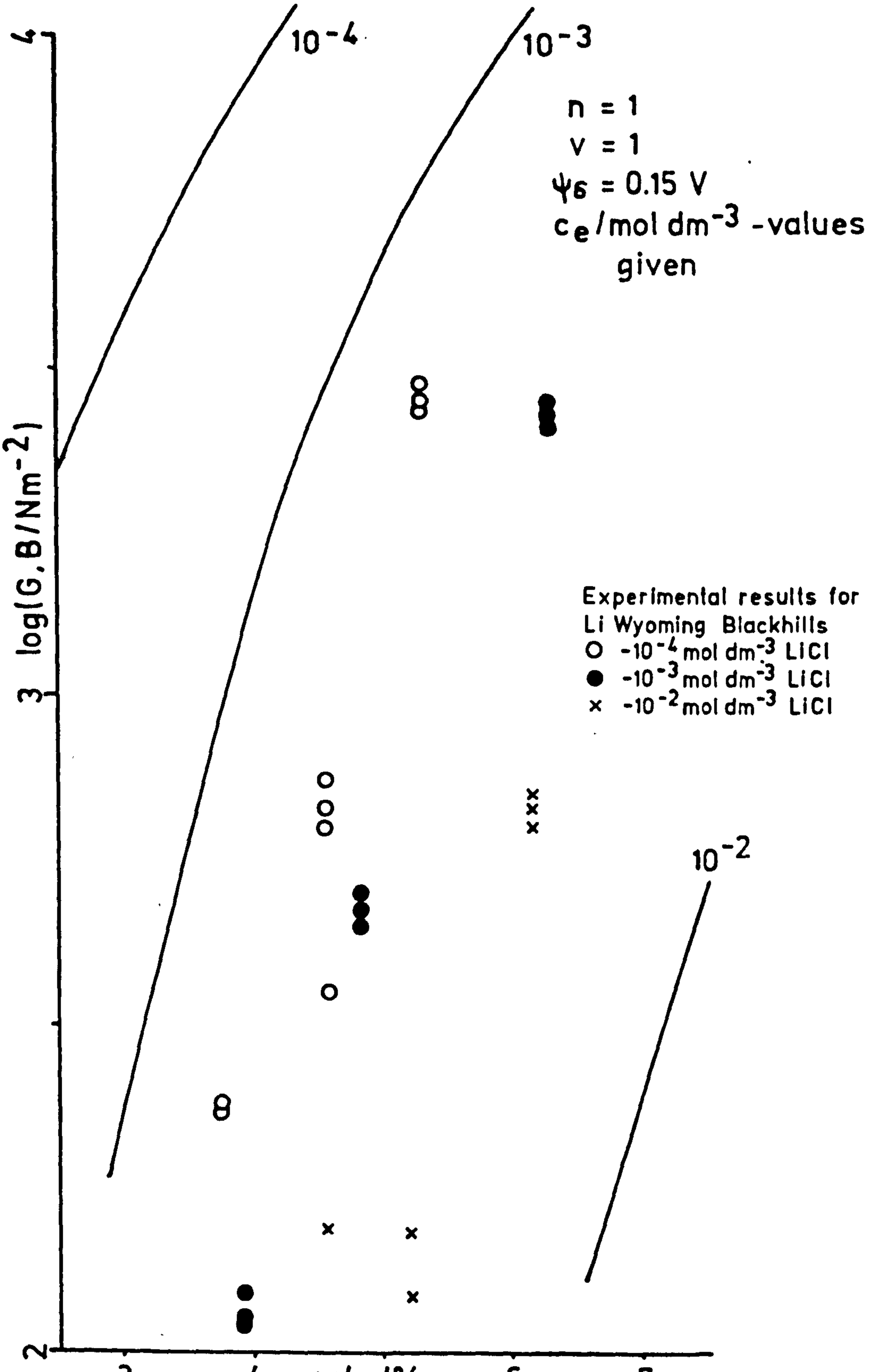

Fig.108: Verwey and Overbeek theory results for infinite parallel plates

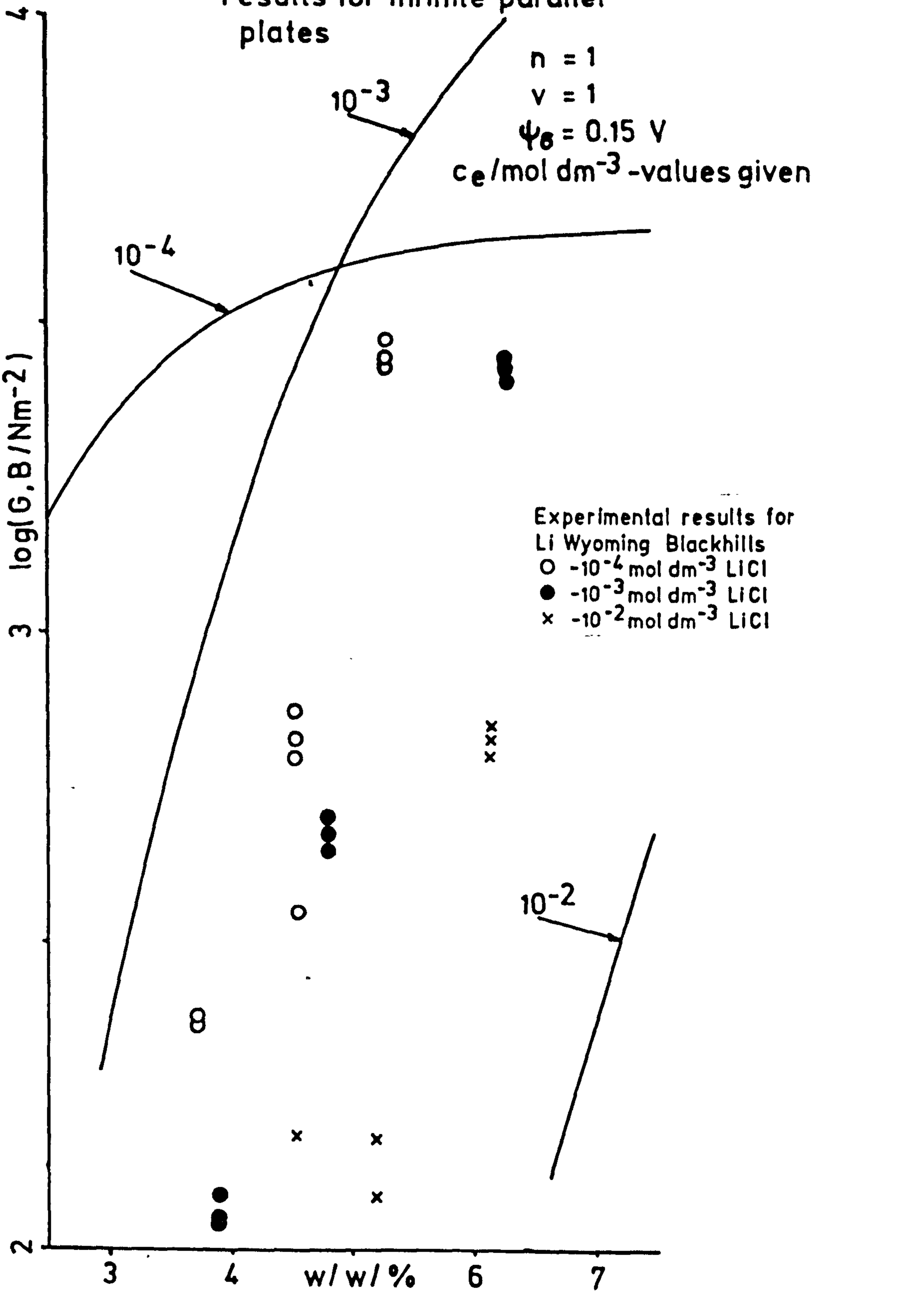

10.2.4 Discussion

Figs. 107 and 108 show that both Langmuir and Verwey and Overbeek theories applied to the infinite parallel plate model give log B vs. w/w curves having similar shape to the experimental log G vs. w/w curves. The theoretical results are, however, a factor of ~100 larger than the experimental results, this difference is far too large to be explained by possible differences between B and G. The theoretical results are also more sensitive to changes in c_e than the experimental results. The theoretical B values are also sensitive to η, although using this model, the differences between the Wyoming and Texas bentonite dispersions cannot be accounted for by alterations of this parameter. The theoretical values of B are relatively insensitive to changes in ψ_δ. The shape of the Langmuir theory curves are in better agreement with the experimental curves at low c_e and higher w/w (i.e. small κHo) than the Verwey and Overbeek theory curves.

In previous work (145) good agreement between theory and experiment was obtained by "fitting" using (higher) effective c_e values. A more quantitative procedure for the calculation of an "effective" κ has recently been suggested by Beresford-Smith and Chan (sect. 8.2.5).

10.2.5 Beresford-Smith and Chan modification

Beresford-Smith and Chan (288, 289, 290, 291) have developed

a theory for deducing the effective electric double layer interaction between colloidal particles in a concentrated dispersion, having a small added electrolyte concentration. This involves modelling a colloidal dispersion as a highly asymmetric electrolyte, where the effective $\kappa(\kappa')$ is given by

$$\kappa' = \left[\frac{10^3 e^2 N_A}{\varepsilon_0 \varepsilon_r kT} \sum_i c_i v_i^2 \right]^{\frac{1}{2}} \qquad (61)$$

where c_i and v_i are the concentration and valency, respectively, of the counter ions necessary to balance the charge on the colloidal particles as well as all species of added electrolyte. Other symbols have the same meanings as in equation 15

or

$$\kappa' = \left[\frac{10^3 e^2 N_A v^2}{\varepsilon_o \varepsilon_r \, bT} \left(c_o + 2c_e \right) \right]^{\frac{1}{2}} \qquad (62)$$

where c_e = concentration of added, symmetrical electrolyte of same valency v as counter ions and c_o = concentration of counter ions necessary to balance the colloidal charge.

c_o may be given by

$$c_o = \frac{\sigma_2}{veN_A} \quad \text{x available particle surface area} \quad \text{mol dm}^{-3} \text{ per dm}^3 \text{ of dispersion} \qquad (63)$$

and, ignoring the edge surface area of the particles,

$$c_o = \frac{2 \times 10^9 \phi \sigma_2}{veN_A n} \quad \text{mol m}^{-3} \tag{64}$$

σ_2 may be calculated from equation 17

$$\sigma_2 = (8 \times 10^3 c_e N_A \varepsilon_o \varepsilon_r kT)^{\frac{1}{2}} \sinh \frac{(ve\psi_\delta)}{(2kT)} \tag{17}$$

Hence κ' is now dependent upon ψ_δ and ϕ as well as c_e and v.

Substituting κ' and the effective electrolyte concentration ($= c_e + co/2$) into equations 59 or 60 means that B may be calculated, taking into account the Beresford-Smith and Chan theory.

Fig. 109 shows that the use of the Beresford-Smith and Chan modification gives curves having similar shape to the experimental data. The data for $c_e = 10^{-4}$ mol dm^{-3} is in quite good agreement with the theory. However, the theoretical prediction for $c_e = 10^{-3}$ and 10^{-2} mol dm^{-3} are $\sim$100 and $\sim 5 \times 10^7$ times too low respectively.

Figs. 110 and 111 show the effects of changing ψ_δ on the theoretical prediction. Changes in ψ_δ have little effect on the shape of the log B on w/w curves (fig. 110) although the magnitude of B is affected (fig. 111), reaching a maximum value at a finite value of ψ_δ. This is because changes in ψ_δ now not only affect B directly (by changing γ in equation 60) but there is an opposing effect upon σ_2 (and therefore c_o and κ') which predominates at high ψ_δ. This latter effect is also dependent upon ϕ.

Fig.109: Theoretical results with Beresford-Smith and Chan modification for infinite parallel plate model

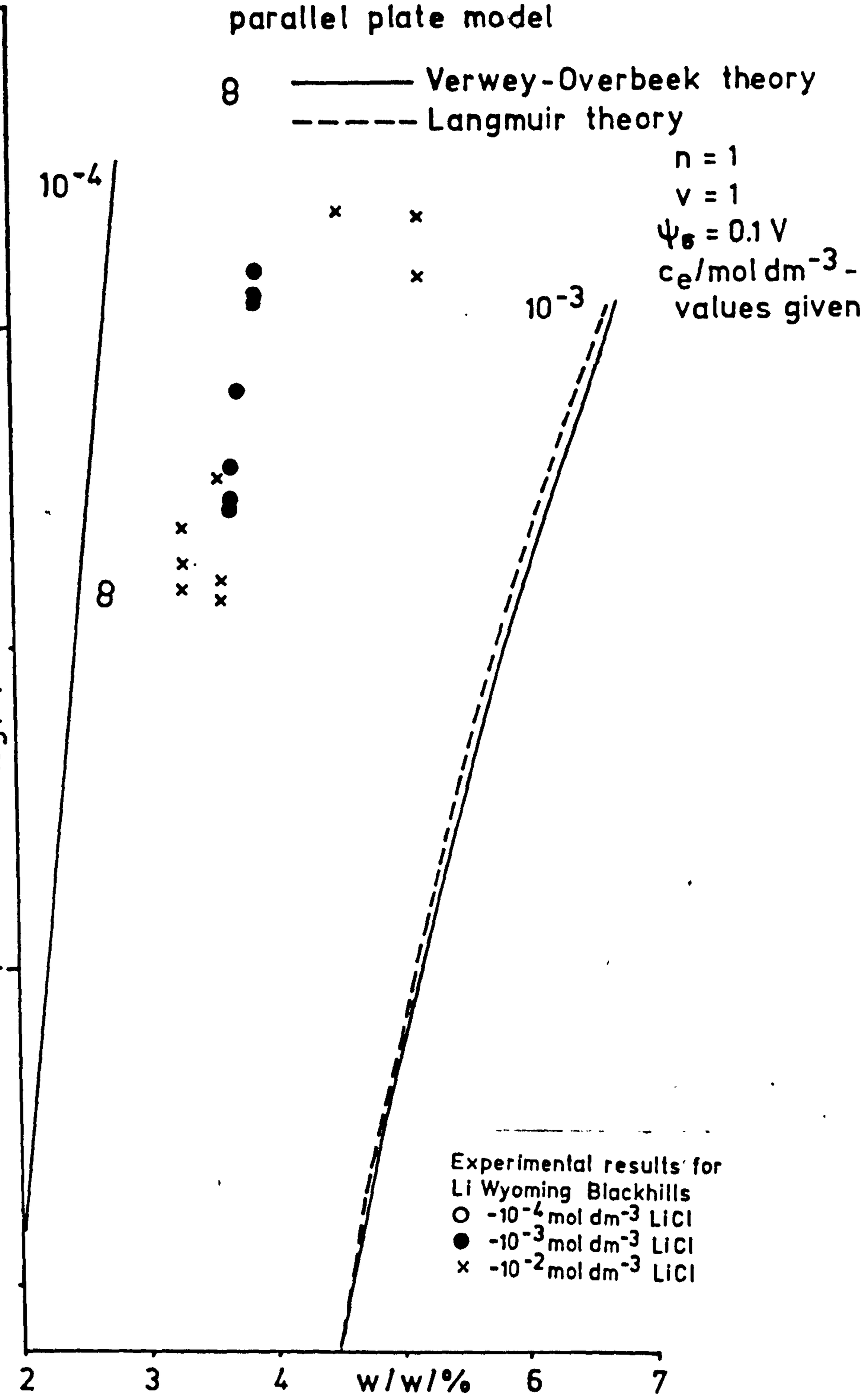

Fig.110: Theoretical results using Beresford-Smith and Chan theory

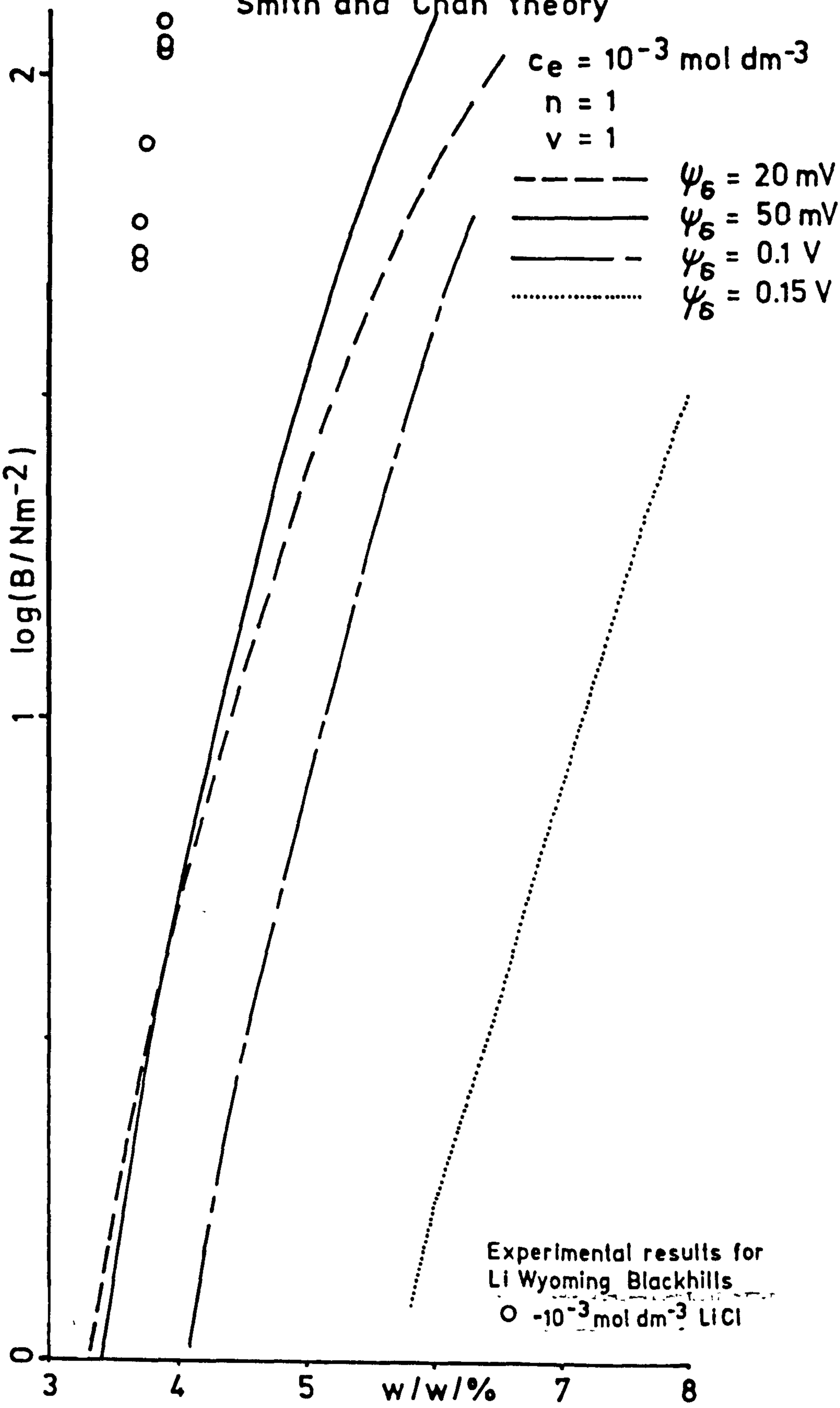

Fig.111: Theoretical results for Beresford-Smith and Chan theory

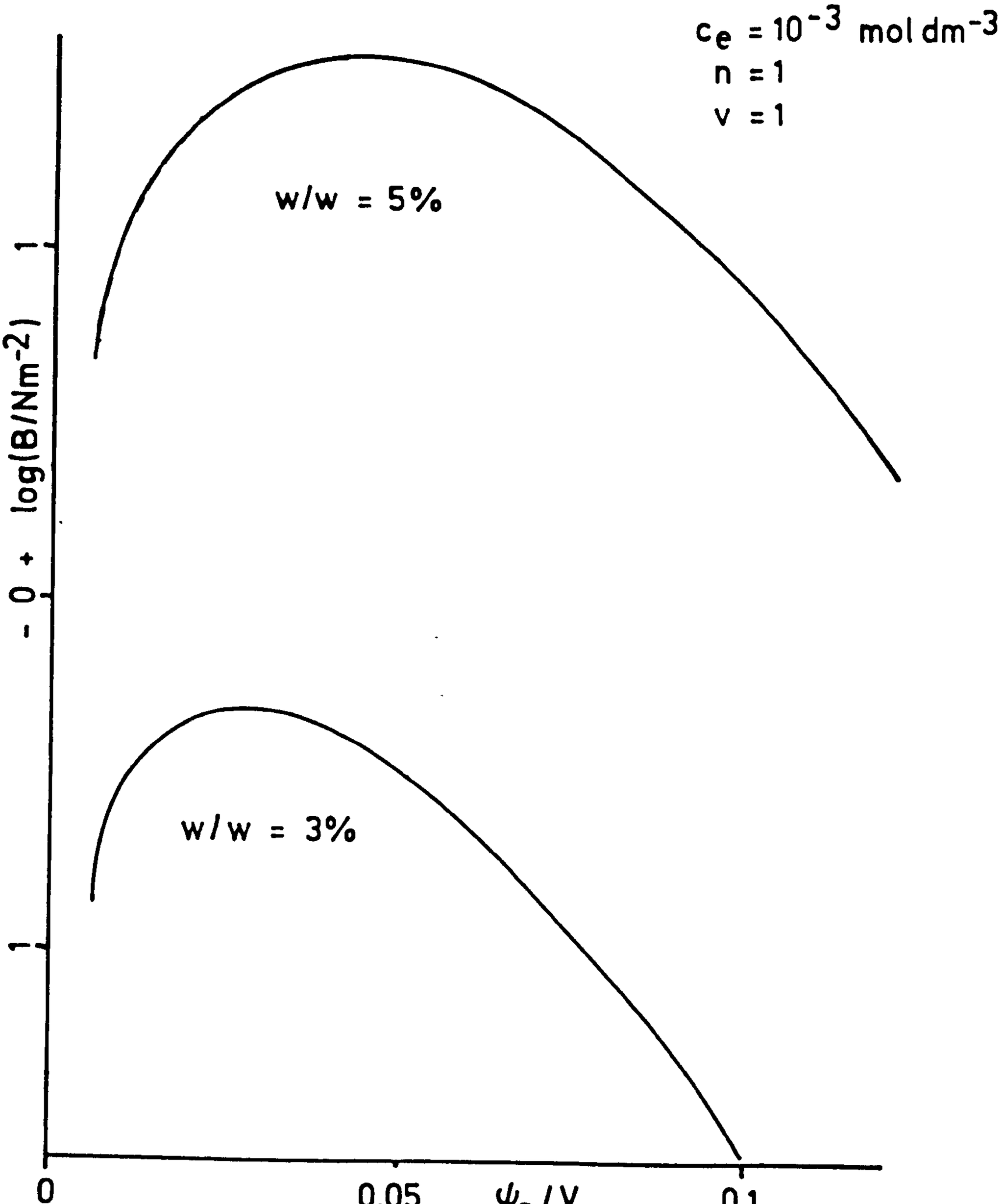

Since $\kappa' > \kappa$ (289) (see table 16) the Langmuir (sect. 8.2.2) and Verwey and Overbeek (sect. 8.2.3) theories, now give identical results over the range of experimental results obtained (fig. 109).

Table 16 shows the effective electrolyte concentrations calculated using the Beresford-Smith and Chan modification.

Table 16: Effective electrolyte concentrations calculated using Beresford-Smith and Chan theory, (assuming n = 1).

w/w/%	ψ_δ/V	c_e/mol dm^{-3}	$\frac{\kappa'}{\kappa}$	Effective electrolyte concentration/ mol dm^{-3}		
				$c_e + co/2$	Previous work (145)	
5	0·10	$1x10^{-4}$	3·95	$9·99 \times 10^{-4}$	-	
5	0·10	$1x10^{-3}$	2·66	$3·83 \times 10^{-3}$	-	
5	0·10	$1x10^{-2}$	1·93	$1·91 \times 10^{-2}$	-	
1·5	0·15	$1x10^{-4}$	3·61	$7·89 \times 10^{-4}$	$8·1x10^{-4}$	Li montmorillonite
1·5	0·12	$1x10^{-3}$	2·09	$2·21 \times 10^{-3}$	$1·6x10^{-3}$	Li montmorillonite
1·5	0·10	$1x10^{-2}$	1·50	$1·26 \times 10^{-2}$	$8·2x10^{-3}$	Li montmorillonite
1·5	0·12	$1x10^{-4}$	2·95	$4·81 \times 10^{-4}$	$5·9x10^{-4}$	Na
1·5	0·09	$1x10^{-3}$	1·81	$1·66 \times 10^{-3}$	$5·5x10^{-4}$	Na
10	0·08	$1x10^{-4}$	4·46	$1·36 \times 10^{-3}$	$3·2x10^{-3}$	K
10	0·07	$1x10^{-3}$	2·75	$4·23 \times 10^{-3}$	$6·3x10^{-3}$	K
10	0·05	$1x10^{-2}$	1·77	$1·67 \times 10^{-2}$	$2·2x10^{-2}$	K
85	0·02	$1x10^{-4}$	8·81	$2·02 \times 10^{-2}$	$6·0x10^{-2}$	C_s
85	0·02	$1x10^{-3}$	5·39	$6·62 \times 10^{-2}$	$5·3x10^{-2}$	C_s

Table 16 shows that there is good agreement between the results calculated from Beresford-Smith and Chan theory and the results of

Middleton (145), extrapolatated from low ϕ ($\sim$1·5% w/w) results, for Li and Na montmorillonites although higher ϕ values need to be assumed to obtain reasonable agreement for K and Cs montmorillonites. Table 16 also shows that κ' becomes closer to $\kappa(\kappa'/\kappa \rightarrow 1)$ as ϕ (w/w) or c_e is increased or ψ_δ is reduced.

10.2.6 Discussion

These results suggest that the infinite parallel plate model with the Beresford-Smith and Chan modification could be used to predict the properties of aligned montmorillonite layers (e.g. 2nd and subsequent compression and decompression data from compression studies (145, 146)). However, for disordered montmorillonite dispersions (e.g. this work and first compression results (145)) this model breakes down quantitatively, especially as c_e is increased above $\sim 10^{-4}$ mol dm^{-3} LiCl, although the predicted trends (general shape of the curves and the reduction in B upon increasing c_e, at a given w/w) are qualitatively correct.

CHAPTER ELEVEN

GENERAL DISCUSSION

G E N E R A L D I S C U S S I O N

11.1 MINERALOGY OF TEXAS BENTONITES

The studies carried out on crude samples of Texas bentonite (chapter 5) indicate that the major mineral components are smectite, opal-CT and halloysite. Scanning electron microscopy of the hard Helms bentonite (full face Helms) revealed that most of the halloysite was present at weathered rock surfaces. This is probably because the halloysite was formed by weathering of the smectite mineral at the exposed rock surfaces. It is expected that halloysite may be more widely dispersed through the soft Helms and Clark bentonites. This is due to the more permeable nature of these materials, allowing more extensive weathering and/or mechanical mixing of surface and bulk regions.

The opal-CT is more completely dispersed through the hard Helms rock than the halloysite. Transmission electron microscopy of carbon replicae of the cleaved rock surface suggested, however, that there seem to be concentrations of opal-CT in small cracks and fissures within the bulk of the rock. The presence of opal-CT in the Texas bentonites has been attributed to the breakdown of radiolaria and diatom etc. skeletons by Henderson et al (16). Much of the opal-CT seems to disperse in water along with the clay mineral components, although it seems likely that some smectite-silica aggregates may be present, as suggested by Chen (10). It is possible that some such aggregates are partially altered volcanic glass particles, i.e. silica-smectite crystal intergrowths.

11.2 DISPERSION PREPARATION

Prior to any careful examination of a colloidal dispersions properties it is important to obtain well characterised dispersion samples. The dispersion preparation procedure used (chapter 6) was generally found to produce dispersions having good reproducibility for a given batch. Variation in properties between individual batches of sample (even those obtained from the same source material) might be expected, due to differences in the particle size distributions (145). It was found to be very important to take care to avoid accidental contamination of samples having electrolyte concentrations less than $\sim 10^{-2}$ mol dm^{-3}, since small additions of electrolyte to such preparations could have large effects on their rheological properties.

The preparation procedure was found to be quite effective at producing reasonably pure montmorillonite dispersions from the Wyoming bentonite samples. However, it was found to be difficult to remove all the opal-CT from the Texas bentonite samples, by "non-chemical" treatments (due to the similarities in particle size and density of opal-CT and smectite). Texas bentonite samples, containing small amounts of halloysite impurity, could be prepared by using "cobbed" material (i.e. that having surface discolourations manually removed).

The very fine fraction samples of montmorillonite might be expected to contain the least amounts of accessory minerals. However, such samples are difficult to prepare in large quantities and they would be expected to undergo rapid dissolution, and subsequent, reactions in dispersion. Such very fine dispersions were found to form gels

having interesting optical properties (i.e. transparent or translucent), which may be worthy of further study.

11.3 RHEOLOGICAL PROPERTIES OF WYOMING BENTONITE DISPERSION

The pulse shearometry results (chapter 8) for the Li Wyoming bentonite dispersions in dilute ($\leq 10^{-2}$ mol dm^{-2}) LiCl solutions can be explained by assuming the system is structured due to electric double layer repulsions. A theory assuming an infinite parallel sheet geometry and only electric double layer forces to be important (chapter 10) may be used to qualitatively explain the results. The experimental log G against w/w of clay have a similar shape to the theoretical predictions. As the LiCl concentration is increased up to 10^{-2} mol dm^{-3} the shear modulus decreases (at a given clay volume fraction). This trend can be explained by a reduction in electric double layer range, and hence interaction energy, upon increasing electrolyte concentration. At such low electrolyte concentration the dispersions are found to be anti-thixotropic (i.e. G decreases with time after mixing). This may be attributed to a relaxation of the system to a more ordered arrangement resulting in an increase in mean interparticle separation and hence reduction in interaction energy.

As the LiCl concentration is increased above 10^{-2} mol dm^{-3} the measured shear modulus increases and the dispersions become thixotropic (G increases with time). Such thixotropic dispersions have generally been believed to be flocculated although there is disagreement as to the arrangement of montmorillonite particles in dispersion (19, 194).

At still higher LiCl concentration (>1 mol dm^{-3}) it seems that there may be a further decrease in shear modulus. The reason for this is not clear (19, 194).

If the counter-ion is changed from Li^+ to Na^+, K^+ and then Cs^+ there is a general shift in the minima in the log G against log c_e curves to lower electrolyte concentrations (fig. 93). This trend may be explained by an increased tendency to tactoid formation and/or reduction in Stern potential as the counter-ion is changed in the series Li^+, Na^+, K^+ to Cs^+. The trend of reducing G, at electrolyte concentrations below the minima, as the counter-ion is changed in the above series can be explained by an increase in tactoid formation giving an increase in interparticle separation and reduction in interaction energy. The increased tendency to tactoid formation, as described above, to be confirmed by the change in optical properties of the dispersions as the counter-ion is changed.

At electrolyte concentrations above the minima in the curves shown in fig. 93 the trends are difficult to explain on the basis of tactoid formation alone.

11.4 COMPARISON OF TEXAS AND WYOMING BENTONITE PROPERTIES

Comparison of the rheological results for the Texas and Wyoming bentonite dispersions (sect. 8.4) indicates that the Texas bentonite preparations consistently give lower measured shear moduli than the Wyoming bentonites under similar clay concentration etc. conditions (figs. 86 - 88 and 94). Possible reasons for this difference in behaviour will now be discussed.

a) Presence of non-dispersing clay minerals in Texas bentonite:

This explanation does not seem likely since X-ray diffraction of the crude samples (sect. 5.3.2) did not provide any evidence for the presence of significant amounts of non-swelling clay minerals (such as vermiculite, illite or chlorite) in the Texas bentonites. No clear evidence was found for the presence of beidellite (sect. 4.3.3, 4.3.4 and 7.3.2) in the Texas bentonites. It is possible that the results of Roberson (12, 13) suggesting the presence of beidellite in Texas bentonite could be explained on the basis of variations in surface charge heterogeneity. The presence of (tetrahedral aluminium containing) beidellite could be checked by solid state ^{27}Al-nuclear magnetic resconance spectroscopy (343, 347, 348, 349).

b) Differences in surface charge density between Texas and Wyoming bentonites:

The CEC determinations (sect. 7. and 4.3.2) suggested that the CEC of the Wyoming bentonite was within the range of variations in CEC of the individual Texas samples. The theoretical calculations (chapter 10) suggest that bulk modulus is relatively insensitive to variation in Stern potential.

c) Differences in surface charge heterogeneity:

This property was not studied in this work. In view of the above (b) small variations in heterogeneity might be considered to have very little effect on properties. Charge heterogeneity would probably have very little effect on the diffuse part of the electric double layer although variations in the inner part of the double layer may affect the tendency towards tactoid formation, for example. The use of Li montmorillonite might be expected to minimise this effect, since such material has the least tendency to form tactoids (sect. 3.2.2).

d) Presence of Ca montmorillonite in Texas bentonite:

The presence of large amounts of Ca montmorillonite is the most likely explanation of the poor rheology of the crude Texas bentonites (fig. 88). This explanation does not seem likely for the purified samples especially in view of the relatively poor rheology of the Li Bentolite L - preparation D sample (fig. 87) which has a very low Ca content (table 33 , appendix 3), due to the combined use of LiCl and EDTA during its preparation (sect. 6.2.liv).

e) Presence of opal-CT in Texas bentonite:

This is considered the most likely explanation for the properties of the Texas bentonite. Opal-CT is the most significant

impurity accessory mineral remaining in the Texas bentonite samples after purification (table 34, appendix 3). Fig. 112 shows a plot of "gelling effectiveness" against opal-CT content. The ordinate axis of fig.112 shows the clay concentration /w/w% required to obtain a shear modulus of 100 Nm^{-2}, the values being obtained from the least squares results given in table 15. The abscissa axis of fig. 112 indicates the amount of cristobalite in the sample as measured by X-ray diffraction (table 34, appendix 3). The measurement of opal-CT by X-ray diffraction is likely to be inaccurate due to the presence of "unseen" amorphous silica phases. However, fig. 112 seems to indicate a clear trend between "gelling ability" and opal-CT content. It is possible that a proportion of the opal-CT in the samples binds the montmorillonite together into aggregates. The existence of such aggregates is suggested by electron microscopy (figs. 55, 73 and 75) (6), although these results may be due to artifacts, and X-ray diffraction studies (10). The presence of such aggregates would increase the mean particle size and thus reduce the particle number concentration which would tend to reduce the clear modulus (appendix 9). Reduction of the mean particle size by centrifugation or high-shear homogenisation (fig. 87) is effective in increasing a dispersions shear modulus, at low electrolyte concentrations at least.

Fig.112: Effect of opal-CT content on "gelling ability" of Li bentonite dispersions

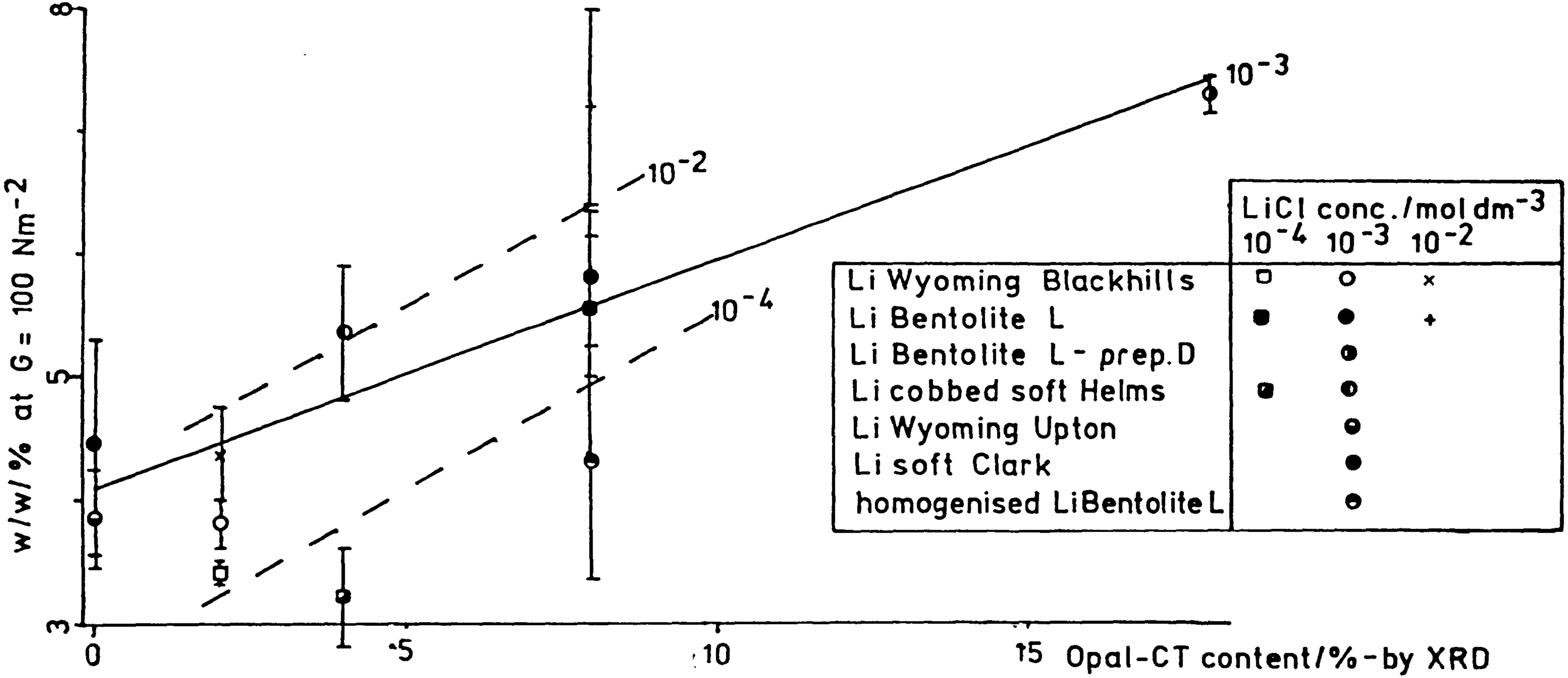

11.5 THEORETICAL MODELS

The results presented in chapter 10 (table 16) indicate that any theoretical models for the prediction of the properties of concentrated aqueous montmorillonite (or other) dispersions must take into account the presence of electric double layer cations as well as added bulk electrolyte, as suggested by Beresford-Smith, Chan and others (288, 289, 290, 291, 145, 192).

The calculations given in appendix 9 suggest that, in more refined theories, it may be necessary to take account of particle ordering effects as suggested by Langmuir (169) and others (493, 208, 345, 346), using statistical mechanics (208, 345, 346, 350).

APPENDIX 1

Calculation of ion site radii

If the cations are arranged in a close-packed sheet on the montmorillonite surface, then the radius of the (circular) site available for each cation can be calculated from the following procedure

surface area per cation = area of circumscribed hexagon

$= 2 \cdot 5980 \times (\text{hexagon side length})^2$

ion site radius = radius of circle inscribed in hexagon

= 0 86602 x hexagon side length

$= 0\ 86602 \times \left(\frac{\text{surface area per cation}}{2 \cdot 59808}\right)^2$

Therefore, for the ideal montmorillonite,

$$\text{ion site radius} = 0 \cdot 86602 \left(\frac{1 \cdot 39v}{2 \cdot 59808}\right)^{\frac{1}{2}} \quad \text{nm}$$

$$= 0 \cdot 63 \sqrt{v} \quad \text{nm}$$

$\therefore$ v = 1 = > ion site radius = 0·63 nm

v = 2 = > ion site radius = 0·90 nm

For interlayer cations

$$\text{ion site radius} = 0 \cdot 63 \sqrt{v/2} \quad \text{nm}$$

$\therefore$ v = 1 = > interlayer ion site radius = 0·45 nm

v = 2 = > interlayer ion site radius = 0·63 nm

These results indicate that there is sufficient space on the mineral surfaces to accommodate the usual solvated and anhydrous cations.

Table 17: Crystal and Stokes radii of solvated metal cation

Cation	crystal radius/nm	Stokes radius of solvated ion/nm in water
Li^+	0·06	0·24
Na^+	0·095	0·18
K^+	0·133	0·13
Cs^+	0·169	
Mg^{2+}	0·065	
Ca^{2+}	0·099	

APPENDIX 2

Pulse Shearometry results

Table 18: Pulse shearometry results for Na Bentolite L

Fig.	NaCl	w/w%	G/Nm^{-2}	(pH = 6·5(±0·5) unless otherwise noted)
	10^{-2}	5·14	351	
	0·1	5·14	67, 70	
	0·5	5·14	365	
	0·2	5·14	141, →71, 91, 105 (1 day after) - Thixotropic	
	$3·3x10^{-3}$	2·8	20, 33, 36, 41 - antithixotropic	
	$3·3x10^{-3}$	2 8	13, 11, 20 (after 3 days)	
	$4·5x10^{-3}$	3·76	118, 96, 91, 91	
	$4·6x10^{-3}$	3·76	54, 74, 60, 67	
	$4·9x10^{-3}$	4·00	84, 87, 87	
	$6·4x10^{-3}$	5·00	225, 216, 216	
	$5·8x10^{-3}$	4·55	99, 105	
	$8·8x10^{-3}$	6·88	650, 630, 601, 607	
	10^{-2}	7·82	1333, 1471, 1429	
	10^{-2}	6·88	120, 122, 129	
	10^{-2}	5·0	85, 120, 135	
	10^{-2}	4·0	87, 105, 78, 114	

Table 19: Pulse Shearometry results for Na Wyoming Blackhills.

pH 6·5±0·5 unless otherwise stated

Fig.	(NaCl)	w/w	G/Nm^{-2}	
	$2·93x10^{-3}$	4·38	1917, 1932, 1770	pH = 3·0±0·1
96	$1·1x10^{-3}$	2·77	391, 446, 458 (not thixotropic)	
	$3 x 10^{-3}$	2·77	70, 70, 76	
	$2·8x10^{-4}$	2·41	282, 286, 282	
96	$1 x 10^{-3}$	2·41	47, 32, 36	
	$3 x 10^{-4}$	2·19	266, 274, 267	
96	$1 x 10^{-3}$	2·19	43, 45, 38	
	$3 x 10^{-3}$	2·19	102 (antithixotropic)	
	$3 x 10^{-4}$	1·68	34, 18, 17	
81	10^{-4}	1·83	111, 115	
81	10^{-4}	1·94	124, 123	
81, 96, 83	10^{-3}	1·93	29, 76, 24, 29	
81, 96, 83	10^{-3}	1·99	45, 47, 52	
	10^{-2}	1·55	38, 44	
93	10^{-4}	3·15	77, 69, 66, →72 (30 minutes)→70 (45 mins).	
93	10^{-3}	3·15	33, 33, 45, →44 (30 minutes)→45 (45 mins).	
93	10^{-2}	3·15	364, 264, 329 →487(30 min)→612(45 min).	
93	0·216	3·15	1487, 3130, 2662 →6373 (45 min).	
93	$\sim 10^{-5}$	3·15	737, 538, 1456, 929	

Table 20: Pulse shearometry results for Li Wyoming Blackhills

Fig.	(LiCl)	w/w/%	G/Nm^{-2}
82	$5x10^{-4}$	6•72	5498, 5341, 5214
82	$5x10^{-4}$	4•29	728, 821, 789
82	$5x10^{-4}$	3•31	88, 94, 91
82	$5x10^{-4}$	2•79	56, 51, 53
82	$5x10^{-4}$	1•80	22, 14, 19, 14
82	10^{-4}	5•32	2923, 2748, 2690
82	10^{-4}	4•56	858, 923, 941 *
82	10^{-4}	3•77	240, 237 (antithixotropic)
82	10^{-4}	2•72	39, 38
80,86,87, 82,83	10^{-3}	6•28	2742, 2636, 2645
80,86,87, 82,83	10^{-3}	4•80	582, 632, 608
80,86,87, 82,83	10^{-3}	3•89	110, 120, 113
80,86,87, 82,83	10^{-3}	3•69	53, 59, 51 (antithixotropic)
82	10^{-2}	6•17	895, 792, 856
82	10^{-2}	5•21	151, 119, 153
82	10^{-2}	3•31	39, 49, 43
82	10^{-2}	3•60	38, 57, 40 (antithixotropic)

Table 20 continued

Fig.	(LiCl)	w/w/%	G/Nm^{-2}	
94	10^{-4}	4•56	801 →888 (after 3 mins)	
94,86,187, 80,82,83	10^{-3}	4•56	449 →349, 429 (after 3 mins)	reserved 16 days after results marked *
94	10^{-2}	4•56	154 →86(after 3 mins)	
94	0•1	4•56	242 →558(after 3 mins)	
94	1	4•56	410 →583(after 3 mins)	
93	$\sim 10^{-5}$	3•63	652, 715 →796(30 mins) →796(45 mins) →840	
93	10^{-4}	3•63	133, 117, 137 →123(30 mins) →130(45 mins) →123	
93	10^{-3}	3•63	70, 75 →79(30 mins) →75(45 mins) →75	
93	10^{-2}	3•63	49, 53 →99(30 mins)	
93	$8•1 \times 10^{-2}$	3•63	625, 589 →1452(30 mins) →1807(45 mins) →2035	
93	0•95	3•63	312, 277 →477(30 mins) →509(45 mins) →1225	
95	10^{-3}	6•04	246, 408, 462 (pH3•45)	
95			310, 371 (pH 4•25)	
95			466, 285, 230, 349 (pH 5•1)	
95			303 (pH 5•8)	
95			203 (pH 6•0)	
95			198 (pH 7•3)	
95			185 (pH 7•4)	
95			199 (pH 8•5)	

Table 20 continued

Fig.	(LiCl)	w/w/%	G/Nm^{-2}
95			141 (pH 8•4)
95			153 (pH 9•3)
95			112 (pH 9•2)
95			87 (pH 10•0)
95		3•72	84 (pH 9•9)
95	0•1	4•08	83, 70 (pH 3•4)
95			48 (pH 4•8)
95			37 (pH 4•7)
95			38 (pH 6•5)
95			38 (pH 6•4)
95			51 35 (pH 7•4)
95			43 (pH 9•4)
95		3•72	39 (pH 9•3)
86	10^{-3}	5•22	3728, 2767, 1352, 3962, 2836 (fine fraction)
-	10^{-3}	2•38	Unmeasurable (coarse fraction)

Table 21: Pulse Shearometry results for Li Bentolite L

Fig.	(LiCl)	w/w	G/Nm^{-2}
84	10^{-4}	7·0	475, 506, 516
84	10^{-4}	5·78	85, 103, 101
84	10^{-4}	4·85	46, 37, 40, 38
84, 94	10^{-4}	4·33	22, 36, 76, 52 *
84,86,87	10^{-3}	7·96	976, 935, 1096
84,86,87	10^{-3}	6·41	99, 97
84,86,87	10^{-3}	5·48	48, 53
84,86,87	10^{-3}	4·43	32, 35, 50, 25
84	10^{-2}	8·54	239, 209, 224
84	10^{-2}	6·59	74, 56, 66
84	10^{-2}	5·02	37, 25, 27
84, 94	10^{-4}	4·33	19, 28 →34(after 3 mins)(22 days after*)
84,86,87, 94	10^{-3}	4·33	37 →43(3 mins.)
84, 94	10^{-2}	4·33	40, 29 →11, 13(3 mins)
94	0·1	4·33	40 →75(3 mins)
94	1	4·33	96 →226(3 mins)
-	10^{-3}	4·05	12

Table 22: Pulse Shearometry results from Li Bentolite L - prep D

Fig.	(LiCl)	w/w/%	G/Nm^{-2}
87	10^{-3}	6·67	59, 53
87	10^{-3}	8·79	400, 408
-	10^{-3}	10·23	1543, 1923, 1594
87	10^{-3}	4·98	294, 320 (fine fraction)
	10^{-3}	5·85	403, 498, 974, 496 (fine fraction)
	10^{-3}	11·55	Unmeasurable (coarse fraction)

Table 23: Pulse Shearometry results for Li-cobbed soft Helms

Fig.	(LiCl)	w/w	G/Nm^{-2}
-	$\sim 10^{-3}$	11·3	503, 476, 470
-	$\sim 10^{-3}$	10·5	365, 359
-	$\sim 10^{-3}$	9·5	784, 688
-	$\sim 10^{-3}$	8·4	~171, ~192
85, 86	$\sim 10^{-3}$	6·1	~76, 161, 228
85	10^{-4}	4·71	247, 227, 235*
-	10^{-4}	4·71	197 (26 days after *)
85	10^{-4}	7·69	1529, 1757, 1623
85	10^{-4}	7·77	1497, 1679, 1571
-	$\sim 10^{-4}$	5·99	180, 160, 155
-	10^{-4}	3·68	(~)2
-	$\sim 10^{-4}$	7·85	137, 153
-	$\sim 10^{-3}$	8·17	150, 148
85, 86	10^{-3}	6·93	385
85, 86	10^{-3}	6·20	205, 202
85, 86	10^{-3}	3·64	80, 6, 9, 35
-	$\sim 10^{-3}$	2·14	(~)1
85	10^{-2}	7·85	186
85, 86	10^{-3}	7·97	1379, 2743, 1715, 1599
85, 86	10^{-3}	7·62	1019, 931
85, 86	10^{-3}	6·68	294, 278
85	10^{-4}	6·58	799, 884
85	10^{-4}	5·45	378, 378
85	10^{-4}	6·29	1081, 2014, 839, 903

Table 24: Pulse shearometry results for Crude dispersions

Fig.	Clay	electrolyte concentrations	pH	w/w	G/Nm^{-2}
-	Wyoming Blackhills	natural	natural pH 9•1	8•29	125
88	Wyoming Blackhills	10^{-3}LiCl	8•0	6•95	109
88	Wyoming Blackhills	10^{-3}LiCl	7•8		33
-	cobbed soft Helms	natural	natural-5•6	31•55	167
88	cobbed soft Helms	10^{-3}LiCl	-	26•34	50, 53
-	Bentolite L	natural	natural-7•0	27•12	36
88	Bentolite L	10^{-3}LiCl	8•1	24•67	195, 110, 50.

Table 25: Pulse shearometry results for Li Wyoming Upton
pH 6•2±0•2

Fig.	(LiCl)	w/w/%	G/Nm^{-2}
80	10^{-3}	2•61	8, 26
80	10^{-3}	3•10	40
80	10^{-3}	5•46	757, 1371, 1188

Table 26: Pulse shearometry results for Li Halloysite
pH 6•1

Fig.	(LiCl)	w/w/%	G/Nm^{-2}	
88	10^{-3}	14•56	3359, 8170, 10237 (thixotropic)	
88	10^{-3}	8•54	925, 676	
-,	10^{-3}	14•56	5000, 5745	measured 5 days after above
-	10^{-3}	8•54	1750, 1037, 962	measured 5 days after above

Table 27: Pulse shearometry results for homogenised Li Bentolite L

Fig.	(LiCl) w/w/%	G/Nm^{-2}
-	$\sim 10^{-5}$ ~ 0.5	~ 1
87	10^{-3} 5.22	211, 215
87	10^{-3} 3.49	82, 102, 49, 54, 30
-	10^{-4} 4.18	400, 388, 370
87	10^{-3} 4.32	47, 47
87	10^{-3} 5.84	553, 560

Table 28: Pulse shearometry results for Li soft Clark 10^{-3}mol dm^{-3} LiCl

Fig.	w/w	G/Nm^{-2}
86	5.02	596, 624
86	4.08	57, 64
86	3.24	43, 45, 42
-	2.46	0, 3
86	3.51	33, 21
86	5.09	95, 87
86	5.90	480, 450

Table 29: Pulse shearometry results for K Wyoming Blackhills

Fig.	(KCl)	w/w	G/Nm^{-2}
83	10^{-3}	5•37	1146, 1316, 1187
83	10^{-3}	4•30	356, 371
83	10^{-3}	2•72	36, 42, 45
93	$\sim 10^{-5}$	3•49	1400, 457, 1731, 673
93	10^{-4}	3•49	72. 107, 88→87 (45 minutes)
93	10^{-3}	3•49	84, 65, 65→92 (30 mins).
93	10^{-2}	3•49	1745, 1746, 1835→4153 (30 mins)→4153 (45 mins)
93	0•118	3•49	1534, 7643, 1322, 2706→9457 (30 mins) →9457 (45 mins)

Table 30: Pulse shearometry results for Cs Wyoming Blackhills

Fig.	(CsCl)	w/w/%	G/Nm^{-2}
83	10^{-3}	1•07	13, 12
83	10^{-3}	2•06	253, 260
83	10^{-3}	3•36	455, 538
83	10^{-3}	3•47	467, 956, 793, 587
83	10^{-3}	4•16	509, 590
93	$\sim 10^{-5}$	3•15	21, 30±2, 16±2, 8±1→8 (45 minutes)
93	10^{-4}	3•15	16
93	10^{-3}	3•15	203, 287±17→453 (30 mins)→487 (45 mins)
93	10^{-2}	3•15	484, 1650, 723, 2368, 5726, 3780±50 →8407 (30 min)→9838 (45 min)
-	0•1	3•15	Unmeasureable

Table 31: Pulse shearometry results for Na Wyoming Upton

Fig.	(NaCl)	w/w	G/Nm^{-2}
81	10^{-3}	3·88	149, 161
81	10^{-3}	2·87	11, 60, 40
81	10^{-3}	3·39	136, 143

Table 32: Pulse shearometry results

Fig.	(LiCl)	w/w	G/Nm^{-2}	Clay
86	10^{-3}	1·31	89, 111	Li Beidellite
86	10^{-3}	4·10	300, 293, 300	Li Milos

APPENDIX 3

Table 33: Chemical composition of clay samples

Percentage compositions by weight obtained by ECLP from XRF analysis

Sample	S_iO_2	Al_2O_3	Fe_2O_3	T_iO_2	CaO	MgO	K_2O	N_2O	Li_2O	Loss on Ign.
WB	69•7	16•7	3•46	0•13	1•71	1•41	0•47	1•34	-	5•0
WU	79•4	12•1	0•82	0•36	0•26	0•05	0•88	1•28	-	4•8
BL	75•3	13•5	0•85	0•22	1•72	2•53	0•11	0•25	-	5•5
CSH	67•2	18•7	1•07	0•30	2•06	3•22	0•19	0•25	-	7•0
SC	68•2	17•3	0•83	0•19	1•02	1•98	1•96	1•17	-	7•4
Mi	59•3	21•5	3•10	0•23	1•48	4•90	0•26	0•38	-	8•8
Halloysite	43•7	38•4	0•26	0•03	0•19	0•18	0•43	0•14	-	16•7
LiWB	62•8	21•6	4•75	0•14	0•14	1•92	0•04	0•20	n.d.	8•5
NaWB	62•7	21•5	4•81	0•14	0•13	1•95	0•02	2•05	-	6•7
LiBL	69•1	18•3	1•20	0•28	0•39	3•23	0•00	0•09	n.d.	7•4
NaBL	62•7	18•7	0•94	0•29	0•14	2•83	0•16	2•61	-	11•6
LiBL/LiEDTA	76•1	14•6	0•92	0•23	0•02	2•19	0•08	0•09	n.d.	5•9
LiCSH	67•5	20•3	1•11	0•30	0•05	2•74	0•10	0•56	n.d.	7•3
NaCSH	72•1	14•6	0•88	0•22	0•03	2•53	0•06	2•06	-	7•6
LiSC	49•7	19•9	0•94	0•18	0•00	3•10	0•00	0•30	1•39	*25•9
LiMi	70•3	17•7	1•96	0•22	0•02	2•60	0•21	0•14	n.d.	6•9

n.d. - not determined

* - obtained by "wet" chemical analysis (276b)

Table 34: Composition of clay samples

Percentage composition by weight estimated by English Clays, Lovering, Pochin & Co. Ltd. from XRD patterns

Sample	Kaolinite	Mica	Quartz	Feldspar	Cristobalite	Alunite
WB	-	<1	9	6	-	-
WU	-	<1	7	3	-	-
BL	-	-	<1	-	29	-
CSH	-	-	1	1	5	-
SC	-	-	1	2	-	-
Mi	<1	<1	2	2	-	-
Halloysite*	-	-	1	-	-	7
LiWB	-	-	1	-	1	-
NaWB	-	-	2	-	1	-
LiBL	-	-	-	-	8	-
NaBL	-	-	-	-	15	-
LiBL/LiEDTA	-	-	-	-	18	-
LiCSH	<1	-	<1	-	3	-
NaCSH	-	-	1	-	3	-
LiMi	-	-	-	-	15	-

Remainder assumed to be montmorillonite except *

APPENDIX 4

Calculation of structural formulae of montmorillonites

(from chemical analyses)

Method 1 Method of fixed anionic charges - assumes 22 anionic changes in the form $O_{10}(OH,F)_2$ are present in the unit formula (43, 257, 258)

Method 2 Method of fixed cationic numbers - assumes an ideal dioctahedral smectite i.e. the sum of the octahedral and tetrahedral cations in the formula equals 6.00 (6).

Structural formulae of the montmorillonites were calculated from the chemical analysis results (appendix 3) making allowance for impurity silica in the form of cristobalite or quartz etc. In some cases the amount of impurity silica estimated from XRD seemed too low to give reasonable answers (i.e. tetrahedral Si > 4), possibly because XRD could not "see" amorphous silica (opal) phases.

The minimum amount of silica impurity needed to give tetrahedral Si < 4.00 was calculated iteratively. The structural formulae were calculated using the computer program given below.

The structural formulae calculated correspond to 0.5 x (unit cell).

Computer program for calculation of Structural Formulae of Dioctahedral Smectites

This program calculates the structural formulae by

1) Correcting the input % by weights for silica impurity and then normalising the total to 100%.

2) The percentage of the oxides of the crystal elements (Si, Al, Mg, Fe) are divided by the relative molecular weights of the oxides and multiplied by the number of cations in the oxide molecule (e.g. Al = % Al_2O_3 x 2/101.96). The percentages of the oxides of the exchangeable ions (assumed to be Ca^{2+}, Na^{+} and K^{+}) are divided by the equivalent weight (e.g. Ca^{2+} = % CaO x (2+)/56.08). This gives the atomic proportions.

3) Method 1 - The atomic proportions of the cations are multiplied by their charges (e.g. Si = 4+) and their totals normalised to 22.

4) Method 2 - The total of the atomic proportions of the crystal cations is normalised to 6.00.

5) For each method the actual amounts in the formula are calculated from the normalising factor.

6) All the Si present is assumed to be in the tetrahedral layer. If Si > 4 then the amount of silica impurity is increased by 1% and the calculation is repeated until Si $\leq$ 4.

7) The remainder of the tetrahedral positions are filled by Al. Any additional Al is assigned to the octahedral layer.

8) All the Mg is assigned to the octahedral layer.

9) The number of equivalents of exchangeable cations is calculated and is put equal to the number of isomorphous substitutions (Al^{3+} for Si^{4+} and Mg^{2+} or Fe^{2+} for Al^{3+} and the amount of Fe^{2+} is calculated.

10) From the total amounts of Fe and Fe^{2+} the amount of Fe^{3+} is calculated.

11) The amount of interlayer Ca^{2+} is calculated by dividing its equivalents by 2.

12) The cec (/eq/100g) is calculated by adding the equivalents of the interlayer cations together.

13) The total no. of octahedral cations is calculated. For an ideal dioctahedral smectite or method 2 this equals 2.

14) The total number of cationic changes is calculated and, assuming 10 oxygen atoms, the number of (OH,F) groups is calculated. For a perfect anionic framework or method 1 this equals 2.

Analysis results for TiO_2 have been ignored.

Structural formulae for uncobbed clays have not been calculated since these are contaminated with iron oxides.

Program Listing

Language - CASIO BASIC

(DEFM 3)

```
10      INPUT "SiO2",A,"Al2O3",B,"Fe2O3",C,"CaO",D,"MgO",E,"K2O",F
20      INPUT "Na2O", G,"Li2O",2(1),"SiO2 IMP",H:R=1
```

```
30      I=A-H:M=100/(I+B+C+D+E+F+G+Z(1)):J=I*M/60.08:
        K=B*M/50.98
40      L=C*M/79.845:.N=D*M/28.04: O=E*M/40.3:
        P=F*M/47.1: Q=G*M/30.99
41      Z(2)=Z(1)*M/19.47
45      IF R=2 THEN 60
50      S=22/(4*J+3*K+3*L+2*O+N+P+Q+Z(2)):
           GOTO 65
60      R=2 : S=6/(J+K+L+O)
65      W=S*J
80      IF W ≤ 4 THEN 100
90      H=H+1: GOTO 30
100     T=N*S:U=P*S:V=Q*S:Z(3)=Z(2)*S
105     X=S*O:Y=T+U+V+W-4-X+Z(3)
115     PRINT "METHOD"; R: SET F2
120     PRINT "Tet.Si="; W, "Tet.Al="; 4-W, "Oct.Al=";
        S*K-4+W
130     PRINT "O.Fe3+="; S*L-Y, "O.Fe2+=";Y,"Oct.Mg=";X
140     PRINT "T.Oct.=";X+S*L+S*K-4+W,+I.Ca2+=";T/2
150     PRINT "I.Na+=";V,"Int.K+=";U,"I.Lit=";Z(3)
151     PRINT "cec=";(N+P+Q+Z(2))*IE3
160     Z=W*2+1.5*S*(K+L)+X+(T+U+V+Z(3))/2
170     PRINT "OH,F=";2*(Z-10):SET N
180     PRINT "SiO2 IMP="; H;"%"
190     IF R=1 THEN 60
200     GOTO 10
```

Results - Table 6 and 11

SiO_2 IMP_{XRD} is the amount of impurity silica estimated from XRD (Appendix 3, Table 34).

SiO_2 IMP_{CALC} is the amount of impurity silica to give results shown.

APPENDIX 5

Schiller Layers

It was noticed that two bottles each containing samples of crude coarse material from Na-hard Helms samples showed evidence of irridescent layers after ∿3 months standing. A photograph of one of these samples is shown in fig. 113.

It seems that (by accident) the conditions in the bottles were such that schiller layers (sect. 3.2.3.2) were formed. In view of the impurities present in the hard Helms samples (sect. 5.3.2) it seems likely that the particles present in the schiller layers may be small (diameter <∿1μm) montmorillonite tactoids (sect. 3.2.2) with possibly significant amounts of accessory silica (opal CT) minerals (sect. 2.3.1) and iron oxides (sect. 2.3.2) present.

Schiller layers were also subsequently noticed to have formed in some Bentolite L dispersions.

Fig. 138 : Photograph of hard Helms clay dispersion exhibiting schiller layers

APPENDIX 6

Stopped-flow birefringence

INTRODUCTION

As previously mentioned (sect. 6.1.7), it is possible to induce birefringence in dispersions of asymmetric particles by the application of an electrial field. It is also possible to induce birefringence by the application of a shear field to such a dispersion (19, 296, 326). It is suggested that stopped-flow spectrometry may be used to measure asymmetric particle sizes. Birefringence in the sample is induced by shear flow and upon cessation of flow the decay of birefringence with time may be analysed in a similar manner to the treatment of Jennings et al (281, 280, 327, 328, 329). The short time scale of study possible with stopped-flow spectrometry (~1ms) means that it is not necessary to damp out Brownian motions, using glycerol, as with the technique of Johnson et al (326).

EXPERIMENTAL

The Hi-Tech stopped-flow spectrometry apparatus, as described previously (164), was used. This apparatus was set up such that the light scattered at an angle of 90^{o} from the dispersion in the observation cell passed into the photomultiplier tube detector. The

wavelength of the incident light was set to 515nm with the monochromator, since the photomultiplier was found to be most sensitive to light scattered from dilute LiWB dispersion at this wavelength. The monochromator slit-width was set to, its maximum value of, 5mm, in order to increase sensitivity. The equipment was switched on, as previously described (164), the photomultiplier supply was set to ∿550V and the equipment was allowed to warm up for 2 hours.

The photomultiplier supply was set to (its maximum rating of) 600V and the filter was set to (its maximum value of) 4. Both reagent reservoirs were filled with dilute (∿0•2%w/w) bentonite dispersion in 10^{-3}mol dm^{-3}LiCl solution. The driving syringes were filled with the dispersion which was then passed into the mixing/ observation cell. The (manual) bias was then adjusted such that the horizontal oscilloscope trace was 2cm above the centre of the display. The apparatus was then set up such that the oscilloscope was triggered when the stopping syringe struck the microswitch on the stopping block, and the resulting oscilloscope trace could be photographed.

At all times during filling or washing of the flow system care was taken not to introduce any air bubbles into the cell, while the light source and the photomultiplier were set at their maximum intensity and sensitivity respectively, since under these circumstances the reflection of a significant amount of light, by an air bubble passing through the cell, could result in damage to the photomultiplier tube.

RESULTS

Under the conditions of operation (164) the dispersion experiences a shear rate of $\sim$3,400 s^{-1} while flowing through the mixing/observation cell. This results in the orientation of the montmorillonite particles and the dispersion becomes birefringent. When the flow stops the particles become randomly oriented. As this happens there is a decay in birefringence with time. With this apparatus the change in scattered light intensity with time is monitored.

Fig. 114 shows an oscilloscope trace obtained for a dispersion of LiBentolite L in 10^{-3} mol dm^{-3} LiCl, it shows the decay of scattered light intensity upon cessarion of the flow until a constant value, corresponding to randomly oriented particles, is obtained approximately 50ms later. Use of the equations of Matsomoto et al (331) and Perrin (333) indicates that this "rotary relaxation time" corresponds to a disc diameter of $\sim$2μm assuming an axial ratio of 500 (giving t$\simeq$4nm). These values are of the expected order of magnitude.

DISCUSSION

It has been demonstrated that it is possible to measure the change of scattered light intensity as aligned montmorillonite particles in dispersion become randomly oriented, using a stopped-flow spectrometer. In principle, therefore, it should be possible

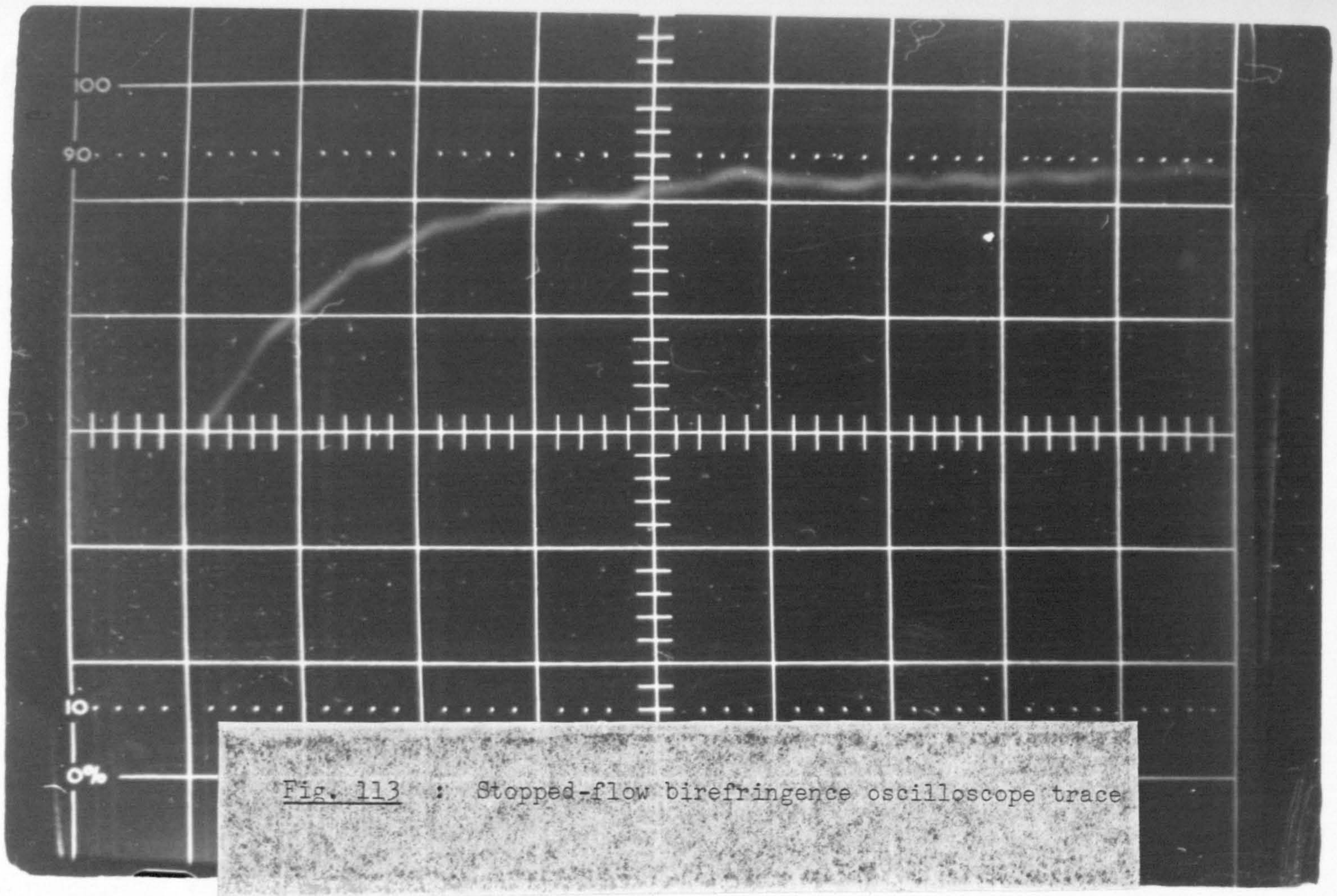

Fig. 113 : Stopped-flow birefringence oscilloscope trace

to modify this apparatus such that the decay of birefringence with time may be measured and hence rotary diffusion coefficients and particle sizes (328, 330, 331, 332, 333) calculated. Initially the effect of volume fraction should be studied, since there may be particle concentration effects, even at low volume fraction (344).

In the application of stopped-flow spectrometry in this way the "dead-time" of the apparatus is irrelevant since upon stopping the flow the "reaction" will (ideally) have proceeded to the same extent at all positions along the observation cell.

APPENDIX 7

X-ray diffraction results

X-ray diffraction (XRD) patterns obtained for heated crude samples of Wyoming Blackhills, Bentolite L and cobbed soft Helms bentonite are shown in figs. 115 - 117 respectively.

XRD patterns obtained for Li Wyoming Blackhills, Li Bentolite L, Li cobbed soft Helms, Na Wyoming Blackhills, Na Bentolite L and Na cobbed soft Helms bentonite are shown in figs. 118 - 123 respectively.

Fig.115: X-Ray diffraction pattern for heated crude Wyoming Blackhills bentonite

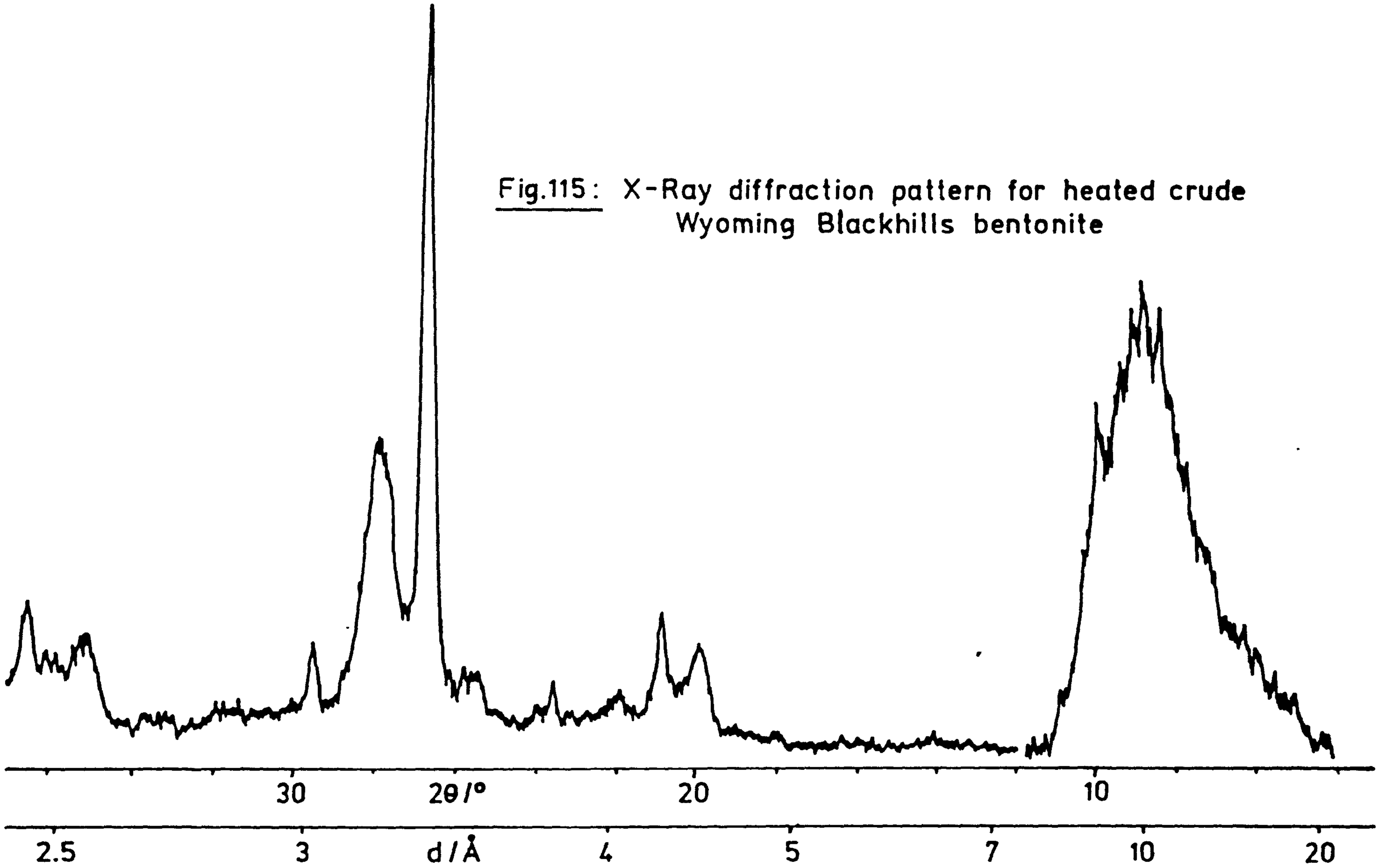

X-Ray diffraction patterns

for heated crude bentonite

samples

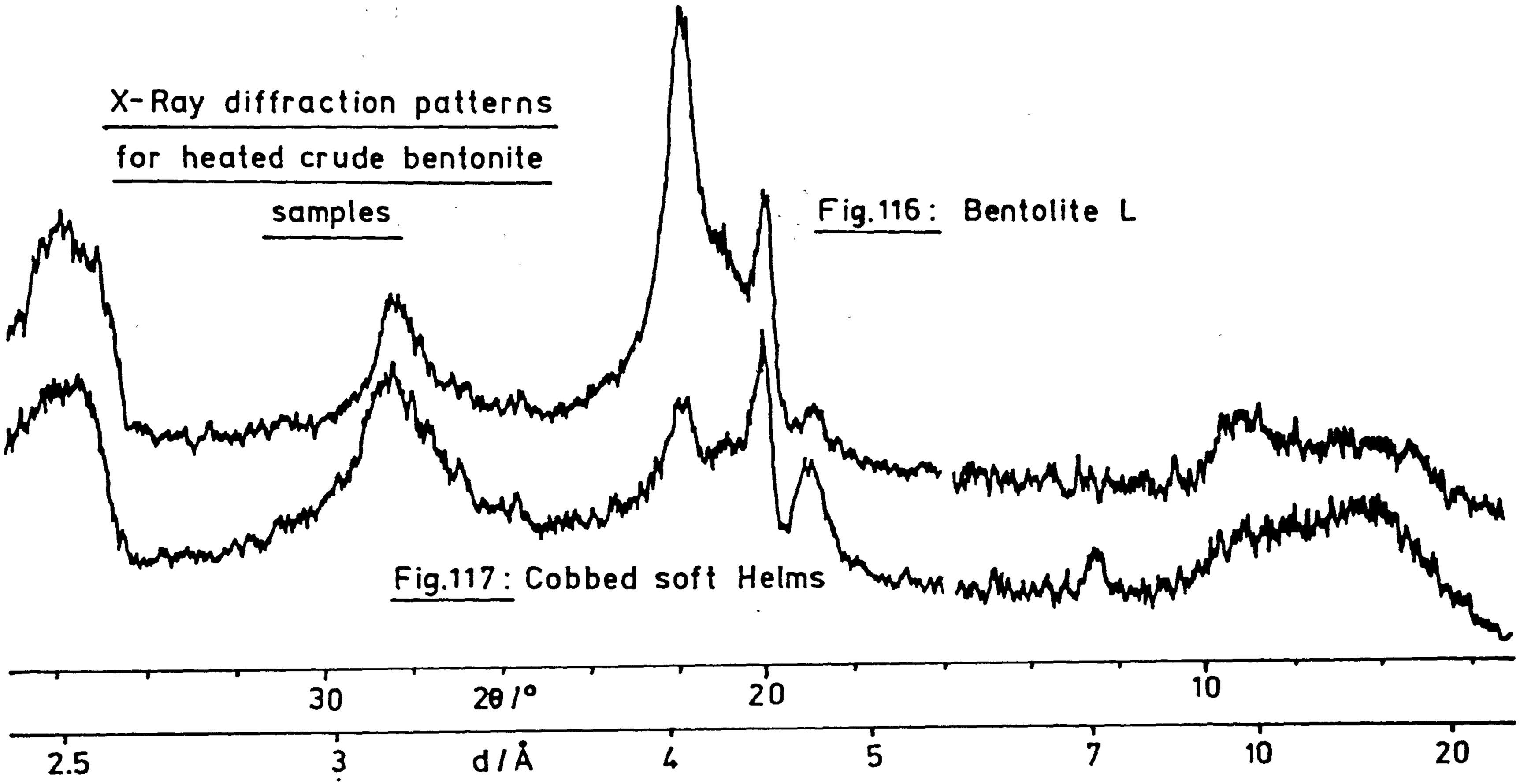

Fig.116: Bentolite L

Fig.117: Cobbed soft Helms

X-Ray diffraction results

fig.118: Li Wyoming Blackhills

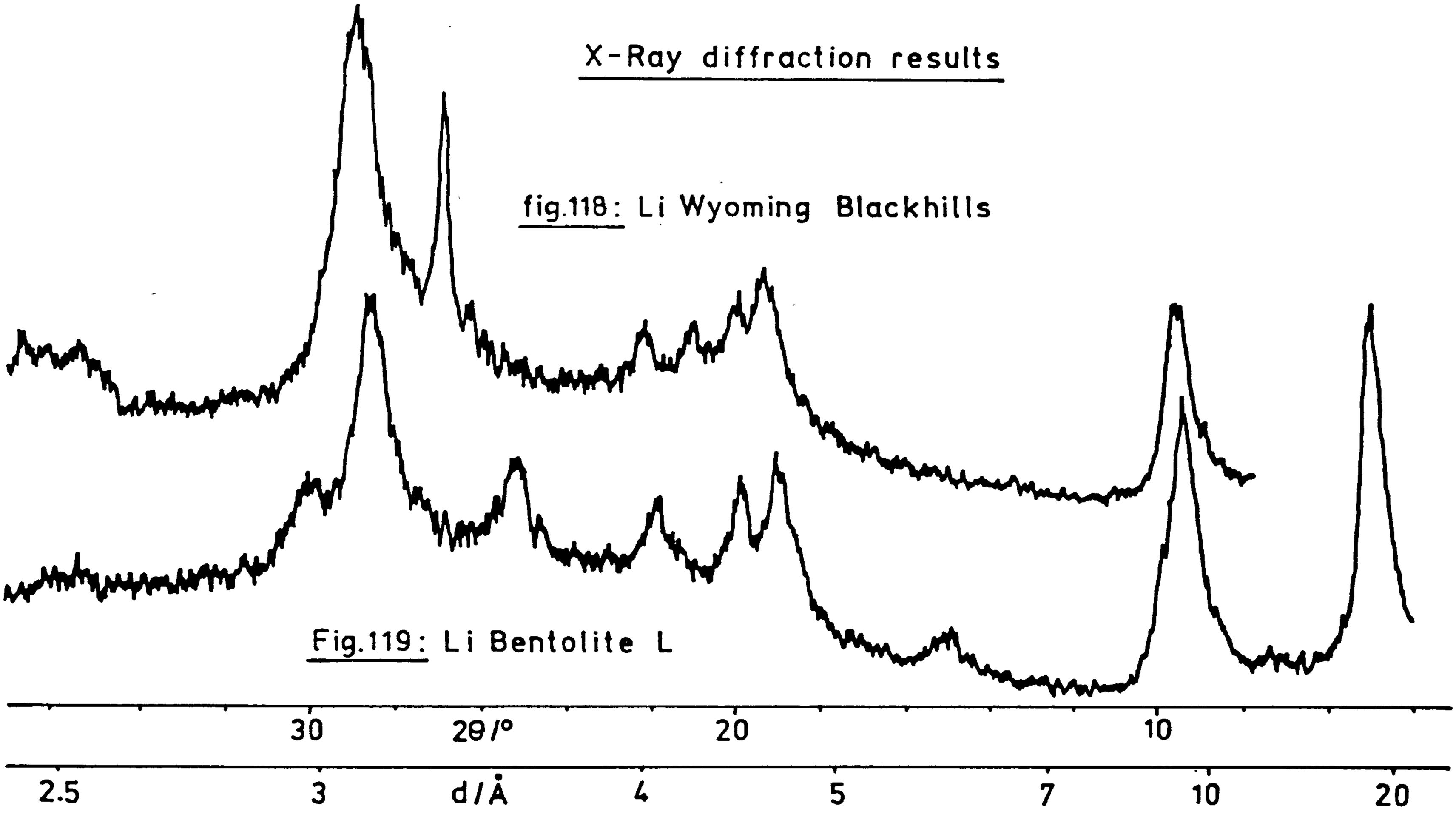

Fig.119: Li Bentolite L

X-Ray diffraction results

Fig.120: Li cobbed soft Helms

Fig.121: Na Wyoming Blackhills

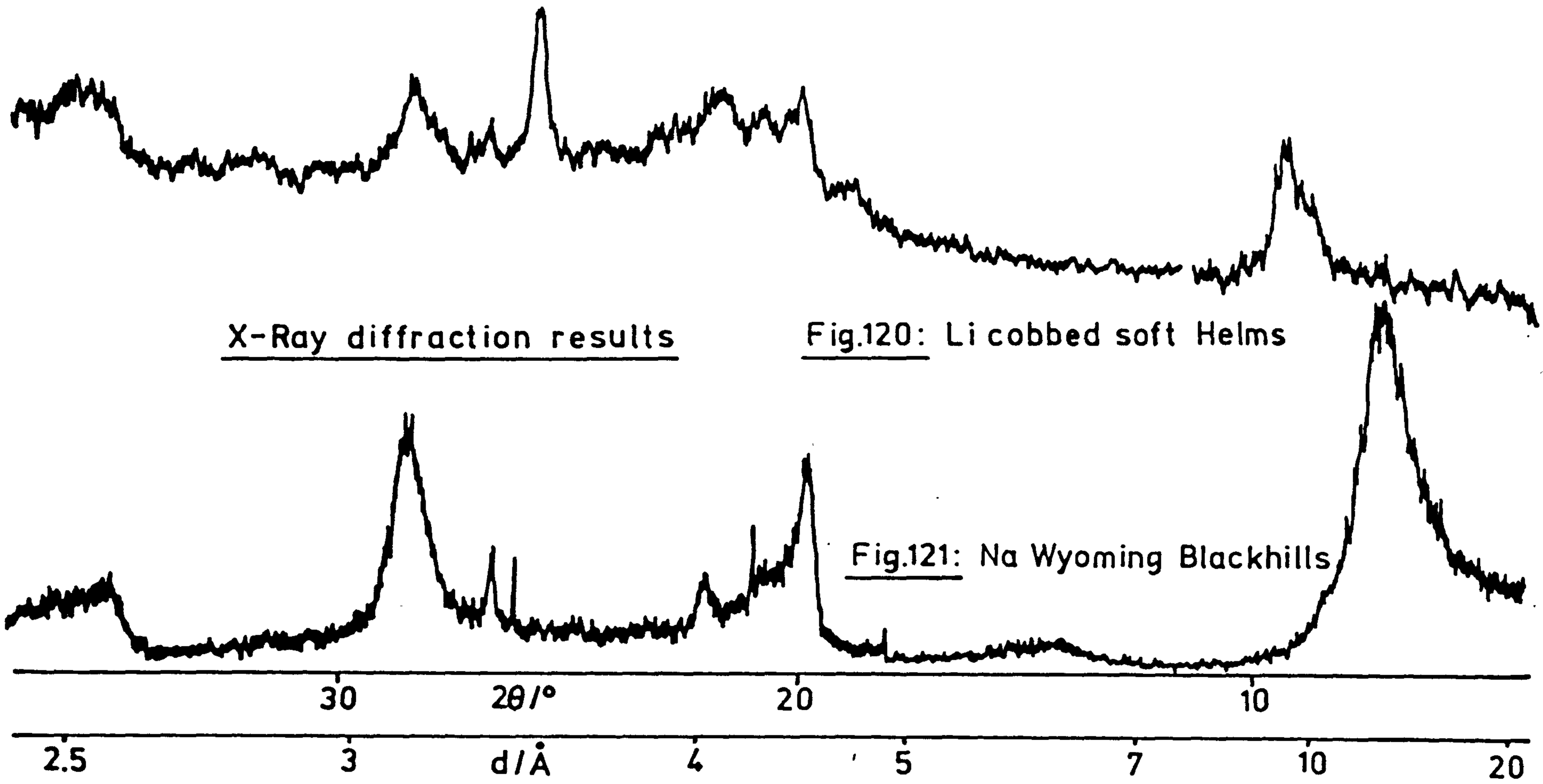

X-Ray diffraction results

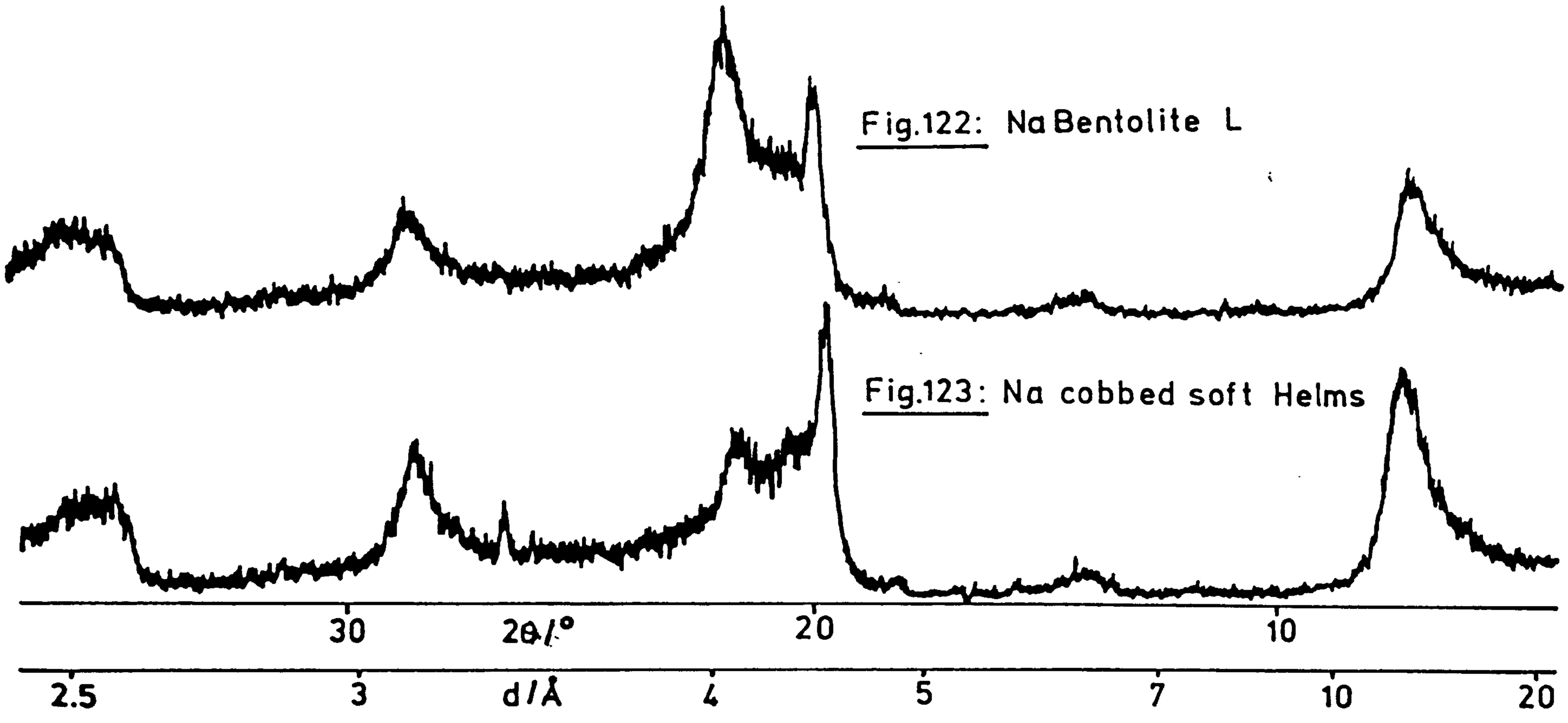

Fig.122: Na Bentolite L

Fig.123: Na cobbed soft Helms

APPENDIX 8

CALIBRATION PLOTS

Calibration plots for the Na^+-selective electrode, Li atomic emmission spectrometry and Ca^{2+}-selective electrode are shown in figs. 125 - 127, respectively.

Fig.125: Sodium electrode calibration plots

o - in water, slope = 56.9 mV

● - in 1 mol dm^{-3} CH_3COONH_4, slope = 56.1 mV
(theoretical slope = 59.16 mV)

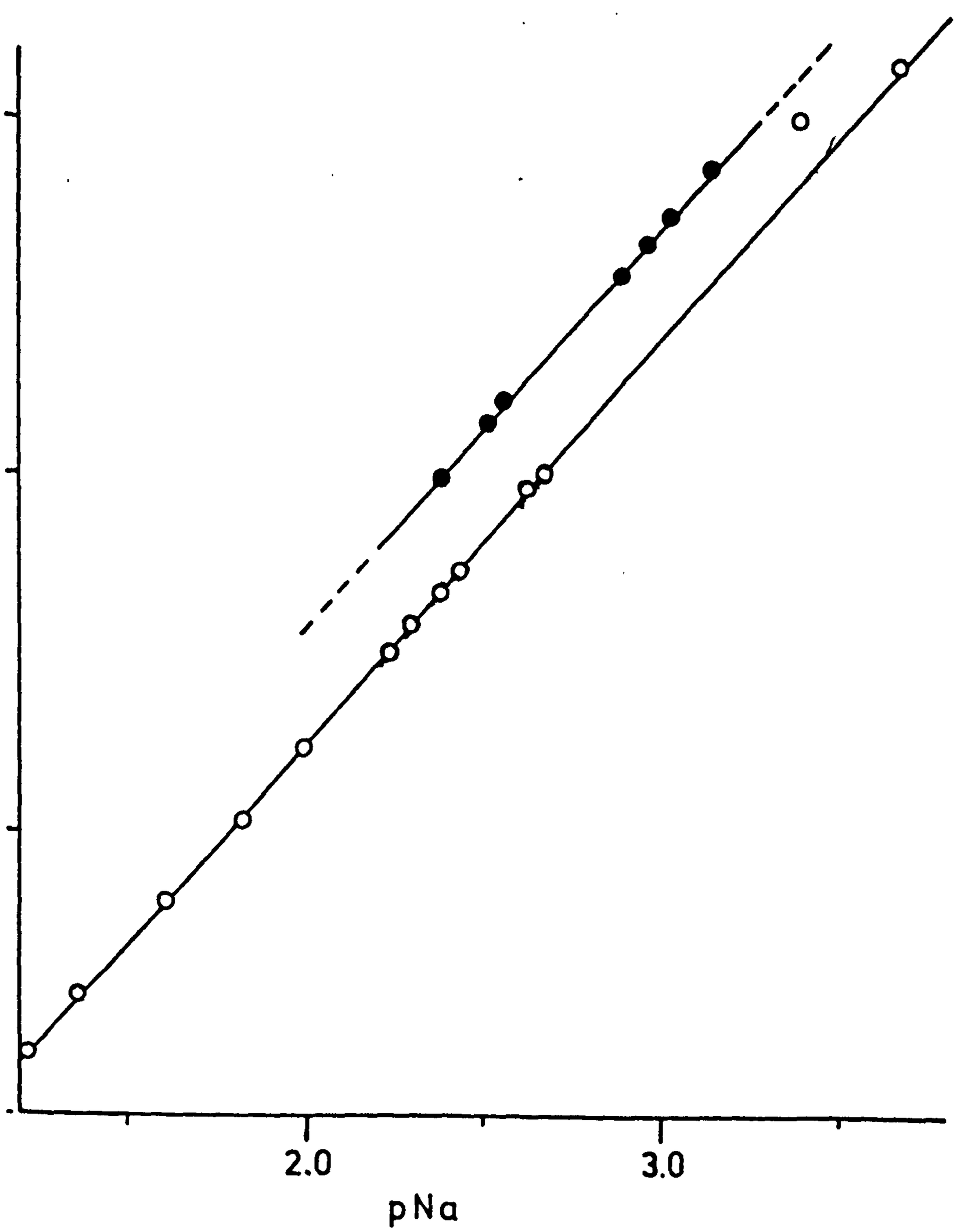

Fig.126: Atomic emmission spectroscopy calibration plot

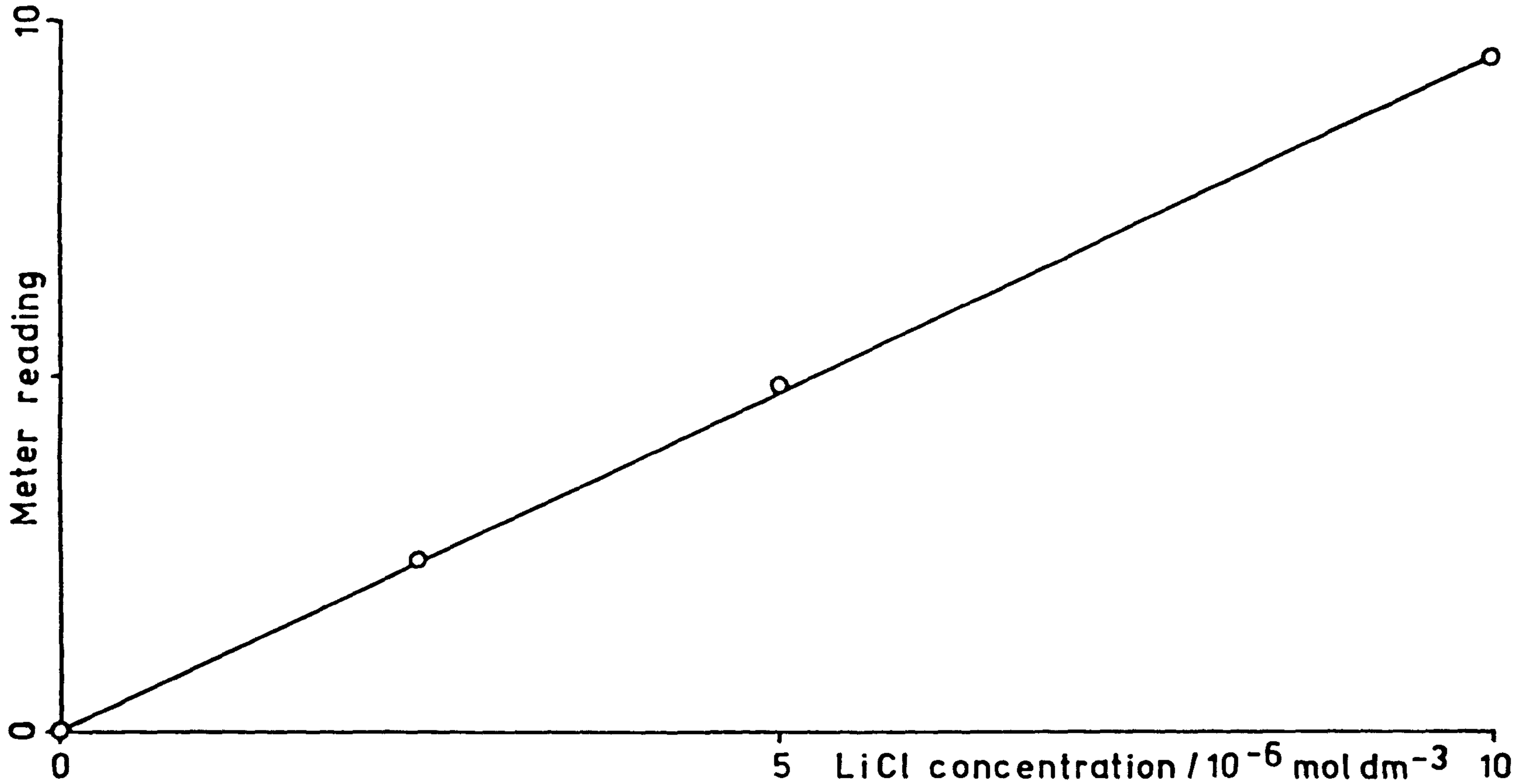

Fig.127: Calcium electrode calibration curve

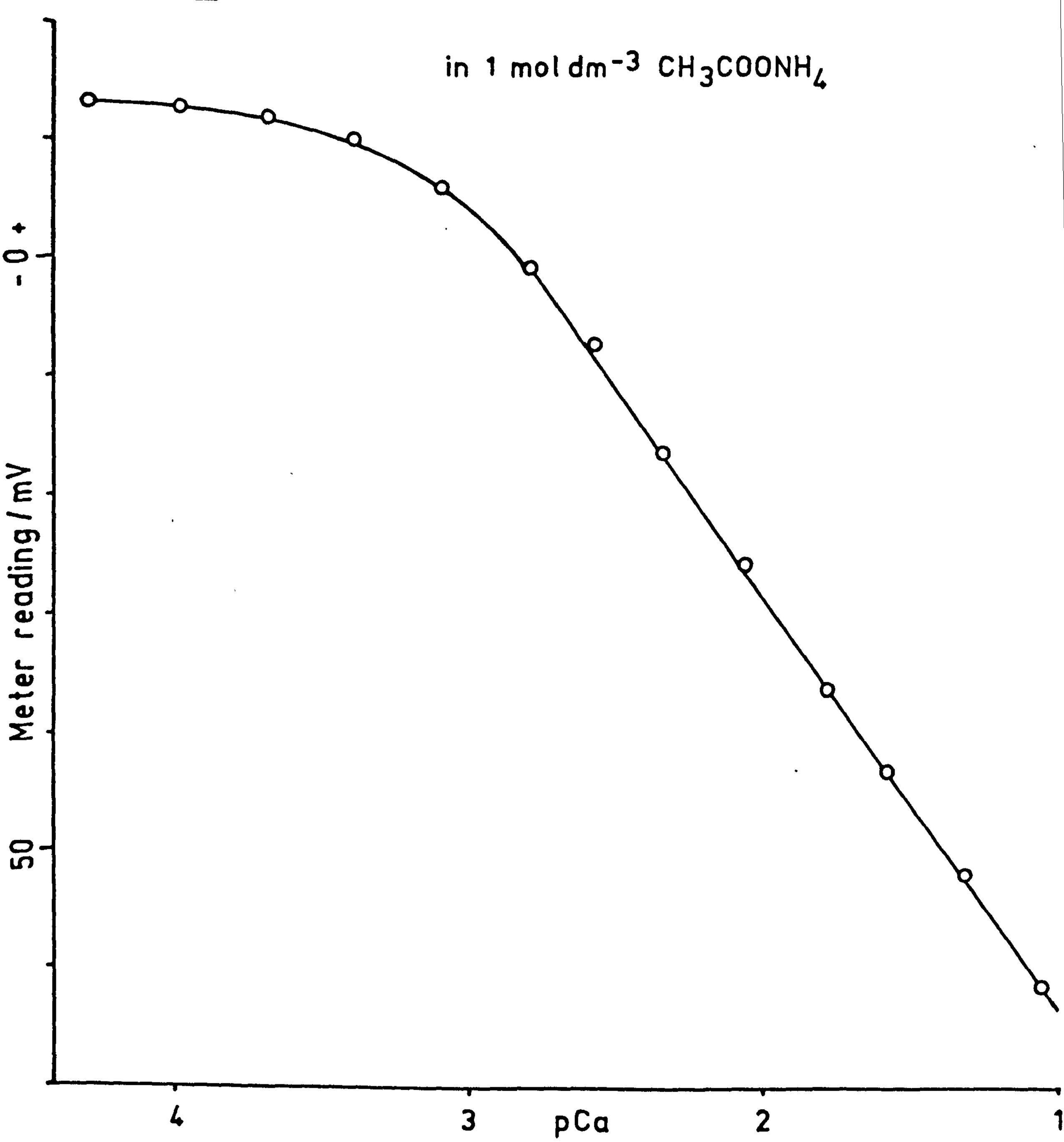

APPENDIX 9

THEORETICAL CALCULATION OF SHEAR MODULI

A9.1 INTRODUCTION

The infinite parallel plate models for the calculation of shear moduli of montmorillonite dispersions, described in chapter 10, have the disadvantage that the interplate separations calculated from equation 56 are probably too large. This seems to be confirmed by X-ray diffraction studies (173, 292). A lower effective interplate separation than that given by equation 56 would give a better quantitative fit of the theoretical model with the experimental data. Such a reduction in Ho may be justified on the basis that in the real montmorillonite dispersion system the individual particles may tend to undergo lateral (edge-edge) swelling (292) and these separate particles may be disordered to some degree (169). Lateral swelling could occur if the edges of the montmorillonite plates carried an effective negative charge, as suggested by Callaghan and Ottewill (192, 196) and Secor and Radke (293).

However, it is not yet known how to obtain the relationship between edge and face separations in a montmorillonite dispersion, although an empirical relationship was obtained by Fukushima (292) for a natural bentonite dispersion. Also, the calculation of the degree of order in the system (sect. A9.3), and the consequent

effects of variations in particle shape and size etc. are difficult.

This appendix describes some relatively simple modifications to the infinite parallel plate models (chapter 10), in an attempt to allow for lateral swelling (A9.2), disorder (A9.3) and attractive interactions (A9.4) in montmorillonite dispersions.

Since the Langmuir and Verwey and Overbeek theories give identical results over the range of experimental results obtained, with the Beresford-Smith and Chan modification (sect. 10.2.5), and since the Langmuir equation (equation 26) cannot be readily integrated to give V_R, the Verwey and Overbeek with Beresford-Smith and Chan theory was used in all the following computations.

A9.2 LATERAL SWELLING (CELL) MODELS

A9.2.1 Introduction

Lateral (edge-edge) swelling of montmorillonite particles in dispersion will result in some ordered lattice arrangement of the plates. It is possible to envisage various three-dimensional arrangements of the particles in a structured dispersion, and the results of such cell models may be used in the calculation of shear moduli (324, 325). However, in structured montmorillonite dispersions (unlike stable monodisperse polystyrene lattices in hexagonal or cubic close-packed arrays (324, 325)) the particle shape(s) and their lattice arrangement are not easily determined. It is possible to calculate results for various particle shapes

(e.g. square, triangular, rectangular, hexagonal, circular or ellipsoidal plates) in a variety of cell arrangements (e.g. simple cubic, body centred cubic, face centred cubic, simple tetragonal, body centred tetragonal or hexagonal unit cells).

The simplest shapes that may be considered to represent montmorillonite particles are the square plate and disc. Close-packing of these shaped particles may be achieved using simple or body centred tetragonal and hexagonal or triclinic cell models respectively. With all of these models some relationship between the edge and face separation of the particles needs to be assumed. This is discussed in sect. A9.2.2. With the body centred tetragonal square plates and triclinic discs models the mode of addition of the interactions of the particles at the first and second co-ordination planes needs to be considered. This is discussed in sect. A9.2.4. The effects of particle shape and size are discussed in sect. A9.2.3.

A9.2.2 Simple tetragonal model

A simple tetragonal unit cell of parallel square plates is shown in fig. 128a. For plates of side length d, thickness/nm t, having an edge separation H_e and a face separation H_f, the volume fraction of montmorillonite is given by

$$\phi = \frac{nd^2}{(d+H_e)^2(H_f+t)} \qquad (65)$$

Fig.128: Unit cell structures

Square plate models

elevation

plan

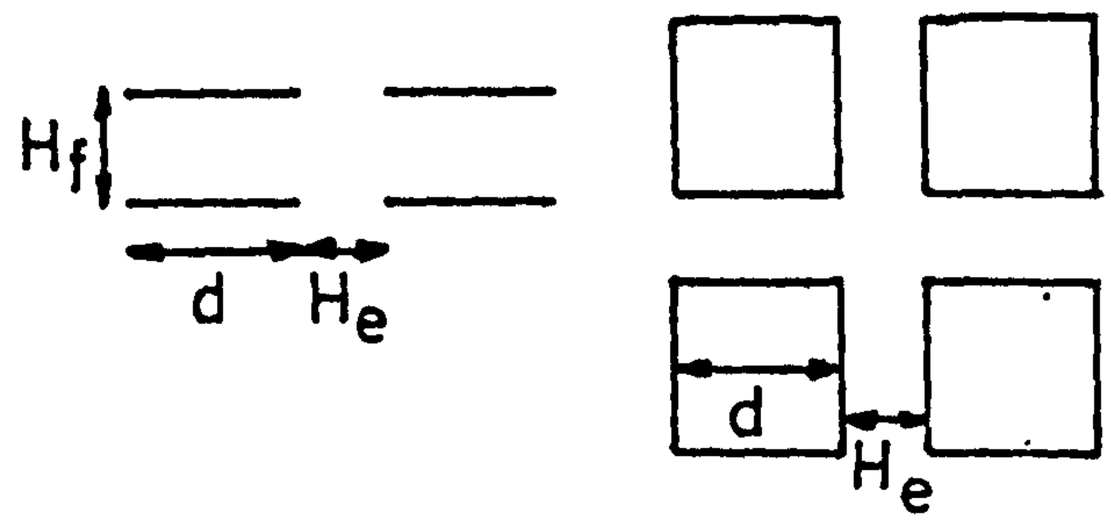

a: Simple tetragonal

b: Body centred tetragonal

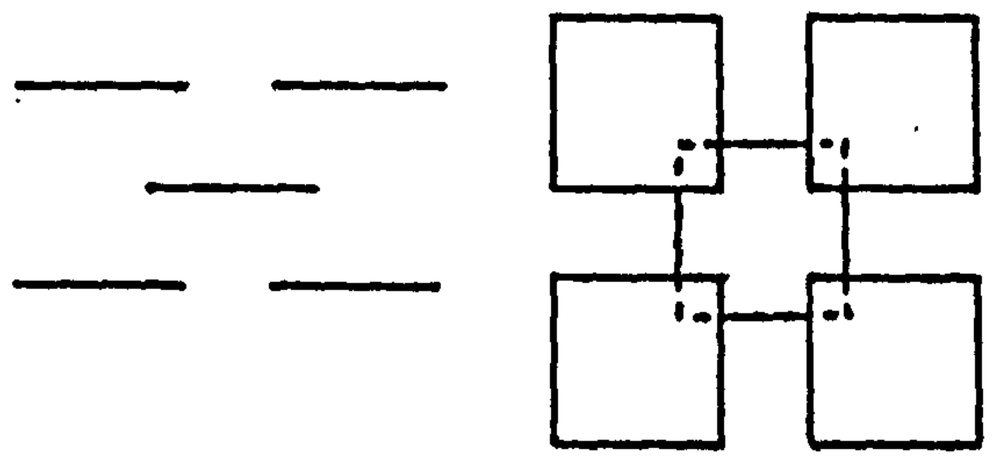

Disc models

c: Body centred tetragonal

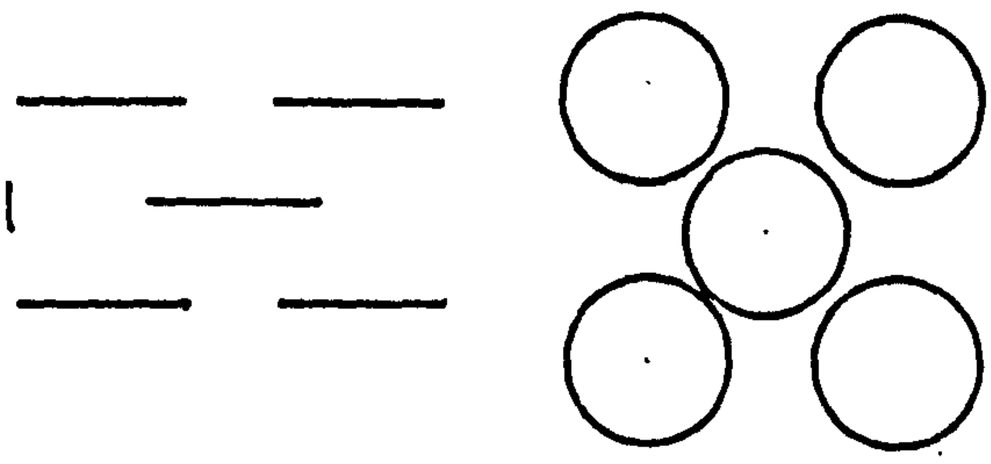

d: Hexagonal

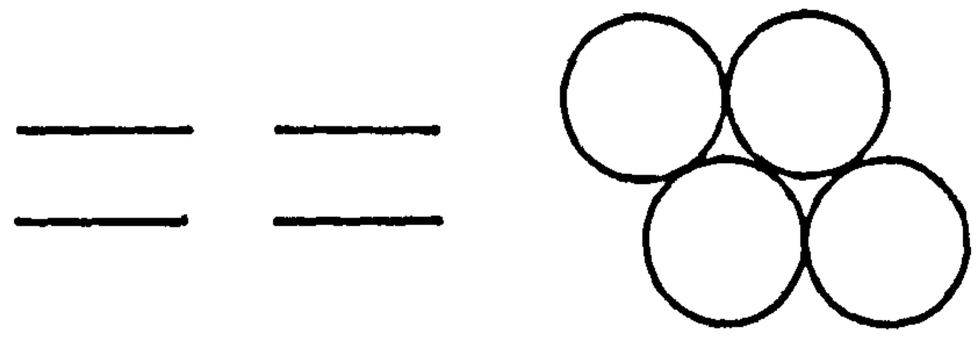

e: Triclinic

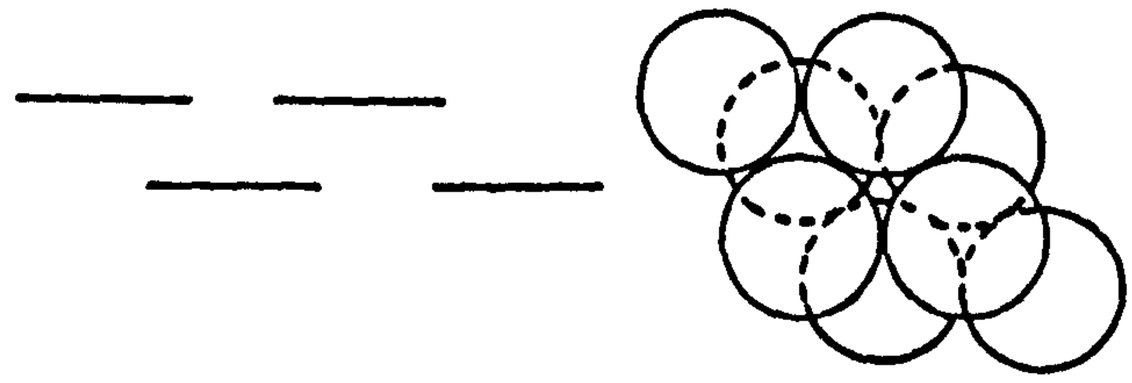

where n is the number of unit (1nm thick) 2:1 layers of montmorillonite per tactoid.

Therefore,

$$H_f = \frac{nd^2}{\phi(d+H_e)^2} - t\ nm \qquad (66)$$

In order to solve equation 66 for H_f the relationship between H_f and H_e needs to be known. Unfortunately, the form of this relationship is difficult to obtain since it would be expected to depend strongly on the form of the potential distribution at the edges of the particles (293). However, an approximation may be made if it is assumed that both the edge and face interactions are given by equation 29. Hence, if it is assumed that the system becomes arranged such that the edge-edge interaction energies are equal to the face-face interaction energies, then (from equation 29)

$$\gamma^2_e \exp(-\kappa' H_e) = \gamma^2_f \exp(-\kappa' H_f) \qquad (67)$$

where γ_e and γ_f are fractions of the edge and face Stern potentials, ψ_e and ψ_δ, respectively, as given by equations 13 and 14.

Therefore,

$$H_f - \Gamma = H_e \qquad (68)$$

where $$\Gamma = \frac{2\ln}{\kappa'}(\gamma_f/\gamma_e) \qquad (69)$$

The relationship between ψ_δ and ψ_e is complicated (293) although if values of 0•1 and 0•04 V respectively are assumed then (see table 35)

$$\Gamma = \frac{1\cdot41}{\kappa'} \qquad (70)$$

Table 35: Effect of chages in ψ_δ and ψ_e upon Γ

ψ_δ/V	ψ_e/V	$\Gamma\kappa'$
0•1	0•04	1•41
0•1	0•05	1•02
0•08	0•04	1•13
0•04	0•02	1•31

Equation 66 now becomes

$$H_f = \frac{nd^2}{(H_f-\Gamma+d)^2\phi} - t\,nm \qquad (71)$$

This equation may be solved iteratively for H_f using the Newton-Raphson method (294). Calculated values of shear modulus obtained using a range of Γ values, given in table 36, suggest that B is relatively insensitive to variations in Γ, over a range of c_e and ψ_δ values. A value of $\Gamma = 1\cdot41/\kappa'$ will be assumed in all the following calculations. Fig. 129 shows some results calculated using the simple tetragonal square plate model.

Table 36: Effect of changes in Γ on B

v=1, w/w = 5%, n = 1, d = 0·5μm, simple tetragonal square plates model

c_e/mol dm^{-3}	ψ_δ/V	Γκ′	log(B/Nm^{-2})
10^{-4}	0·1	1·41	3·35
10^{-4}	0·1	1·02	3·37
10^{-4}	0·08	1·41	3·32
10^{-4}	0·08	1·13	3·34
10^{-4}	0·04	1·41	2·90
10^{-4}	0·04	1·31	2·90
10^{-3}	0·1	3·00	1·65
10^{-3}	0·1	1·41	1·72
10^{-3}	0·1	1·02	1·74
10^{-3}	0·1	0·50	1·77
10^{-2}	0·1	1·41	-3·44
10^{-2}	0·1	1·02	-3·42

A9.2.3 Hexagonal Model

A hexagonal unit cell of parallel discs is shown in fig. 128d. For discs of diamter d, thickness/nm t, having a minimum edge separation H_e and a face separation H_f, the volume fraction ϕ of montmorillonite is given by

$$\phi = \frac{n\pi d^2}{4(d+H_f-\Gamma)^2\phi\cos(\pi/6)} - t \qquad (72)$$

Fig.129: Theoretical results

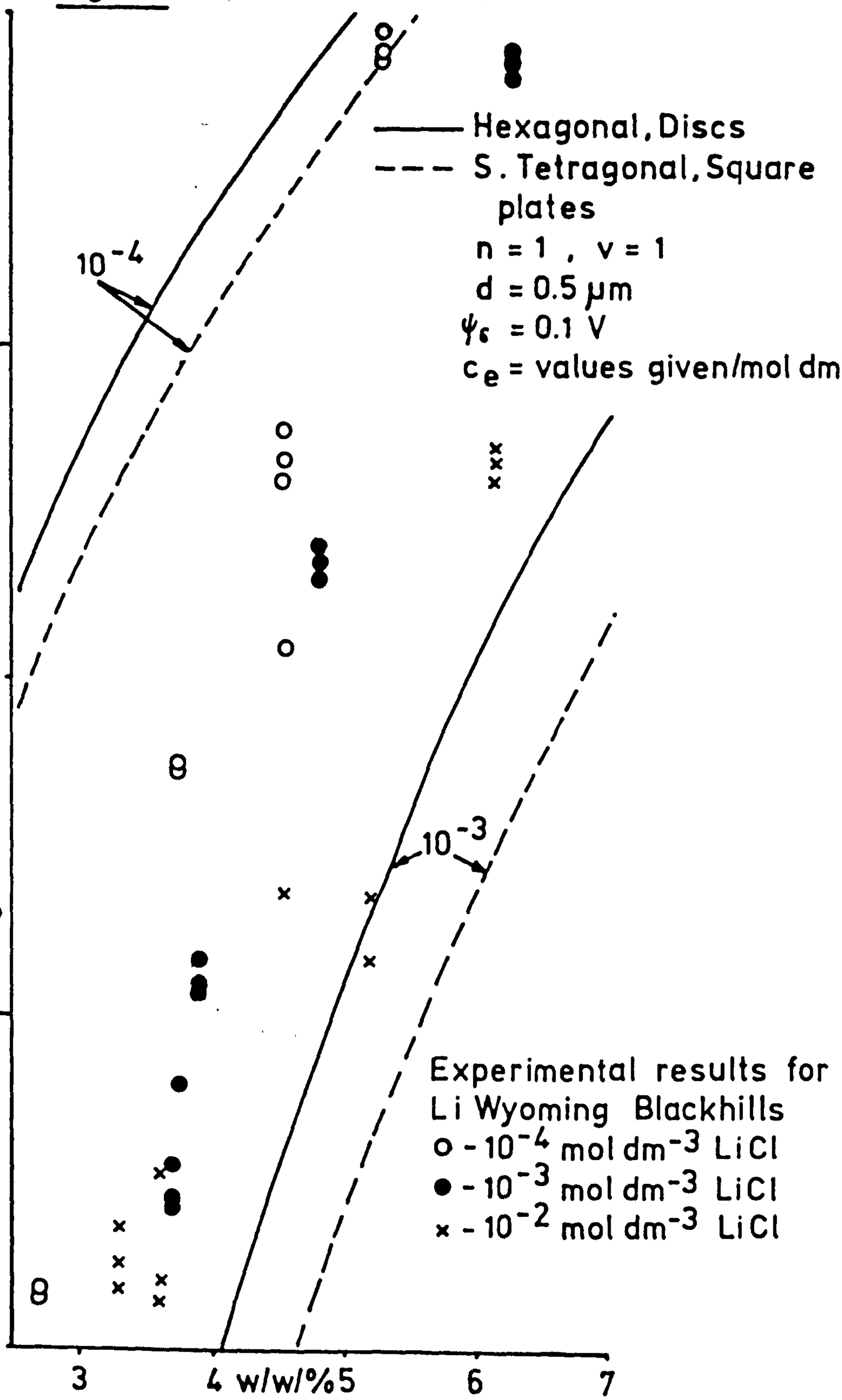

Hence

$$H_f = \frac{n\pi d^2}{4(d+H_f-\Gamma)^2\phi\cos(\pi/6)} \quad -t \qquad (73)$$

which may be solved iteratively for H_f, as with equation 71, and B then calculated. Results for the hexagonal discs model are given in fig. 129. Fig. 129 indicates that the change in particle shape from squares to discs has very little effect on the trend of the results and relatively small quantitative effect. This seems to suggest that in the modelling of polygonal (S- or H-type) montmorillonite particles, the packing geometry of the particles may be of more importance than their actual shape. (Equation 73 differs from equation 71 by the factor $\pi/4\cos(\pi/6)$ ($\simeq$0•907) which is the maximum packing fraction of discs in 2 dimensions). The relationship between particle symmetry and packing behaviour is complex, with 2-dimensional packing fractions of up to 1•0 being possible with some highly asymmetric shapes (295).

Table 37 shows that as particle diameter d is reduced, the theoretical bulk modulus B is increased. This increase in B becomes more marked as d is reduced. This trend of increasing dispersion structure upon decreasing particle size, has been noted experimentally (219, 234), and may be explained by the increase in particle number concentration giving a greater degree of inter-particle interaction.

Table 37: Effect of changes in d on B

Hexagonal discs model, v = 1, n = 1, w/w = 5%, ψ_δ = 0·1V

c_e/mol dm^{-3}	d/μm	log(B/Nm^{-2})
10^{-4}	1·0	3·38
10^{-4}	0·5	3·50
10^{-4}	0·2	3·82
10^{-3}	2·0	1·58
10^{-3}	1·0	1·75
10^{-3}	0·5	2·07
10^{-3}	0·2	2·87
10^{-3}	0·1	3·80
10^{-2}	1·0	-3·40
10^{-2}	0·5	-2·59

A9.2.4 Triclinic model

If the hexagonal unit cell structure is distorted such that the discs become arranged in a body-centred type array, a triclinic cell (fig. 127e) is formed. For the triclinic structure

$$\phi = \frac{n\pi d^2}{4(H_f+t)(d+H_e)^2\cos(\pi/6} \qquad (72)$$

i.e. identical to the hexagonal model (sect. A9.2.3). However (for H_e<d) the co-ordination arrangement results in each disc being "exposed" to two other discs at different separations having

different degrees of overlap.

Overlap of plates in different "co-ordination planes" (c.f. co-ordination shells for ordered dispersions of spherical particles (200)) in a triclinic (or body centred tetragonal) structure may alter the interactions between them. The means of addition of interactions in this situation is not obvious and several procedures may be used. One such approach will now be described.

If it is assumed that the amount of interaction (or B) is proportional to the degree of overlap of plates (i.e. generalized Maxwell body assumption for solids (225)) and interaction only occurs between exposed areas of plates (as suggested in fig. 130a), then

$$B = B_1 A_1 + B_2 (1-A_1) \qquad (74)$$

where B_1 and B_2 are the bulk moduli for plates at the 1st and 2nd co-ordination planes, respectively and A_1 is the relative area of at the first co-ordination plane. If H_1 and H_2 are the separation of plates at the first and second co-ordination planes respectively, then

$$H_1 = H_f \qquad (75)$$

$$H_2 = 2H_f+t \qquad (76)$$

where H_f is given by equation 73. Hence B_1 and B_2 may be calculated for H_1 and H_2, respectively using equations 60 and 62 and then B

Fig.130a: Maxwell body model for interaction between exposed areas of plate

Schematic diagram

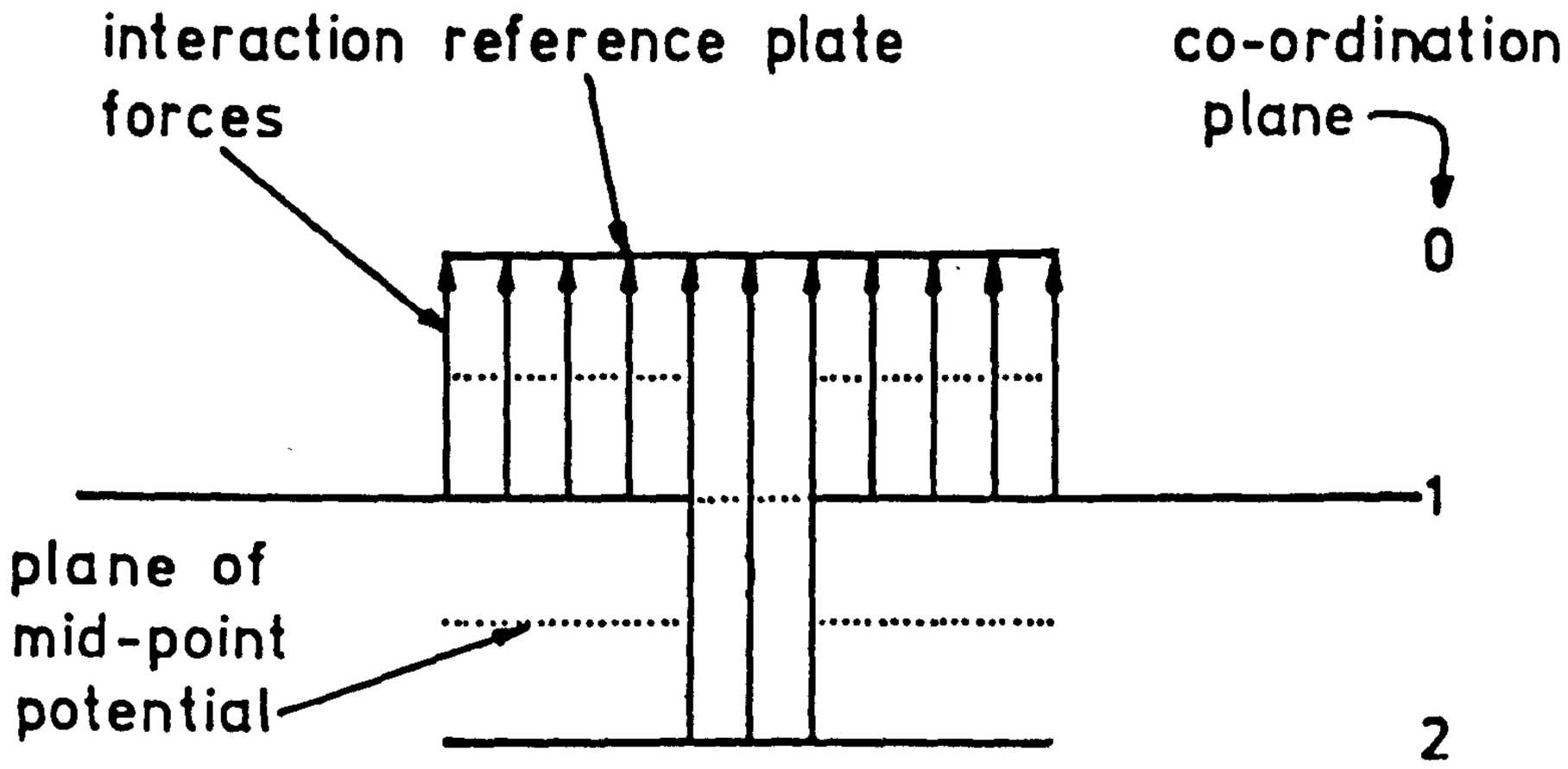

Fig.130b: Possible edge effect

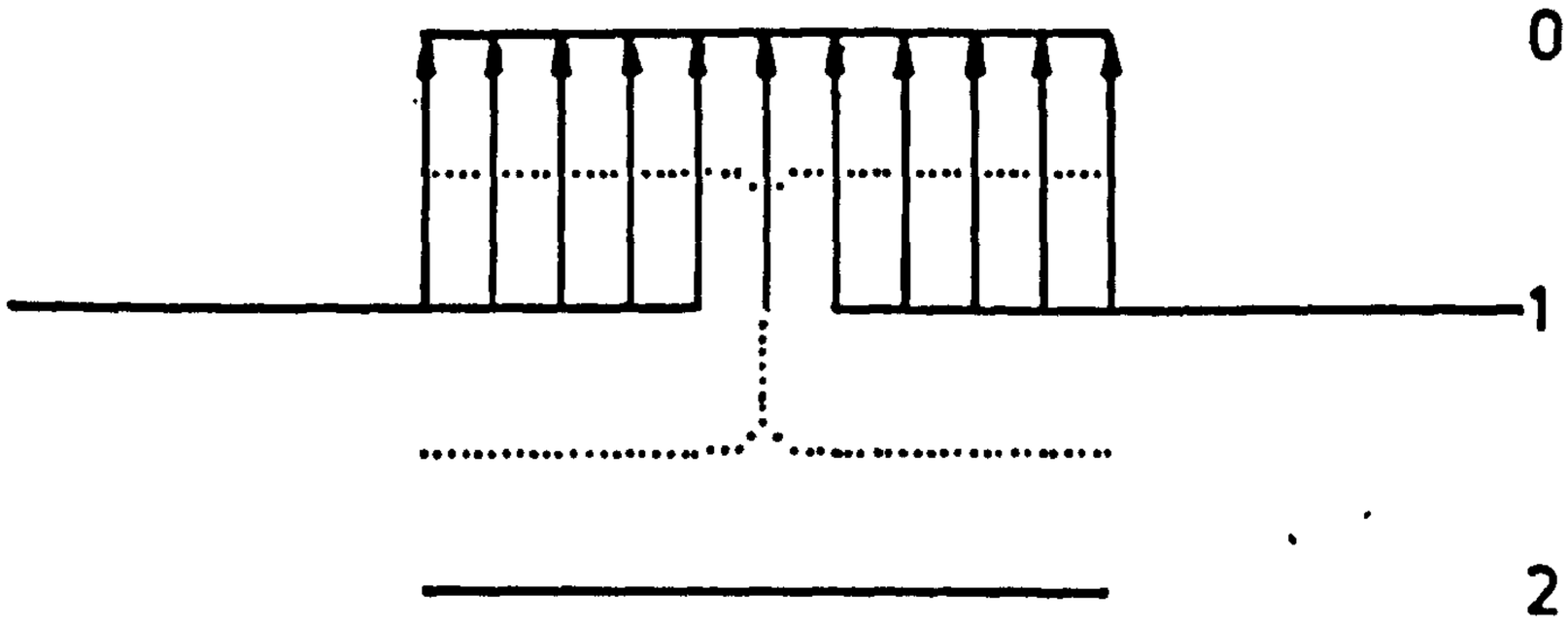

obtained from equation 74. For the triclinic unit cell of discs A_1 may be obtained from equation 77.

$$A_1 = \frac{2}{\pi} \cos^{-1}\left[\frac{(d+H_e)}{2d\cos(\pi/6)}\right] \qquad (77)$$

Results calculated for this model are given in fig. 131. There are only small quantitative differences between these results and those calculated for the hexagonal discs model (fig. 129), however.

A9.2.5 Discussion

Difficulties are involved in the estimation of possible effects due to "hidden" areas of plate, i.e. all areas not indicated to interact in fig. 130a, and edge electric double layer effects, as suggested in fig. 130b. The shape of the iso-potential distribution of spaces in the first co-ordination plane could be calculated by extending the mathematical treatment of Secor and Radke (293) to an ordered, concentrated dispersion system. Although it seems reasonable to suggest that the shape of the mid-point potential contour would have a form similar to that of the dotted line given in fig. 130b, i.e. it would more nearly approximate to that for infinite parallel plates than that given in fig. 130a. In this case the simple tetragonal (sect. A9.2.2) or the hexagonal (sect. A.9.2.3) models may be more valid than the triclinic model (sect. A.9.2.4) discussed.

The results described in this section (A9.2) suggest that the cell model chosen is relatively unimportant, with variations in particle shape or arrangement giving small quantitative variation in the results, the general trends being similar.

The cell models indicate (table 37, fig. 131) that a reduction in particle size brings about an increase in B. This may be explained by an increase in particle number concentration bringing about an increased interaction energy via a reduction in mean interparticle separation.

A9.3 DISORDERED MODELS

A9.3.1 Introduction

All of the cell models described (sect. A9.2) assume that the montmorillonite particles are monodisperse, have identical shape to each other and are arranged in a well-ordered lattice. None of these requirements are likely to be met by natural montmorillonite dispersions, which would be expected to exhibit some degree of disorder or heterogeneity.

Causes of disorder in montmorillonite, possible reasons for failure of the cell models described previously, are given below

a) Changes in "effective shape" of particles - while square plate particles may be able to pack very well, the "effective shape" of the electric double layer around such a particle would be expected to be different

Fig.131: Theoretical results for Triclinic, Discs

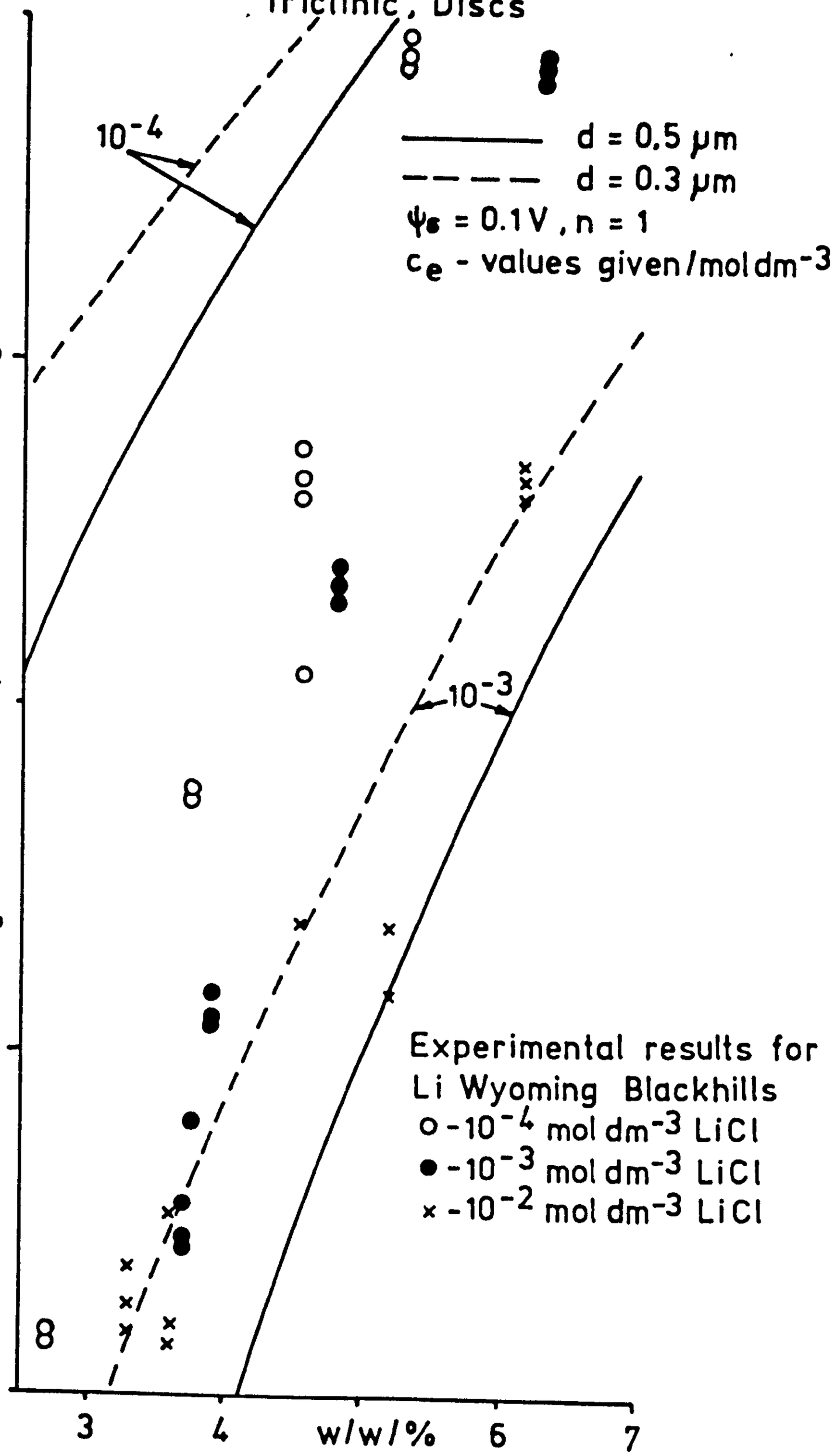

to that of the actual particle, i.e. an ellipsoid-type shape (293), and hence the packing behaviour may be quite different.

b) Differing shape of individual montmorillonite particles.

c) Polydispersity of montmorillonite particles.

d) Entropy effects in dispersion (section 3.2.3).

e) Associated minerals - all the above effects may be modified by the presence of minerals other than montmorillonite in the dispersion.

Although the structure of a concentrated montmorillonite system is complicated, the various examples of disorder in such systems may be classified (203) as

i) voids

ii) edge-face stacking

iii) regions of gross particle folding

iv) ordered domains, and

v) regions of non-parallel stacking.

Fig. 132 shows schematically how the different types of disorder alter the particle separations and orientations from that of the ordered system (cell model)(fig. 132a). The theoretical treatment of a disordered system, such as disordered crystals (299, 301), is difficult, involving the use of statistical mechanics. The situation for a disordered montmorillonite dispersion is likely to be even more complicated than that for crystals because of the effects of variations in particle size and shape, as well as thermal motion, on disorder.

As mentioned previously (sect. 3.2.3), the degree of order in a montmorillonite dispersion is dependent upon the volume fraction ϕ

Fig.132: Disorder in plate systems

Schematic

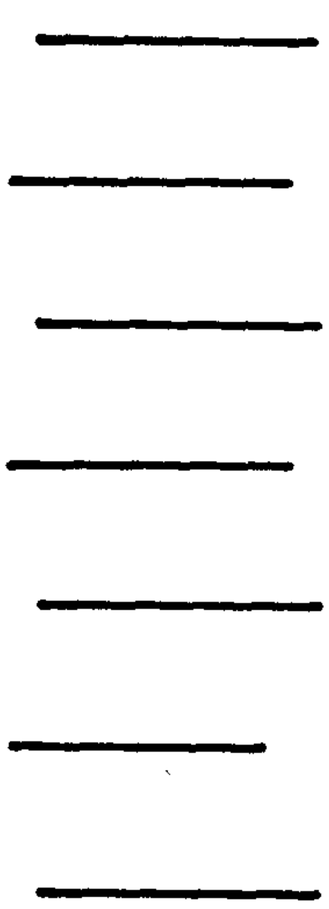

a: ordered domains

b: voids

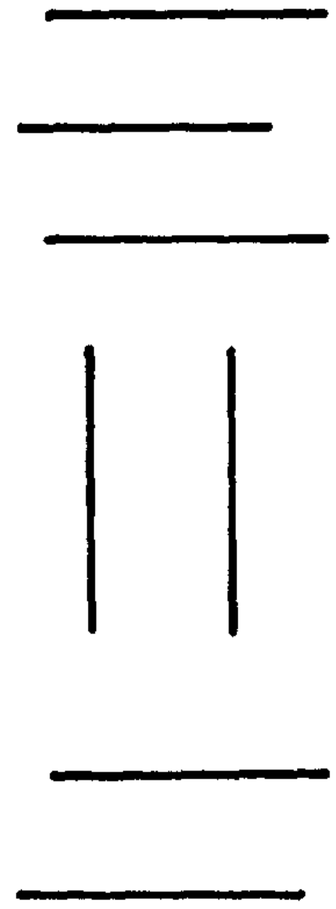

c: edge-face stacking

d: particle folding

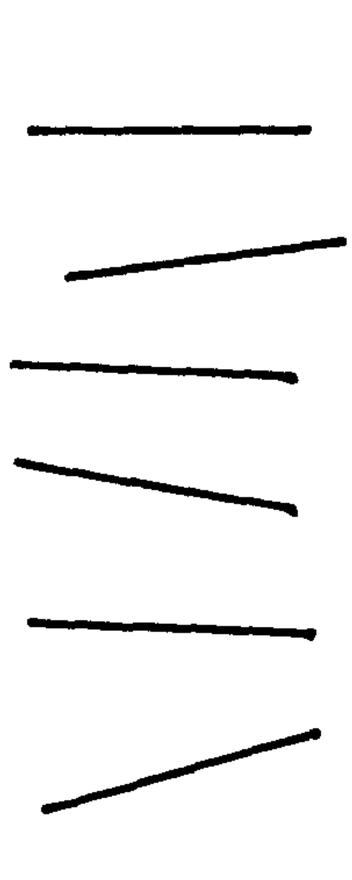

e: non-parallel stacking

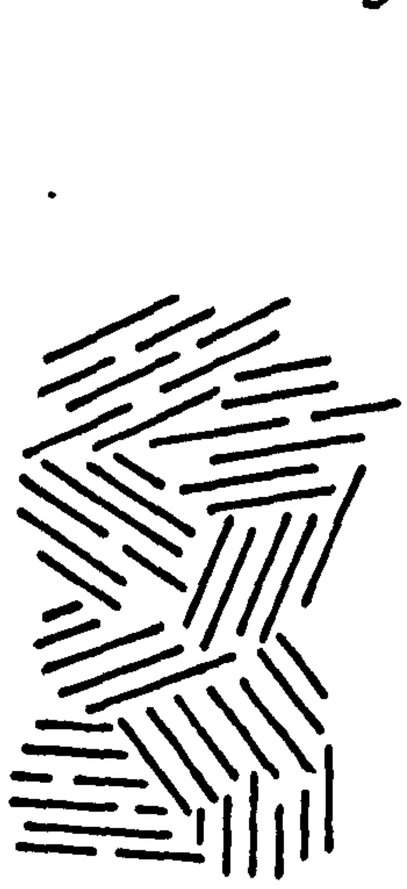

f: random orientation of ordered domains

of clay present. At low ϕ montmorillonite dispersions are isotropic, with the particles having random orientations (169). As ϕ is increased, a point is reached (Onsager transition)(208) where ordered domains are formed (169) as a separate phase within the disordered phase. As ϕ is increased still further, the ordered domains grow to fill the available volume and the dispersion becomes structured. The structure of such concentrated dispersions would be expected to consist of randomly oriented ordered domains of aligned particles separated by, disordered, grain boundaries. The degree of order in such systems may be altered experimentally by the application of shear (169) or electrical (280, 281, 297, 298, 300) fields, or by temperature changes. Such changes in the ordering of these sytems would be expected to alter the rheological properties by changing the size and/or degree of orientation of the ordered domains. The importance of such changes in the degree of ordering of montmorillonite dispersions is demonstrated by the differences between the first (disordered) and subsequent (ordered) compression curves (145).

As already mentioned, the theoretical treatment of disordered systems is considerably more difficult than that for ordered systems, although by the use of various approximations, qualitative effects of disorder may be estimated.

One possible approach would be to model the system as a concentrated emulsion (or foam) in which the disperse phase of the emulsion acts as the ordered montmorillonite domains and the dispersion medium as the grain boundaries. This approach would seem to indicate that the shear modulus increases as the size of the ordered domains

decreases (302), as expected (from compression studies (145). There are, however, theoretical difficulties with this approach, e.g. calculation of ordered domain sizes. The emulsion model will not be discussed further here.

Since thermal motion of particles is a prime cause of disorder*, it may be useful to consider the consequences of the thermal motion (Brownian motion) of montmorillonite particles on the dispersion structure. Such motions may have a significant effect on the particle interactions in colloidal systems (312). If the montmorillonite particles in an ideal (close-packed) lattice structure (at OK*) are allowed to undergo Brownian motion then the system will tend to become disordered.

Montmorillonite particles may undergo translational, rotational and vibrational motions. These motions will result in diffusion of the particles until potential energy barriers (e.g. those due to electric double layer repulsions) larger than the particle energies are encountered. If the distance over which particles diffuse, before encountering a significant potential energy barrier is relatively small then they would tend to remain "fixed" in the ordered lattice structure, having restricted thermal motion. If, however, particles can diffuse relatively long distances between encounters then, as the particles

---

* An ideal system at a temperature of OK (absolute zero) has zero entropy (299, 303, 304). This is unlikely to occur for a montmorillonite dispersion because disorder, due to variations in particle size and shape, would remain "frozen-in". Such disorder may be termed "static disorder", with that due to thermal motion being referred to as "dynamic disorder (299).

have a greater freedom to move with respect to each other, the system will tend to become disordered. Such processes would continue until equilibrium was reached when the rate of disruption of order by thermal motions equalled the rate of formation of ordered domains, such that the overall entropy of the system was maximum (sect. 3.2.3).

If the manner in which the separation and orientation of the particles change upon disordering the system can be estimated, by consideration of the thermal motions of the colloidal particles, then this can be introduced into the model.

A9.3.2 Effects of thermal motion

Montmorillonite particles in dispersion may undergo random thermal translational, rotational and vibrational motions (fig. 133). The effects of such motions will now be discussed.

A9.3.2.1 Translational motions

Montmorillonite particles in dispersion may undergo random translational motion in any direction. If such motions are considered with reference to the initial position of a particle, then they may be resolved into motions along the three, mutually perpendicular, a, b and c axes, as shown in fig. 133. The average translational kinetic energy along a given axis is $\frac{1}{2}kT$ per particle (296, 304). If the particles arranged in an ordered lattice

Fig.133: Thermal motions of disc-shaped particles

a: Translational motion

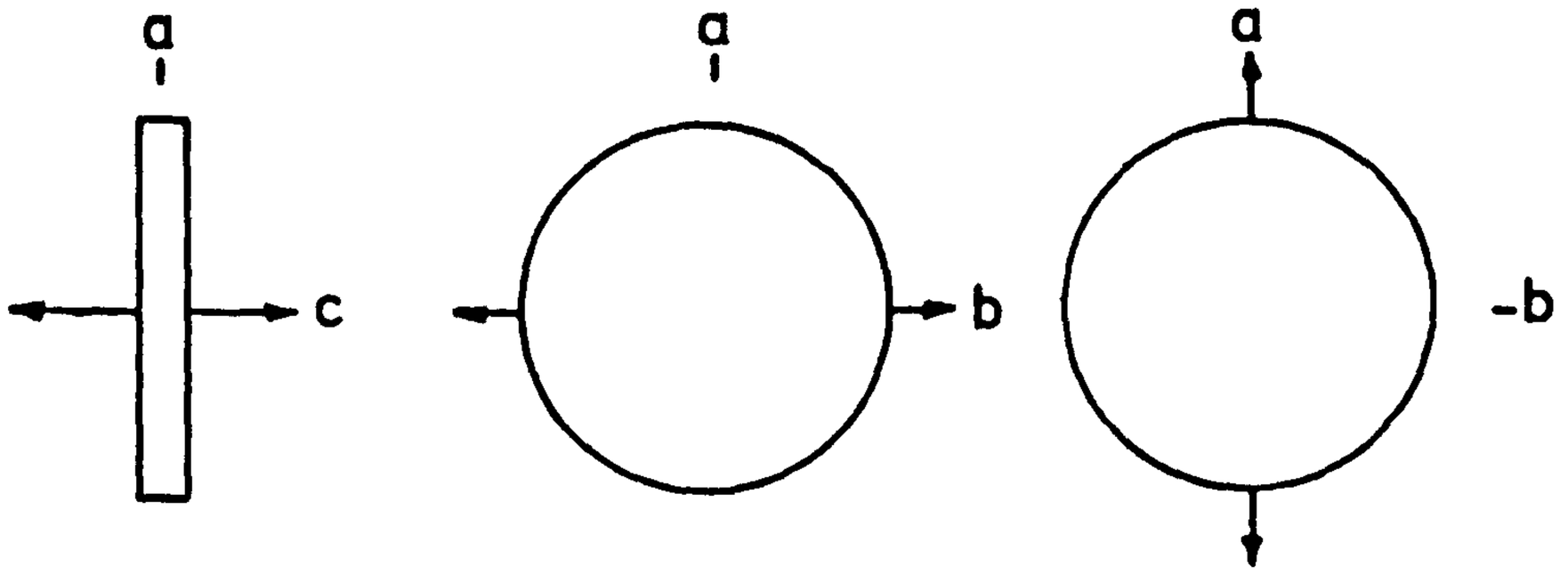

b: Rotational motion

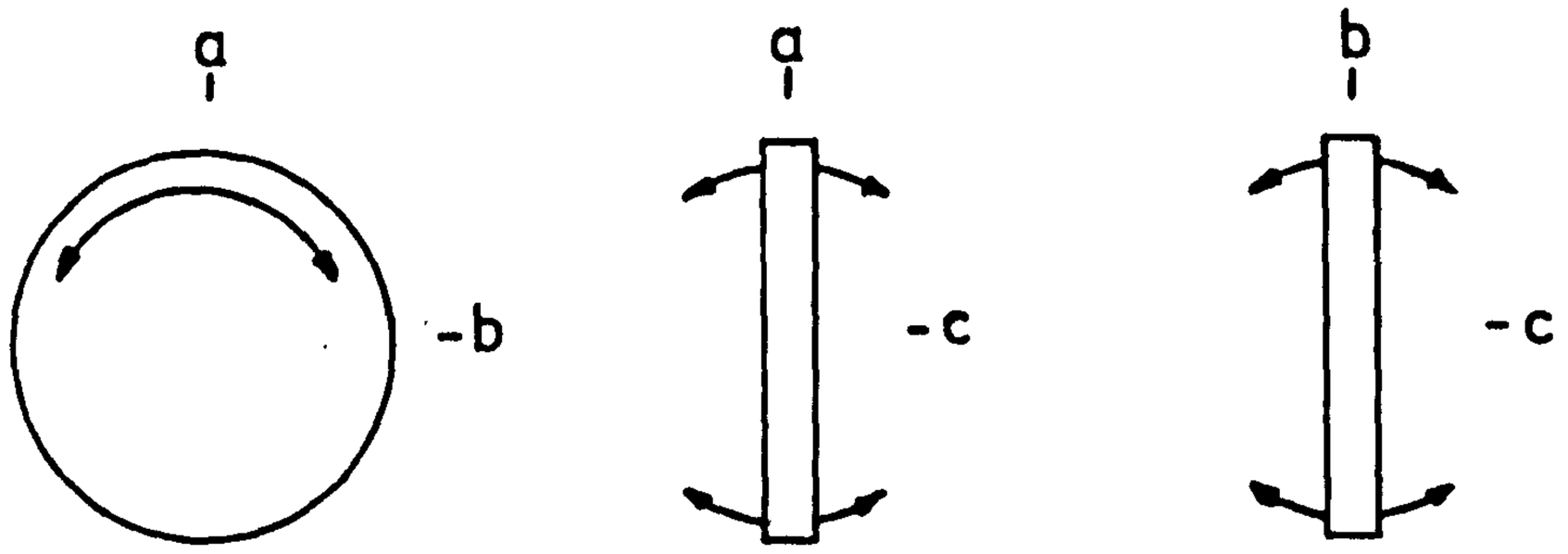

c: Vibrational motion

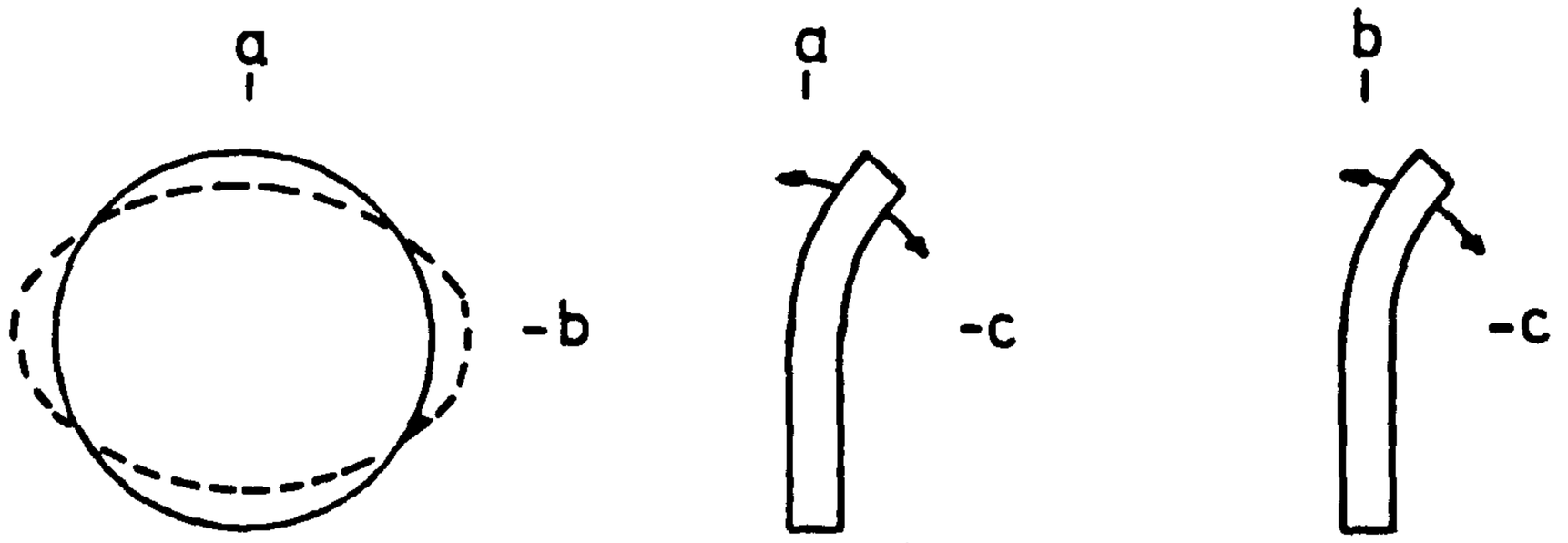

arrangement, e.g. the hexagonal model, are allowed to undergo translational motion then their relative positions may change.

Translational motions along the c axis, perpendicular to the disc face, will result in a change of H_f. If regions of particles are considered to diffuse towards each other then this will result in a localised decrease in H_f as the particles in such domains become more concentrated. The remaining particles in the system will now have a greater freedom of movement (193, 208) and may rotate to fill any available void space, i.e. the system becomes disordered. The extent to which the system becomes disordered will depend upon how such motion is restricted by potential energy barriers due to the electric double layers around the particles.

If the particles in a hexagonal unit cell are considered to diffuse towards each other, along the c axis, until their mean thermal energy ($\frac{1}{2}kT$) balances the increase in potential energy upon approach then the interplate separation H_f' may be obtained by solving

$$V_T(H_f') = V_T(H_f) + \tfrac{1}{2}kT \text{ per particle} \qquad (78)$$

where $V_T(H_f')$ and $V_T(H_f)$ are the total potential energies at separations H_f' and H_f (the unperturbed unit cell separation) respectively. Assuming $V_T = V_R$ (160), then

$$V_R(H_f') = V_R(H_f) + \frac{2kT}{\pi d^2 n} \quad Jm^{-2} \qquad (79)$$

where d = mean disc diameter.

If this value of H_f' is used in the calculation of B, as before, then the model is effectively assumed to be as shown in fig. 132c, with the particles in the ordered domains having a hexagonal arrangement, with face-face separations H_f'.

Translational motion of the discs in a lateral direction, along the a and b axes, is also possible. This will tend to reduce H_e within the ordered domains. This may be allowed for by substitution of H_f' for H_f in equation 68.

Lateral translational motions will also tend to change the value of A_1, i.e. the hexagonal structure will tend to be distorted towards some triclinic array. Since the differences between results calculated for hexagonal (sect. A9.2.3) and triclinic (sect. A9.2.4) arrays are small, and an infinite parallel plates-type electric double layer distribution is being assumed (sect. A9.2.5), this effect may be ignored.

The results of calculations of B using H_f' values obtained using equation 79 are shown in fig. 133 and will be discussed in sect. A9.3.2.4.

A9.3.2.2 Rotational motions

Rotational motions about the a or b axes may give alterations in the interactions between particles (fig. 133b). Rotational motions about the c axis (fig. 133b) will have no

effect on particle interaction for circular discs and may be ignored. The mean rotational thermal energy will be $\frac{1}{2}kT$ about each of the a and b axes (fig. 133), which will be equivalent to a mean rotational energy of kT about an axis in the same plane as and at an angle of 45^{o} to the a and b axes, assuming no bending of the disc occurs (sect. A9.3.2.3). Since all axes passing through the disc centre and in the plane of the disc are equivalent, the rotational motion may be considered by studying rotation about any such axis having a mean energy of kT.

If rotation is considered to occur such that V_R is increased by kT per particle, then an effective particle separation $H_f"$ and corresponding value for B may be calculated, in a similar manner to that used for the calculation of H_f' (sect. A9.3.2.1).

i.e. $$V_R(H_f") = V_R(H_f') + kT \text{ per particle} \qquad (80)$$

or from equation 78

$$V_R(H_f") = V_R(H_f) + 3kT/2 \text{ per particle} \qquad (81)$$

Calculated values of B, using this modification for rotation, are compared with experimental results in figs. 134 and 135. These results will be discussed in sect. A9.3.2.4.

Fig.134: Theoretical results for Hexagonal, Discs

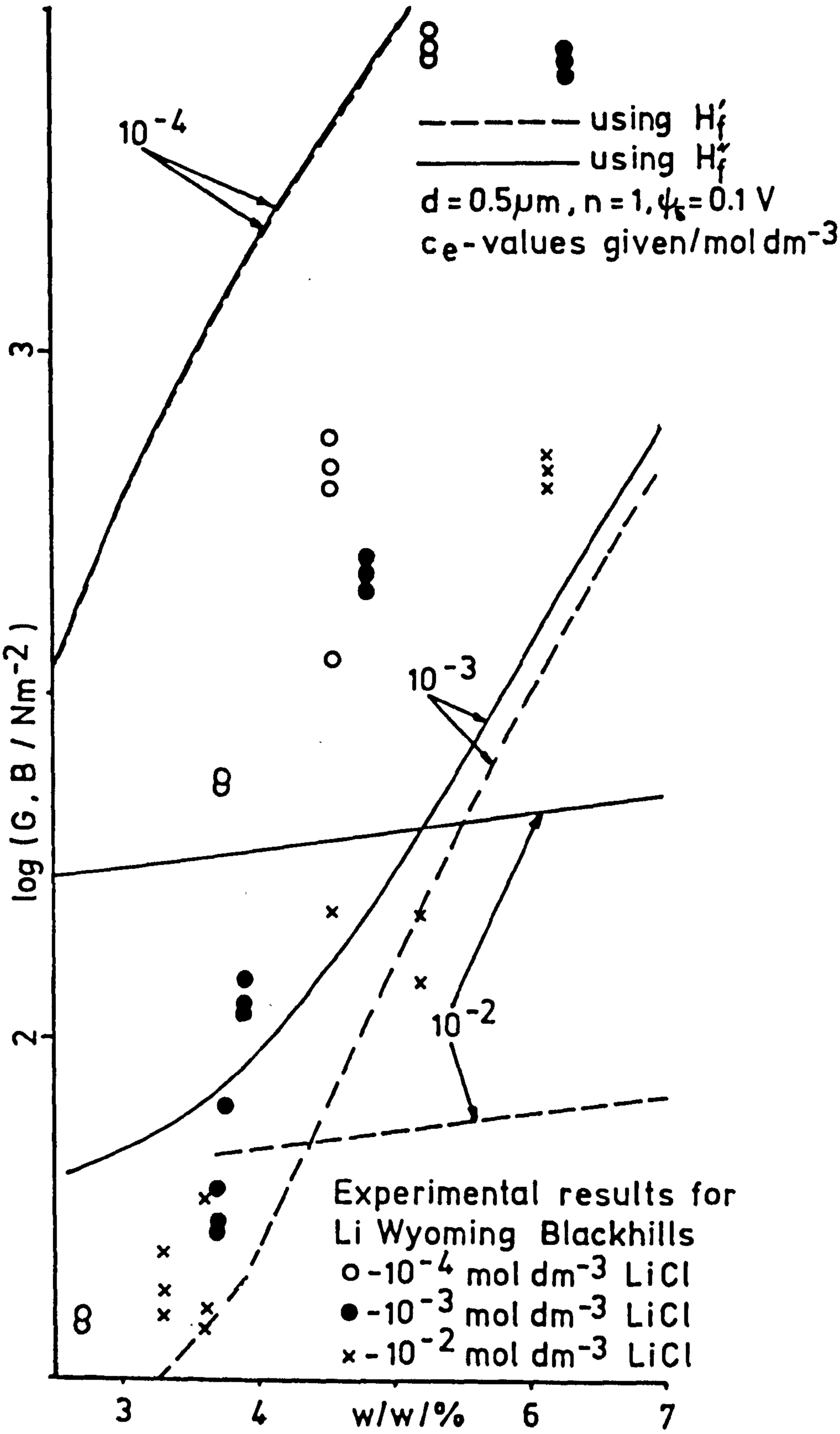

Fig.135: Theoretical results for Hexagonal ,Discs

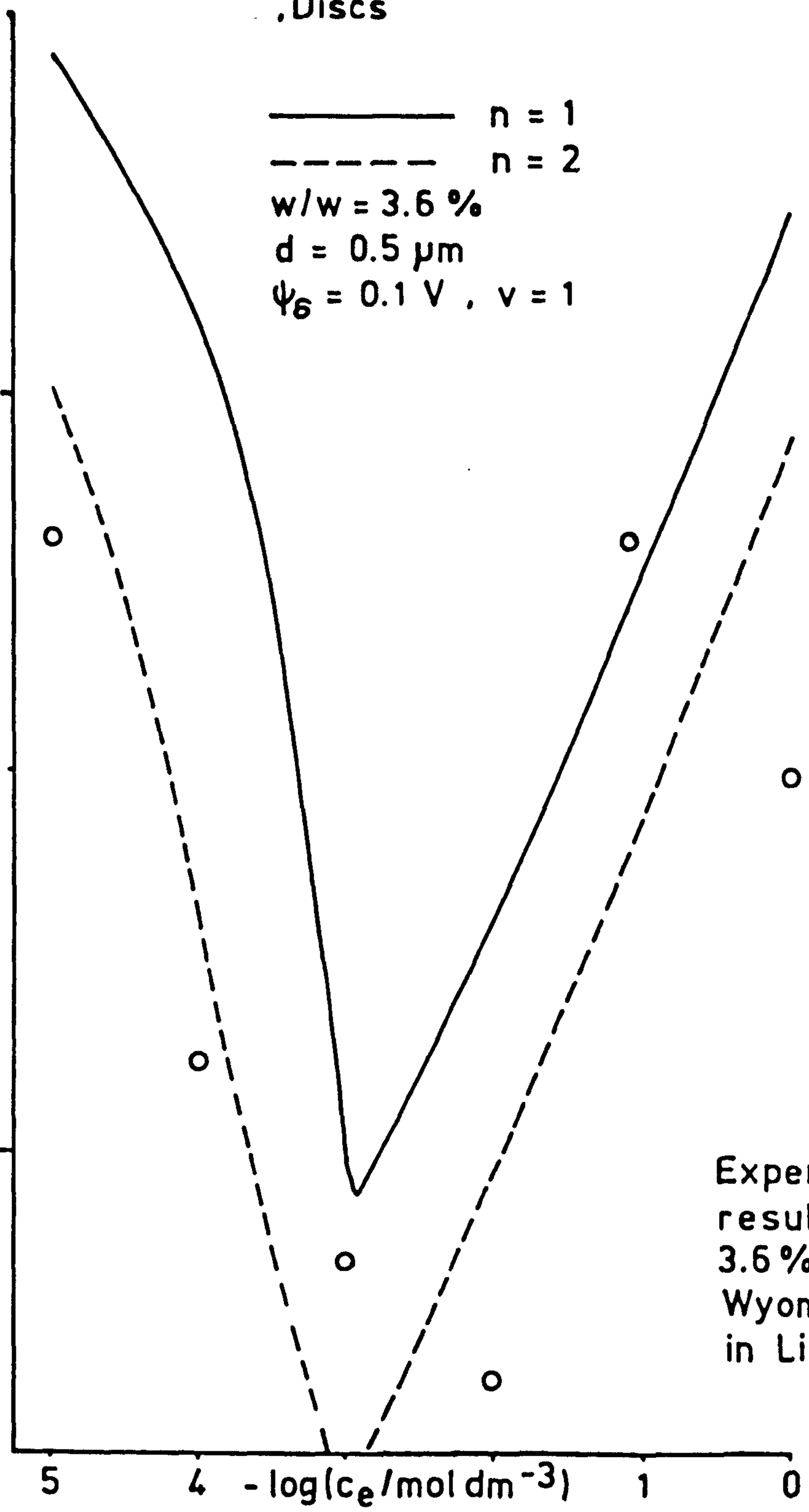

A9.3.2.3 Vibrational motions

Vibrated motions of disc shaped particles (fig. 133c) will not be considered, since their effect upon particle interactions may be neglected because quantum effects are important (304).

A9.3.2.4 Discussion

Figs. 134 and 135 show that the introduction of disorder into the hexagonal model has a considerable effect. The results at $c_e = 10^{-4}$mol dm^{-3} are identical to the non-disordered cell system. However, as the electrolyte concentration is increased the effects of disorder become more important with the theoretical curves generally moving closer to the experimental data. This increase in disorder upon increasing electrolyte concentration is due to the reduction of the range of the electric double layer repulsions allowing greater freedom of particle motion (193, 208, 345, 346). This effect has been noted with other concentrated colloidal systems (305). The tendency of an increase in disorder, caused by addition of electrolyte, to increase B is due to a "hardening" of the potential energy curve (fig. 9) at the interaction distance.

Fig. 135 shows that this model gives a reasonable qualitative description of the change in elastic properties

with electrolyte concentration. The results seem to suggest that the increase in shear modulus G as c_e is increased above some critical electrolyte concentration ($\sim 10^{-2}$ mol dm^{-3} LiCl for LiWB) is due, at least in part, to a decrease in order of the system.

The relatively small change upon changing the increase in V_R from $\frac{1}{2}kT$ to $\frac{3}{2}kT$ (fig. 134 - compare results using H_f' and H_f'') suggests that the assumption of mean thermal energies rather than a distribution of energies may be reasonable.

A9.4 ATTRACTIVE INTERACTIONS

So far the attractive interactions between montmorillonite particles in dispersion have been ignored, as suggested by Langmuir (169). The effects of including the attractive interactions will now be considered.

Equation 37 may be written in the form

$$B = H_o \frac{\partial^2 V_R}{\partial H_o^2} + H_o \frac{\partial^2 V_A}{\partial H_o^2} \qquad (82)$$

The calculation of the first term in the above expression has already been described (sect. 10.2). V_A may be given by equation 30.

$$V_A = \left[\frac{-A}{12\pi} \frac{1}{H_o^2} + \frac{1}{(H_o+2t)^2} - \frac{2}{(H_o+t)^2} \right] \quad Jm^{-2} \qquad (30)$$

where A is the non-retarded Hamaker constant and may be set equal to $2{\cdot}2 \times 10^{-20}$J (175).

Therefore,

$$H_o \frac{\partial^2 V_A}{\partial H_o^2} = \frac{-AH_o}{2\pi}\left[\frac{1}{H_o^4} + \frac{1}{(H_o+2t)^4} - \frac{2}{(H_o+t)^4}\right] \quad Nm^{-2} \qquad (83)$$

This may then be substituted into equation 82 and B calculated. The effects of this modification are shown in figs. 136 and 137. These show that at low electrolyte concentrations there is little effect due to the attractive interaction. However at $c_e > \sim 10^{-2}$mol dm^{-3} there is a marked reduction of B (fig. 137), until at high c_e ($> \sim 0{\cdot}1$mol dm^{-3}) B becomes negative when $V_A > V_R$, i.e. flocculation occurs.

Negative values of B are due to attractive interactions between particles. However, such systems of flocculated particles may show elastic properties (219, 325), and hence the absolute value of B could be taken. The results of this modification are shown in fig. 138, which shows that as c_e is increased above the point where the minimum in B occurs (at $\sim 10^{-1}$mol dm^{-3}) B then increases very rapidly.

There is some experimental evidence for a decrease in G of montmorillonite dispersions at very high electrolyte concentrations (fig. 93 (19)). These theoretical predictions (fig. 138) of a decrease in B under similar conditions should be treated with caution since there are theoretical and experimental difficulties with such flocculated systems because of the time dependent nature of the rheological behaviour.

Fig. 138 shows the results of calculations using the disordered,

Fig.136 : Theoretical results for
Hexagonal, Discs,
including attractive interaction

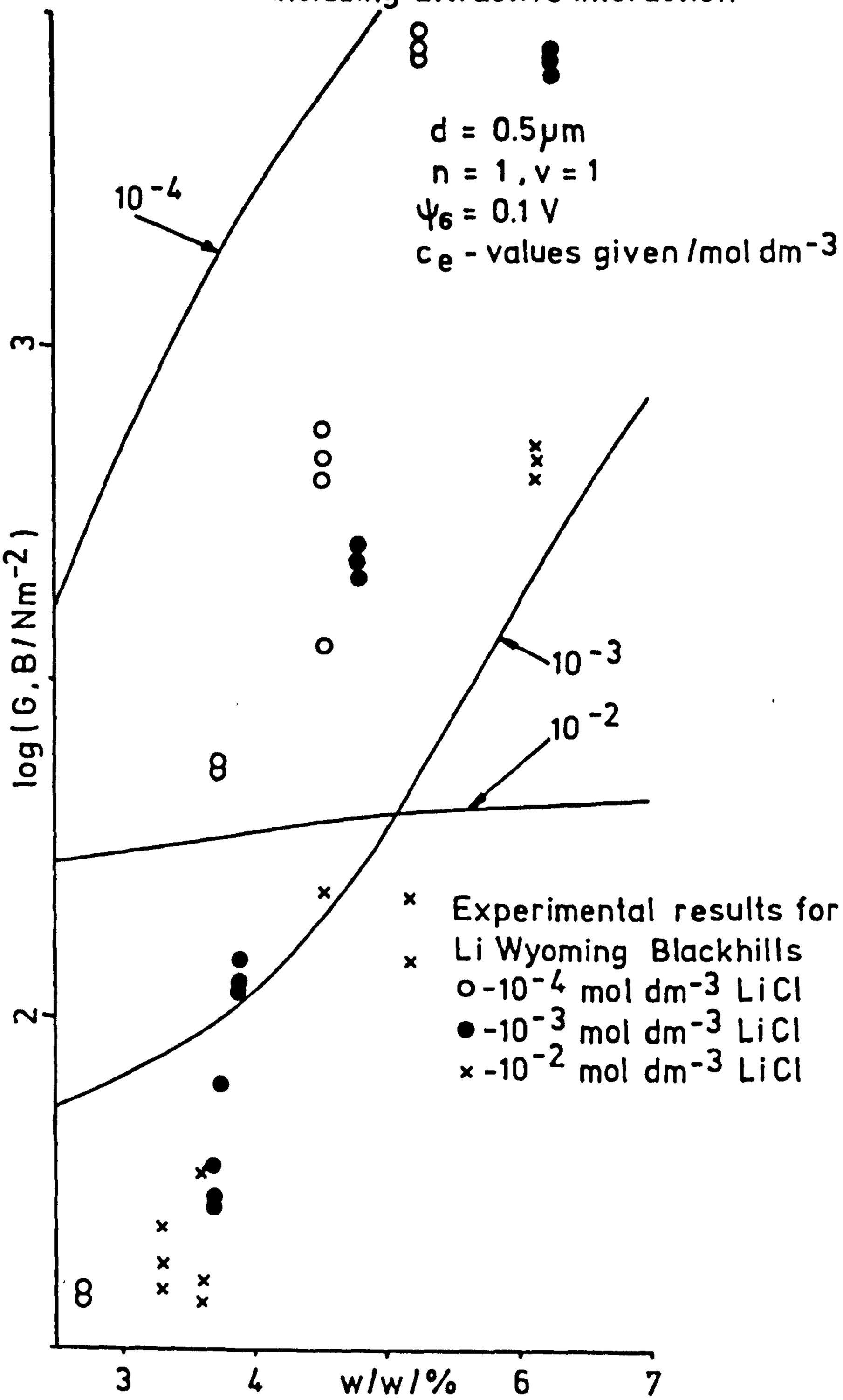

Fig.137 : Theoretical results for Hexagonal, Discs, including attractive interaction

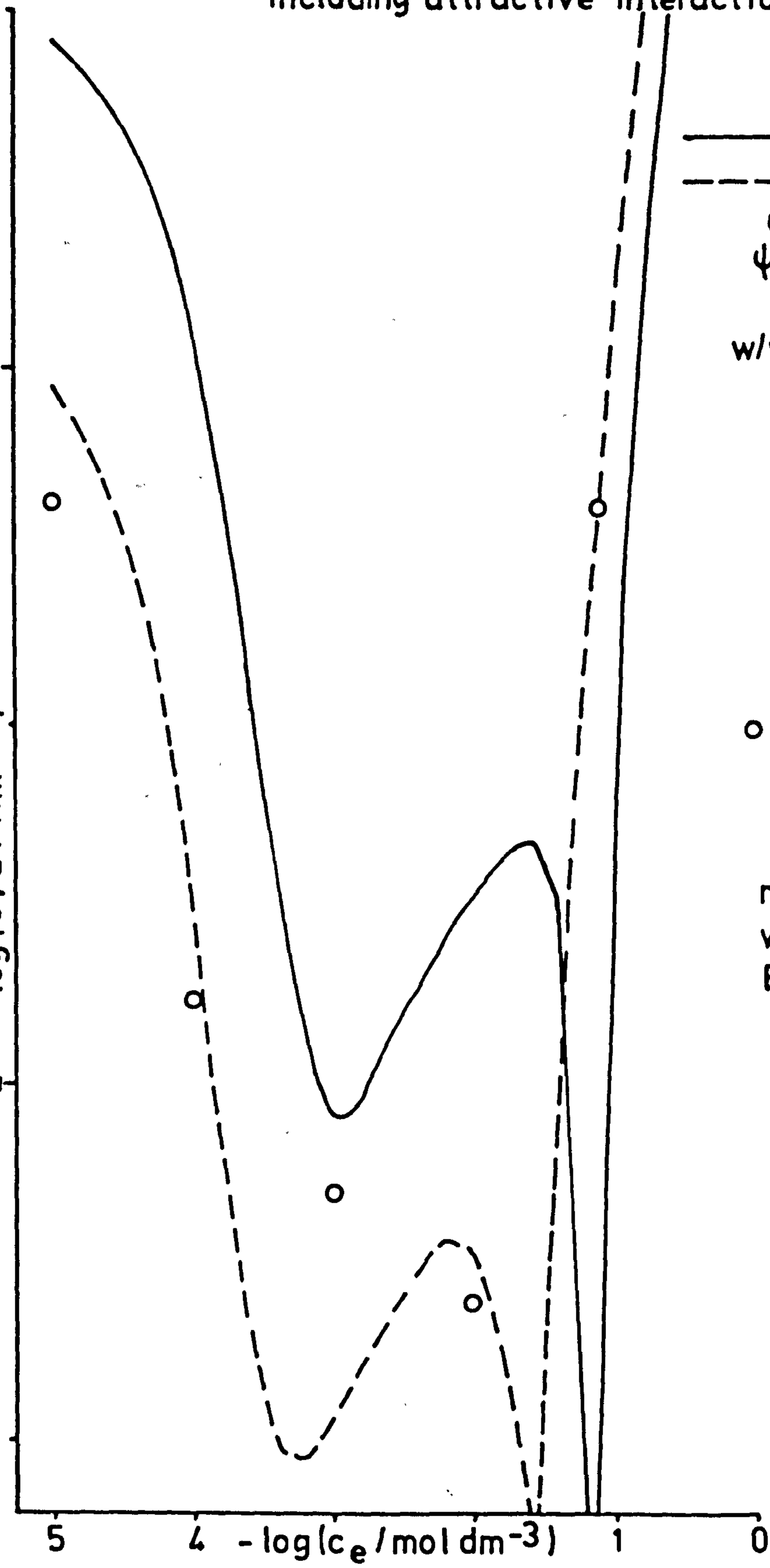

Fig.138: Theoretical results

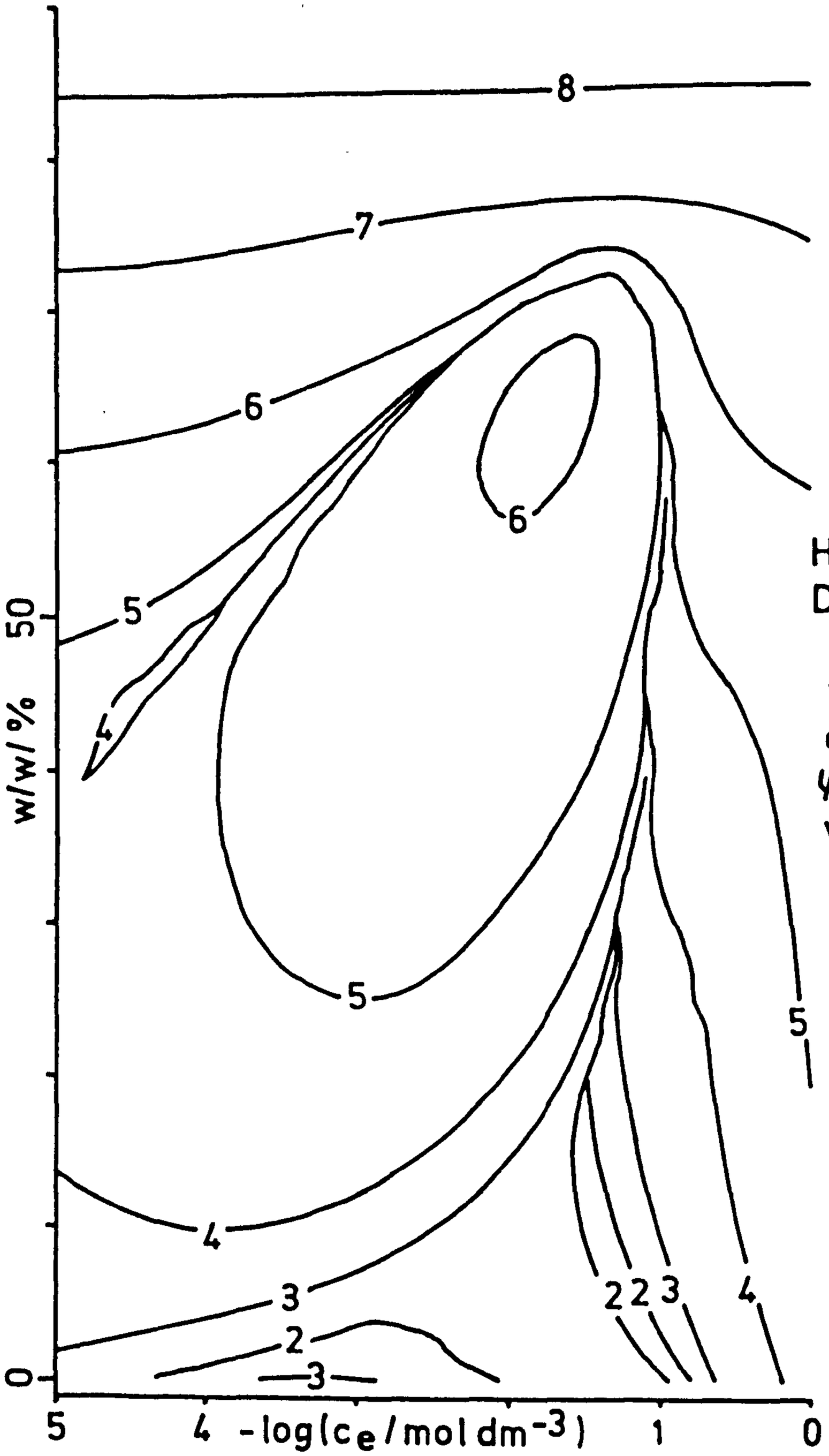

hexagonal discs model, including attractive interactions, described above. Fig. 138 is a "phase diagram" plot of w/w of montmorillonite against electrolyte concentration. All points along the lines on the plot have a constant value of Log B given. This plot suggests that the rheological behaviour of montmorillonite dispersions may be very complicated. The "phase diagram" given by Forsyth et al (193), obtained by statistical mechanics, suggest that there may be some qualitative validity of fig. 138. It needs to be pointed out, however, that there are many theoretical simplifications involved in the results shown in fig. 138, e.g. possible changes in tactoid formation (n) with changing volume fraction or electrolyte concentration are not accounted for. Also there would be practical difficulties involved in obtaining experimental evidence for many of the trends shown in fig. 138, e.g. polydispersity and solubility of clay particles.

APPENDIX 10

Thank you (Uncle) John "Les Holloway" (Demerry) Dimery, for assistance with electron microscopy, Pen-Kem electrophoresis and many other little things that I've forgotten; (Lesmo/Max) Les "What do you want it for?" (Smallpiece/vonKorbinn) Corbin, for showing me how to extinguish a Laboratory fire; Sue Corbin, for keeping Les under control; Iris Stephens, for cleaning my coffee mug (when necessary); Jim (Fergie-Woodentops) Fergie-Woods, for having a silly surname; (Cuddly) Steve "zot zot" Lubetkin (as seen on T.V.), for advice on the use of Dog Nobblers; (Auntie) Jean Proctor, for being wonderful; (Evil) Bob Newton, for advice on hi-fi and demonstrating the "Killer" skittles technique; Roly Harbron, for darts exhibitions (I've still got the scars!); (Super) Sue Partridge, for jolly well attempting to jolly well teach me to jolly well speak jolly Queen's jolly English; (Cuddly) Dudley Thompson, for TEM AND EPMA; Jimbo Goodwin, for not interfering too much; (Billy) Sarah "That's a nasty little mess!" Burkitt, for cuddles; Dave Skuse, for fishing trips; Craig (C^2N) Nunn, for advice on cooking 3-alarm chili con carne and knowing everything (especially about Texas); (Divna Auntie) Vanja Marković, for teaching me to speak Serbo Croat (badly); (Chopper) Charlie Jeffrey, for advice on flying helicopters and Brownian dynamics; Ian Livsey, for demonstrating the "Smokescreen" skittles technique; (Sgt. Maj.) Sara Papworth, for keeping me in order with her rod of iron; (Nobber) Neal Williams, for demonstrating the "I can't quite

bowl as slow as Rex despite the use of my special belt" skittles technique; Roy (Yozzer) Hughes, for incomprehensible discussions on statistical mechanics; (Young Map) Pamela Clayton, for wearing a very silly lab coat; (Mandy) Andy "You're a really great bloke" - SMACK-Mackie, for giving me a bad back; (Cheeky) Chiu Lam, for being little; (Lovely) Louise Marshall, for supplying me with aspirins during the writing of this thesis; Mary McBride, for advice on travelling on Irish Railways; Dai (Beaker) Thomas for having a ridiculous hairstyle; (Philthy) Phil Taylor, for demonstrating the "I can bowl even faster than Evil Bob" skittles technique; (Ozzy) Martin Smith, for "letting" us beat his skittles team; David Hodge, for advice on the use of an umbrella; (Jolly) Jill Lye, for being jolly; Guru Satgurunathan, for cocktails; Sandra Bourne, for advice on barn dancing; Ian (great hairy wassock) Metcalfe, for being a kindred spirit (?); Dawn Metcalfe, for playing Mhing; (Styrene) Sarah Rickard, for making me laugh; Cathy Elliott, for telling me I was handsome (once); Dave Schechter, for demonstrating the "I can try and bowl faster than Philthy Phil" skittles technique; Trev Crowley, for supplying free fumigation service; Steve (Grapefruit) Lenon, for going to Australia; Bruce Johnson, for advice on all matters concerning Bendigo; Tracy ..... "I'm sorry, but I've forgotten your name", for kisses; Susan Davies and the rest of the staff of the Worsley Chemistry Library, for being so helpful; Smiles Brewing Co. and anyone else it may concern.

REFERENCES

1. Knight, W.C., Eng. Min. J., 63 (1897) 600
2. Knight, W.C., Eng. Min. J., 66 (1898) 491
3. Ross, C.S. and Shannon, E.V., J. Am. Ceram. Soc., 9 (1926) 77
4. Wright, P.C., J. Geol. Soc. Aust., 15 (1968) 347
5. Grim, R.E., Clay Mineralogy, 2nd ed., McGraw-Hill, New York (1968)
6. Grim, R.E. and Güven, N., Bentonites, Dev. Sed., 24, Elsevier, Amsterdam (1978)
7. Larsen, D.H., Calif. Div. Mines Geol. Bull., 169 (1959) 269
8. Cairns-Smith, A.G., Sci. Amer., 252 (1985) 74
9. Chelf, C.R., Min. Res. Circ., 43, University of Texas (1942), in ref. 10
10. Chen, P.Y., Ph.D. thesis, University of Texas (1968)
11. van Olphen, H. and Fripiat, J.J., Data handbook for clay materials and other non-metallic minerals, Pergamon, Oxford (1979)
12. Roberson, H.E., Ph.D. thesis, University of Illinois (1959)
13. Roberson, H.E., J. Sed. Petrol., 34 (1964) 401
14. Brindley, G.W. and Brown, G. (eds.), Crystal structures of clay minerals and their X-ray identification, Mineralogical Society, London (1980)
15. Brown G., chapter 6 in ref. 14
16. Henderson, J.H., Jackson, M.L., Syers, J.K., Clayton, R.N. and Rex, R.W., Clays Clay Miner., 19 (1971) 229
17. Whitten, D.G.A. and Brooks, J.R.V., A dictionary of geology, Penguin, Harmondsworth (1982)
18. Bailey, S.W., chapter 1 in ref. 14
19. van Olphen, H., An introduction to clay colloid chemistry, 2nd ed., Wiley, New York (1977)
20. Zvyagin, B.B., Soviet Phys. Cristallogr., 2 (1957) 388
21. Radoslovich, E.W., Nature (Lond.), 191 (1961) 67
22. Zvyagin, B.B., Soviet Phys. Cristallogr., 5 (1960) 32

23. Newnham, R.E., Mineralog. Mag., 32 (1961) 683
24. Radoclovich, E.W., Am. Miner., 48 (1963) 76
25. Hendricks, S.B., Z. Kristallogr. Kristallgeom., 100 (1939) 509
26. Geise, R.F., Clays Clay Miner., 21 (1973) 145
27. Weickowski, T. and Wiewióra, A., Clays Clay Miner., 24 (1976) 219
28. Geise, R.F., and Datta, P., Am. Miner., 58 (1973) 471
29. Cruz, M., Jacobs, H. and Fripiat, J.J., Proc. Intl. Clay Conf. 1972, Madrid, Division de Ciencias C.S.I.C., Madrid (1973) 35.
30. Brindley, G.W. and Goodyear, J., Mineralog. Mag., 28 (1948) 407
31. Churchman, G.J. and Carr, R.M., Am. Miner., 57 (1972) 914
32. Churchman, G.J., Aldrich, L.P. and Carr, R.M., Clays Clay Miner., 20 (1972) 241
33. Hughes, I.R., N.Z.J.Sci., 9 (1966) 103
34. Harrison, J.L. and Greenberg, S.S., Clays Clay Miner., 9 (1962) 374
35. Bates, T.F., Hildebrand, F.A. and Swineford, A., Am. Miner., 35 (1950) 463
36. Sudo, T., Shimoda, S., Yotsumoto, H. and Aita, S., Electron micrographs of clay minerals, Dev. Sed., 31, Elserier, Amsterdam and Kodansha, Tokyo (1981)
37. Brindley, G.W., chapter 2 in ref. 14
38. Mitra, G.B. and Bhattacherjee, S., Acta Crystallogr., B31 (1975) 2851
39. Hendricks, S.B., Am. Miner., 23 (1938) 295
40. Hendricks, S.B. and Jefferson, M.E., Am. Miner., 23 (1938) 863
41. Weaver, C.E. and Pollard, L.D., The chemistry of clay minerals, Dev. Sed., 15, Elsevier, Amsterdam (1973)
42. Damour, A.A. and Salvetat, D., Ann. Chim. Phys. ser. 3, 21 (1847) 376
43. Ross, C.S. and Hendricks, S.B., U.S. Geol. Surv., Prof. Pap. 205B (1945) 23
44. Berthier, P., Ann. Chim. Phys., 36 (1827) 22
45. Larsen, E.S. and Steiger, G., Am. J. Sci., ser. 5, 15 (1928) 1
46. Ross, C.S. and Kerr, P.F., J. Sed. Petrol., 1 (1931) 55
47. Grover, J.W., Am. Miner., 20 (1935) 475
48. Larsen, E.S. and Wherry, E.T., J. Wash. Acad. Sci., 15 (1925) 465
49. Grim, R.E. and Rowland, R.A., Am. Miner., 27 (1942) 746

50. Nixon, H.L. and Weir, A.H., Miner. Mag., 31 (1957) 413
51. Weir, A.H. and Greene-Kelly, R., Am. Miner., 17 (1962) 137
52. Méring, J. and Oberlin, A., chapter 6 in ref. 314
53. Hofmann, U., Weiss, A., Koch, G., Mehler, A. and Scholz, A., Natl. Acad. Sci., Publ. 465 (1956) 273
54. Glaeser, R., Mantine, I. and Méring, J., Bull. Grpe. fr. Argiles, 19 (1967) 125
55. Hamilton, J.D., Clay Miner., 9 (1971) 107
56. Radoslovich, E.W., Am. Miner., 47 (1962) 617
57. Radoslovich, E.W., and Norrish, K., Am. Miner., 47 (1962) 599
58. Veitch, L.G. and Radoslovich, E.W., Am. Miner., 48 (1963) 62
59. Grim, R.E., Bray, R.H. and Bradley, W.F., Am. Miner., 22 (1937) 813
60. Levinson, A.A., Am. Miner., 40 (1955) 41
61. Dixon, J.B. and Weed, S.B. (eds.), Minerals in soil environments, Soil Science Society of America, Madison, Wisc. (1977)
62. Barnhisel, R.I., chapter 10 in ref. 61
63. Eggleston, R.A. and Bailey, S.W., Am. Miner., 52 (1967) 673
64. Rich, C.I., Clays Clay Miner., 16 (1968) 15
65. Occelli, M.L., Ind. Eng. Chem. Prod. Res. Dev., 22 (1983) 553
66. Pinnavaia, T.J., Science, 220 (1983) 365
67. Endo, T., Mortland, M.M. and Pinnavaia, T.J., Clays Clay Miner., 28 (1980) 105
68. Manos, C.G., Mortland, M.M. and Pinnavaia, T.J., Clays Clay Miner., 32 (1984) 93
69. Reynolds, R.C., chapter 4 in ref. 14
70. Sawnley, B.L., chapter 12 in ref. 61
71. Greenland, D.J. and Hayes, M.H.B. (eds.), The chemistry of soil constituents, Wiley, Chichester (1978)
72. Brown, G., Newman, A.C.D., Rayner, J.H. and Weir, A.H., chapter 2 in ref. 71
73. Weaver, C.E., Am. Miner., 41 (1956) 202
74. Earley, J.W., Brindley, G.W., McVeagh, W.J. and Vanden Heuvel, R.C., Am. Miner., 41 (1956) 258
75. Shimoda, S., Clays Clay Miner., 17 (1969) 179

76. Cole, W.F., Clay Miner., 6 (1966) 261
77. Thompson, G.R. and Hower, J., Clays Clay Miner., 23 (1975) 289
78. Weir, A.H. and Rayner, J.H., Clay Miner., 10 (1974) 173
79. Hower, J. and Mowatt, T.C., Am. Miner., 51 (1966) 825
80. Wilding, L.P., Smeck, N.E. and Drees, L.R., chapter 14 in ref. 61
81. Frondel, C., Dana's system of mineralogy, 7th ed., vol. III Silica minerals, Wiley, New York (1962)
82. Dennen, W.H., Geochim. Cosmochim. Hata, 30 (1966) 1235
83. Crook, K.A.W., Sedimentology, 11 (1968) 171
84. Krinsley, D.H. and Smalley, I.J., Science, 180 (1973) 1277
85. Fenner, C.N., Am. J. Sc., 36 (1913) 331
86. Jones, J.B. and Segnit, E.R., J. Geol. Soc. Aust., 18 (1972) 419
87. Berry, L.G., Mason, B and Dietrich, R.V., Mineralogy, 2nd ed., Freeman, San Fransisco (1983)
88. Rockett, T.J. and Foster, W.R., Am. Miner., 52 (1967) 1233
89. Flörke, O.W., Ber. Deut. Keram. Ges., 38 (1961) 89.
90. Jones, J.B., Segnit, E.R. and Nickson, N.M., Nature (London), 198 (1963) 1191
91. Jones, J.B., Sanders, J.V. and Segnit, E.R., Nature (London), 204 (1964) 990
92. Jones, J.B. and Segnit, E.R., J. Geol. Soc. Aust., 18 (1971) 57
93. Pollard, C.O. and Weaver, C.E., J. Sed. Petrol., 43 (1973) 1072
94. Henmi, T. and Parfitt, R.L., Clays Clay Miner., 28 (1980) 57
95. Henmi, T. and Wada, K., Am. Miner., 61 (1976) 379
96. Wada, K., chapter 16 in ref. 61
97. Sudo, T. and Shimoda, S. (eds.), Clays and Clay minerals of Japan, Dev. Sed., 26, Elsevier, Amsterdam (1978)
98. Wada, K., chapter 4 in ref. 97
99. Siever, R. and Scott, R.A., chapter 14 in Breger, I.A. (ed.), Organic geochemistry, Pergamon, Oxford (1963)
100. Güven, N. and Pease, R.W., Clays Clay Miner., 23 (1975) 187
101. Brown, T.E., Ph.D. thesis, University of Texas (1963)
102. MacEwan, D.M.C., chapter 4 in Brindley, G.W. (ed.), X-ray identification and crystal structures of clay minerals, Mineralogical Society, London (1951)

103. Gast, R.G., chapter 2 in ref. 61
104. McAtee, J.L., Clays Clay Miner., 5 (1958) 279
105. Jonas, E.C. and Roberson, H.E., Clays Clay Miner., 13 (1966) 223
106. Stul, M.S. and Mortier, W.J., Clays Clay Miner., 22 (1974) 391
107. Rengasamy, P., van Assche, J.B. and Uytterhoeven, J.B., J. Chem. Soc. Faraday Trans I, 72 (1976) 376
108. Byrne, P.J.S., Clays Clay Miner., 2 (1954) 241
109. Sudo, T., Hayashi, H. and Shimoda, S., Clays Clay Miner., 9 (1962) 378
110. Sawhney, B.L., Clays Clay Miner., 20 (1972) 93
111. Heifferich, F., Ion Exchange, McGraw-Hill, New York (1962)
112. Pauley, J.L., J. Am. Chem. Soc., 76 (1954) 1422
113. Jenny, H., J. Phys. Chem., 36 (1932) 2217
114. Cloos, P., Fripiat, J.J., Poncelet, G. and Poncelet, A., Bull. Soc. Chim. Fr., 42 (1965) 215
115. Gast, R.G., Soil Sci. Soc. Am. Proc., 33 (1969) 37
116. Neal, C. and Cooper, D.M., Clays Clay Miner., 31 (1983) 367
117. Bolt, G.H., J. Colloid Sci., 10 (1955) 206
118. Babcock, K.L., Hilgardia, 34 (1963) 417
119. Norrish, K., Disc. Faraday Soc., 18 (1954) 120
120. Borchardt, G.A., chapter 9 in ref. 61
121. Patterson, S.H., Ph.D. thesis, University of Illinois (1955)
122. Hanshaw, B.B., Clays Clay Miner., 12 (1964) 397
123. Weaver, C.E. and Beck, K.C., Geol. Soc. Am., Spec. Pap., 134
124. Schachtschabel, P., Kolloid Beih., 51 (1940) 199
125. Kelley, W.P. and Cummins, A.B., Soil Sci., 11 (1921) 139
126. Hofmann, U and Endell, J., Ver. Deut. Chem. Beih., 35 (1939) 708
127. Hofmann, U. and Klemen, R., Z. Anorg. Chem., 262 (1950) 95
128. Weaver, C.E., Am. Miner., 43 (1958) 839
129. Field, R.J., Ph.D. thesis, University of Bristol (1986)
130. MacEwan, D.M.C. and Wilson, M.J., chapter 3 in ref. 14
131. The Economist, 289 (7315) (1983) 89
132. Suquet, H., de la Calle, L. and Pezerat, H., Clays Clay Miner., 23 (1975) 1
133. Bradley, W.F., Grim, R.E. and Clark, G.F., Z. Kristallogr. Kristallgeom., 97 (1937) 216

134. Mooney, R.W., Keenan, A.G. and Wood, L.A., J. Am. Chem. Soc., 74 (1952) 1367
135. Glaeser, R. and Méring, J., C.R. Lebd. Séanc. Acad. Sci., 267 (1968) 436
136. Méring, J., Trans. Faraday Soc., 42B (1946) 205
137. Farmer, V.C. and Russell, J.D., Clays Clay Miner., 15 (1971) 121
138. Mathieson, A. McL. and Walker, G.F., Am. Miner., 39 (1954) 231
139. Mathieson, A. McL., Am. Miner., 43 (1958) 216
140. Shirozu, H. and Bailey, S.W., Am. Miner., 51 (1966) 1124
141. Hougardy, J., Stone, W.E.E. and Fripiat, J.J., J. Chem. Phys., 64 (1976) 3840
142. Fripiat, J.J., (ed.), Advanced techniques for clay mineral analysis, Dev. Sed., 34, Elsevier, Amsterdam (1982)
143. Stone, W.E.E., chapter 4 in ref. 142
144. Middleton, S.R., M.Sc. thesis, University of Bristol (1973)
145. Middleton, S.R., Ph.D. thesis, University of Bristol (1978)
146. Lubetkin, S.D., Middleton, S.R. and Ottewil, R.H., Phil. Trans. R. Soc. Lond., A311 (1984) 353
147. MacEwan, D.M.C., Nature, Lond., 154 (1944) 577
148. Bradley, W.F., Am. Miner., 30 (1945) 704
149. MacEwan, D.M.C., Clays Clay Miner., 9 (1960) 431
150. Foster, W.R., Sarius, J.G. and Waite, J.M., Clays Clay Miner., 3 (1955) 296
151. Cebula, D.J. and Ottewill, R.H., Clays Clay Miner., 29 (1981) 73
152. Schramm, L.L. and Kwak, J.C.T., Soil Sci., 137 (1984) 1
153. Martin Vivaldi, J.L.M., MacEwan, D.M.C. and Rodriguez Gallego, M., Proc. Intl. Clay Cont., Stockholm, 1 (1963) 45, Pergamon, Oxford
154. Russel, J.D. and Farmer, V.C., Clay Miner. Bull., 5 (1964) 443
155. Moum, J., Rao, C.N. and Ayyar, T.S.R., Clays Clay Miner., 21 (1973) 89
156. Stern, O., Z. Electrochem., 30 (1924) 508
157. Gouy, G., J. Physique, 9 (1910) 457
158. Chapman, D.L., Phil. Mag., 25 (1913) 475

159. Overbeek, J.Th.G., chapter 4 in Kruyt, H.G., (ed.) Colloid Science, vol. 1, Elsevier, Amsterdam (1952)
160. Verwey, E.J.W. and Overbeek, J.Th.G., Theory of the stability of lyophobic colloids, Elsevier, Amsterdam (1948)
161. Chan, D.Y.C., Pashley, R.M. and Quirk, J.P., Clays Clay Miner., 32 (1984) 131
162. Novich, B.E. and Ring, T.A., Clays Clay Miner., 32 (1984) 74
163. Reerink, H. and Overbeek, J.Th.G., Disc. Faraday Soc., 18 (1954) 74
164. Howarth, L.G., M.Sc. thesis, University of Bristol (1982)
165. London, F., Z. Physik., 63 (1930) 245
166. Derjaguin, B.V. and Landau, L., Acta Physicochim. U.R.S.S., 14 (1941) 633
167. Derjaguin, B., Trans. Faraday Soc., 36 (1940) 203
168. Derjaguin, B., Acta Physicochim. U.R.S.S., 10 (1939) 333
169. Langmuir, I., J. Chem. Phys., 6 (1938) 873
170. Dube, G.P., Indian J. Phys., 17 (1943) 189
171. Levine, S., Trans. Faraday Soc., 42B (1946) 102
172. Viani, B.E., Low, P.F. and Roth, C.B., J. Colloid Interface Sci., 96 (1983) 229
173. Barclay, L.M. and Ottewill, R.H., Spec. Disc. Faraday Soc., 1 (1970) 138
174. Derjaguin, B.V. and Churaev, N.V., J. Colloid Interface Sci., 49 (1974) 249
175. Israelachvili, J.N. and Adams, G.E., J. Chem. Soc. Faraday Trans. I 74 (1978) 975
176. Pashley, R.M., J. Colloid Interface Sci., 83 (1981) 531
177. Pashley, R.M. and Israelachvili, J.N., J. Colloid Interface Sci., 97 (1984) 446
178. Pashley, R.M. and Israelachvili, J.N., J. Colloid Interface Sci., 101 (1984) 511
179. Hamaker, H.C., Rec. trav. chim., 55 (1936) 1015
180. Hamaker, H.C., Rec. trav. chim., 56 (1937) 3
181. Kallman, H. and Willstäter, M., Naturw., 20 (1932) 952

182. De Boer, J.H., Trans. Faraday Soc., 32 (1936) 10

183. Hamaker, H.C., Physica, 4 (1937) 1058

184. Lifshitz, E.M., Soviet Phys. J.E.T.P., 2 (1956) 73

185. Dzyaloshinkskii, E.E., Lifshitz, E.M. and Pitaevskij, L.P., Soviet Phys. J.E.T.P., 37 (1960) 161

186. Derjaguin, B.V., Abricossova, I.I. and Lifshitz, E.M., Q. Rev. Chem. Soc., 10 (1956) 295

187. Tabor, D. and Winterton, R.H.S., Proc. Roy. Soc., A312 (1969) 435

188. Israelachvili, J.N. and Tabor, D., Proc. Roy. Soc., A331 (1972) 19

189. Sheludko, A., Colloid Chemistry, Elsevier, Amsterdam (1966)

190. Kitchener, J.A., Recent Progr. Surface Sci., 1 (1964) 51

191. Warkentin, B.P., Ph.D. thesis, Cornell University (1956)

192. Callaghan, I.C., Ph.D. thesis, University of Bristol (1975)

193. Forsyth, P.A., Marčelja, J.S., Mitchell, D.J. and Ninham, B.W., Adv. Colloid Interface Sci., 9 (1978) 37

194. Rand, B., Pekenć, E., Goodwin, J.W. and Smith, R.W., J. Chem. Soc. Faraday I, 76 (1980) 225

195. Swartzen-Allen, S.L. and Matijenć, E., Chem. Rev., 74 (1974) 385

196. Callaghan, I.C. and Ottewill, R.H., Faraday Disc. Chem. Soc., 57 (1974) 110

197. Schramm, L.L. and Kwak, J.C.T., Clays Clay Miner., 30 (1982) 40

198. Jessen, F.W. and Morgan, N., AIME Petroleum Trans., 216 (1959) 455

199. Forslind, E. and Jacobsson, A., chapter 4 in Franks, F. (ed.), Water, vol 5, Plenum, New York (1975)

200. Ottewill, R.H. p.503 in ref. 286

201. Kahn, A., J. Colloid Sci., 13 (1958) 51

202. Blackmore, A.V. and Miller, R.D., Soil Sci. Soc. Amer. Proc., 25 (1961) 169

203. Cebula, D.J., Thomas, R.K., Middleton, S., Ottewill, R.H. and White, J.W., Clays Clay Miner., 27 (1979) 39

204. Kleijn, W.B. and Oster, J.D., Clays Clay Miner., 30 (1982) 383
205. Banin, A. and Lahav, N., Israel J. Chem., 6 (1968) 235
206. Shainberg, I. and Otoh, H., Israel J. Chem., 6 (1968) 251
207. Dufey, J.E. and Banin, A., Soil Sci. Soc. Amer. J., 43 (1979) 782
208. Onsager, L., Ann. N.Y. Acad. Sci., 51 (1949) 627
209. M'Ewen, M.B. and Pratt, M.I., Trans. Faraday Soc., 53 (1957) 535
210. M'Ewan, M.B. and Mould, D.L., Trans. Faraday Soc., 53 (1957) 548
211. M'Ewan, M.B. and Mould, D.L., Nature, Lond., 166 (1950) 437
212. Cebula, D.J., Thomas, R.K. and White, J.W., J. Chem. Soc. Faraday I, 76 (1980) 314
213. Bernal, J.D. and Fankuchen, I., Nature, Lond., 139 (1937) 923
214. Zocher, H., Z. Anorg. Allg. Chem., 147 (1925) 91
215. Hiffner, P.A. and Krieger, I.M., J. Phys. Chem., 73 (1969) 2386
216. Barclay, L., Harrington, A. and Ottewill, R.H., Kolloid Z.Z. Polym., 250 (1972) 655
217. Hachisu, S., Kobayashi, Y. and Kose, A., J. Colloid Intervace Sci., 42 (1973) 342
218. Straley, J.P., Mol. Cryst. Liqu. Cryst., 22 (1973) 333
219. Tadros, Th.F., Chem. Ind., (1985) 210
220. Bergmann, P., Löw-Beer, P. and Zocher, H., Z. Physik. Chem. A181 (1938) 301
221. Marković, I., M.Sc. thesis, University of Bristol (1980).
222. Talibodeen, O., Ads. Sci. Techn., 1 (1984) 235
223. Goodwin, J.W., in Goodwin, J.W. (ed.), Colloidal dispersions, Royal Society of Chemistry, Special Publication No. 43, London (1982)
224. Reiner, M., Physics Today, 17 (1969) 62
225. Ferry, J.D., Viscoelastic properties of polymers, 3rd ed., Wiley, New York (1980)
226. Gittus, J., Creep, viscoelasticity and creep fracture in solids, Applied Science, Barking (1975)
227. Goodwin, J.W., Ph.D. thesis, University of Bristol (1972)
228. Uvarov, E.B., Chapman, D.R. and Isaacs, A., A dictionary of science, 4th ed., Penguin, London (1971)

229. Zwanzig, R. and Mountain, R.D., J. Chem. Phys., 43 (1965) 4464
230. van Olphen, H., Clays Clay Miner., 4 (1956) 204
231. Smith, R.W., M.Sc. thesis, University of Bristol (1973)
232. Nehme, O., M.Sc. thesis, University of Bristol
233. Bingham, E.C., NBS Scientific Paper No. 278 (1916)
234. Mungan, N., Ph.D. thesis, University of Texas (1962)
235. Brown G., Phil. Trans. R. Soc. Lond., A311 (1984) 221
236. Anderson, J.E., Ph.D. thesis, University of Texas (1965)
237. McBride, E.F., Lindermann, W.L. and Freeman, P.S., Bur. Econ. Geol., Rept. Inv. no. 63, University of Texas (1968) Lithology and petrology of the Gueydon (Catahoula) formation in south Texas
238. Wilcox, R.E., U.S. Geol. Surv. Bull., 1028-N (1959) 409
239. Slaughter, M. and Earley, J.W., Geol. Soc. Am., Spec. Pap. No. 83 (1965)
240. Jonas, E.C., Personal communication (1975) in ref. 11
241. Krauskopf, K.B., Geochim. Cosmochim. Acta, 10 (1956) 1
242. Yoshimura, T. and Kohyama, N., J. Miner. Soc. Japan, 15 (1981) 210
243. Senkagi, A.L., Dixon, J.B., Hossner, L.R., Abder-Ruhman, M. and Fanning, D.S., Clays Clay Mixer., 32 (1984) 259
244. Hagner, A.F., Am. Miner., 24 (1939) 67
245. Gormley, I.P. and Addison, J., Clay Miner., 18 (1983) 153
246. Todor, D.N., Thermal analysis of minerals, Abacus, Tunbridge Wells (1976)
247. Kohyama, N., Fukushima, K. and Fukami, A., Clays Clay Miner., 26 (1978) 25
248. Occelli, M.L. and Tindwa, R.M., Clays Clay Miner., 31 (1983) 22
249. Oades, J.M., Clays Clay Miner., 32 (1984) 49
250. Tuck, J.J., Hall, P.L., Hayes, M.H.B., Ross, P.K. and Poinsignon, C., J. Chem. Soc., Faraday Trans. I., 80 (1984) 309
251. Hall, P.L., Harrison, R., Hayes, M.H.B., Tuck, J.J. and Ross, D.K., J. Chem. Soc., Faraday Trans. I, 79 (1983) 1687

252. Wilson, M.J., Russell, J.D. and Tait, J.M., Contrib. Mineral. Petrol., 47 (1974) 1
253. Farmer, V.C. and Russell, J.D., Spectrochim. Acta, 20 (1974) 1149
254. Tarte, P., Silicates Ind., 28 (1963) 345
255. Tarte, P., Spectrochim. Acta, 23A (1967) 2127
256. Reference clay minerals, API, project 49, Columbia University, New York (1951)
257. Marshall, C.E., Z. Kristallogr., 91 (1935) 433
258. Marshall, C.E., The colloid chemistry of silicate minerals, Academic Press, New York (1949)
259. Brown, G. and Brindley, G.W., chapter 5, in ref. 14
260. Hsu, P.H., Clays Clay Miner., 16 (1968) 303
261. Blum, L. and Stell, G., J. Chem. Phys., 71 (1979) 42
262. Salacuse, J.J. and Stell, G., J. Chem. Phys., 77 (1982) 3714
263. Bates, T.F., Selected electron micrographs of clays and other fine-grained minerals, Circular No. 51, College of mineral industries, Pennsylvania State University (1958)
264. Robinson, D., Personal communication, University of Bristol (1984)
265. Cairns-Smith, A.G., The genetic take over and the mineral origins of life, Cambridge University Press, Cambridge (1982)
266. Mehra, O.P. and Jackson, M.C., Clays Clay Miner., 7 (1960) 317
267. Vanderhoff, J.W., vanden Hul, H.J., Tausk, R.J.M. and Overbeek, J.Th.G., chapter in Goldfinger, G. (ed.), Clean Surfaces, Dekker, New York (1970)
268. van den Hul, H.J. and Vanderhoff, J.W., Br. Polym. J., 2 (1970) 121
269. van den Hul, H.J. and Vanderhoff, J.W., J. Colloid Interface Sci., 28 (1968) 336
270. Correns, C.W., Einführung in die Mineralogie, Springer-Verlag, Berlin (1949)
271. Eeckman, J.P. and Landelout, H., Kolloid Z., 178 (1961) 99
272. Paver, H. and Marshall, C.E., J. Soc. Chem. Ind. (Lond.), 53 (1934) 750
273. Heyding, R.D., Ironside, R., Norrish, A.R. and Prysiazniuk, R.Y., Can. J. Chem., 38 (1960) 1003

274. Overbeek, J.Th.G., J. Colloid Sci., 8 (1953) 593
275. Bradfield, R., J. Phys. Chem., 28 (1924) 170
276. Smith, D.N., Private communication, ECLP Ltd.: a(1984); b(1985)
277. Fey, M.V. and Le Roux, J., Clays Clay Miner., 25 (1977) 285
278. Greene-Kelley, R., J. Soil Sci., 4 (1953) 233
279. Ericsson, T., Linares, J. and Lotse, E., Clay Miner., 19 (1984) 85
280. Oakley, D.M. and Jennings, B.R., J. Colloid Interface Sci., 91 (1983) 188
281. Jennings, B.R. and Oakley, D.M., Clay Miner., 17 (1982) 313
282. Goetz, P.J. and Penniman, J.G., Colloid Interface Sci., 4 (1976) 241
283. System 3000, Automated electrokinetics analyser, PenKem, Inc., Bedford Hills, N.Y.
284. The Pulse Shearometer instruction manual, Rank Brothers, Bothsham, Cambridge
285. Hurlbut, C.S. (ed.), Dana's manual of mineralogy, 18th ed., Wiley, New York (1959)
286. Poehlein, G.W., Ottewill, R.H. and Goodwin, J.W. (eds.), Science and Technology of polymer colloids, vol 2, Martinus-Nijhoff, The Hague (1983)
287. Goodwin, J.W., p.552 in ref. 286
288. Beresford-Smith, B. and Chan, D.Y.C., Chem. Phys. Lett., 92 (1982) 474
289. Beresford-Smith, B. and Chan, D.Y.C., Faraday Discuss. Chem. Soc., 76 (1983) 65
290. Beresford-Smith, B., Chan, D.Y.C. and Mitchell, D.J., J.Colloid Interface Sci., 105 (1985) 216
291. Beresford-Smith, B., Ph.D. thesis, Australian National University, Canberra (1985)
292. Fukoshima, Y., Clays Clay Miner., 32 (1984) 320
293. Secor, R.B. and Radke, C.J., J. Colloid Interface Sci., 103 (1985) 237

294. Korn, G.A. and Korn, T.M., Mathemetical handbook for scientists and engineers, 2nd ed., McGraw-Hill, New York (1968)

295. MacGillavry, C.H., Symmetry aspects of M.C. Escher's periodic drawings, Oosthoek, Utrecht (1965)

296. Shaw, D.J., Introduction to colloid and surface chemistry, 2nd ed., Butterworth, London (1970)

297. Kovganich, N.Y., Deinaga, Y.F. and Popko, K.K., Ukr. Khim. Zh., 44 (1978) 209

298. Kovganich, N.Y., Deinaga, Y.F., Popko, K.K. and Petruk, A.S., Ukr. Khim. Zh., 43 (1977) 1237

299. Parsonage, N.G. and Staveley, L.A.K., Disorder in crystals, Clarendon, Oxford (1978)

300. Marshall, L., Ph.D. thesis, University of Bristol, to be published

301. Sherwood, J.N. (ed.), The plastically crystalline state - Orientationally disordered crystals, Wiley, Chichester (1979)

302. Princeu, H.M., J. Colloid Interface Sci., 91 (1983) 160

303. Barrow, G.M., Physical Chemistry, 3rd ed., McGraw Hill, New York (1973)

304. Atkins, P.W., Physical Chemistry, 2nd ed., Oxford University Press (1982)

305. Cebula, D.J., Goodwin, J.W., Jeffrey, G.C., Ottewill, R.H., Parentich, A. and Richardson, R.A., Faraday Discuss. Chem. Soc., 76 (1983) 37

306. Bell, C.F., Principles and applications of metal chelation, Oxford University Press (1977)

307. Singh, S.S. and Brydon, J.E., Soil Sci., 103 (1967) 162

308. Singh, S.S. and Miles, N.M., Soil Sci., 126 (1978) 323

309. Singh, S.S., Canadian J. Soil Sci., 62 (1982) 549

310. Goodman, H., Personal communication, English Clays, Lovering, Pochin and Co. Ltd. (1984)

311. Findlay, A.D., M.Sc. thesis, University of Bristol (1985)

312. Adamczyk, Z., Czarnecki, J. and Warszyński, P., J. Colloid Interface Sci., 106 (1985) 299

313. Thompson, D.W., Personal communication, University of Bristol (1985)

314. Gard, J.A., (ed.), The electron-optical investigation of clays, Mineralogical Society Monograph no. 3, Mineralogical Society, London (1971)

315. Comer, J.J., specimen preparation, chapter 3 in ref. 314
316. Corbet, H.C. and Wollfes, J., Proc Stockholm Conf. Electron Microsc., Almquist and Wiksell, Stockholm (1956) 334
317. Jennings, B.R., Private communication, Brunel University (1984)
318. Michaels, A.S. and Bolger, J.C., Ind. Eng. Chem. Fundam., 1 (1962) 153
319. Warkentin, B.P. and Yong, R.N., Clays Clay Miner., 9 (1962) 210
320. Granquist, W.T., Clays Clay Miner., 6 (1957) 207
321. van Olphen, H., Discuss. Faraday Soc., 11 (1951) 82
322. Webster, J.R.P., M.Sc. thesis, University of Bristol (1984)
323. Cairns-Smith, A.G., Seven clues to the origin of life - a scientific detective story, Cambridge University Press, Cambridge (1985)
324. Buscall, R., Goodwin, J.W., Hawkins, M.W. and Ottewill, R.H., J. Chem. Soc., Faraday Trans. I., 78 (1982) 2889
325. Partridge, S.J., Ph.D. thesis, University of Bristol (1985)
326. Johnson, S.J., Frattini, P.L. and Fuller, G.G., J. Colloid Interface Sci., 104 (1985) 440
327. Morris, V.J., Foweraker, A.R. and Jennings, B.R., Adv. Mol. Relax. Interact. Process., 12 (1978) 65
328. Morris, V.J., Foweraker, A.R. and Jennings, B.R., Adv. Mol. Relax. Interact. Process., 12 (1978) 201
329. Morris, V.J., Foweraker, A.R. and Jennings, B.R., Adv. Mol. Relax. Interact. Process., 12 (1978) 211
330. Boeckel, G., Geuzling, J.C., Weill, G. and Benoit, H., J. Chim. Phys., 59 (1962) 999
331. Matsumoto, M., Watanabe, H. and Yoshioka, K., Biopolymers, 12 (1973) 1729
332. Benoit, H., Annals. Phys., 6 (1951) 561
333. Perrin, F., J. Phys. Radium, 5 (1934) 497
334. Jackson, M.L., Soil chemical analysis - Advanced course, published by author, University of Wisconsin, Madison (1956)
335. Jackson, M.L., Soil chemical analysis, Prentice-Hall, New Jersey (1958)

336. Jackson, M.L., chapter 8 in Rich, C.I. and Kunze, G.W. (eds.), Soil clay mineralogy, University of North Carolina Press (1964)
337. Kunze, G.W., p.568 - 577 in Methods of soil analysis, part 1, American Society of Agronomy, Madison (1965)
338. Buscall, R., Goodwin, J.W., Hawkins, M.W. and Ottewill, R.H., J. Chem. Soc., Faraday Trans. I, 78 (1982) 2873
339. Hunter, R.J., Aust. J. Chem., 16 (1963) 774
340. Hauser, E.A. and Reed, C.E., J. Phys. Chem., 41 (1937) 911
341. Hauser, E.A. and Reed, C.E., J. Am. Chem. Soc., 58 (1936) 1822
342. Burgess, J., Metal ions in solution, Ellis Harwood, Chichester (1978)
343. Goodman, P.A. and Stucki, J.W., Clay Miner., 19 (1984) 663
344. Petkanchin, I.B. and Suong, T.T., Colloids Surfaces, 16 (1985) 127
345. Dickinson, E., in Everett, D.H. (ed.), Specialist Periodical Reports, Colloid Science, 4 (1983) 150
346. Hayter, J.B., Faraday Discuss. Chem. Soc., 76 (1983)
347. Thompson, J.G., Clay Miner., 19 (1984) 229
348. Sanz, J. and Serratosa, J.M., Clay Miner., 19 (1984) 113
349. Müller, D., Gessner, W., Behrens, H.J. and Scheler, G., Chem. Phys. Lett., 79 (1981) 59
350. Gass, D.M., J. Chem. Phys., 54 (1971) 1898

It's getting late for scribbling and scratching

on the paper

Something's going to give under this pressure

And the cracks are already beginning to show ...

Fish, Derek W. Dick, 1985